

**MOLECULAR MODELLING AND DYNAMIC SIMULATION OF SOME  
CORROSION INHIBITORS IN ACIDIC MEDIUM**

**BY**

**ABDULLAHI UMAR BELLO**

**DEPARTMENT OF CHEMISTRY,  
FACULTY OF PHYSICAL SCIENCES,  
AHMADU BELLO UNIVERSITY,  
ZARIA, NIGERIA**

**NOVEMBER, 2018**



MOLECULAR MODELLING AND DYNAMIC SIMULATION OF SOME  
CORROSION INHIBITORS IN ACIDIC MEDIUM

BY

Abdullahi Umar BELLO, B.Sc. Chemistry (BUK) 2012

P13SCCH8017

A THESIS SUBMITTED TO THE SCHOOL OF POSTGRADUATE STUDIES,  
AHMADU BELLO UNIVERSITY, ZARIA  
IN PARTIAL FULFILLMENT OF THE REQUIREMENTS FOR THE AWARD  
OF MASTER OF SCIENCE DEGREE IN PHYSICAL CHEMISTRY

DEPARTMENT OF CHEMISTRY,  
FACULTY OF PHYSICAL SCIENCES,  
AHMADU BELLO UNIVERSITY,  
ZARIA, NIGERIA

NOVEMBER, 2018

## DECLARATION

I declare that the work in the Dissertation entitled “**MOLECULAR MODELLING AND DYNAMIC SIMULATION OF SOME CORROSION INHIBITORS IN ACIDIC MEDIUM**” has been performed by me in the Department of Chemistry, under the supervision of Prof. A. Uzairu and Dr. G. A. Shallangwa. The information derived from the literature has been duly acknowledged in the text and a list of references provided. No part of this dissertation was previously presented for another higher degree at any university.

Abdullahi Umar Bello

-----

-----

Name of student

Signature

Date

## CERTIFICATION

This Dissertation entitled “**MOLECULAR MODELLING AND DYNAMIC SIMULATION OF SOME CORROSION INHIBITORS IN ACIDIC MEDIUM**” by Abdullahi Umar Bello meets the regulation governing the award of the degree of Master of Science of Ahmadu Bello University, Zaria, and is approved for its contribution to knowledge and literary presentation.

Prof. A. Uzairu (Chairman, Supervisory Committee)	_____	_____
	(Signature)	Date

Dr. G. A. Shallangwa (Member, Supervisory Committee)	_____	_____
	(Signature)	Date

Prof. A. O. Oyewale Head of Department	_____	_____
	(Signature)	Date

Prof. S. Z. Abubakar Dean, School of postgraduate Studies	_____	_____
	(Signature)	Date

## **DEDICATION**

This work is dedicated to Almighty Allah (S.W.T), without Him I would not have been able to achieve this feat. To his Messenger Prophet Muhammad (S.A.W). To my parents, late Alhaji Bello Umar and Malama Saratu Imam as well as my wife Saratu Muhammad and well-wishing relatives and friends.

## ACKNOWLEDGEMENT

All praise and glory is due to Allah (S.W.T) for his showers of blessings throughout my research work to complete the research successfully. May Allah's Peace and Blessings be upon Prophet Muhammad (S.A.W) and his family.

I would like to thank, Prof. A. Uzairu and Dr. G. A. Shallangwa for their support, advice and guidance throughout the research periods and compilations of this Dissertation.

I am also highly indebted to my mother Malama Saratu Imam and my late father, Alhai Bello Umar for all their efforts on me. May the Almighty Allah grant them Aljannatul Firdausi (Amin).

I am very much thankful to my wife, my brothers and sisters for their love, understanding, prayers and continuing support to complete this research work. If I continue to mention names I will not finish.

I am equally using this medium to express my sincere gratitude to all the staff and students of the Department of Chemistry, Ahmadu Bello University, Zaria. I really enjoyed a good learning and working relationship with you all.

## Table of contents

Cover page.....	i
Fly leaf.....	ii
Title Page.....	iiError!
<b>Bookmark not defined.</b>	
DECLARATION .....	iv
CERTIFICATION.....	v
DEDICATION .....	vi
ACKNOWLEDGEMENT .....	vii
Table of Contents.....	viii
List of Tables.....	xii
List Figures.....	of xiii
List Schemes.....	of xv
List of Abbreviations.....	xvii
Abstract .....	xviii
<b>CHAPTER ONE.....</b>	<b>1</b>
<b>1.0 INTRODUCTION .....</b>	<b>1</b>
<b>1.1 Background to the study.....</b>	<b>1</b>
<b>1.2 Research problem.....</b>	<b>4</b>
<b>1.3 Justification to the research .....</b>	<b>5</b>
<b>1.4 Research Questions .....</b>	<b>6</b>
<b>1.5 Theoretical Frame Work.....</b>	<b>6</b>
<b>1.6 Aim and Objectives .....</b>	<b>8</b>
<b>1.7 The Significance of the Study .....</b>	<b>8</b>
<b>CHAPTER TWO.....</b>	<b>9</b>
<b>2.0 LITERATURE REVIEW.....</b>	<b>9</b>
2.1 Corrosion.....	9
2.1.1 Importance of Corrosion Studies.....	9
2.1.2 Conditions necessary for corrosion.....	10

2.1.3 Classification of Corrosion.....	10
2.1.4 Factors Influence Corrosion.....	11
2.1.5 Electrochemical theory of corrosion.....	12
<b>2.2 Types of Corrosion</b> .....	<b>14</b>
2.2.1 General or uniform corrosion.....	14
2.2.2 Pitting corrosion.....	14
2.2.3 Stress corrosion cracking .....	14
2.2.4 Intergranular corrosion.....	15
2.2.5 Corrosion fatigue.....	15
2.2.6 Filiform corrosion .....	15
2.2.7 Crevice corrosion .....	15
2.2.8 Galvanic or bi-metallic corrosion.....	16
2.2.9 Fretting corrosion .....	16
2.2.10 Erosion corrosion .....	16
2.2.11 Selective leaching or demetalification .....	16
<b>2.3 Cost of Corrosion</b> .....	<b>16</b>
<b>2.4 Methods of Corrosion Protection</b> .....	<b>17</b>
2.4.1 Application of protective coatings .....	17
2.4.2 Polarize or shift the potential of the metal .....	17
2.4.3 Cathodic protection.....	18
2.4.4 Materials selection.....	18
2.4.5 Corrosion inhibitors.....	19
<b>2.6 Literature Review on Inhibition of steel corrosion in Acidic Medium</b> .....	<b>21</b>
<b>2.7 Theoretical studies of Corrosion Inhibitors</b> .....	<b>25</b>
<b>2.8 Quantum Chemical studies</b> .....	<b>27</b>
2.8.1 Quantum Chemical studies on corrosion inhibitors .....	27
<b>2.9 Quantitative Structure Activity Relationship Study (QSAR)</b> .....	<b>29</b>
2.9.1. QSAR on corrosion inhibitors.....	30
<b>2.10 Molecular dynamic simulation</b> .....	<b>31</b>
2.10.1 Molecular dynamic simulation on corrosion inhibitors .....	31
<b>CHAPTER THREE</b> .....	<b>32</b>
<b>3.0 MATERIALS AND METHODS</b> .....	<b>32</b>

<b>3.1 Materials</b> .....	32
3.1.1 Data collection.....	33
<b>3.2 Methods</b> .....	42
2.2.1 Geometry Optimization.....	43
3.2.2 Quantum chemical calculation.....	46
<b>3.3 QSAR Methods</b> .....	48
3.3.2 Training and test sets.....	53
3.3.3 QSAR Model Building.....	57
3.3.4 Procedure involved in building GFA models.....	58
3.3.5 Evaluation of the QSAR model.....	61
3.3.6 Applicability Domain.....	64
3.4.1 Building Steel Crystal .....	68
3.4.2 Solution Construction.....	72
3.4.3 Importing inhibitor and Molecular optimization.....	76
3.4.5 Molecular dynamic simulation.....	81
<b>CHAPTER FOUR</b> .....	84
<b>4.0 RESULTS</b> .....	82
<b>4.1 Quantum Chemical studies, GFA Derived models for %IEand molecular dynamics simulation studies of amino acids/analogous derivatives</b> .....	84
<b>4.2 Quantum Chemical studies, GFA Derived models for %IEand molecular dynamics simulation studies of Imidazole derivatives</b> .....	96
<b>4.3 Quantum Chemical studies, GFA Derived models for %IEand molecular dynamics simulation studies of Triazole derivatives</b> .....	96
<b>CHAPTER FIVE</b> .....	120
<b>5.0 DISCUSSION OF RESULTS</b> .....	120
<b>5.1 Quantum Chemical studies, GFA-QSAR Derived models for %IEand molecular dynamics simulation studies of amino acids derivatives</b> .....	120
5.1.2 Quantitative structure–activity relationship (QSAR) Studies for Amino Acids Derivatives.....	125
5.1.3 Molecular Dynamic Simulation Studies for Amino Acids Derivatives .....	127
<b>5.2 Quantum Chemical studies, GFA Derived models for %IEand molecular dynamics simulation studies of Imidazole derivatives</b> .....	129
5.2.2 Quantitative structure–activity relationship (QSAR) Studies for Imidazole Derivatives.....	133

5.2.3 Molecular Dynamic Simulation Studies for Imidazole Derivatives .....	134
<b>5.3 Quantum Chemical studies, GFA Derived models for %IEand molecular dynamics simulation studies of Triazole derivatives.....</b>	<b>135</b>
5.3.2 Quantitative structure–activity relationship (QSAR) Studies for Triazole Derivatives.....	138
5.3.3 Molecular Dynamic Simulation Studies for Imidazole Derivatives .....	139
5.4 Comparison of the Effectiveness of AM, IM and TR in Inhibiting Corrosion of Steel.....	140
<b>CHAPTER SIX.....</b>	<b>141</b>
<b>6.0 SUMMARY, CONCLUSION AND RECOMMENDATIONS .....</b>	<b>143</b>
<b>6.1 Summary of the Findings .....</b>	<b>143</b>
<b>6.2 Conclusion.....</b>	<b>144</b>
<b>References .....</b>	<b>146</b>

## List of Tables

Table 3.1: Amino Acids Derivatives and Their Experimental Inhibition Efficiency(%IE)	34
Table 3.1: Amino Acids Derivatives and Their Experimental Inhibition Efficiency (%IE) (Continued)	34
Table 3.1. : Amino Acids Derivatives and Their Experimental Inhibition Efficiency(% IE)(Continued)	35
Table 3.2: Imidazole Derivatives and Their Experimental Inhibition Efficiency (% IE)	37
Table 3.2: Imidazole Derivatives and Their Experimental Inhibition Efficiency (% IE) (Continued)	37
Table 3.3: Triazole Derivatives and Their Experimental Inhibition Efficiency (% IE)	38
Table 3.3: Triazole Derivatives and Their Experimental Inhibition Efficiency (% IE) (Continued)	39
Table 3.3: Triazole Derivatives and their Experimental Inhibition Efficiency (%IE) (Continued)	40
Table 3.3: Triazole Derivatives and their Experimental Inhibition Efficiency (%IE) (Continued)	41
Table 3.4 Minimum Recommended Values of Validated Parameters for Generally Acceptable QSAR	63
Table 4.2: Optimized Structures, E-HOMO and E-LUMO and of the Studied Inhibitors (AM)	87
Table 4.3: External Validation for Model 4.1	90
Table 4.4: Calculation of Predictive $R^2_{pred}$ . of Model 4.1	91
Table 4.6: Adsorption Energy, Binding Energy, Shortest Bond Distances and Inhibition Efficiencies (%IE) of the AM-Studied Inhibitors	95
Table 4.7: Selected Quantum Chemical Parameters for the Studied Inhibitors IM (Imidazole Derivatives)	97
Table 4.8: Optimized Structures, E-HOMO and E-LUMO of the Studied Inhibitors(IM)	98
Table 4.9: External Validation for Model 4.4	101
Table 4.10: Calculation of Predictive $R^2_{pred}$ . of Model 4.4	102

Table 4.11: Comparison of Experimental, Predicted and Residual %IE of Model 4.4103

Table 4.12: Adsorption Energy, Binding Energy, Shortest Bond Distances and Inhibition Efficiencies (% IE) of the IM-Inhibitors106

Table 4.13: Selected Quantum Chemical Parameters for the Studied Inhibitors, TR (Triazole Derivatives)108

Table 4.13: Selected Quantum Chemical Parameters for the Studied Inhibitors, TR (Triazole Derivatives) (Continued)109

Table 4.14: Optimized Structures, E-Homo and E-Lumo and of the Studied Inhibitors (TR). 110

Table 4.15: External Validation for Model4.7113

Table 4.16: Calculation of Predictive  $R^2_{pred}$ . of Model 4.7114

Table 4.17: Comparison of Experimental, Predicted and Residual %IE of Model 4.7115

Table 4.18: Adsorption Energy, Binding Energy, Shortest Bond Distances and Inhibition Efficiencies (% IE) of the Studied Inhibitors, Triazoles Derivatives, (TR) 118

Table 4.18: Adsorption Energy, Binding Energy, Shortest Bond Distances and Inhibition Efficiencies (%IE) Of The Studied Inhibitors, Triazoles Derivatives, (TR) (Continued) 119

## List of Figures

Figure 1.1: World Consumption of Corrosion Inhibitors	3
Figure 2.1: The Basic Corrosion Cell Consists of an Anode, a Cathode, an Electrolyte, and a Metallic Path for Electron Flow.	13
Figure 3.1: Spartan'14 Graphic Interface	44
Figure 3.2: File Browser	45
Figure 3.3: Spartan' 14 Calculations Dialog Box.	45
Figure 3. 4: Qsar Methodology Flowchart	49
Figure 3.5: Spartan' 14 Molecular Properties Dialog	50
Figure 3.6: Material Studio Interface	50
Figure 3.7: Imported Corrosion Inhibitors With Their Inhibition Efficiencies	51
Figure 3.8. Models Dialog For Selecting Descriptors To Be Computed	53
Figure 3.9: Dataset Division Software.	55
Figure 3.10: Dataset Division Software.	55
Figure 3.11: "Save File" Dialog Box	55
Figure 3.12: Dialog Box For Imputing The Percent of The Training Set	56
Figure 3.13: Output File Format of Training Set Compound	57
Figure 3.15: Material Studio's Study Table Window Interface- B	60
Figure 3.18: Md Simulation Methodology Flowchart	69
Figure 3.20: Forcite Geometry Optimization Dialog	70
Figure 3.21: Cleave Surface Dialog	71
Figure 3.23: Symmetry Supercell Calculation Dialog, Setup Tab	74
Figure 3.24: Build Fe-Crystal Symmetry Supercell	75
Figure 3.27: Material Studio 3d-Atomistic Interface For Drawing Molecules	78
Figure 3.28: Amorphous Cell Calculation Dialog, Setup Tab	78
Figure 3.29: Amorphous Cell Construction Dialog	79
Figure 3.30: Solvent Molecules	79

Figure 3.32: Imported Inhibitor Molecule	80	
Figure 3.33: Built Corrosion System	81	
Figure 3.34: Forcite Dynamics Dialog	82	
Figure 3.35: Forcite Dynamics Dialog, Dynamics Tab	83	
Figure 4.1: Experimental Against Predicted Inhibition Efficiency (% IE) For Amino Acids Derivatives	89	
Figure 4.2: The Williams Plot, the Plot of Standardized Residuals versus the Leverage Value for Amino Acids Derivatives.		97
Figure 4.3: Molecular Dynamic System of Fe, Inhibitor Molecule and Acidic Layer	94	
Figure 4.4: Experimental Against Predicted Inhibition Efficiency (% IE) For Imidazole Derivatives	100	
Figure 4.5: The Williams Plot, the Plot of Standardized Residuals versus the Leverage Value for Imidazole Derivatives.	104	
Figure 4.6: Equilibrium Adsorption Configurations of Inhibitor, IM-1 on Fe (1 1 0) Surface	105	
Figure 4.7: Experimental Against Predicted Inhibition Efficiency (% IE) for Triazole Derivatives	112	
Figure 4.8: The Williams Plot, the Plot of Standardized Residuals versus the Leverage Value for Triazole Derivatives.	116	
Figure 4.9: Equilibrium Adsorption Configurations of TR-1 on Fe (1 1 0) Surface	117	

### **List of Schemes**

Scheme 4.1: GFA Derived QSAR Models for % IE of Amino acids derivatives	86
Scheme 4.2: GFA Derived QSAR Models for % IE of Imidazole derivatives	97
Scheme 4.3: GFA Derived QSAR Models for % IE of Triazole derivatives	109

### **List of abbreviations**

B3LYP	Becke's three-parameter hybrid functional
DFT	Density functional theory
IE	Inhibition Efficiency
MD	Molecular dynamic
GFA	Genetic Function Approximation
1D-3D	One to three dimensional descriptor respectively.
QSAR	Quantitative structure activity relationship
CI	Corrosion Inhibitors
CR	Corrosion Rate
AM	Amino derivatives
IM	Imidazole derivatives
TR	Triazole derivatives

## Abstract

The corrosion inhibition performance of amino acids, imidazole and triazole derivatives in an aqueous acidic medium on steel surfaces have been investigated by the quantum chemical calculation, QSAR analysis, and molecular dynamics (MD) simulation methods. Density functional theory (B3LYP/6-31G\*) quantum chemical calculation method was used to find the optimized geometry of the studied inhibitors. Quantum chemical parameters such as energy of the highest occupied molecular orbital (E-HOMO), the energy of the lowest unoccupied molecular orbital (E-LUMO), energy band gap  $\Delta E$ , Dipole Moment, electrophilicity index ( $\omega$ ), chemical softness ( $\sigma$ ), chemical hardness ( $\eta$ ) and fraction of electron transfer from the inhibitors molecule to the metallic surface ( $\Delta N$ ) have been calculated and well discussed. Additionally, a linear quantitative structure-activity relationship (QSAR) model was built by Genetic Function Approximation (GFA) method to run the regression analysis and establish a correlation between the computed descriptors and the experimental corrosion inhibition efficiencies which were used to predict the corrosion inhibition efficiencies of the studied inhibitors. The prediction of corrosion efficiencies of these inhibitors nicely matched the experimental measurements. The correlation parameters obtained for the best model in each of the three series are the squared correlation coefficients ( $R^2$ ) of 0.871, 0.942 and 0.862, adjusted squared correlation coefficients ( $R^2_{adj}$ ) value of 0.818, 0.908 and 0.822, Leave one out (LOO) cross-validation coefficients ( $Q^2$ ) value of 0.750, 0.795 and 0.706, the external validations ( $R^2_{pred}$ ) of 0.857, 0.983 and 0.835. These indicate that the generated models were excellent for verifying with internal and external validation parameters. Furthermore, molecular dynamics simulation is applied to search the best adsorption configuration of inhibitor over Fe (1 1 0) surface. It is further confirmed by the MD simulations that adsorption of the inhibitor molecules on the metallic surfaces mainly occurred by chemical adsorption phenomenon. Thus, Quantum chemical studies, QSAR analysis along with MD simulation may be very powerful tool for the rational designing of several promising corrosion inhibitors and in prediction of their inhibition efficiencies.



## CHAPTER ONE

### 1.0 INTRODUCTION

#### 1.1 Background to the study

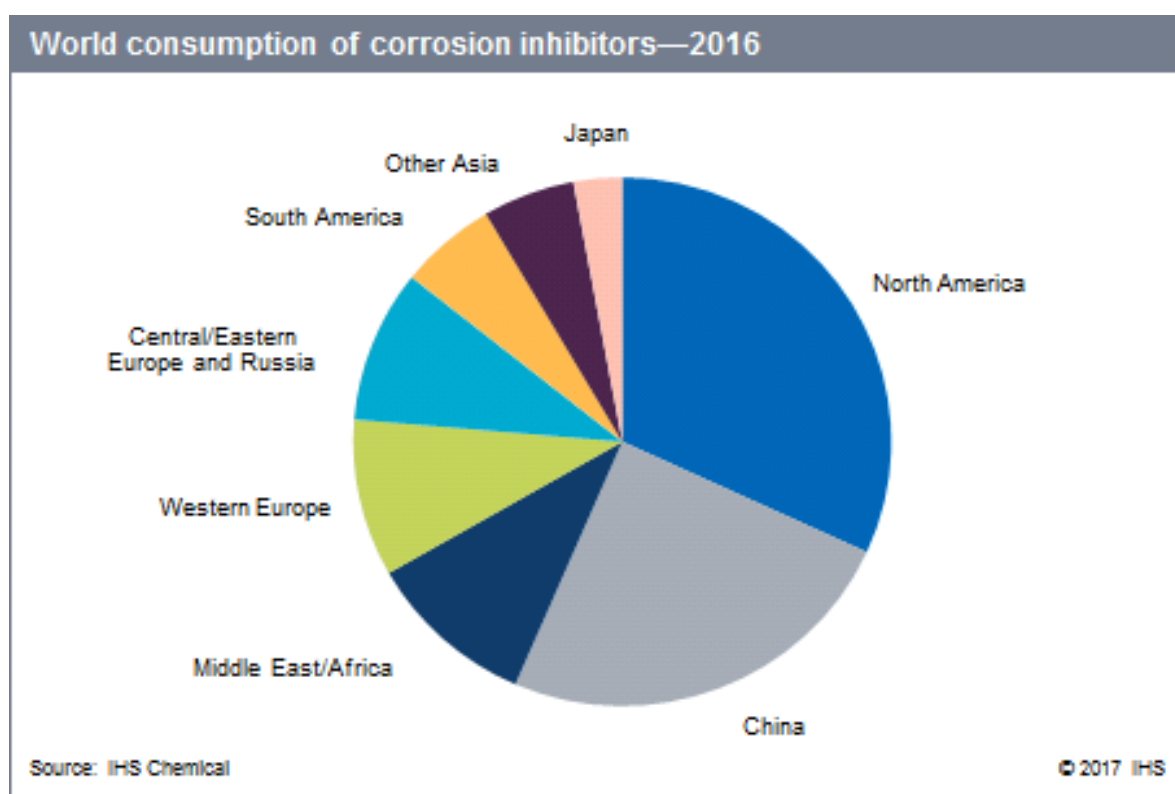
Corrosion is an undesirable process that affects several areas of industrial activity, especially the oil industry, resulting in huge economic losses (Szkarska-Smialowska and ZS-Smialowska, 2005). It is a common problem for steel and directly impacts its cost and safety. The corrosion of iron can cause structural damage and lead to changes in the mechanical and chemical properties of plants, vessels, pipes, and other processing equipment. Several countries have attempted to relate the cost of corrosion to their gross national product. The annual cost of corrosion worldwide was estimated at \$ 2.2 Trillion in 2010, which was about 3 % of the world's gross domestic product of \$ 73.33 Trillion (Al Hashem, 2011; Obot, 2014). Preventing the corrosion of steel has played an important role in various industries, especially in the chemical and petrochemical processing industries that employ the use of steel (Singh *et al.*, 2016). Although it is not possible to completely avoid the corrosion process there are several ways to prevent it or slow down the corrosion rate (Nwankwo *et al.*, 2016). Several organic compounds especially those that contain N, O, S, and P heteroatoms, as well as  $\pi$ -electron systems have been previously used as corrosion inhibitors for metals in aqueous solutions (Murulana *et al.*, 2012; Zhao *et al.*, 2014). Although many heterocyclic compounds have been successfully used as corrosion inhibitors in several metallic systems, most of them were toxic and non-biodegradable (Eddy and Mamza, 2009).

With the current advancement of environmental safety, researchers were focused on the environmentally friendly corrosion inhibitors. Amino acids which were non-toxic,

easily available and completely soluble in aqueous media are considered to be the most promising green inhibitors (Lyon, 2004). So also, Azoles and particularly their derivatives are known as efficient corrosion inhibitors (Kuznetsov and Kazansky, 2008). For example, some derivatives of benzimidazole have been demonstrated as excellent inhibitors for metals and alloys in acidic solution, and exhibit different inhibition performance with the difference in substituent groups and substituent positions on the imidazole ring (Ahamad and Quraishi, 2009; Tang *et al.*, 2013; Zhang *et al.*, 2012). In recent years, N- and S-containing triazole derivatives have attracted more attention for their excellent corrosion inhibition performance (Wang *et al.*, 2004). Not only can some N- and S-containing triazole compounds give very high values of inhibition efficiency, but they can bring down the hydrogen permeation current to a considerable extent (Muralidharan *et al.*, 1995). In contrast to most commercial acid corrosion inhibitors which are highly toxic, many N- and S-containing triazole derivatives are environmentally friendly corrosion inhibitors (Bentiss *et al.*, 1999). In the past two decades, the research in the field of “green” corrosion inhibitors has been addressed toward the goal of using cheap, effective molecules at low or “zero” environmental Impact (Obot and Obi-Egbedi, 2010). The pie chart in Figure 1.1 shows world consumption of corrosion inhibitors on a value basis as at 2016 (Anonymous, 2017).

Several experimental techniques have been used to study the corrosion and corrosion inhibition in acid solution such as weight-loss method, potentiodynamic polarization, electrochemical impedance spectroscopy (EIS), and so on (Amin and Ibrahim, 2011; Zhang *et al.*, 2008). However, experiments are usually time-consuming, expensive, and deficient in elucidating the inhibition mechanism of the system at the Sub-atomic and molecular levels (Wazzan *et al.*, 2016). Therefore, quantum chemical calculation and

molecular dynamics simulation were recommended as potent and fast tools to assist in the interpretations of experimental findings and to overcome such deficiencies (Atalay *et al.*, 2006; Ebenso *et al.*, 2010). Quantum chemical methods have already proven to be very useful in determining the molecular structure as well as elucidating the electronic and reactivity centers of a compound (Gece, 2008). Recently, theoretical prediction of the efficiency of corrosion inhibitors has become very popular in parallel with the progress in computational hardware and the development of efficient algorithms which assisted the routine development of molecular quantum mechanical calculations (Saha and Banerjee, 2015).



**Figure 1.1: World Consumption of Corrosion Inhibitors**

Quantitative structure-activity relationships (QSAR) has been a subject of intense interest in the field of medicinal chemistry in determining the molecular structure as well as

elucidating the electronic structure and reactivity (Kraka and Cremer, 2000), but to a less extent in the field of corrosion (Bentiss *et al.*, 2003; El Sayed *et al.*, 2012). However, in recent years, quantitative structure-activity relationship (QSAR) has aroused many researchers' interest in the studies of corrosion inhibitors (Zhao *et al.*, 2014). The success of the QSAR approach can be explained by the insights offered for the structural determination of chemical properties, and the possibility of estimating the properties of the new chemical compounds without any need for them to be synthesized and tested (Asadollahi *et al.*, 2011). However, the success of any QSAR model depends on the accuracy of input data, selection of the appropriate descriptors, statistical tools, and most important validation of the developed models (Tong *et al.*, 2005; Tropsha *et al.*, 2003) It has been proved to be very helpful for predicting the inhibition efficiencies of novel corrosion inhibitors(Zhao *et al.*, 2014).

Moreover, with the advances in computational chemistry and the development of new algorithms, theoretical methods have been used to investigate corrosion inhibition mechanism and to design new and environment-friendly corrosion inhibitors. Molecular dynamics (MD) simulation was recently considered as a modern tool to study the adsorption behavior of the inhibitor molecules on the metallic surfaces of interest (Wazzan *et al.*, 2016). In recent years, most of the theoretical Molecular dynamics (MD) simulation calculations have not yielded desirable results because they have been performed on an isolated molecule in vacuum without considering corrosion medium(Khaled, 2008). Since the interactions of the inhibitor-metallic surface in a corrosion medium were not taken into account, these calculations do not provide full pictures of the inhibition mechanism.

## **1.2 Research problem**

Organic compounds have been reported to be effective metals corrosion inhibitors in various media. The adsorption layer formed between the compounds, acting as an inhibitor, and the metal surface is one of the main factors that control the inhibition efficiency. Other factors responsible for the formation of a strong adsorption layer on the metal surface are inhibitor's molecular structure and size, number and type of substituents on the inhibitor molecules and the type of adsorption (whether it is a physisorption or chemisorption) (Palomar-Pardavé *et al.*, 2012; Sherif, 2006).

Several experiments were extensively carried out to determine the influence of these factors. However, experiments are usually time-consuming, expensive, and deficient in elucidating the inhibition mechanism of the system at the sub-atomic and 3D-molecular levels (Wazzan *et al.*, 2016). Therefore, quantum chemical calculation, molecular modeling and dynamic simulation were recommended as potent and fast tools to assist in the interpretations of experimental findings and to relate it with the molecular properties of the inhibitor.

### **1.3 Justification to the research**

Experimental approaches used for corrosion study were often costly and time-consuming since large-scale trial experiments are required. Therefore, computational techniques which can overcome these shortcomings are required. This research will contribute to computational prediction and identification of highly efficient and environmentally friendly compounds for corrosion inhibition of steel.

#### **1.4 Research Questions**

- i. What are the dominant structural features responsible for the inhibition efficiency of the studied inhibitors against corrosion of steel in acidic media?
- ii. Which of the derivatives of the studied inhibitors have the highest binding energy based on molecular dynamic simulation?
- iii. What is the dominant substituent influencing the high binding energy of the studied inhibitors?

#### **1.5 Theoretical Frame Work**

Quantitative structure-activity relationships (QSAR) has been a subject of intense interest in the field of medicinal chemistry in determining the molecular structure as well as elucidating the electronic structure and reactivity (Kraka and Cremer, 2000), but to a less extent in the field of corrosion (Bentiss *et al.*, 2003; El Sayed *et al.*, 2012). The concept of assessing the efficiency of a corrosion inhibitor with the help of computational chemistry is to search for compounds with desired properties using chemical intuition, experience and a mathematically quantified and computerized form. Once a correlation between the structure and activity or property is found, any number of compounds, including those not yet synthesized, can be readily predicted employing computational methodology (El Sayed *et al.*, 2012) via a set of mathematical equations which are capable of representing accurately the chemical phenomenon under study (Asadollahi *et al.*, 2011). However, the success of any QSAR model depends on the accuracy of input data, selection of the appropriate descriptors, statistical tools, and most importantly validation of the developed model (Gece,

2008). A major step in constructing the QSAR models is to find a set of molecular descriptors that represent variation in the structural properties of the molecules.

With the improvement of sophisticated software and hardware related computational supportive systems, computer-aided simulation has been explored as an easy and powerful tool from where we can investigate the complex system in corrosion process and may successfully predict their relative inhibition efficiency well in advance. In this occasion, proper theoretical modeling and corresponding quantum chemical calculation is very efficient for exploring the relationship between the molecular properties of the inhibitors and its corrosion inhibition efficiencies (Gece and Bilgiç, 2010; Sun *et al.*, 2012). Corrosion inhibition capability of the molecules can be determined by the frontier molecular orbital energies, energy gap, dipole moment, global hardness, softness, a fraction of electron transfer from the inhibitors molecule to the metallic surface etc. Kokalj recently proposed that only quantum chemical approach alone is not sufficient enough to envisage the inhibition efficiency trend of the inhibitors molecules (Kokalj, 2010). In many cases, results obtained from DFT cannot be correlated well with obtained experimental findings (Ebenso *et al.*, 2010; Quraishi, 2013). In such circumstances, a precise modeling of experimentation should be emphasized to correlate the theoretical results with the experimental inhibition effectiveness.

In real practice, modeling of an experiment can only provide the actual interfacial interactions between the concerned metallic surface and inhibitor molecules. As a result, recently molecular dynamics (MD) simulation has emerged as a modern tool from where we can reasonably predict actual interfacial configuration and adsorption energies of the surface adsorbed inhibitor molecules. Till date, only a few certain groups are working on it to get the interaction, as well as the binding energy of surface, adsorbed inhibitor

molecules. Obot and Gasem recently employed MD simulation to study the adsorption behavior of pyrazine derivatives on the steel surface (Obot and Gasem, 2014). Xia *et al* (2008) explored the correlation between the structural conformation of the imidazoline derivatives and their corresponding inhibition efficiencies by employing MD.

## **1.6 Aim and Objectives**

The aim of this study is to investigate computationally inhibitory action and interaction of the Amino acids, Imidazole and Triazole derivatives as potential steel corrosion inhibitors.

This aim will be achieved through the following objectives:

- i. Data collection.
- ii. Optimization of starting geometries of the molecules.
- iii. Computation of molecular descriptors.
- iv. Splitting of the dataset into training and test set.
- v. Building of QSAR models.
- vi. Selection of the best QSAR model.
- vii. Validation of the QSAR models.
- viii. Molecular dynamics simulation

## **1.7 The Significance of the Study**

This study is based on the premise that corrosion inhibition and protection of metals/alloys play very important role in the chemical, manufacturing, construction, food,

and beverages, oil and gas industry of the economy. The study therefore provides the basis for the evaluation of amino acids, imidazole and triazoles derivatives as suitable alternatives to highly expensive and non-environmentally friendly corrosion inhibitors of steel.

## **CHAPTER TWO**

### **2 LITERATURE REVIEW**

#### **2.1 Corrosion**

Corrosion may be defined as a destructive phenomenon, chemical or electrochemical, which attacks any metal or alloy reacting with the surrounding environment and in extreme cases may cause structural failure. Corrosion can be also defined as the deterioration of material by reaction with its environment. The corrosion occurs because of the natural tendency for most metals to return to their natural state; e.g., iron in the presence of moist air will revert to its natural state, iron oxide. Metals can be corroded by the direct reaction of the metal with a chemical; e.g., zinc will react with dilute sulfuric acid, and magnesium will react with alcohols(Nimmo and Hinds, 2003).

##### **2.1.1 Importance of Corrosion Studies**

The importance of corrosion studies is two folds. The first is economic, including the reduction of material losses resulting from the wasting away or sudden failure of piping, tanks, metal components of machines, ships, hulls, marine, structures...etc. The second is conservation, applied primarily to metal resources, the world's supply of which is limited, and the wastage of which includes corresponding losses of energy and water resources

accompanying the production and fabrication of metal structures (Clark and Varney, 1962; Moore, 2013).

### 2.1.2 Conditions necessary for corrosion

For the purpose of this thesis, electrochemical corrosion is the most important classification of corrosion. Four conditions must exist before electrochemical corrosion can proceed:

- i. There must be something that corrodes (the metal anode).
- ii. There must be a cathode.
- iii. There must be continuous conductive liquid path (electrolyte, usually condensate and salt or other contaminations).
- iv. There must be a conductor to carry the flow of electrons from the anode to the cathode.

This conductor is usually in the form of metal-to-metal contact such as in bolted or riveted joints. The elimination of any one of the four conditions will stop corrosion (Jones, 1996).

### 2.1.3 Classification of corrosion

All metallic materials consist of atoms having valence electrons which can be donated or shared. In a corrosive environment the components of the metallic material get ionized and the movement of the electrons sets up a galvanic or electrochemical cell which causes oxidation, reduction, dissolution or simple diffusion of elements. The metallurgical approach of corrosion of metals is in terms of the nature of the alloying characteristics, the phases existing and their inter-diffusion under different environmental conditions. In fact, the process of corrosion is a complex phenomenon and it is difficult to predict the exclusive effect or the individual role involved by any one of the above mentioned

processes. Based on the above processes, corrosion can be classified in many ways as low temperature and high temperature corrosion, direct oxidation and electrochemical corrosion, etc. The preferred classification is: Dry or chemical corrosion and wet or electrochemical corrosion(Moniz *et al.*, 1986). The other type are:

- i. Chemical corrosion: In which the metal is converted into its oxide when the metal is exposed to a reactive gas or non-conducting liquids.
- ii. Electrochemical corrosion: The formation of hydrous oxide film occurs when the metal is immersed in a conducting liquid containing dissolved reactive substance. The reaction is considered to take place at the metal solution interface, due to the heterogeneity on the metal surface, which creates local anodic and cathodic sites on the metal.

#### 2.1.4 Factors influence corrosion

The nature and extent of corrosion depend on the metal and the environment. The important factors which may influence the corrosion process are:

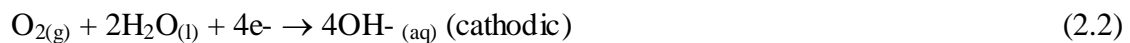
- i. Nature of the metal, nature of the environment and the corrosion products.
- ii. Temperature.
- iii. Concentration of electrolyte.
- iv. Electrode potential.
- v. Aeration.
- vi. Agitation.
- vii. Hydrogen over voltage and pH of the electrolyte(Moniz *et al.*, 1986).

### 2.1.5 Electrochemical theory of corrosion

Electrochemistry is a branch of chemistry dealing with relationships between electricity and chemical reactions. It involves oxidation and reduction (redox) reactions. Corrosion is an example of a type of electrochemical reaction, since a substance -oxidizing agent- oxidizes a metal in its environment. In the natural environment, oxygen gas is a good oxidizing agent. Most metals have lower reduction potentials than  $O_2$ ; therefore, they are easily oxidized in the presence of oxygen. Metals such as gold, silver and platinum are not so easily oxidized and are sometimes referred to as noble metals. The reasons for the lack of oxidation in these noble metals are varied and sometimes complex. One of the most familiar corrosion processes is the oxidation of iron (rusting). Iron metal is spontaneously oxidized in the presence of  $O_2$  and an aqueous electrolyte solution (see Figure 2.1). Physical strains (scratches, dents, bends, etc...) present on the iron are more easily oxidized than other areas. This directly relates to physics, i.e., the way electric fields are generated at the surface of the metal. Stronger fields are generated at the physically strained parts of the metal. The result is that these regions are anodic (oxidation occurs) and simultaneously different areas are cathodic regions at which a reduction reaction (usually of  $O_2$ ) occurs (Moore, 2013). The iron atom gives up two electrons to form the  $Fe^{2+}$  ion as in equation (2.1):



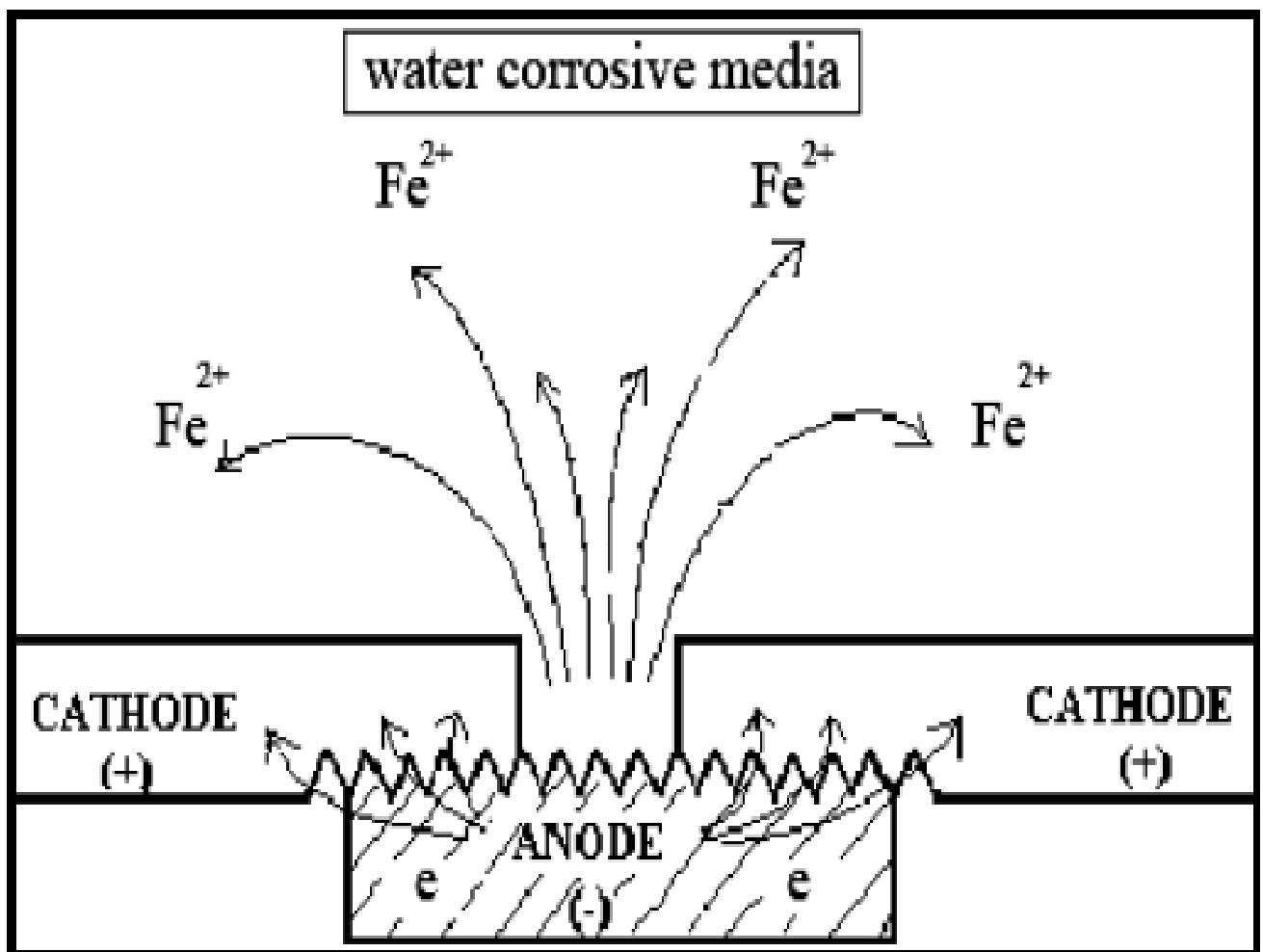
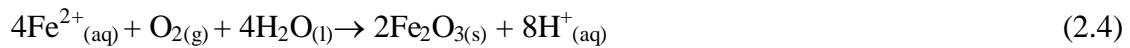
The electrons that are released flow through the iron metal to the cathodic region where they react with oxygen as shown in equation (2.2):



These two half reactions together give the overall reaction as given in equation 2.3:



$\text{Fe}^{2+}$  is eventually oxidized further to  $\text{Fe}^{3+}$ , in the compound iron (III) oxide (rust) as presented in equation 2.4:



**Figure 2.1: The basic corrosion cell consists of an anode, a cathode, an electrolyte, and a metallic path for electron flow.**

## 2.2 Types of Corrosion

### 2.2.1 General or uniform corrosion

Differences in electrical potential occur on the surface of a piece of metal due to small differences in chemical composition, phase differences, amount of cold work, etc. These differences set up small corrosion cells each with an anode and cathode. Corrosion continues until the metal is consumed or the film of rust formed on the surface sets up a barrier to the electrolyte (Jones, 1996).

### 2.2.2 Pitting corrosion

Pitting corrosion is a complex but important problem that is at the root of many corrosion failures. It has been studied in detail for many years, yet crucial phenomena remain unclear. In pitting corrosion, the surface of the metal is attacked in small-localized areas. Organisms in water or breaks in a passive film can initiate corrosion. In pitting corrosion very little metal is removed from the surface but the effect is marked. In passivated metals or alloys that are exposed to solutions containing aggressive anions, primarily chloride, pitting corrosion results in local dissolution leading to the formation of cavities or (holes) (Moniz *et al.*, 1986; Moore, 2013).

### 2.2.3 Stress corrosion cracking

Stress corrosion occurs due to the simultaneous influence of static tensile stresses and a corrosive environment and this is specific to a particular metal. The stresses may be internal such as those caused by cold work, welding, and heat treatment or external forces caused by mechanical stresses set up by assembly practices. A good example of this form of corrosion is 316 stainless steel in marine environments. 316 stainless steel was

developed to withstand attacks in chloride environments, but if stressed the steel will fail by stress corrosion cracking(Jones, 1996).

#### 2.2.4 Intergranular corrosion

Corrosion occurs at the grain boundaries due to a difference in potential between the anodic grain boundaries and the cathodic grains. "Sensitized" stainless steels, where carbides have been precipitated in the grain boundaries during improper heat treatment or in the heat-affected zone of a weld, are particularly susceptible to intergranular corrosion(Moore, 2013).

#### 2.2.5 Corrosion fatigue

Corrosion fatigue occur due to the repeated cycling stresses in a corrosive environment(Moniz *et al.*, 1986).

#### 2.2.6 Filiform corrosion

Filiform corrosion appears as a network of corrosion trails, of a wormlike structure, particularly beneath thin organic coatings. Salts containing chlorides, which have been left on the surface prior to coating, are suspected(Jones, 1996).

#### 2.2.7 Crevice corrosion

Crevice corrosion occurs when there is a difference in ion, or oxygen, concentration between the metal and its surroundings. Oxygen starvation in an electrolyte at the bottom of a sharp V-section will set up an anodic site in the metal that then corrodes rapidly(Clark and Varney, 1962).

#### 2.2.8 Galvanic or bi-metallic corrosion

Galvanic corrosion takes place between two different metals, or coatings, which are joined together in the presence of an electrolyte. Each metal has a potential different from any other metal when placed in an electrolyte. A series can be built up of all the metals relative to each other (Moniz *et al.*, 1986).

#### 2.2.9 Fretting corrosion

Fretting corrosion occurs when two or more parts rub against each other. The rubbing action removes the corrosion products and exposes new metal to the electrolyte (Moore, 2013).

#### 2.2.10 Erosion corrosion

Erosion is the removal of metal by the movement of fluids against the surface. The combination of erosion and corrosion can provide a severe rate of corrosion (Moore, 2013).

#### 2.2.11 Selective leaching or demetalification

Demetalification is the removal of one of the alloying elements in an alloy by the electrolyte. This results in a "spongy" metal. Typical example is the removal of zinc in chloride waters from brass (Moniz *et al.*, 1986).

### **2.3 Cost of Corrosion**

Corrosion is not only dangerous, but also costly, with annual damages in the billions of dollars. Apart from the monetary loss cause by corrosion, consider some of the direct and indirect effects of corrosion which contribute to these costs:

- i. Replacement of corroded equipment.
- ii. Unscheduled plant shutdowns for replacement.

- iii. Process upsets resulting from corrosion.
- iv. Product contamination.
- v. Product loss from a vessel that has corroded.
- vi. Otherwise unnecessary preventive maintenance.
- vii. Over design to allow for corrosion.
- viii. Inability to use otherwise desirable materials.

While the economic costs are frightening, we must consider them to be of secondary importance to the potential loss of life and damage to the environment problems, which can have widespread effects upon modern industrial businesses. It is essential, therefore, for operators of industrial process plants to have a program for controlling corrosion(Obot, 2014).

## **2.4 Methods of Corrosion Protection**

### 2.4.1 Application of protective coatings

Metallic structures can be protected from corrosion in many ways. A common method involves the application of protective coatings made from paints, plastics or films of noble metals on the structure itself (e.g., the coating on tin cans). These coatings form an impervious barrier between the metal and the oxidant but are only effective when the coating completely covers the structure. Flaws in the coating have been found to produce accelerated corrosion of the metal(Jones, 1996).

### 2.4.2 Polarize or shift the potential of the metal

Another method of reducing corrosion is to polarize or shift the potential of the metal enabling it to act as a cathode (rather than an anode) in an electrochemical cell. One example is the galvanizing of steel with a coating of zinc. The iron and zinc then function

as the electrodes of a cell. Zinc is the more readily oxidized metal of the pair and functions as the anode and corrodes, while the iron functions as the cathode. The zinc is used up and protection is effective as long as some zinc remains. Sacrificial anodes work on the same principal but use an external electrode made from a readily oxidized metal; this form of protection is commonly used on buried pipelines(Sastri, 2012).

#### 2.4.3 Cathodic protection

Cathodic protection using an impressed current derived from an external power supply is a related form of protection in which the metal is forced to be the cathode in an electrochemical cell. For example, most cars now use the negative terminal on their batteries as the ground. Besides being a convenient way to carry electricity, this process shifts the electrical potential of the chassis of the car, thereby reducing (somewhat) its tendency to rust(Sastri, 1998, 2012).

#### 2.4.4 Materials selection

Basic recommendations for eliminating corrosion are materials selection which are summarized as follows:

- i. Use corrosion-resistant materials including plastics and non-metallic in severe environments.
- ii. Avoid dissimilar metal couples.
- iii. Avoid the use of back-to-back structural shapes, selection of appropriate material shall be considered, such as stainless steel. In addition, alternate structural shapes shall be considered such as C- or d-shaped channel, especially in highly corrosive areas.
- iv. Avoid the use of alloys susceptible to stress-corrosion(Sastri, 1998, 2012).

#### 2.4.5 Corrosion inhibitors

Corrosion inhibitors can be added to solutions in contact with metals (e.g. inhibitors are required in the antifreeze solution in automobile cooling systems). These compounds can prevent either the anode or the cathode reaction of corrosion cells; one way that they can do this is by forming insoluble films over the anode or cathode sites of the cell. Examples of anodic inhibitors are sodium phosphate or sodium carbonate while zinc sulfate and calcium or magnesium salts act as cathodic inhibitors. New forms of paints are being developed which take advantage of similar properties. These paints promise to nearly eliminate corrosion in applications like painted car fenders, etc(Akalezi *et al.*, 2012; Sastri, 1998, 2012).

#### **2.5 Corrosion Inhibition in Acid Solutions by Organic Inhibitors**

Acid solutions are widely used in industry, where the most important fields of application are acid pickling, industrial acid cleaning, and oil well acidizing. Because of general aggressive nature of acid solutions, the practice of inhibition is commonly used to reduce the corrosive attack on metallic materials. The selection of appropriate inhibitors mainly depends on the type of acid, its concentration, temperature and velocity of flow, the presence of dissolved organic and/or inorganic substances, and on the type of metallic material exposed to the action of the acidic solution(Obot and Obi-Egbedi, 2010; Sastri, 2012).Occasionally, they act as cathodic, anodic or together, as cathodic and anodic inhibitors, nevertheless, as a general rule, act through a process of surface adsorption, designated as a film- forming. Naturally, the occurrence of molecules exhibiting a strong affinity for metal surfaces compounds showing good inhibition efficiency and low environmental risk(Yaro *et al.*, 2013). These inhibitors build up a protective hydrophobic

film adsorbed molecules on the metal surface, which provides a barrier to the dissolution of the metal in the electrolyte. They must be soluble or dispersible in the medium surrounding the metal (Sastri, 1998, 2012).

The efficiency of an organic inhibitor depends on the:

- i. Chemical structure, like the size of the organic molecule;
- ii. Aromaticity and/or conjugated bonding, as the carbon chain length;
- iii. Type and number of bonding atoms or groups in the molecule (either  $\pi$  or  $\sigma$ );
- iv. Nature and the charges of the metal surface of adsorption mode like bonding strength to the metal substrate;
- v. The ability for a layer to become compact or cross-linked,
- vi. Capability to form a complex with the atom as a solid within the metal lattice;
- vii. Type of the electrolyte solution like adequate solubility in the environment(Sanyal, 1981).

The efficiency of these organic corrosion inhibitors is related to the presence of polar functional groups with S, O or N atoms in the molecule, heterocyclic compounds, and pi electrons, generally have hydrophilic or hydrophobic parts ionizable. The polar function is usually regarded as the reaction center for the establishment of the adsorption process(Yaro *et al.*, 2013). The organic acid inhibitor that contains oxygen, nitrogen and/or sulfur is adsorbed on the metallic surface blocking the active corrosion sites. Although the most effective and efficient organic inhibitors are compounds that have  $\pi$ -bonds, it presents biological toxicity and environmental harmful characteristics(El-Haddad, 2013). Since the metal surface covered is proportional to the inhibitor concentrates, the concentrations of the inhibitor in the medium is critical(Roberge, 1999; Sherif, 2006).

## 2.6 Literature Review on Inhibition of steel corrosion in Acidic Medium

Corrosion in oilfields occurs at all stages from downhole to surface equipment and processing facilities. It appears as leaks in tanks, casings, tubing, pipelines, and other equipment (Finšgar and Jackson, 2016; Osman and Shalaby, 2003). Corrosion problems are usually connected with operating problems and equipment maintenance, leading to recurrent partial and even total process shutdown, resulting in severe economic losses (Garcia-Arriaga *et al.*, 2010). Typically, highly concentrated acids, between 5 and 28 wt.%, are used in the well during the acidic stimulation process and cause serious corrosion issues. It is almost impossible to prevent corrosion, however it is possible to control it (Brondel *et al.*, 1994).

To control the corrosion damage of well tubulars, mixing tanks, coiled tubings, and other metallic surfaces, acids need to be inhibited by the use of an effective corrosion inhibitor solution (now commonly organic compounds)(de Queiroz Baddini *et al.*, 2007; Quraishi and Jamal, 2000). A corrosion inhibitor is a chemical substance that is effective in very small amounts when added to a corrosive environment to decrease the corrosion rate of the exposed metallic material. Organic compounds in recent decades, including triazole derivatives (Collins *et al.*, 1993), tetrazole derivatives (Dafali *et al.*, 2003), thiadiazole derivatives (Es-Salah *et al.*, 2004), cysteine (Ezeoke *et al.*, 2012), substituted uracils (Ferreira *et al.*, 2004), and imidazole derivatives (Finšgar and Milošev, 2010) were proved as excellent corrosion inhibitors in acid media. The following is the literature review on some related organic inhibitors against steel corrosion in acidic medium.

Some amino acids have been found to be good inhibitors for the corrosion of mild steel in HCl. Amino acids are nontoxic, relatively cheap and easy to produce with purities

greater than 99%. At the present time there are more than 200 different amino acids known to occur in nature (Ashassi-Sorkhabi *et al.*, 2004). Most of the natural amino acids are the alpha amino acids which contain carboxyl and amino groups bonded to the same carbon atom (Bazzi *et al.*, 1995).

Some researchers investigated the inhibitory effect of three amino acids (alanine (Ala), glycine (Gly) and leucine (Leu)) against steel corrosion in HCl solutions using potentiodynamic polarization method (Ashassi-Sorkhabi *et al.*, 2004). Corrosion data such as corrosion rate, corrosion potential ( $E_{corr}$ ) and corrosion resistance ( $R_p$ ) were determined by extrapolation of the cathodic and anodic Tafel region. Adsorption isotherm was investigated by weight loss measurement. The effect of inhibitor concentration and acid concentration against inhibitor action was investigated. The inhibition efficiency depends on the type of amino acid and its concentration. The inhibition effect ranged from 28 to 91%. The amino acids acted as a corrosion inhibitor in HCl solution through adsorption on the steel surface and the adsorption also supported the Langmuir adsorption isotherm (Gece, 2008).

The inhibition effects of tryptamine (TA) on the corrosion behaviour of ARMCO iron in 0.5 M deaerated  $H_2SO_4$  using potentiodynamic curves (PCM) and electrochemical impedance spectroscopy (EIS) was also studied (Moretti *et al.*, 2004). TA was found to be an effective ARMCO iron inhibitor, even at higher temperature and for long term exposure. Inhibition efficiencies, calculated by PCM and EIS, ranged from 90% to 99% and did not diminish over time and as the temperature increased. TA adsorption followed Bockris–Swinkels adsorption isotherm (Moretti *et al.*, 2004). The effect of cysteine on the corrosion of 304L stainless steel in 1 M  $H_2SO_4$  using open-circuit potential measurements, anodic polarization curves, electrochemical impedance spectroscopy (EIS) and scanning electron

microscopy (SEM) was also determined (Silva *et al.*, 2006). The results obtained indicated that the effect of cysteine was concentration dependent.

Other studies reported evaluated the electrochemical performance of 1-diethylamino-propan-2-ol (EAP) and 1, 3-bis-diethylamino-propan-2-ol (DEAP) for brass in simulated atmospheric water using potentiodynamic curves and electrochemical impedance spectroscopy (EIS) (Gao and Liang, 2007; Kiani *et al.*, 2008; Zerfaoui *et al.*, 2004). The experimental results indicated that the investigated compounds retarded the anodic dissolution of brass. The experimental data was partly supported by density functional theoretical (DFT) and quantum chemical analysis.

Popova and his co-workers investigated benzimidazole, 2-aminobenzimidazole, 2-mercaptobenzimidazole, 1-benzylbenzimidazol, and 1,2-dibenzylbenzimidazole as corrosion inhibitors for mild steel in deaerated 1 mol/L HCl solution (Popova *et al.*, 2004). They reported that all five diazoles have pronounced corrosion inhibition properties, whereas the latter three were particularly effective. Subsequently, they have reported that 8 benzimidazole derivatives exhibit a corrosion inhibition effect for mild steel in 1 mol/L HCl at 20<sup>0</sup>C (Popova *et al.*, 2004). Their %IE increases with increased corrosion inhibitor concentration and they mainly act as mixed-type inhibitors. The %IE of these compounds has the following order: 5(6)-nitrobenzimidazole < benzimidazole < 2-methylbenzimidazole < 5(6)-carboxybenzimidazole < 2-hydroxymethylbenzimidazole < 2-aminobenzimidazole \_ 2-benzimidazolylacetonitrile < 2-mercaptobenzimidazole. Furthermore, the researchers investigated 5 different azole compounds as corrosion inhibitors for mild steel in 1 mol/L HCl at 20<sup>0</sup>C. The %IE trend of these compounds was reported to have the following order: indole \_ 1H-benzotriazole \_ benzothiazole > benzimidazole. On the other hand, the addition of benzothiadiazole to the HCl solution even

promoted corrosion rate compared with the non-inhibited solution (Popova *et al.*, 2007). The authors also reported that the %IE of these compounds, except benzothiadiazole, increases with increased corrosion inhibitor concentration and that they act as mixed-type inhibitors by predominantly reducing the rate of the anodic reaction.

Triazole and triazole-type compounds containing nitrogen and sulfur have attracted more attention because of their excellent corrosion inhibition performance (Lebrini *et al.*, 2011). New triazole derivatives have been continuously synthesized and investigated as inhibitors of metal corrosion in acidic solutions (Martinez and Metikoš-Huković, 2003). The triazole derivatives have special affinity towards metal surface displacing water molecules on the surface. In addition, they possess abundant  $\pi$ -electrons and unshared electron pairs on the nitrogen atom that can interact with d-orbitals of iron to provide a protective film.

Some researchers studied benzotriazole as an inhibitor for the corrosion inhibition of mild steel in 1 N citric acid using weight loss method. The results obtained indicated that the corrosion inhibition efficiency of the benzotriazole varied with the temperature and acid concentrations (Matheswaran and Ramasamy, 2010). Also, it was found that the corrosion inhibition behaviour of benzotriazole was better when the concentration of inhibitor was increased. Kinetic treatment of the results showed first order kinetics. Li and his co-workers synthesized two triazole derivatives [1-phenyl-2-(5-(1,2,4) triazol-1-ylmethyl-(1,3,4) oxadiazol-2-ylsulphonyl)-ethanone (PTOE) and 2-(4-tert-butyl-benzylsulphonyl)-5-(1,2,4) triazol-1-ylmethyl-(1,3,4) oxadiazole (TBTO)] as new corrosion inhibitors for the corrosion of mild steel in 1 M hydrochloric acid (Li *et al.*, 2011). The inhibition efficiencies of the different inhibitors were evaluated using weight loss and electrochemical techniques such as electrochemical impedance spectroscopy (EIS) and polarization curves. The results

obtained from electrochemical investigation revealed that these compounds acted as mixed-type inhibitors retarding the anodic and cathodic corrosion reactions and did not change the mechanism of either hydrogen evolution reaction or mild steel dissolution. The adsorption of the inhibitors obeyed the Langmuir adsorption model. The effect of molecular structure on the inhibition efficiency of the inhibitors was investigated using *ab initio* calculations while electronic properties such as the energy of the highest occupied molecular orbital (HOMO), the energy of the lowest unoccupied molecular orbital (LUMO), dipole moment ( $\mu$ ) and molecular orbital densities were also calculated.

## 2.7 Theoretical studies of Corrosion Inhibitors

Traditionally, the performance of inhibitive action is found out by the weight loss measurements, potentiodynamic polarization, and electrochemical impedance spectroscopy. However, these experimental methodologies are costly, time-consuming and sometimes unable to explore inhibition mechanisms (Taylor *et al.*, 2015). According to quantum mechanics, all the information one needs to know about a system can be obtained from the wavefunction, which, in turn, is obtained as the solution to the Schrodinger equation (2.5), in which the quantum mechanical operator H contains the physical terms that contribute to the system energy and E is an eigenvalue (Levine *et al.*, 2000).

$$H\Psi = E\Psi \quad (2.5)$$

$\Psi$  is the quantum mechanical wave function that is related to the probability density of the electrons in the system (this density,  $\rho$ , is given by  $|\Psi|^2$ ). Any observable quantity  $\langle A \rangle$  can be determined by taking the expectation value of the appropriate quantum mechanical operator A, applied to the wave function via the equation (2.6):

$$\langle A \rangle = \int_{-\infty}^{+\infty} \Psi^* A\Psi dx = \langle \Psi/A/\Psi \rangle \quad 2.6$$

The angular brackets on the right introduce Dirac notation and the \* indicates the complex conjugate(Levine *et al.*, 2000).

Over the latter half of the 20th century, powerful techniques were derived alongside the development of microcomputers that allowed the wave functions of molecular systems to be obtained with great accuracy(Taylor *et al.*, 2015). Unfortunately, deducing inhibitor efficiency directly from the wave function is nontrivial: the operator representing inhibitor efficiency must somehow capture all the relevant information regarding the target material and environment! Instead, Vosta and Eliasek and then, later, many others(Gholami *et al.*, 2013; Vosta and Eliasek, 1971) introduced the approach utilized in drug design, of attempting to correlate readily computable molecular descriptors (such as the dipole moment or energies of the frontier molecular orbitals) with the inhibitor efficiencies obtained from experiment, using the method of linear (and, later, non-linear) regression (QSAR). The systems of equations derived that relate inhibitor efficiency to molecular properties are generally opaque to the underlying physics involved in inhibition. Consequently, Corrosion inhibition capability of the molecules can be determined by the frontier molecular orbital energies, energy gap, dipole moment, global hardness, softness, a fraction of electron transfer from the inhibitors molecule to the metallic surface etc.

However, Kokalj recently proposed that only quantum chemical approach alone is not sufficient enough to envisage the inhibition efficiency trend of the inhibitors molecules(Kokalj, 2010). In many cases, results obtained from DFT cannot be correlated well with obtained experimental findings(Murulana *et al.*, 2012; Quraishi, 2013). In this circumstances, a precise modeling of experimentation should be emphasized to correlate the theoretical results with the experimental inhibition effectiveness. In real practice, modeling of an experiment can only provide the actual interfacial interactions between the

concerned metallic surface and inhibitor molecules. As a result, recently molecular dynamics (MD) simulation has emerged as a modern tool from where we can reasonably predict actual interfacial configuration and adsorption energies of the surface adsorbed inhibitor molecules(Wazzan *et al.*, 2016).

## **2.8 Quantum Chemical studies**

Quantum chemical methods and molecular modeling techniques enable the definition of a large number of molecular quantities characterizing the reactivity, shape, and binding properties of a complete molecule as well as of molecular fragments and substituents. The use of theoretical parameters presents two main advantages: firstly, the compounds and their various fragments and substituents can be directly characterized on the basis of their molecular structure only; and secondly, the proposed mechanism of action can be directly accounted for in terms of the chemical reactivity of the compounds under study (Gece, 2008).

Quantum chemically derived parameters are fundamentally different from experimentally measured quantities, although there is some natural overlap. Unlike experimental measurements there is no statistical error in quantum chemical calculations. There is inherent error however, associated with the assumptions required to facilitate the calculations. In most cases the direction but not the magnitude of the error is known (Levine *et al.*, 2000). In using quantum chemistry-based parameters with a series of related compounds, the computational error is considered to be approximately constant throughout the series.

### **2.8.1 Quantum Chemical studies on corrosion inhibitors**

Ma *et al.* (2006) attempted to find theoretical parameters to characterize inhibition property of three nitrogen-heterocyclic compounds, namely 3,5-dimethyl-1H-pyrazole, pyridine and 2-(3-methyl-1H-pyrazol-5-yl)pyridine against steel corrosion by using an ab initio method employing the HF/LANL2DZ basis set. According to their results, corrosion inhibition efficiency is related to the HOMO energy. They also investigated the interaction between inhibitor molecules and one iron atom and found that the lower the value of combined energy, the more stable the formed complex, the better the inhibitive property.

A detailed calculation of the molecular structure of benzimidazoles was performed by El Sayed and co-workers using the B3LYP/6-31G\* method to explore possible correlations between corrosion inhibition efficiencies and a number of quantum molecular properties, such as EHOMO, ELUMO, total negative charge on molecules and linear solvation energy relationship parameters. Furthermore, bivariate correlations using two trial personal correlation coefficient and linear regression analyses were performed by stepping method (El Sayed *et al.*, 2008). A comparison of the inhibition efficiencies of a series of benzimidazoles indicated that their inhibition effect has been closely related to the orbital energies (EHOMO and ELUMO), Log P, dipolar-polarizability factor ( $p^*$ ) and the total negative charge on the molecule. It has been concluded that a composite index of more than three quantum chemical parameters should be considered to characterize the inhibition efficiency of molecules. Quantum chemical studies of corrosion inhibition of steel in acidic medium by some triazole, oxadiazole and thiadiazole derivatives were conducted by El Ashry *et al.* (2006) in a similar manner.

Zhang *et al.* (2005) studied the inhibition efficiencies of imidazole, benzimidazole and their derivatives using the B3LYP/6-31G\* method. They calculated a number of quantum chemical parameters, such as EHOMO, ELUMO, energy gap, charge distribution,

dipole moment, and molecular connectivity index (MCI) which reveals the steric hindrance effect of the molecule. According to their results, the EHOMO was the most statistically significant term influencing the corrosion inhibition efficiencies. The greater the EHOMO, the greater is the inhibition efficiency.

## **2.9 Quantitative Structure Activity Relationship Study (QSAR)**

Quantitative structure–activity relationship (QSAR) models are regression or classification models used in the chemical and biological sciences and engineering. Like other regression models, QSAR regression models relate a set of "predictor" variables (X) to the potency of the responsevariable (Y), while classification QSAR models relate the predictor variables to a categorical value of the response variable. In QSAR modeling, the predictors consist of physico-chemical properties or theoretical molecular descriptors of chemicals; the QSAR response-variable could be a biological activity of the chemicals. QSAR models first summarize a supposed relationship between chemical structures and biological activity in a data-set of chemicals. Second, QSAR models predict the activities of new chemicals (Tropsha *et al.*, 2003).

Recently, quantitative structure-activity relationship (QSAR) has aroused many researchers' interest in the studies of corrosion inhibitors (El Sayed *et al.*, 2012; Zhao *et al.*, 2014). The advantage of this approach lies in the fact that it requires only the knowledge of the chemical structure. Additionally, it has been proved to be very helpful for predicting the inhibition efficiencies of novel corrosion inhibitors (Zhang *et al.*, 2005).The concept of assessing the efficiency of a corrosion inhibitor with the help of computational chemistry is to search for compounds with desired properties using chemical intuition, experience and a mathematically quantified and computerized form. Once a correlation between the structure

and activity or property is found, any number of compounds, including those not yet synthesized, can be readily predicted employing computational methodology (Karelson *et al.*, 1996) via a set of mathematical equations which are capable of representing accurately the chemical phenomenon under study (El Sayed *et al.*, 2012).

#### 2.9.1. QSAR on corrosion inhibitors

El Ashry and Senior in (2011) studied the corrosion activity of lauric hydrazide and its salts as corrosion inhibitors using quantum chemical calculation and QSAR the result revealed the effect of inclusion quantum chemical parameters to improve corrosion inhibition efficiency. Khaled (2011) reported that the corrosion inhibition of 1,3-Pyrimidine derivatives as corrosion inhibitors using genetic algorithm and QSAR model technique the activity of this compound show similarities with experimental (Khaled, 2011).

Inhibition and adsorption efficiency of cysteine, glycine, leucine and alanine on mild steel in hydrochloric acid was investigated and the result define the effect of various concentration of the amino acid inhibited the corrosion of mild steel and the correlation between the theoretical obtained from (QSAR) with experimental was found to be excellent (Eddy *et al.*, 2011).

However, Masoud and others explained the inhibition performance of aminopyridine as corrosion inhibitor using quantum chemical calculation the correlation was found to be good between the theoretical and experimental corrosion inhibition (Masoud *et al.*, 2010). Therefore the most effective way to obtain a complete set of data without necessarily performing an experiment is the application of quantitative structure activity relationship (QSAR) (Pourbasheer *et al.*, 2014). Once QSAR model is established

the activity of the molecules can be predicted and know which structural features play a significant role in the activity.

## **2.10 Molecular dynamic simulation**

Molecular dynamics (MD) is a computer simulation method for studying the physical movements of atoms and molecules. The atoms and molecules are allowed to interact for a fixed period of time, giving a view of the dynamic evolution of the system. In the most common version, the trajectories of atoms and molecules are determined by numerically solving Newton's equations of motion for a system of interacting particles, where forces between the particles and their potential energies are often calculated using interatomic potentials or molecular mechanics force fields. The method was originally developed within the field of theoretical physics in the late 1950s (Alder and Wainwright, 1959; Fermi *et al.*, 1955) but is applied today mostly in chemical physics, materials science and the modelling of biomolecules. Because molecular systems typically consist of a vast number of particles, it is impossible to determine the properties of such complex systems analytically; MD simulation circumvents this problem by using numerical methods.

### **2.10.1 Molecular dynamic simulation on corrosion inhibitors**

Recently, Khaled applied molecular simulation tools to optimize the structure of adsorbed triazole derivatives. The iron/inhibitor/solvent interfaces were simulated and the charges on the inhibitor molecules as well as their structural parameters were calculated in the presence of solvent effects. According to the experimental and theoretical data,

aminotriazole was the best inhibitor among triazole, aminotriazole and benzotriazole(Khaled, 2008).

Hu and Dai investigated the adsorption behavior of glutamic acid and aspartic acids on Cu (001) surface in gas phase and found that both of the two inhibitors could be adsorbed on the Cu surface firmly due to the interaction between polar groups and copper surface(Hu and Dai, 2012). Fu and others researched the inhibition behavior of four amino acids compounds on Fe(110) surface in aqueous and found that these four amino acids compounds can be absorbed on the iron surface through the heteroatoms and heterocyclic ring(Fu *et al.*, 2010).

Obot and Gasem (2014) recently has employed MD simulation to study the adsorption behavior of pyrazine derivatives on the steel surface. Xia and co-workers explored the correlation between the structural conformation of the imidazoline derivatives and their corresponding inhibition efficiencies by employing MD(Xia *et al.*, 2008).

## **CHAPTER THREE**

### **3.0 MATERIALS AND METHODS**

#### **3.1 Materials**

This work was carried out in-silico, the hardware and software that was used include: Dell Intel(R)Core(TM)i7-5500U CPU), 16.00GB RAM @ 2.400GHz 2.400GHz processor on Windows 8.1 Pro 64-bit Operating system, x64-based processor, Spartan 14v.1.1.0 software, Material studios 8.0, ChemDraw ultra 12.0 and Microsoft office Excel 2013.

### 3.1.1 Data collection

Twenty-five amino acids/analogues derivatives, twenty imidazole and thirty-one triazole derivatives as potential steel corrosion inhibitors were collected from the literature (Babić-Samardžija *et al.*, 2005; Hluchan *et al.*, 1988; Khaled and Hackerman, 2003), (Aljourani *et al.*, 2009; Khaled, 2003; Popova *et al.*, 2003; Tang *et al.*, 2013) and (Bentiss *et al.*, 1999; Deng *et al.*, 2012; González-Olvera *et al.*, 2013; Gurudatt *et al.*, 2015; Ma *et al.*, 2017; Ouici *et al.*, 2015; Quraishi and Sardar, 2002; Quraishi *et al.*, 2012; Wang *et al.*, 2004) respectively which was used for this present study. The chemical structure of each compound in the data sets was drawn with ChemDraw ultra V12.0, named and saved as \*.cdx file. Their molecular structures and experimental inhibition efficiencies were shown in Table 3.1, 3.2 and 3.3 respectively.

**Table 3.1: Amino acids Derivatives and Their Experimental Inhibition Efficiency (%IE)**

Inhibitor	Structure	%IE
AM-1		50
AM-2		59

AM-3	63
AM-4	47
AM-5	80
AM-6	52
AM-7	39
AM-8	73
AM-9	53

---

**Table 3.1: Amino acids Derivatives and Their Experimental Inhibition Efficiency (%IE) (Continued)**

Inhibitor	Structure	%IE
AM-10		51

AM-11	87
AM-12	75
AM-13	67
AM-14	34
AM-15	43
AM-16	77.4
AM-17	75.1

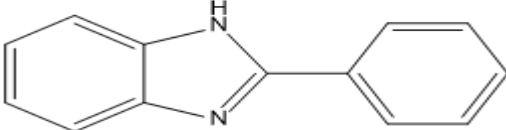
---

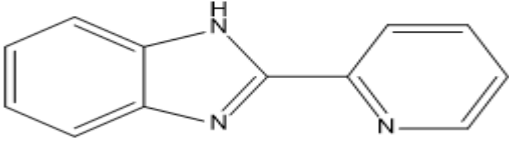
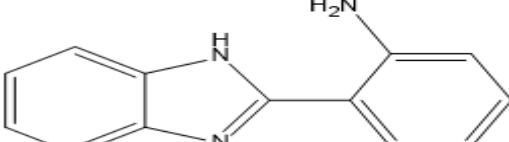
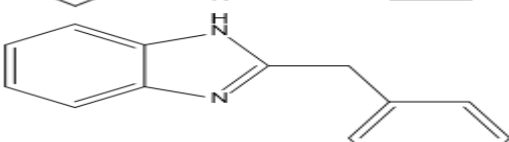
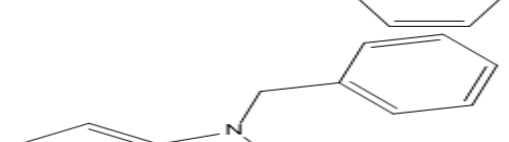
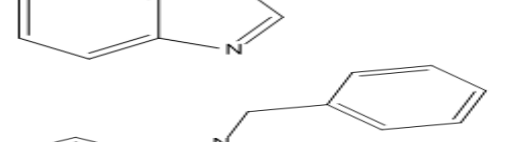
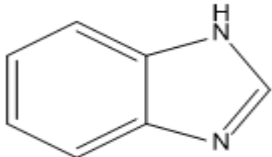
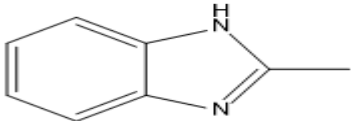
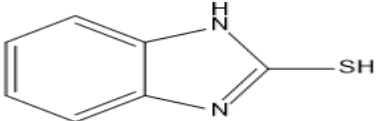
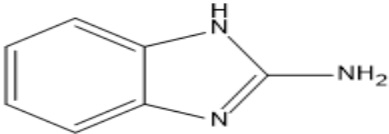
**Table 3.1. : Amino acids Derivatives and Their Experimental Inhibition Efficiency (%IE) (Continued)**

Inhibitor	Structure	%IE
AM-18		41

AM-19	71
AM-20	63.62
AM-21	71.79
AM-22	63.24
AM-23	66.83
AM-24	49.88
AM-25	60.09

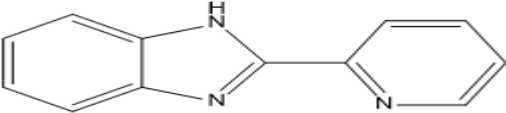
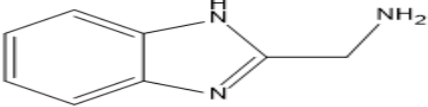
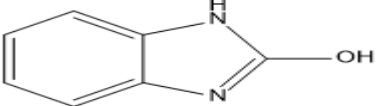
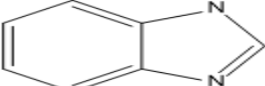
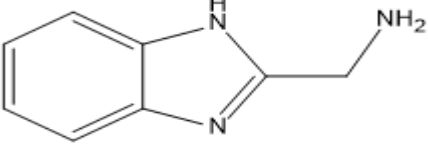
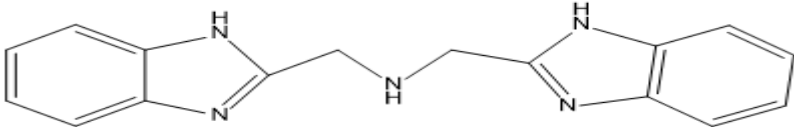
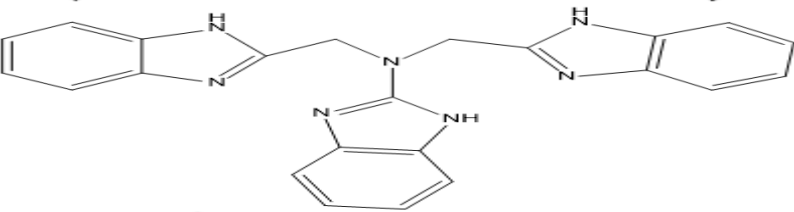
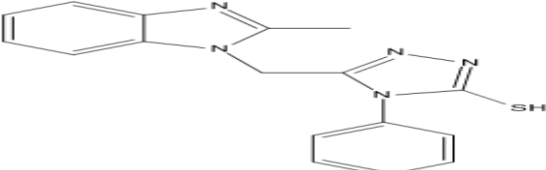
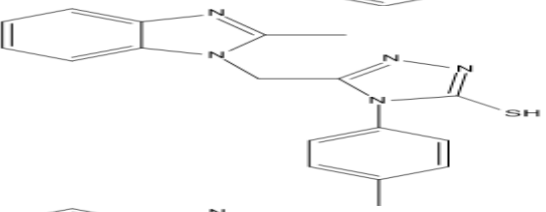
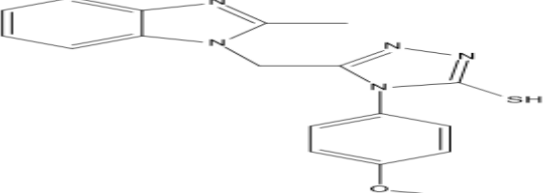
**Table 3.2: Imidazole Derivatives and Their Experimental Inhibition Efficiency (%IE)**

Inhibitor	Structure	%IE
IM-1		85

IM-2		90
IM-3		93
IM-4		93
IM-5		95
IM-6		96
IM-7		52.2
IM-8		57.1
IM-9		88.7
IM-10		75.99

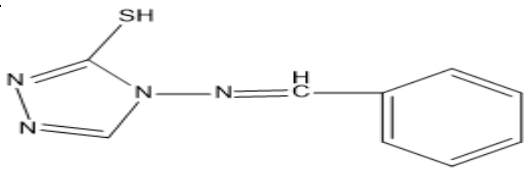
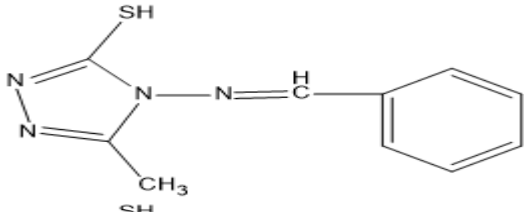
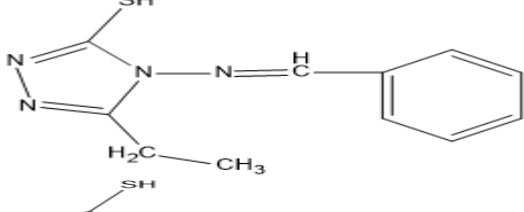
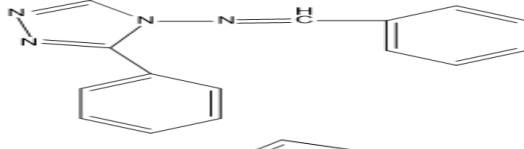
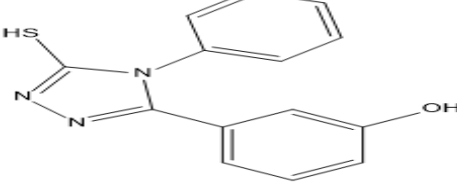
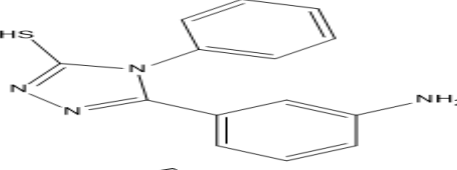
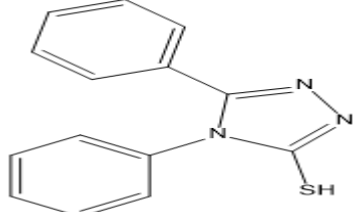
**Table 3.2: Imidazole Derivatives and Their Experimental Inhibition Efficiency (%IE)  
(Continued)**

Inhibitor	Structure	%IE
-----------	-----------	-----

IM-11		72.40
IM-12		62.32
IM-13		57.07
IM-14		50.34
IM-15		72.2
IM-16		91.8
IM-17		92.0
IM-18		87.1
IM-19		83.9
IM-20		81.1

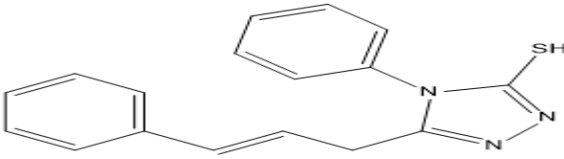
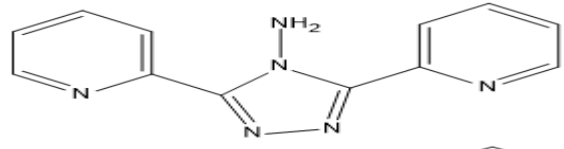
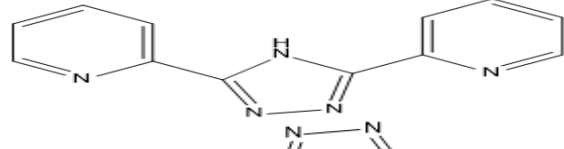
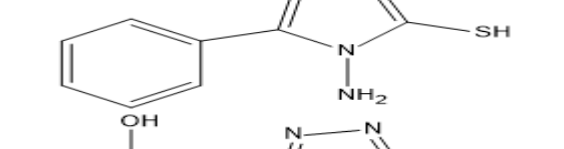
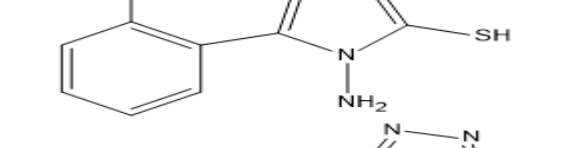
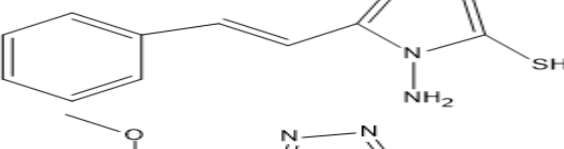
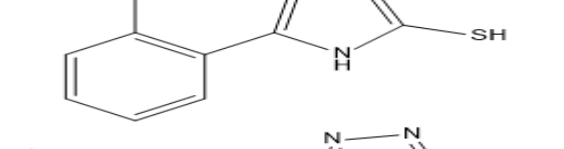
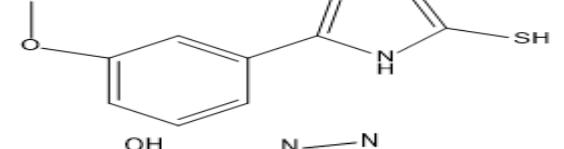
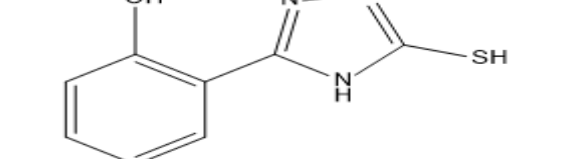
**Table 3.3: Triazole Derivatives and Their Experimental Inhibition Efficiency (%IE)**

Inhibitor	Structure	%IE
-----------	-----------	-----

TR-1		91.43
TR-2		92.63
TR-3		95.53
TR-4		97.48
TR-5		73.0
TR-6		83.4
TR-7		84.2

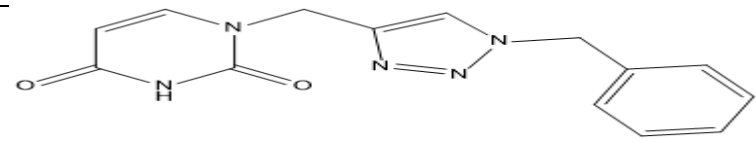
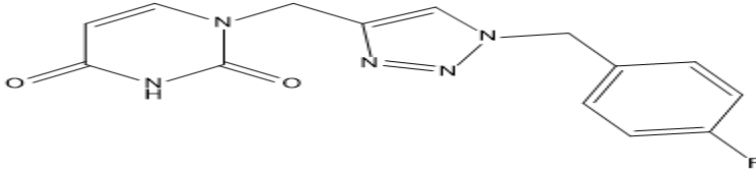
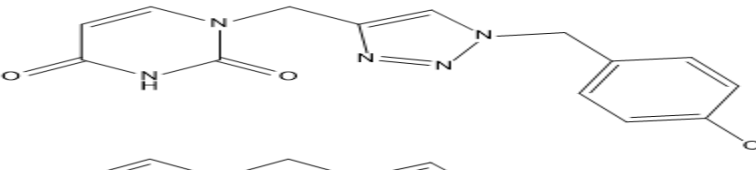
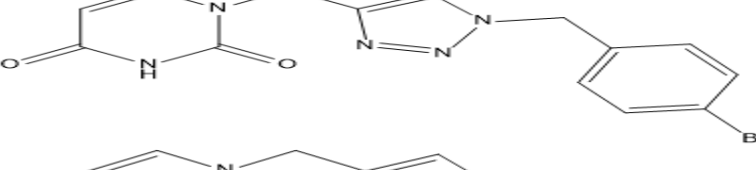
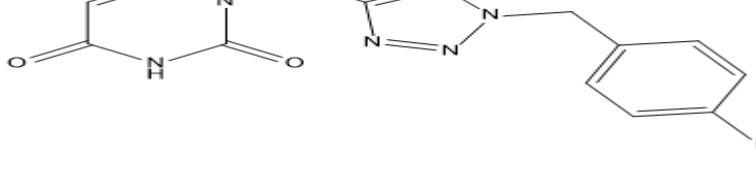
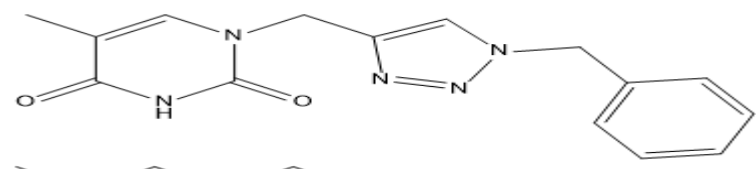
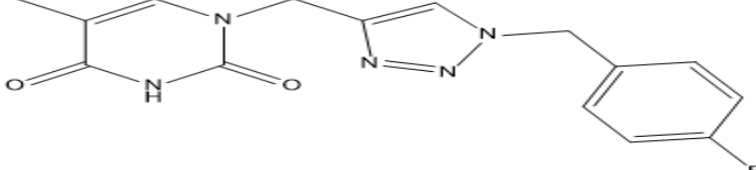
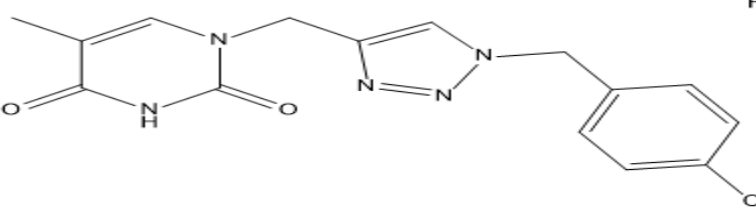
**Table 3.3: Triazole Derivatives and Their Experimental Inhibition Efficiency (%IE)  
(Continued)**

Inhibitor	Structure	%IE
-----------	-----------	-----

TR-8		87.3
TR-9		74.7
TR-10		68.1
TR-11		91.0
TR-12		92.9
TR-13		95.2
TR-14		98.36
TR-15		98.16
TR-16		96.73

**Table 3.3: Triazole Derivatives and Their Experimental Inhibition Efficiency (%IE)  
(Continued)**

Inhibitor	Structure	%IE
-----------	-----------	-----

TR-17		93.1
TR-18		95.6
TR-19		95.9
TR-20		96.1
TR-21		92.9
TR-22		90.2
TR-23		95.0
TR-24		95.0

**Table 3.3: Triazole Derivatives and Their Experimental Inhibition Efficiency (%IE)  
(Continued)**

Inhibitor	Structure	%IE
-----------	-----------	-----


TR-25		95.0
TR-26		94.9
TR-27		58.2
TR-28		94.7
TR-29		77.57
TR-30		84.11
TR-31		94.92

### 3.2 Methods

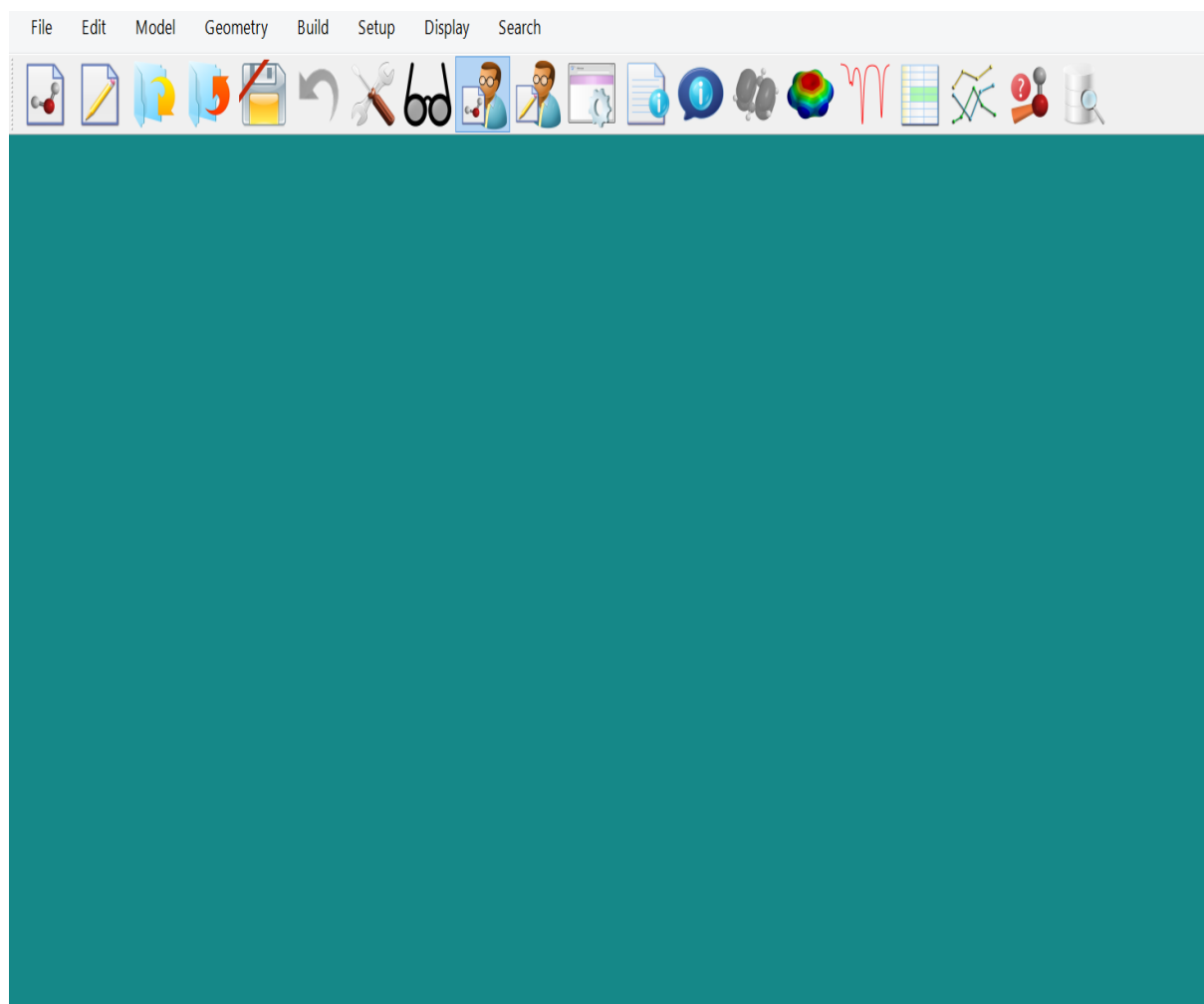
### 3.2.1 Geometry optimization

The 2-D structures of the data set compounds drawn using ChemDraw Ultra 12.0 was imported into Spartan 14 V1.1.4 Wave function package where they were converted to 3-D form and subjected to energy minimization in order to remove their strain energies. The computational method invoked for calculating geometries in the present study is Density Functional Theory (DFT) method in combination with the B3LYP functional with 6-311+G (d,p) basis set (Larif *et al.*, 2013). The B3LYP hybrid functional of DFT method uses Becke's three-parameter functional (B3) and incorporates a blend of HF with DFT exchange terms associated with the gradient-corrected correlation functional of Lee, Yang, and Parr (LYP)(Becke, 1993).

The various procedures deployed in molecular optimization using Spartan 14 V1.1.0 were highlighted thus: Spartan 14 software was launched by double clicking on the icon on the desktop of the laptop specified in section 3.1 above creating its interface or work space shown in Figure 3.1. By clicking on the file menu → Open button on the menu bar, a file browser propped up, in the file name box of the window, the name of the molecule saved as cdx file drawn with chemdraw was indicated in Figure 3.2. All files option was selected from the small window next to file name to allow the Spartan Software recognize the cdx file.

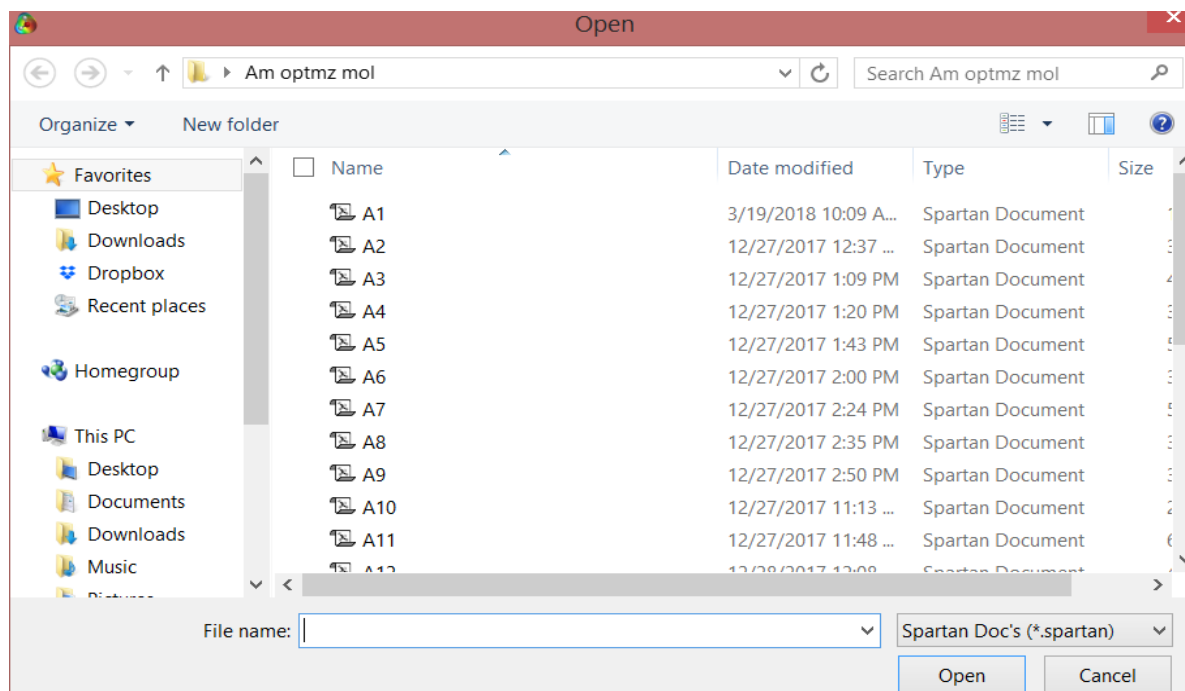
By clicking Open on the window, the molecule was imported to the Spartan's interface. By selecting View  option on the tool menu interface, the structure of the molecule was completely imported unto the interface. The energy of the imported molecule was minimized by selecting build → minimize options on the menu bar. The molecule was

represented using the ball and spoke option in the model menu. The minimum energy geometry of the molecule was calculated by selecting set up → calculations menus on the menu bar causing the appearance of a dialog box shown in Figure 3.3. On the dialog box, equilibrium geometry was selected from the leftmost checkbox to the right of calculate menu. This specifies optimization of equilibrium geometry.

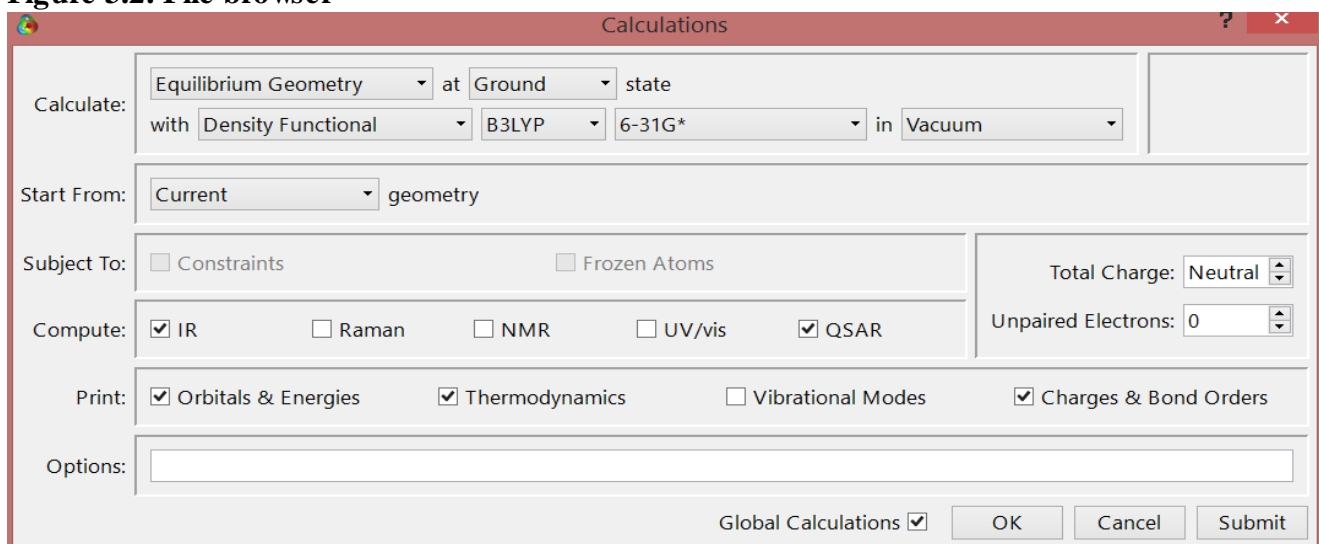


**Figure 3.1: Spartan'14 graphic interface**

Using the state checkbox in the dialog box, ground state was selected. Through the leftmost checkbox on the second row, right of calculate menu, the type of calculation (molecular mechanics, semi-empirical or DFT) was specified.



**Figure 3.2: File browser**



**Figure 3.3: Spartan' 14 Calculations dialog box.**

Directly below the state check box on the second row of calculate menu is the check box for indicating the calculation type. Here, Becke's three-parameter hybrid functional (B3LYP) for DFT calculation was selected. The 6-31G\* basis was selected for DFT

calculation through the last checkbox on the second row of calculate menu on the dialogue box. The check box directly right of the start from menu was used to select the geometry of the molecule, current geometry was selected in all calculations. The compute menu was used to specify the properties of the molecule to be computed. The check boxes for QSAR and IR were marked in this section. The print menu was used to mark the checkboxes for orbital energies, thermodynamics, charges and bond order. Calculations dialogue was existed by clicking on submit at bottom. At the completion of the calculation, a notification that calculation has completed appeared. This notification was removed by clicking Ok that appears on the screen. Through the file menu on the Spartan interface, the optimized molecule was saved as sdf\* file in a folder. This procedure was appropriately applied to all other molecules in each of the data sets.

### 3.2.2 Quantum chemical calculation

Density functional theory (DFT) is a worldwide accepted *ab initio* approach for modelling ground state properties of molecules of interest. In the last few decades, DFT has become popular due to its accuracy in carrying out theoretical calculation in lesser time with a much lesser amount of investment. In this Dissertation, quantum chemical calculations were carried out with SPARTAN 14.0 Wave-Function programming Package. The various procedures deployed in molecular optimization using Spartan 14 V1.1.0 generate the relevant Quantum chemical descriptors. The Quantum chemical descriptors computed include the energy of the highest occupied molecular orbital (*E-HOMO*), the energy of the lowest unoccupied molecular orbital (*E-LUMO*) and dipole moment ( $\mu$ ). The quantum chemical reactivity indices such as energy band gap ( $\Delta E = ELUMO - EHOMO$ ), chemical hardness ( $\eta$ ), chemical softness ( $\sigma$ ), electrophilicity index ( $\omega$ ), global electronegativity ( $\chi$ )

and the number of transferred electrons ( $\Delta N$ ) were derived from the frontier molecular orbital energies ( $E_{HOMO}$  and  $E_{LUMO}$ ) using appropriate relations (Equations 3.1–3.7) as previously reported in literature (Nwankwo *et al.*, 2016; Saha and Banerjee, 2015).

$$\Delta E = E_{LUMO} - E_{HOMO} \quad 3.1$$

$$\eta = -\frac{1}{2}(E_{HOMO} - E_{LUMO}) \quad 3.2$$

$$\sigma = \frac{1}{\eta} = -\left(\frac{2}{E_{HOMO} - E_{LUMO}}\right) \quad 3.3$$

$$\bar{\mu} = \frac{1}{2}(E_{HOMO} + E_{LUMO}) \quad 3.4$$

$$\omega = \frac{\bar{\mu}^2}{2\eta} \quad 3.5$$

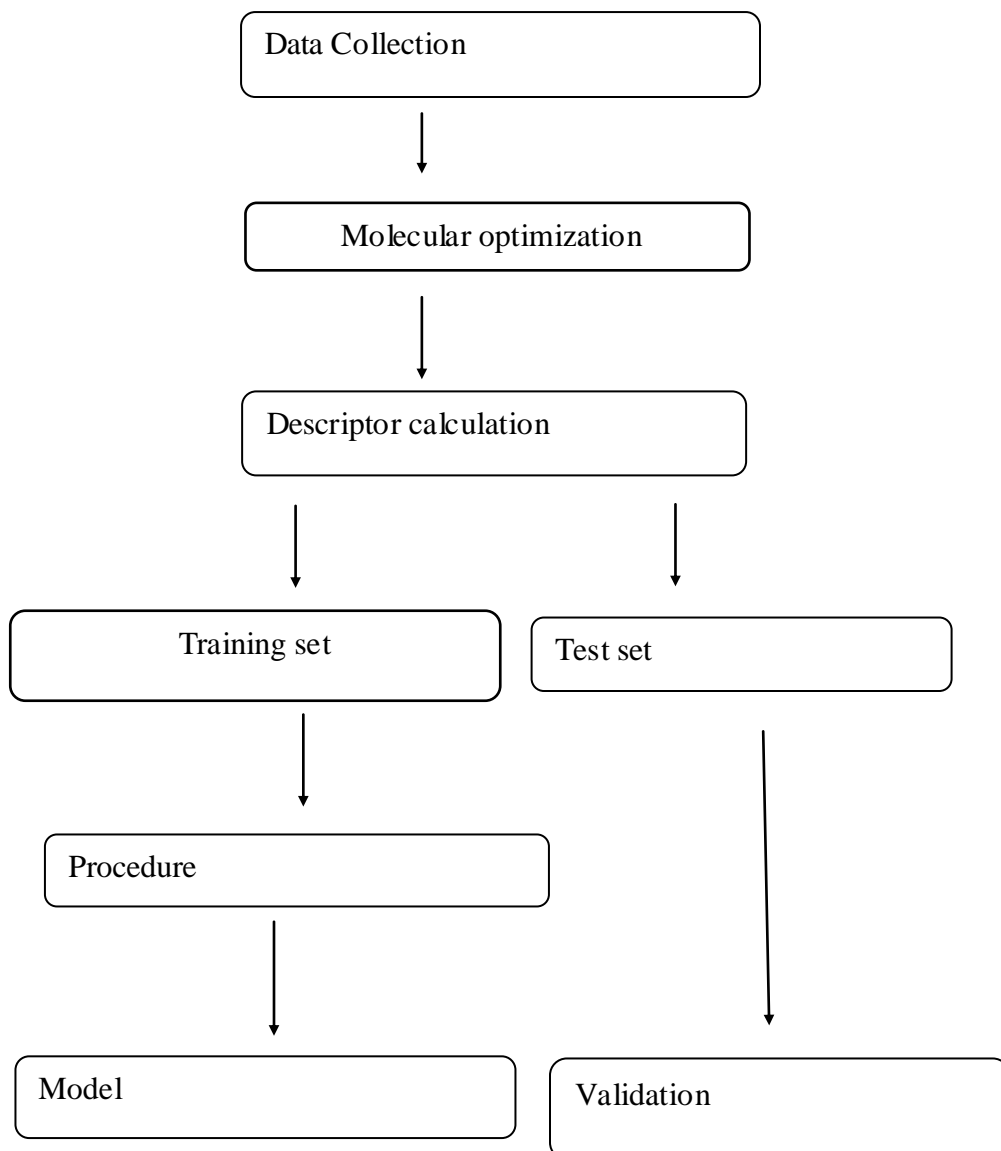
$$\chi = \frac{-(E_{HOMO} + E_{LUMO})}{2} \quad 3.6$$

$$\Delta N = \frac{\chi_{Fe} - \chi_{inh}}{2(\eta_{Fe} + \eta_{inh})} \quad 3.7$$

Where  $\chi_{Fe} = 7eV$ ,  $\eta_{Fe} = 0$  (Musa *et al.*, 2012)

### 3.3 QSAR Methods

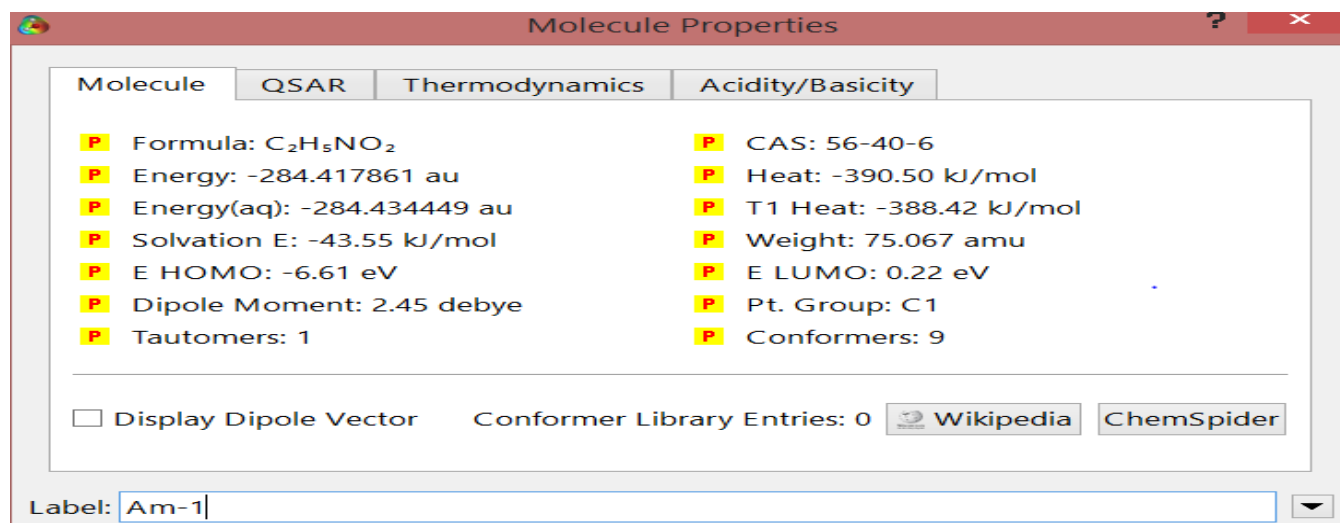
In the present study, QSAR studies were performed using Hansch's approach (Hansch and Fujita, 1964). In Hansch's approach, structural properties of compounds are calculated in terms of different physicochemical parameters and these parameters are correlated with the experimental inhibition efficiency (%IE) through equation using regression analysis. The various steps are presented in a flowchart in Figure 3.4



### Figure 3. 4: QSAR methodology flowchart

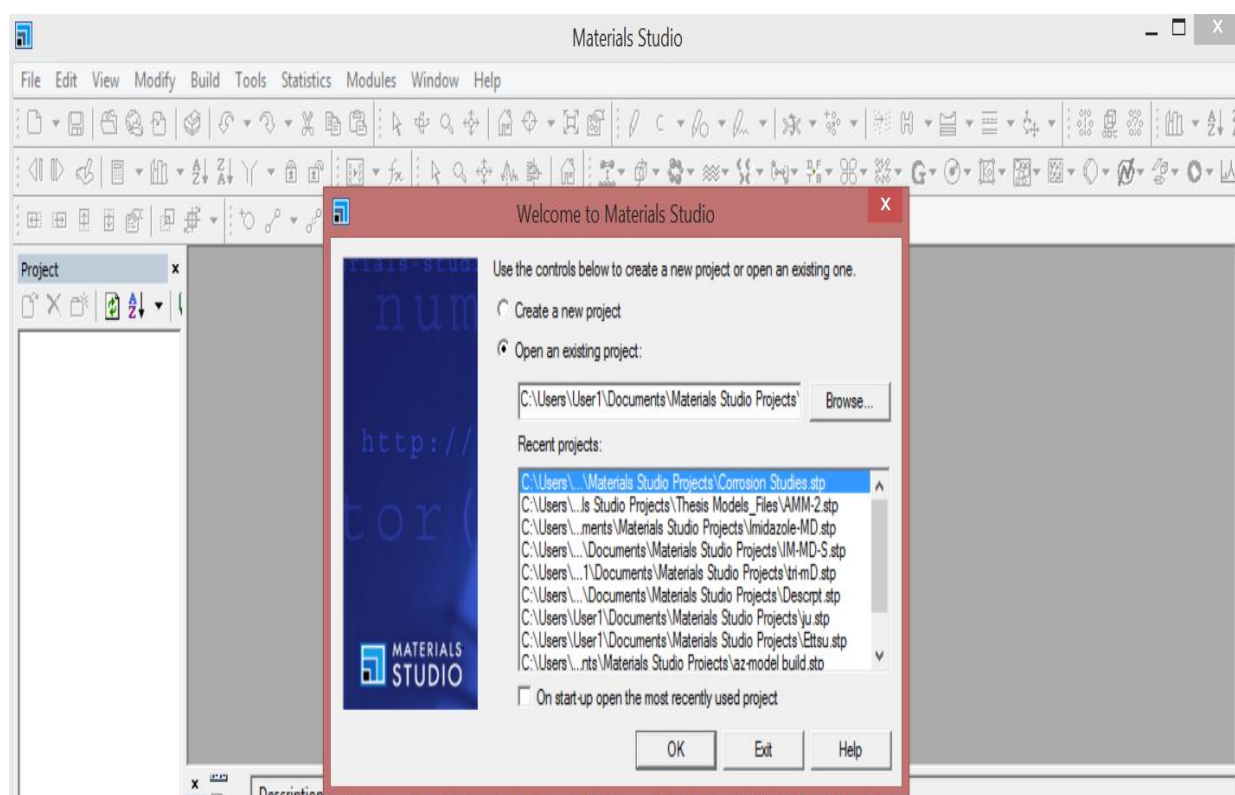
#### 3.3.1 Computing molecular descriptors using Spartan 14 and Material studio soft wares.

By launching the Spartan 14 software, its interface (see Figure 3.1) was created. The optimized molecule's structural file saved as *\*sdf* file as described in section 3.2.1 was imported unto the interface by clicking the *file menu* → *open* option on the menu bar resulting to the propping of a file browser (see Figure 3.2). On the file browser, the folder containing the optimized molecule was indicated via the *file name* checkbox at the bottom of the browser. The molecule was selected from its folder and *all files* (\*) selected. By clicking on the *open* option also at the bottom of the browser, optimized molecule was imported unto the interface of Spartan 14 software. The properties of the molecule were then accessed by selecting *display* → *properties* options on menu bar prompting the propping up a window shown in Figure 3.5. The properties of the molecule were then accessed via the *molecule*, *QSAR*, *thermodynamic* and *acidity/basicity* menus of the window by selecting appropriate menu. The same procedures apply to all molecules in the data set.



**Figure 3.5: Spartan' 14 Molecular properties dialog**















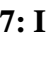
The Material studio software was launched by double clicking the Material studio icon to create its interface shown in Figure 3.6. On the interface, Selecting File | New... from the menu bar open the New Document dialog. Then Study Table was Selected.SD file was imported which contains both the structural and experimental data required. Edit | Insert From... from the menu bar was selected.




**Figure 3.6: Material studio interface**

The Structures folder was browsed and Corrosion.sd file was double-clicked. The structures are inserted into the first column of the study table. The second column contain corrosion inhibition data for the imported molecules as presented in Figure 3.7.

Column A in the study table was selected. Clicking on the column heading cell provides an easy way to select all of the data in the column.

	Structures	%E					
1	 am1.	50					
2	 am2.	59					
3	 am3.	63					
4	 am4.	47					
5	 am5.	80					
6	 am6.	52					
7	 am7.	39					
8	 am8.	73					
9	 am9.	53					
10	 am10.	51					
11	 am11.	87					
12	 am12.	75					
13	 am13.	67					
14	 am14.	34					
15	 am15.	43					

**Figure 3.7: Imported corrosion inhibitors with their inhibition efficiencies**

The Models button  on the QSAR Models toolbar was clicked to open the models dialog. The models dialog is the key component for managing models. A model in QSAR is a process that takes a set of inputs and provides a set of outputs. At this point in a typical QSAR study to calculate descriptors. These are models which take a single structure as an input and provide a single number or group of closely related numbers as outputs. QSAR simplifies this task by providing a variety of models which calculate a diverse set of descriptors. These can be browsed using the models dialog. The Models dialog should now

look like the one shown in Figure 3.8. The descriptors to be computed was selected and the Run button on the models dialog was clicked. This launches a job to calculate the selected Descriptors and add the results to the study table. The Job Explorer will also open, allowing you to monitor the status of the QSAR Models job. Once the job is complete, a Job Completed dialog is displayed.

	A	B	C	D	E	F	G	H	I	J	K
	Structures	%E									
1	am1.	50									
2	am2.	59									
3	am3.	63									
4	am4.	47									
5	am5.	80									
6	am6.	52									
7	am7.	39									
8	am8.	73									
9	am9.	53									
10	am10.	51									
11	am11.	87									
12	am12.	75									
13	am13.	67									
14	am14.	34									
15	am15.	43									
	am16.	77.40000000									

Output	Category	Model	Class	Engine
Atomic charges	Charges	DMol3 Periodic	simulation	DMol3
Density of states	Density of sta...	DMol3 Periodic	simulation	DMol3
Rotatable bonds	Structural	Fast Descriptors	descriptor	Fast Descriptors
Hydrogen bond donor	Structural	Fast Descriptors	descriptor	Fast Descriptors
Hydrogen bond acceptor	Structural	Fast Descriptors	descriptor	Fast Descriptors
Chiral centers	Structural	Fast Descriptors	descriptor	Fast Descriptors
AlogP	Thermodynamic	Fast Descriptors	descriptor	Fast Descriptors
AlogP98	Thermodynamic	Fast Descriptors	descriptor	Fast Descriptors
Molecular refractivity	Thermodynamic	Fast Descriptors	descriptor	Fast Descriptors
Molecular flexibility	Topological	Fast Descriptors	descriptor	Fast Descriptors
Balaban indices	Topological	Fast Descriptors	descriptor	Fast Descriptors
Wiener index	Topological	Fast Descriptors	descriptor	Fast Descriptors
Zagreb index	Topological	Fast Descriptors	descriptor	Fast Descriptors
Kappa indices	Topological	Fast Descriptors	descriptor	Fast Descriptors
Subgraph counts	Topological	Fast Descriptors	descriptor	Fast Descriptors
Chi indices	Topological	Fast Descriptors	descriptor	Fast Descriptors
Valence modified chi indices	Topological	Fast Descriptors	descriptor	Fast Descriptors
Information content	Information	Fast Descriptors	descriptor	Fast Descriptors
E-state keys	E-state keys	Fast Descriptors	descriptor	Fast Descriptors
Structure	Structure	Forcite Energetics	simulation	Forcite
Total energy	Energies	Forcite Energetics	simulation	Forcite

Run Run Later Help

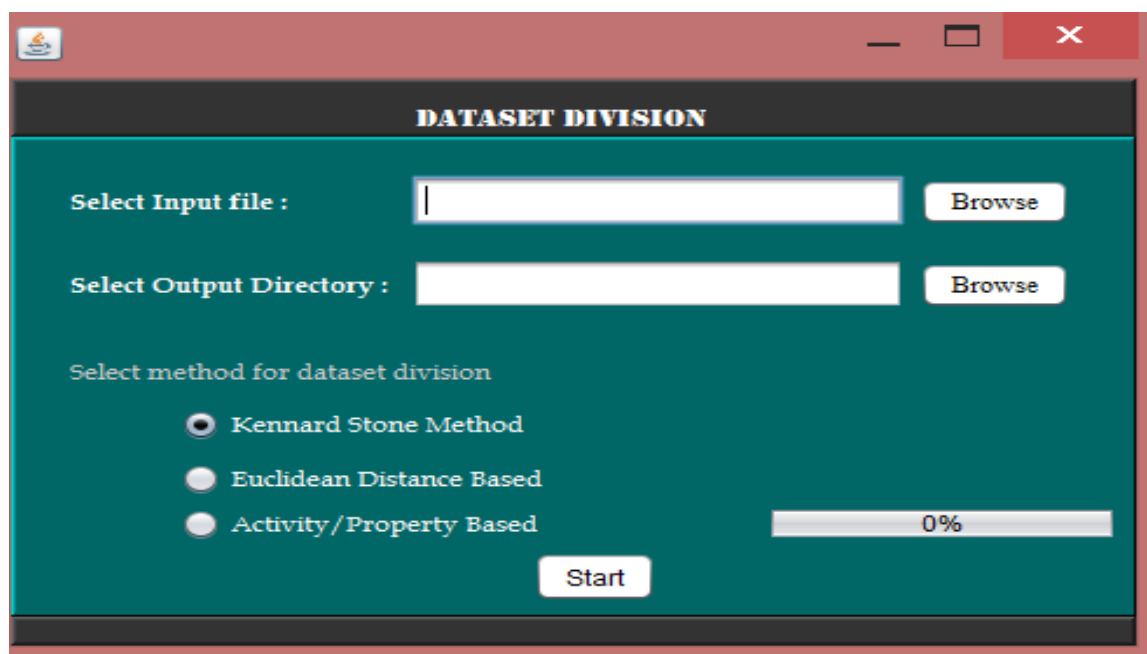
### **Figure 3.8. Models dialog for selecting descriptors to be computed**

#### 3.3.2 Training and test sets

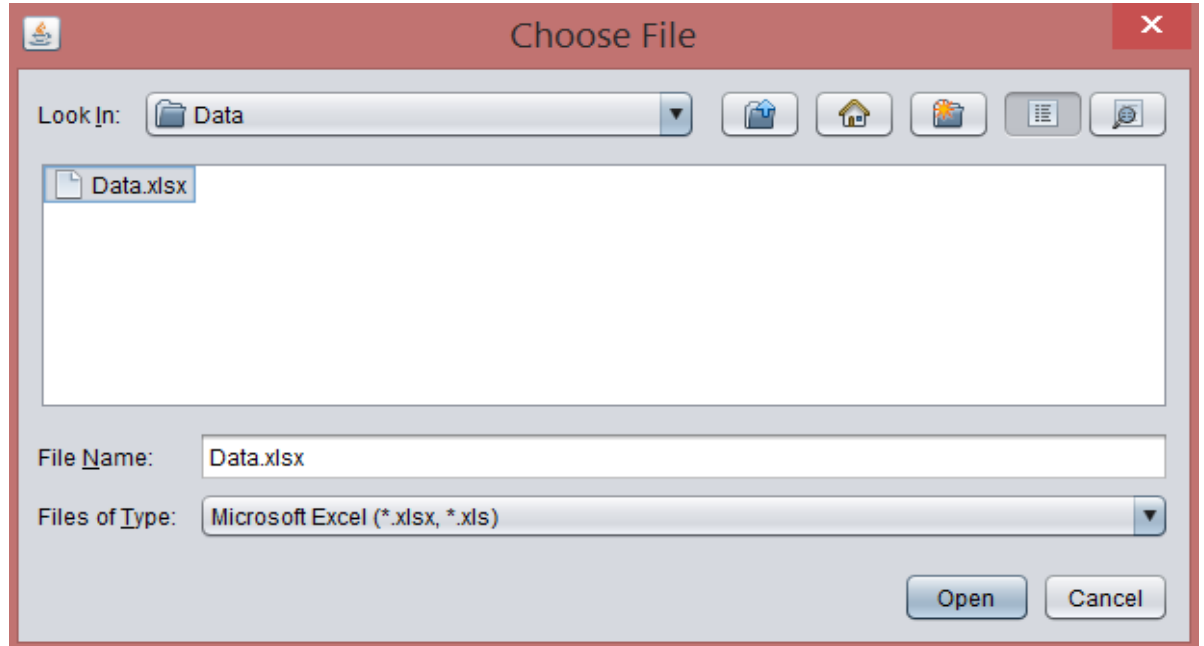
In order to obtain validated QSAR models, the descriptors (1D-3D) generated from the Spartan 14 and Material studio soft wares were divided into training (70%) and test (30%) sets. The training set was used to generate the model, while the test set were used for the external validation of the model. In this study, the division was performed using the Kennard-Stone algorithm (Kennard and Stone, 1969).

The procedures deployed in dividing the datasets into training and test sets using dataset Division GUI 1.2 program are highlighted thus: dataset Division GUI 1.2 program was launched by double-clicking on the icon on the desktop of the laptop as shown in Figure 3.9. By clicking on Select Input file (Browse), a dialog box appeared. Choose file name saved in the data folder were entered in the check box provided and open option button were clicked. By clicking on browse option at right side of the interface corresponding to the icon 'select input file' at the left side of the software, the choose file dialog box where the file containing the data set was imported into the software as shown in Figure 3.10. Moreover, select output directory (Browse) in the dialog box was clicked, save dialog box file name (e.g. Inhibitors) was written in the file name box and the save button was clicked (see Figure 3.11). By clicking on the start bottom, input dialog box appeared as in Figure 3.12. Percent of training set compounds (70% in this case) while the rest 30% for the test set, OK bottom was clicked. The result of the calculation was provided

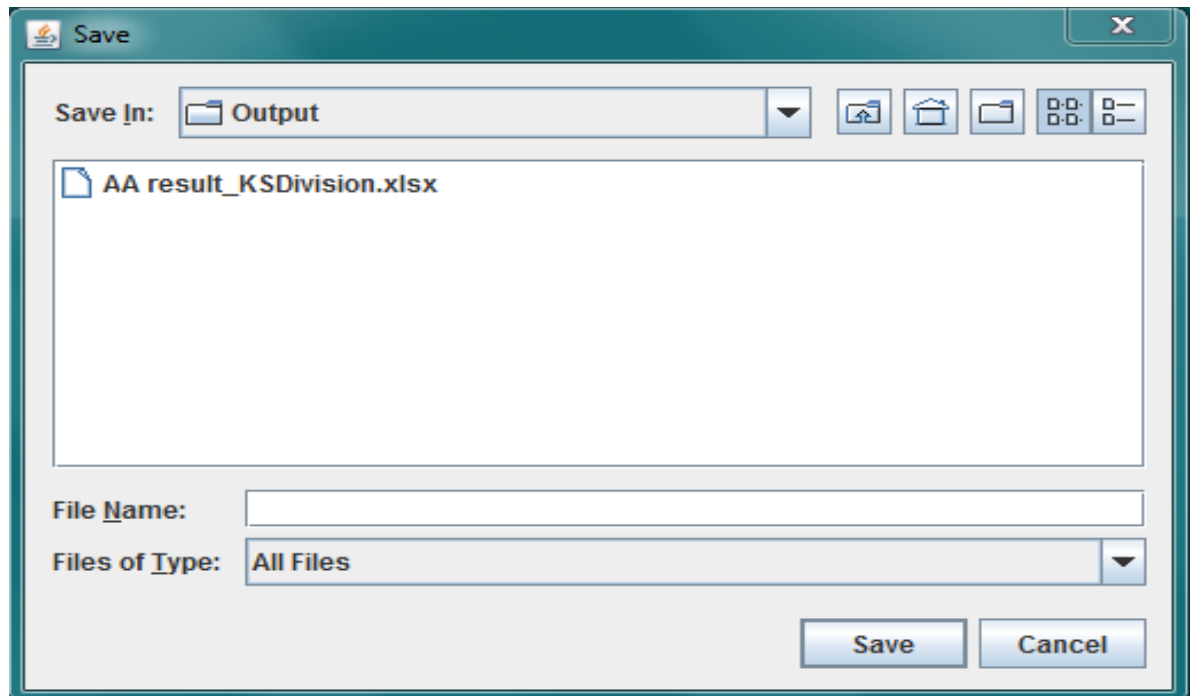
as Training and Test sets as showed in figure 3.13 and 3.14 respectively in the data set division excel folder output.



**Figure 3.9: Dataset Division software.**



**Figure 3.10: Dataset Division software.**



**Figure 3.11: "Save file" dialog box**

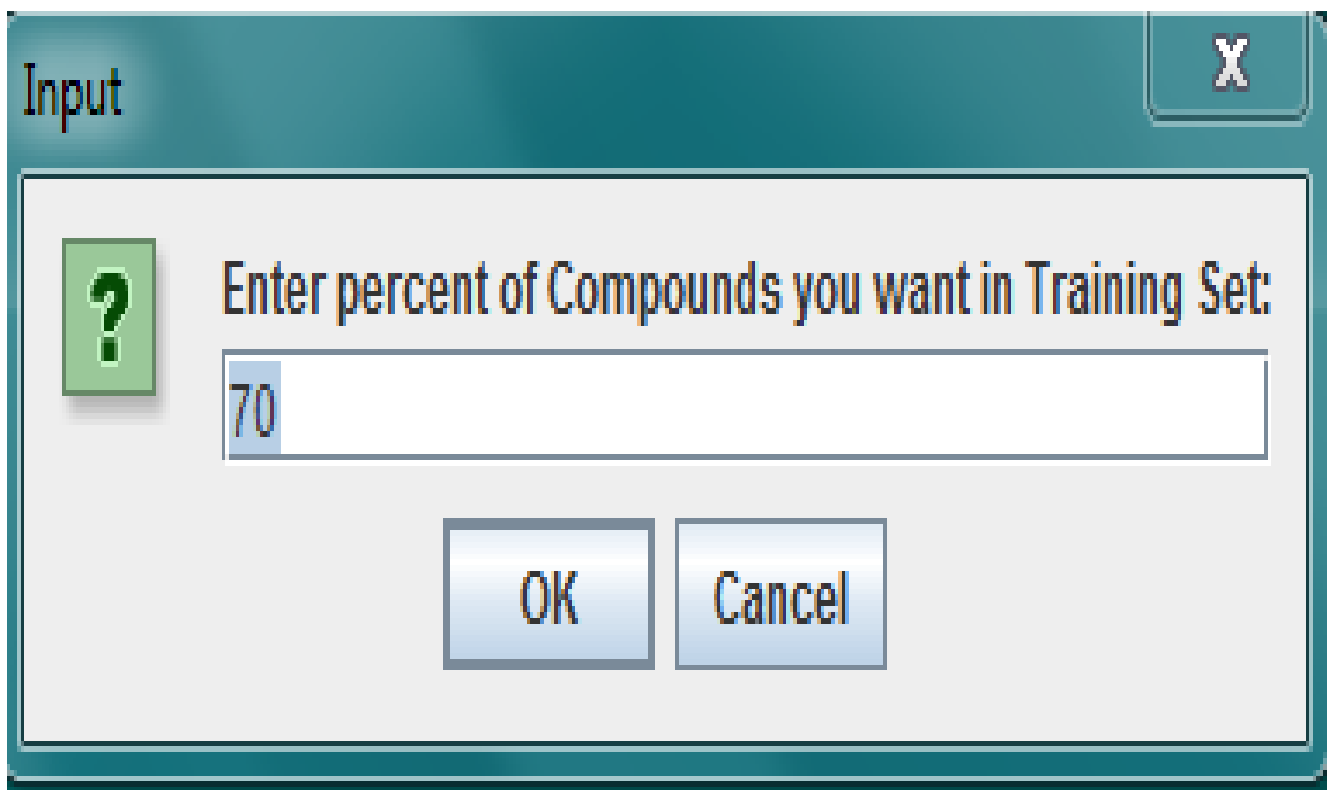


Figure 3.12: Dialog box for imputing the percent of the training set

	A	B	C	D	E	F	G	H	I	J	K	L	M
1	Inhibitors	%IE	E HOMO(e	Dipole Mo	E LUMO	Log P	PSA	Polarizabil	DE	n	b	H	w
2	2	86.8	-5.45	3.75	0.1	-0.86	45.877	51.07	5.55	2.775	0.36036	-2.675	9.92843
3	3	88.8	-5.83	2.26	-0.36	0.35	20.673	51.65	5.47	2.735	0.365631	-3.095	13.09932
4	4	97.8	-5.96	3.76	-0.42	0.5	8.938	58.71	5.54	2.77	0.361011	-3.19	14.0939
5	5	98.2	-5.81	3.56	-0.33	1.81	8.799	67	5.48	2.74	0.364964	-3.07	12.91211
6	6	76.3	-5.89	3.5	-0.22	-0.55	20.545	51.69	5.67	2.835	0.352734	-3.055	13.22956
7	7	71.2	-5.87	4.83	-1.37	1.04	26.881	56.79	4.5	2.25	0.444444	-3.62	14.74245
8	8	69.4	-6.01	2.9	-0.31	-1.63	46.047	52.57	5.7	2.85	0.350877	-3.16	14.22948
9	9	60.1	-5.74	2.21	0	-0.22	40.697	50.75	5.74	2.87	0.348432	-2.87	11.81995
10	11	68.4	-6.55	4.66	-0.2	0.68	51.387	47.68	6.35	3.175	0.314961	-3.375	18.08262
11	12	88.8	-5.93	40.3	-0.9	2.05	48.772	54.78	5.03	2.515	0.397614	-3.415	14.66525
12	13	60.2	-5.86	4.63	0.57	0.74	59.211	47.49	6.43	3.215	0.311042	-2.645	11.24611
13	14	38.1	-6.21	3.64	0.7	-0.42	59.186	45.97	6.91	3.455	0.289436	-2.755	13.11177
14	15	93.1	-6.59	3.38	-1.04	0.39	64.9	62.51	5.55	2.775	0.36036	-3.815	20.19399
15	16	95.6	-6.63	3.85	-1.07	-0.14	64.847	62.89	5.56	2.78	0.359712	-3.85	20.60328
16	20	90.2	-6.32	3.99	-0.9	0.57	64.727	64.02	5.42	2.71	0.369004	-3.61	17.6585
17	22	95	-6.39	2.01	-0.96	0.43	64.449	65.13	5.43	2.715	0.368324	-3.675	18.33389
18	23	95	-6.41	1.92	-0.98	0.7	64.56	65.49	5.43	2.715	0.368324	-3.695	18.53398
19	25	85.8	-5.93	5.59	-1.48	3.46	36.649	68.93	4.45	2.225	0.449438	-3.705	15.27132

**Figure 3.13: Output file format of Training set compound**

	A	B	C	D	E	F	G	H	I	J	K	L	M
1	Inhibitors	%IE	E HOMO(e	Dipole Mo	E LUMO	Log P	PSA	Polarizabil	DE	n	b	H	w
2	1	60	-6.07	3.44	-0.34	-0.81	20.62	50.19	5.73	2.865	0.34904	-3.205	14.71468
3	10	87.1	-6.59	4	-1.2	0.08	38.728	49.62	5.39	2.695	0.371058	-3.895	20.44296
4	17	95.9	-6.66	4.05	-1.1	0.26	64.744	63.62	5.56	2.78	0.359712	-3.88	20.92562
5	18	96.1	-6.66	4.03	-1.09	0.53	64.762	63.98	5.57	2.785	0.359066	-3.875	20.90926
6	19	92.9	-6.65	3.79	-1.08	1.06	64.814	64.54	5.57	2.785	0.359066	-3.865	20.80148
7	21	95	-6.38	3.13	-0.95	0.03	64.634	64.39	5.43	2.715	0.368324	-3.665	18.23425
8	24	94.9	-6.4	2.06	-1.09	1.23	64.582	66.08	5.31	2.655	0.376648	-3.745	18.61822
9	26	86.5	-6.04	4.58	-1.53	0.94	43.697	67.05	4.51	2.255	0.443459	-3.785	16.15282
10	27	93.1	-6	5.57	-1.51	-0.04	50.049	69.29	4.49	2.245	0.445434	-3.755	15.82728

**Figure 3.14: Output file format of Test set compound format**

### 3.3.3 QSAR Model Building

In Material studio software version 8, the regression analysis was performed on the experimentally determined inhibition efficiencies (dependent variables) and the generated descriptors (independent variables) using genetic function approximation (GFA) method in material studio software version 8. It is a distinctive characteristic of GFA that it could create a population of models rather than a single model and it has ability to perform better correlation analysis. GFA algorithm, selecting the basic functions genetically, developed better models than those made using stepwise regression methods. The models were estimated using the “lack of fit” (LOF), which was measured using a slight variation of the original Friedman formula, so that best model received the best fitness score (Wu *et al.*, 2015).

In Materials Studio version 8, LOF is measured using a slight variation of the original Friedman formula (Friedman, 1990). The revised formula equation (3.8) is:

$$\text{LOF} = \text{SSE} / \left(1 - \frac{c+dp}{M}\right)^2 \quad (3.8)$$

Where SSE is the sum of squares of errors, c is the number of terms in the model, other than the constant term, d is a user-defined smoothing parameter, p is the total number of descriptors contained in all model terms (ignoring the constant term) and M is the number of samples in the training set. Unlike the commonly used least squares measure, the LOF measure cannot always be reduced by adding more terms to the regression model. While the new term may reduce the SSE, it also increases the values of c and p, which tends to increase the LOF score. Thus, adding a new term may reduce the SSE, but actually increases the LOF score. By limiting the tendency to simply add more terms, the LOF measure resists over fitting better than the SSE measure (Khaled, 2011).

The GFA algorithm approach has a number of important advantages over other standard regression analysis techniques. It builds multiple models rather than a single model (Accelrys Inc., 2007). It automatically selects which features are to be used in the models and is better at discovering combinations of features that take advantage of correlations between multiple features (Khaled, 2008). GFA incorporates Friedman's lack-of-fit (LOF) error measure, which estimates the most appropriate number of features, resists over fitting, provides information not available from the standard regression analysis and allows control over the smoothness of fit. Also, it can use a larger variety of equation term types in the construction of its models.

### 3.3.4 Procedure involved in building GFA models

The Material studio software version 8 was launched from the desk top prompting a pop up of the windows (work space window and project window) shown in Figure 3.6. By selecting the options, create a new project → Ok on the propped up window, a file browser

appeared. Through the file name option on the browser, the name of the file was indicated and saved as project files (\*.stp) causing the appearance of full Material studio work space. By clicking the file → new project menus via the menu bar of the work space, a file browser propped up. Through the file name option checkbox of the browser, the file name of the new project was indicated and saved as project files (\*.stp). Through the file menu on the menu bar of the work space, study table was created by selecting new →study table → Ok options on a propped up document window shown in causing the appearance of the material studio study table shown in Figure 3.15. The descriptors (descriptors of the training set from section 3.2.6) with the corresponding inhibition efficiency (dependent variable/ %IE) were copied, pasted and highlighted unto the first column of material studio's Study table excel sheet interface as shown in Figure 3.15. In addition, all the molecular descriptors (independent variables) were copied and pasted unto the remaining column of material studio's Study table excel sheet interface (Figure 3.15). The options: Statistics → model building → genetic function approximations were selected.

A Genetic function approximation window shown in Figure 3.15 appeared at the top left corner of the workspace from where the boxes against the predictor variables (descriptors) were marked via the variable selection menu of the window, the Population and Generation were set to 1,000 and 2,000 respectively via the parameter menu. The number of top equations returned was set to 3, Mutation probability was set to 0.1, and the smoothing parameter was set to 0.5 in line with standard settings used in GFA – QSAR study. Equation length (expected number of descriptors in a model) was adjusted by clicking equation data → Initial or Maximum equation length menus on GFA window. The predictor variables (descriptors) was selected as in Figure 3.15. By clicking the Ok button,

calculations commenced immediately. The models were scored based on the one with the least Friedman's LOF.

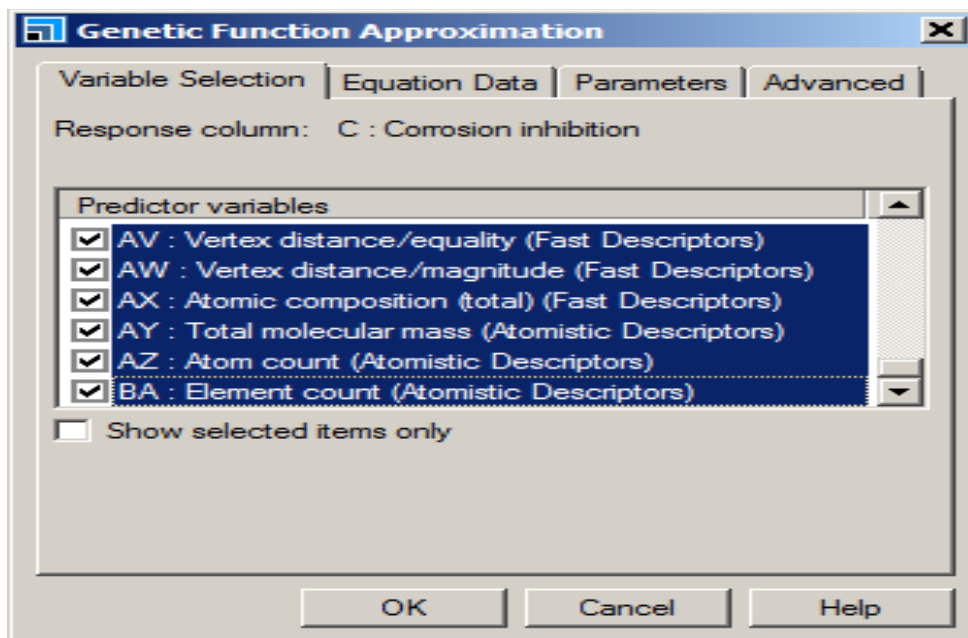
The screenshot displays the 'Genetic Function Approximation' dialog box in the top-left corner, which is used for configuring a genetic algorithm. The dialog has four tabs: 'Variable Selection', 'Equation Data', 'Parameters', and 'Advanced'. The 'Parameters' tab is active, showing the following settings:

- Population: 1000
- Maximum generations: 5000
- Number of top equations returned: 3
- Mutation probability: 0.1
- Scoring: Friedman LOF (selected in a dropdown menu)
- Scaled LOF smoothness parameter: 0.5

Below the dialog box, a portion of a data table is visible. The table has columns labeled B through G, representing different properties. The rows are numbered 8 through 15. The values in the table are as follows:

	B	C	D	E	F	G
8	60.10000000	-5.74000000	2.21000000	0	-0.22000000	40.69700000
9	68.40000000	-6.55000000	4.66000000	-0.20000000	0.68000000	51.38700000
10	88.80000000	-5.93000000	40.30000000	-0.90000000	2.05000000	48.77200000
11	60.20000000	-5.86000000	4.63000000	0.57000000	0.74000000	59.21100000
12	38.10000000	-6.21000000	3.64000000	0.70000000	-0.42000000	59.18600000
13	93.10000000	-6.59000000	3.38000000	-1.04000000	0.39000000	64.90000000
14	95.60000000	-6.63000000	3.85000000	-1.07000000	-0.14000000	64.84700000
15	90.20000000	-6.32000000	3.99000000	-0.90000000	0.57000000	64.72700000
	95	-6.39000000	2.01000000	-0.96000000	0.43000000	64.44900000

Figure 3.15: Material Studio's Study table window interface- B



**Figure 3.16: Generic Function Approximation dialog, Variable Selection tab**

### 3.3.5 Evaluation of the QSAR model

The predictive ability of the best model was evaluated by internal and external validation parameters. The validation parameters were compared with the minimum recommended standards for a generally acceptable QSAR model (Veeramy *et al.*, 2011). The various internal and external validation parameter used in this study are presented as:

- i.  $R^2$  (the square of the correlation coefficient): Describes the fraction of the total variation attributed to the model. The closer the value of  $R^2$  is to 1.0, the better the regression and equation explains the Y variable.  $R^2$  is the most commonly used internal validation indicator and is expressed as in equation (3.9):

$$R^2 = 1 - \frac{\sum(Y_{obs} - Y_{pred})^2}{\sum(Y_{obs} - Y_{training})^2} \quad (3.9)$$

Where,  $Y_{obs}$ ;  $Y_{pred}$ ;  $Y_{training}$  are the experimental property, the predicted property and the mean experimental property of the samples in the training set, respectively. The minimum recommended value for this parameter was shown in Table 3.4(Wu *et al.*, 2015).

- ii. Adjusted  $R^2$  ( $R^2_{adj}$ ):  $R^2$  value varies directly with the increase in number of regressors i.e. descriptors, thus,  $R^2$  cannot be a useful measure for the goodness of model fit. Therefore,  $R^2$  is adjusted for the number of explanatory variables in the model. The adjusted  $R^2$  is defined as in equation (3.10):

$$R^2_{adj} = 1 - (1 - R^2) \frac{N-1}{N-P-1} = \frac{(N-1)R^2 - P}{N-P+1} \quad (3.10)$$

Where  $p$  = number of independent variables in the model and  $N$  = sample size(Abdulfatai *et al.*, 2017). The minimum recommended value for this parameter was shown in Table 3.4

- iii.  $Q^2$  (Leave one out cross validation coefficient): The LOO cross validated coefficient ( $Q^2$ ) is given by equation (3.11):

$$Q^2 = 1 - \frac{\sum(Y_p - Y)^2}{\sum(Y - Y_m)^2} \quad (3.11)$$

Where  $Y_p$  and  $Y$  represent the predicted and observed activity respectively of the training set and  $Y_m$  the mean activity value of the training set. The minimum recommended value for this parameter was shown in Table 3.4 (Brandon and Aline, 2015).

- iv.  $R^2_{\text{pred}}$ :  $R^2_{\text{pred}}$  is termed the predictive  $R^2$  of a development model and is an important parameter that is used to test the external predictive ability of a QSAR model. The predicted  $R^2$  value is calculated by equation (3.12):

$$Pred. R^2 = 1 - \frac{\sum [Y_{(te)} - Y_{Pred (te)}]^2}{\sum [Y_{(te)} - Y_m (tr)]^2} \quad (3.12)$$

$Y_{\text{pred}}(\text{test})$  and  $Y(\text{test})$  indicate predicted and observed activity values respectively of the test set compounds and  $Y_m(\text{tr})$  indicates mean activity value of the training set. The minimum recommended value for this parameter was shown in Table 3.4 (Veerasingam *et al.*, 2011).

**Table 3.4 Minimum recommended values of validated parameters for generally acceptable QSAR**

Symbol	Name	Value
$R^2$	Coefficient of determination	$\geq 0.6$
$P_{(95\%)}$	Confidence interval at 95% confidence level	$< 0.05$
$Q^2$	Cross validation coefficient	$< 0.5$
$R^2_{\text{ext}}$	Coefficient of determination for external test set	$\geq 0.6$

$R^2 - Q^2$  Difference between  $R^2$  and  $Q^2$   $\leq 0.3$

$N_{\text{ext. test set}}$  Minimum number of external test set  $\geq 5$

---

### 3.3.6 Applicability Domain

The applicability domain (AD) of QSAR model was used to verify the prediction reliability, identify the problematic compounds and predict the compounds with an acceptable activity that fall within the domain. The most common methods used for determination of the AD of QSAR models have been described by Grammatica that used the leverage values for each compound (Tropsha *et al.*, 2003). The leverage approach allows the determination of the position of a new chemical in the QSAR model, i.e. whether a new chemical will lie within the structural model domain or outside of it. The leverage approach along with the Williams Plot is used to determine the applicability domain in all QSAR models. To construct the William Plot, the leverage  $h_i$  for each chemical compound in which QSAR model was used to predict its property was calculated according to the equation (3.13):

$$h_i = x_i(X^T X)^{-1}x_i^T \quad (3.13)$$

Where,  $x$  refers to the descriptor vector of the considered compound and  $X$  Represents the descriptor matrix derived from the training set descriptor values. The warning leverage ( $h^*$ ) was determined as in equation (3.14):

$$h^* = \frac{3(p+1)}{N} \quad (3.14)$$

Where  $N$  is the number of training compounds and  $p$  is the number of descriptors in the model.

The generation of the williams plot; The original descriptor matrix was copied and pasted on an already opened excel worksheet, this was done by clicking on the right button on the key pad of the laptop to bring up a drop down menu from which the paste special menu was selected (see Figure 3.17). Dialogue box was displayed. Transpose option was checked and ok was selected to give the transpose of the original matrix. The transposed version ( $X_{Tr} = m \times n$ ) of the original descriptor matrix ( $X_{tr}$ ) generated was multiplied by the original matrix  $X_{tr}$  by highlighting a section of the worksheet such that the number of columns on the highlighted section is equal to the number of columns of the original matrix and the number of rows equal to that of the number of rows of the transposed matrix. In the first cell of the highlighted section `MMULT (array1, array2)` was typed. Array 1 is the range of cells covered by the original matrix on the worksheet e.g. E2:G5, while array 2 is the range of cells covered by the transpose. These ranges were selected by highlighting the sections covered by the respective matrices on the work sheet matrix as shown in Figure 3.12. The `CTRL+ SHIFT + ENTER` was pressed to give the result of the multiplication. The inverse of the result of the multiplication was found by first highlighting a section on the worksheet where the result of the operation will be displayed, the number of rows and columns on this section should be the same as that of the matrix whose inverse is being sought. In the first cell of the highlighted section (Figure 3.17) `=Transpose (Range)` was typed, 'range' is the range of cells covered by the matrix to be transposed e.g. A2:G5. `CTRL+ SHIFT + ENTER` was pressed to give the result of the operation. The original  $X_{tr}$ , the inverse  $(X_{Tr} X_{tr})^{-1}$  and the transposed matrix  $X_T$  were multiplied using the same

multiplication steps described above to obtain an  $n \times n$  symmetric matrix (hat matrix) whose diagonal elements (leverages) describe the distance of each training set compound to the structural centroid of the model, the leverages were extracted from the hat matrix. The calculation of the hat matrix as well as the extraction of the diagonal elements (leverages) for the test/external validation set compound entering the model, was performed as for the training set described above with slight modification. A transposed version ( $X_{Te/ext}^T = m \times n$ ) of the original descriptor matrix of test data  $X_{Te/ext}$  was generated, a clone version of the inverse matrix solved above for the training data  $(X_{Tr}^T X_{Tr})^{-1}$  was also generated, the original  $X_{Te/ext}$ , the inverse  $(X_{Tr}^T X_{Tr})^{-1}$  and the transposed matrix  $X_{Te/ext}^T$  were multiplied. The leverages from both training and test sets hat matrices were plotted as a function of the standardized residuals to obtain the Williams plot.

	A	B	C	D	E	F	G	H	I	J	K	L	M	N	O	P	Q	R	S
1																			
2					E HOMO	e Dipole Mo	E LUMO	Log P											
3		1	-5.45	3.75	0.1	-0.86													
4		1	-5.83	2.26	-0.36	0.35													
5		1	-5.96	3.76	-0.42	0.5			1	1	1	1	1	1	1	1	1	1	1
6		1	-5.81	3.56	-0.33	1.81			-5.45	-5.83	-5.96	-5.81	-5.89	-5.87	-6.01	-5.74	-6.55	-5.93	-5.86
7		1	-5.89	3.5	-0.22	-0.55			3.75	2.26	3.76	3.56	3.5	4.83	2.9	2.21	4.66	40.3	4.63
8		1	-5.87	4.83	-1.37	1.04			0.1	-0.36	-0.42	-0.33	-0.22	-1.37	-0.31	0	-0.2	-0.9	0.57
9		1	-6.01	2.9	-0.31	-1.63			-0.86	0.35	0.5	1.81	-0.55	1.04	-1.63	-0.22	0.68	2.05	0.74
10		1	-5.74	2.21	0	-0.22													
11		1	-6.55	4.66	-0.2	0.68													
12		1	-5.93	40.3	-0.9	2.05													
13		1	-5.86	4.63	0.57	0.74			=MMULT(										
14		1	-6.21	3.64	0.7	-0.42													
15		1	-6.59	3.38	-1.04	0.39													
16		1	-6.63	3.85	-1.07	-0.14													
17		1	-6.32	3.99	-0.9	0.57													
18		1	-6.39	2.01	-0.96	0.43													
19		1	-6.41	1.92	-0.98	0.7													
20		1	-5.93	5.59	-1.48	3.46													

Figure 3.17: Excel Worksheet for calculating leverages

### 3.4 Molecular Dynamics Simulation Methods

The molecular dynamics simulation was carried out to describe the interaction between the inhibitor molecules and the metallic surface. The adsorption locator module implemented in the Materials studio 8.0 software from Accelrys was used for the simulation. The inhibitor molecules were modeled and optimized using the Condensed-phase Optimized Molecular Potentials for Atomistic Simulation Studies (COMPASS) force field. COMPASS is a robust and well-developed force field that was derived based on fitting against a wide range of experimental data for organic and inorganic compounds

(Wymyslowski *et al.*, 2014). This informs its suitability for treating metal and non-metal containing systems. The whole system was performed at 298K controlled by the Andersen thermostat with fixed number-volume-energy (microcanonical) ensemble, with a time step of 1.0 fs, simulation time of 50ps. The MD simulation was carried out in a simulation box (24.82 Å × 24.82 Å × 45.27 Å) with periodic boundary conditions. The box includes a Fe slab, an acid solution layer, and an inhibitor molecule. For the iron surface, Fe (110) surface was selected as the studied surface for that Fe (110) was density packed surface and was the most stable (Khaled, 2008). The iron crystal contained ten layers and seven layers near the bottom were frozen. The density of the acid solution layer was set at 1.0 gcm<sup>-3</sup>. The adsorption and binding energy values in solution was calculated by equation (3.15) and (3.16) respectively (Saha and Banerjee, 2015).

$$E_{adsorption} = E_{Total} - (E_{Fe_{surface}} + E_{solution} + E_{Inhibitor}) \quad (3.15)$$

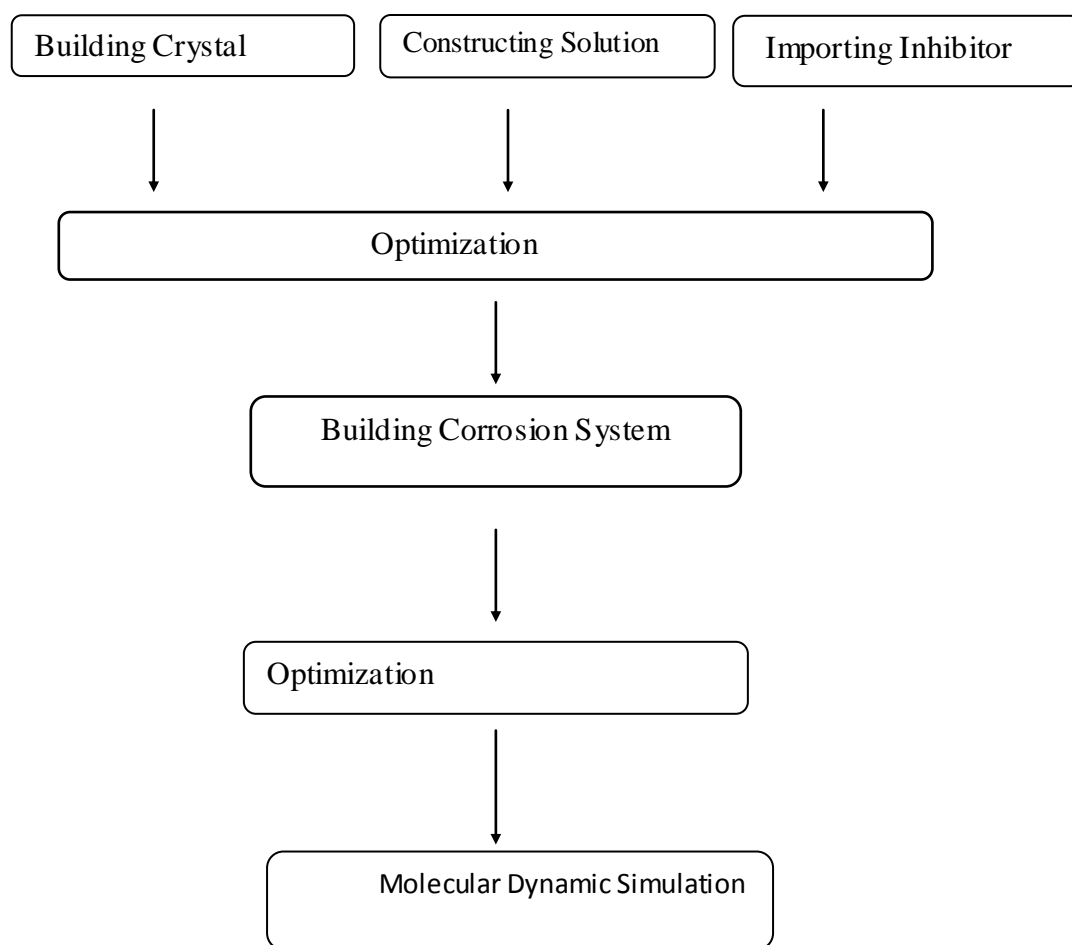
$$E_{adsorption} = E_{binding} \quad (3.16)$$

The various steps are presented in a flowchart in Figure. 3.18

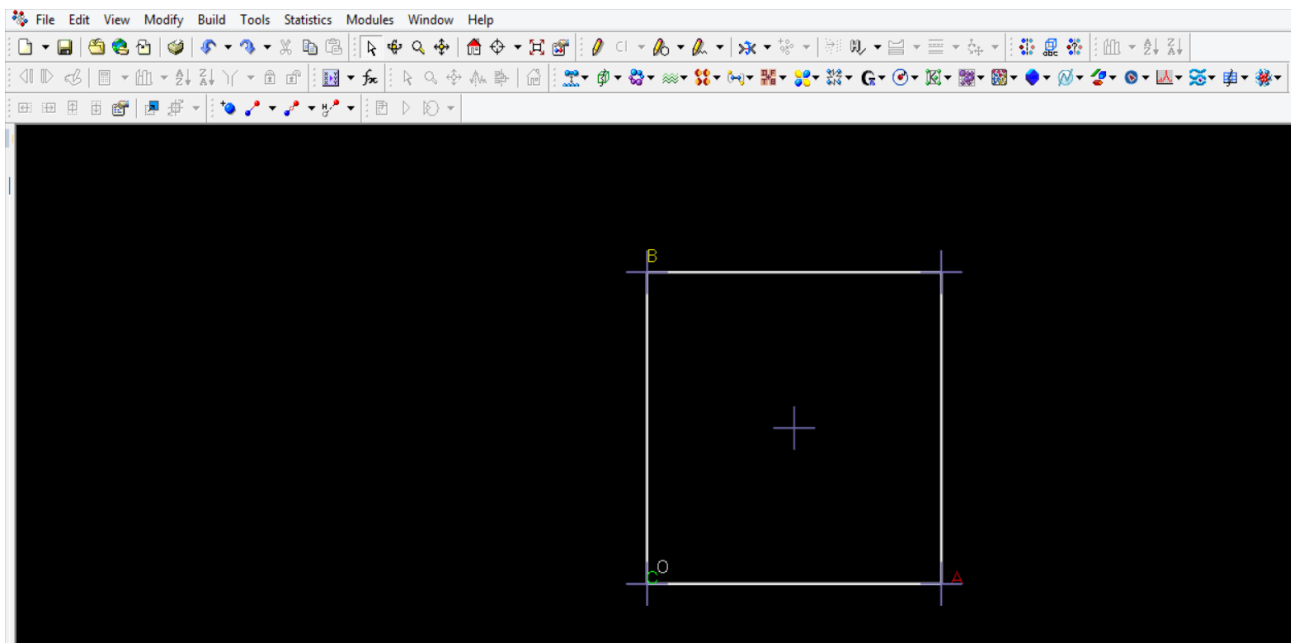
### 3.4.1 Building Steel Crystal

Materials Studio has an extensive structure library containing many common metals surface (Fe-crystal was used, since the steel used in the wet laboratory experiment is has 98.3 percent weight of Fe). In the Project Explorer, the root project icon was right-clicked and Import... from the shortcut menu was selected to open the Import Document dialog. Navigating to Structures\pure metals and Fe was imported as shown in Figure 3.19. Before

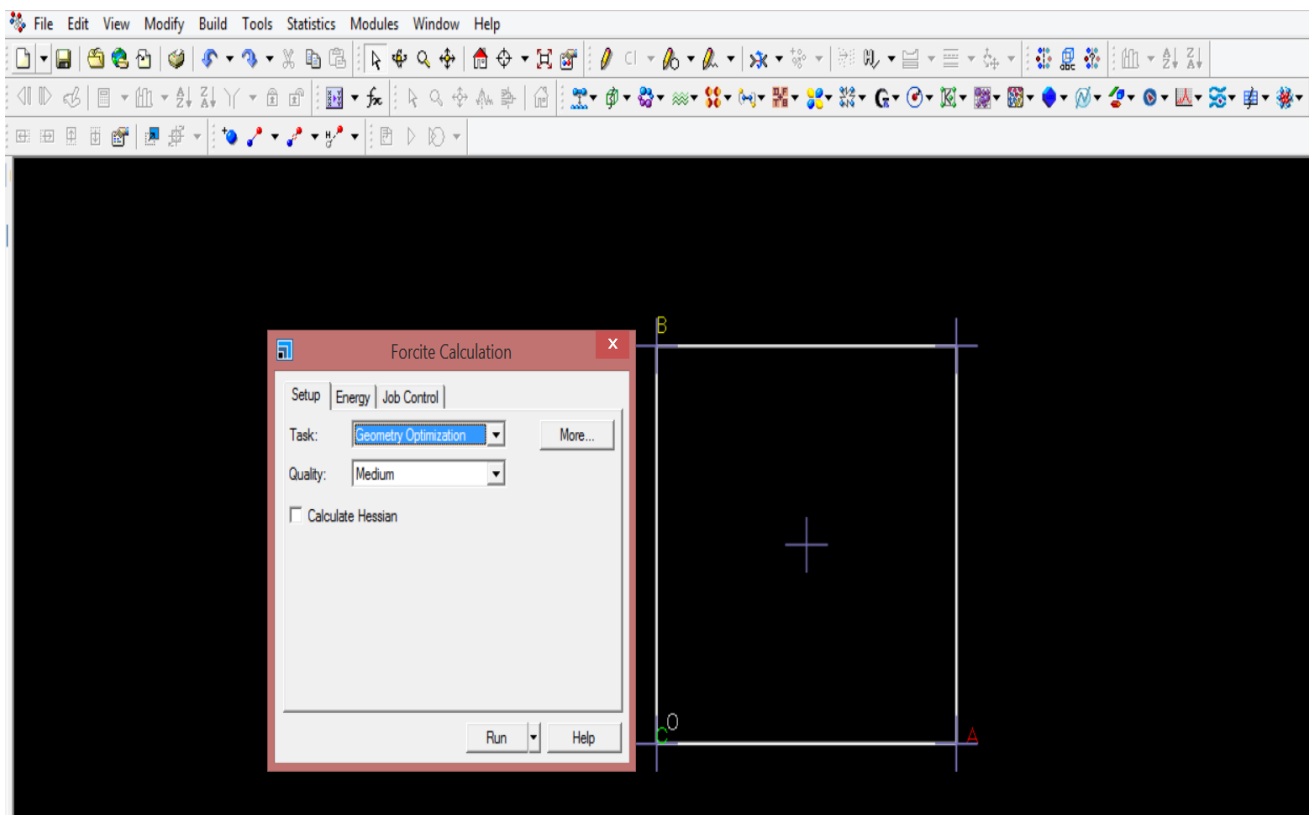
cleaving the surface, the crystal structure was optimized. On the Setup tab on the Forcite Calculation dialog the More... button was clicked to open the Forcite Geometry Optimization dialog (Figure 3.20). The Optimize cell checkbox was checked and the dialog was closed. As this is a 3D periodic structure, one can choose to either optimize the cell and atomic positions or just the atomic positions. In this case, the cell and atomic positions was choosed and optimized. Forcite optimize the structure within the symmetry constraints. The Run button was clicked and the Forcite Calculation dialog was closed.



**Figure 3.18: MD Simulation methodology flowchart**

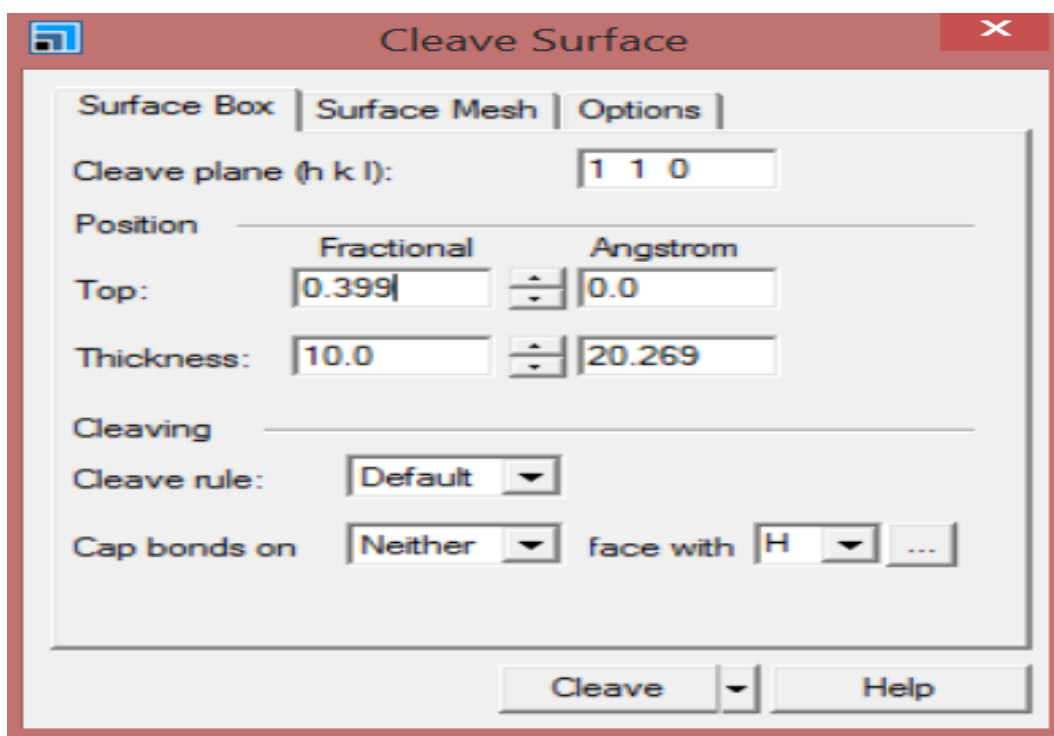


**Figure 3.19: Imported Fe unit cell structure**



**Figure 3.20: Forcite Geometry Optimization dialog**

Now to cleave the crystal to show the active 110 surface. The optimized Fe.xsd document was opened. Build | Surfaces | Cleave Surface was chosen to open the Cleave Surface dialog. The Cleave plane was Changed to 1 1 0 and the TAB key pressed. In Fe.xsd, a blue box is displayed with the cleave plane displayed as a solid blue line and the depth displayed by dotted lines. The spinners was used to increase the Fractional Top to 0.399 and the Fractional Thickness to 10.0. The Cleave button was clicked and the dialog closed as presented in Figure 3.21. The display was changed by Right clicking on the back ground of 3D atomistic view and Display Style selected. *Ball and stick* was Selected and Stick radius = 0.1 and Ball radius = 0.4 values was set respectively as seen in Figure 3.22.




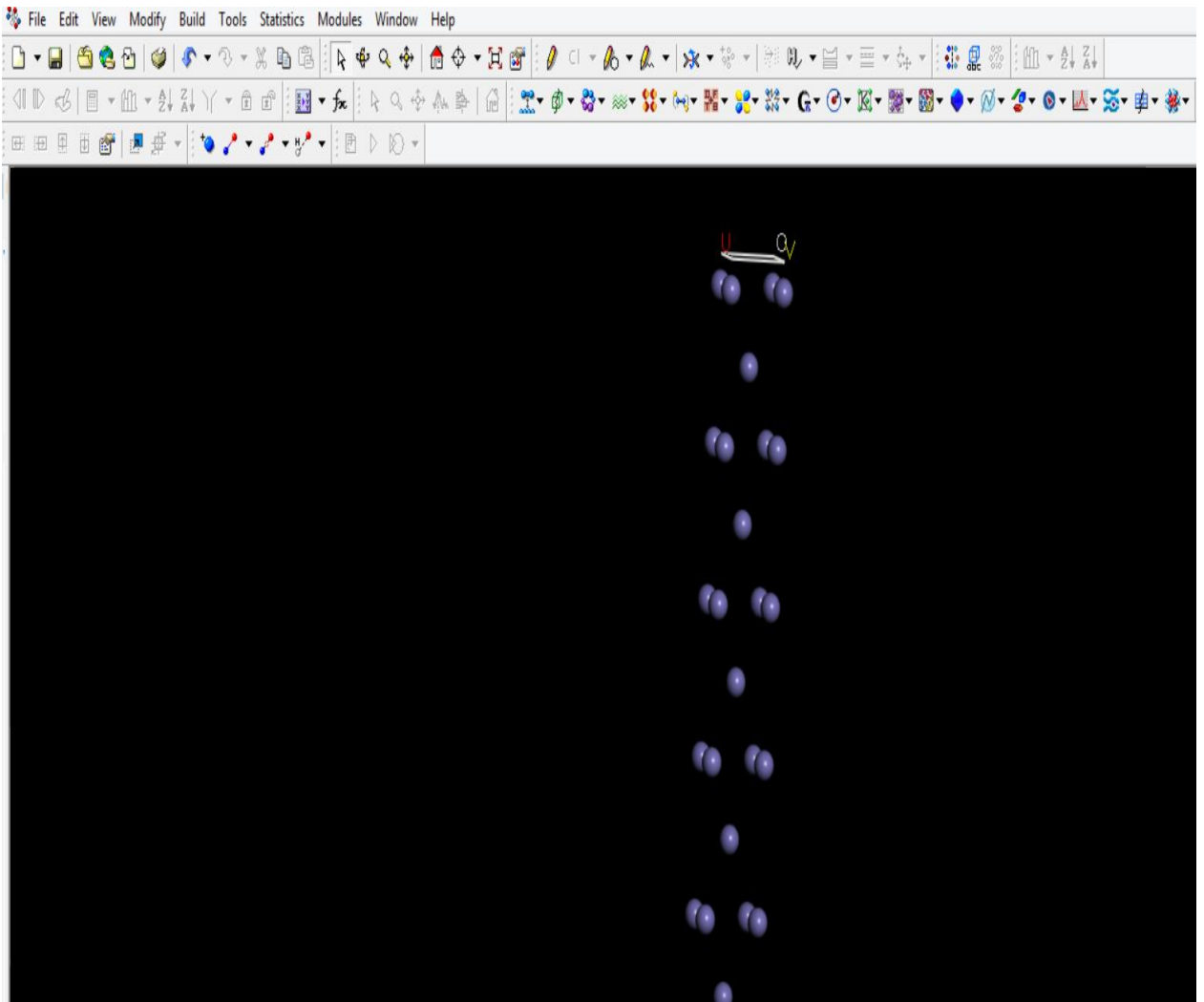
**Figure 3.21: Cleave Surface dialog**

To build symmetry super cell. **Build | Symmetry | Supercell** from the menu bar was Selected to open the **Supercell** dialog. The **Supercell range was** increased to **10** for **U** and **V** (Figure 3.23). The **Create Supercell** button was clicked and the dialog window closed. The built Fe-crystal Symmetry Supercell are shown in Figure 3.24

To build the vacuum slab. **Build| Crystals| Build Vacuum Slab**. Was Selected in **Build Vacuum Slab Crystal** dialog and then the vacuum thickness was changed from 10.00 Å to 25.00 Å and the **Build** button was clicked (see Figure 3.25). The built Fe-crystal in a Vacuum Slab are shown in Figure 3.26

#### 3.4.2 Solution Construction

All solvents molecules such as water, hydroxonium ion and chloride ion models were drawn in Materials Studio using the available drawing tools. While each system was unique, they all shared similar construction, optimization and modeling methods. To begin construction a new 3D atomistic file was created and named Solution. Drawing tools allowed for the placement of both single atoms and bonds. Helpful tools in this process included the add hydrogen and clean tools. The add-hydrogen tool adds hydrogen atoms to all atoms based on missing atoms and the Lewis theory of bonding as shown in Figure 3.27. After building, they were then placed into an amorphous cell using the Amorphous Cell module in Materials Studio by selecting Amorphous Cell  from the Modules toolbar and choose Calculation or select **Modules | Amorphous Cell | Calculation** from the menu bar. This opens the Amorphous Cell Calculation dialog (see Figure 3.28 and Figure 3.29).



**Figure 3.22: Cleaved Fe-Surface inform of Ball and stick display style**

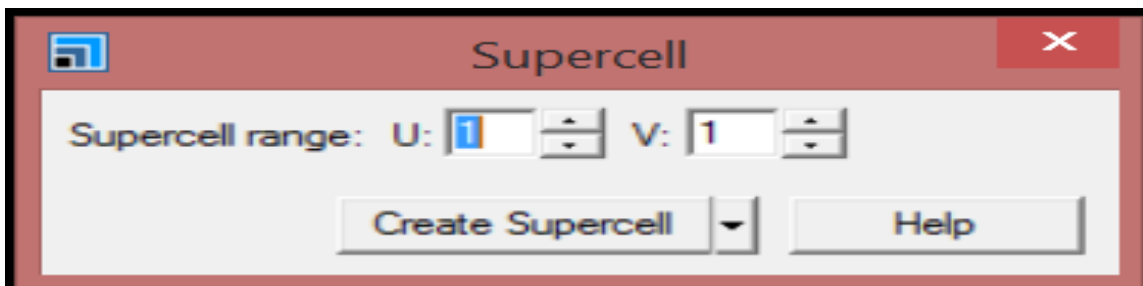
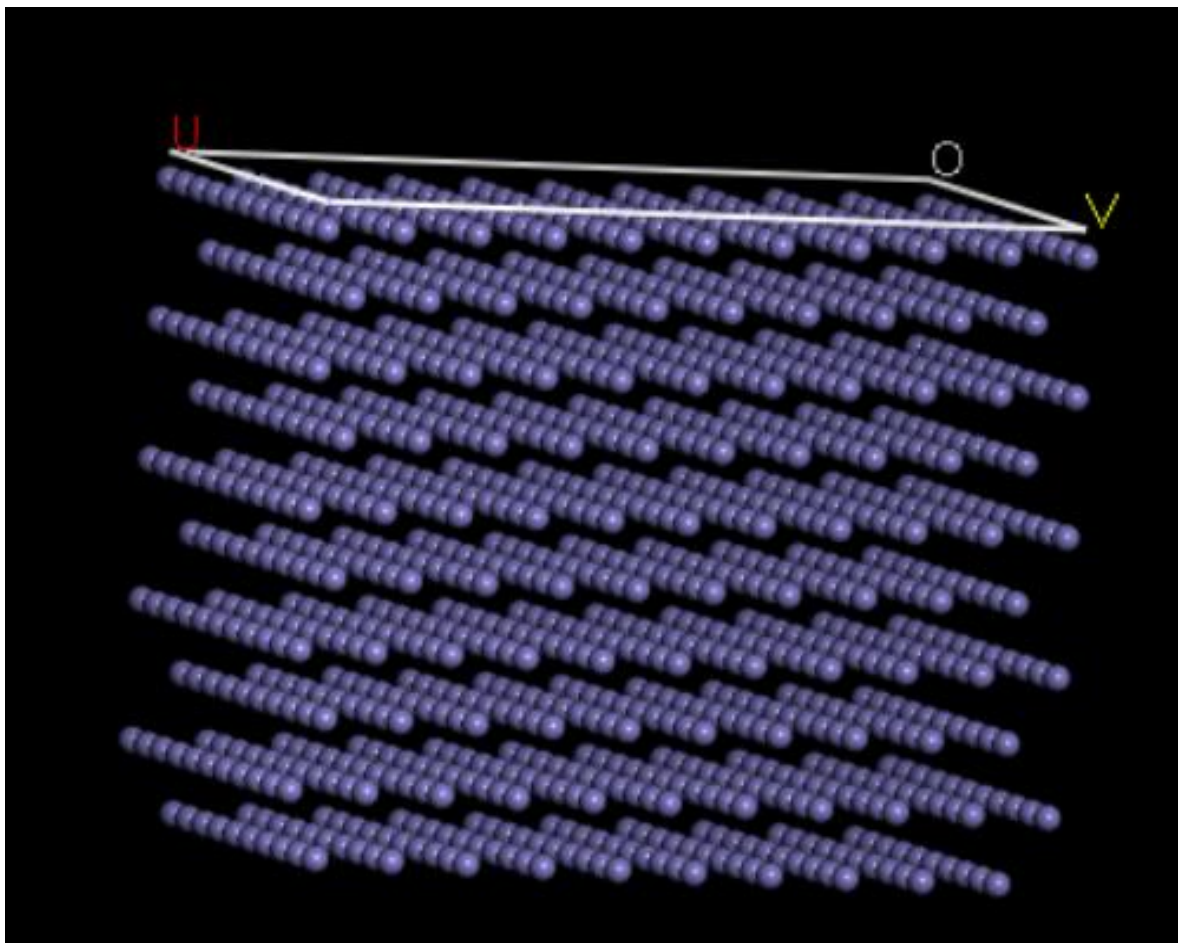
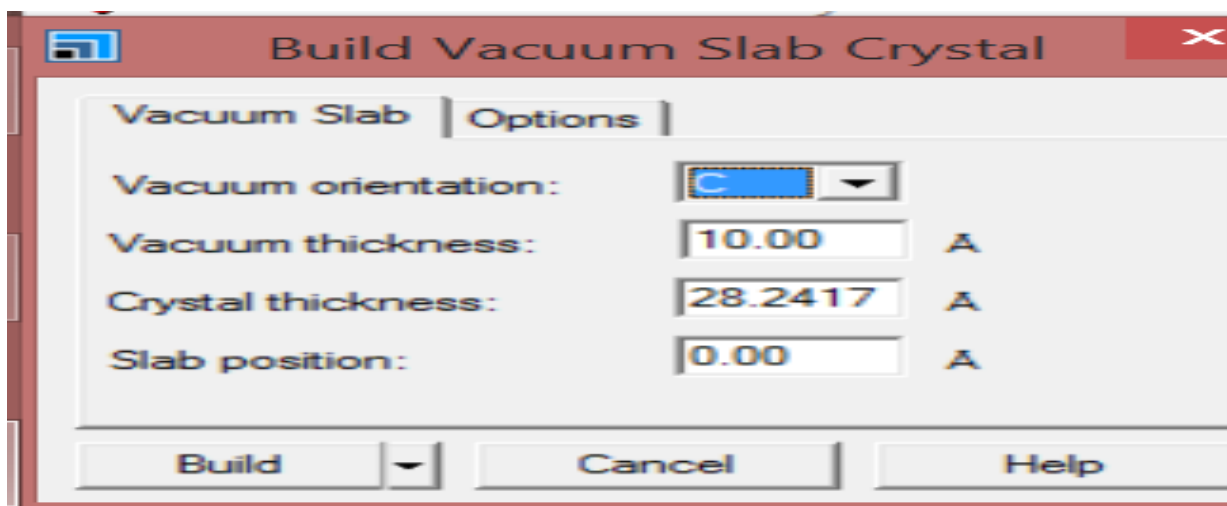


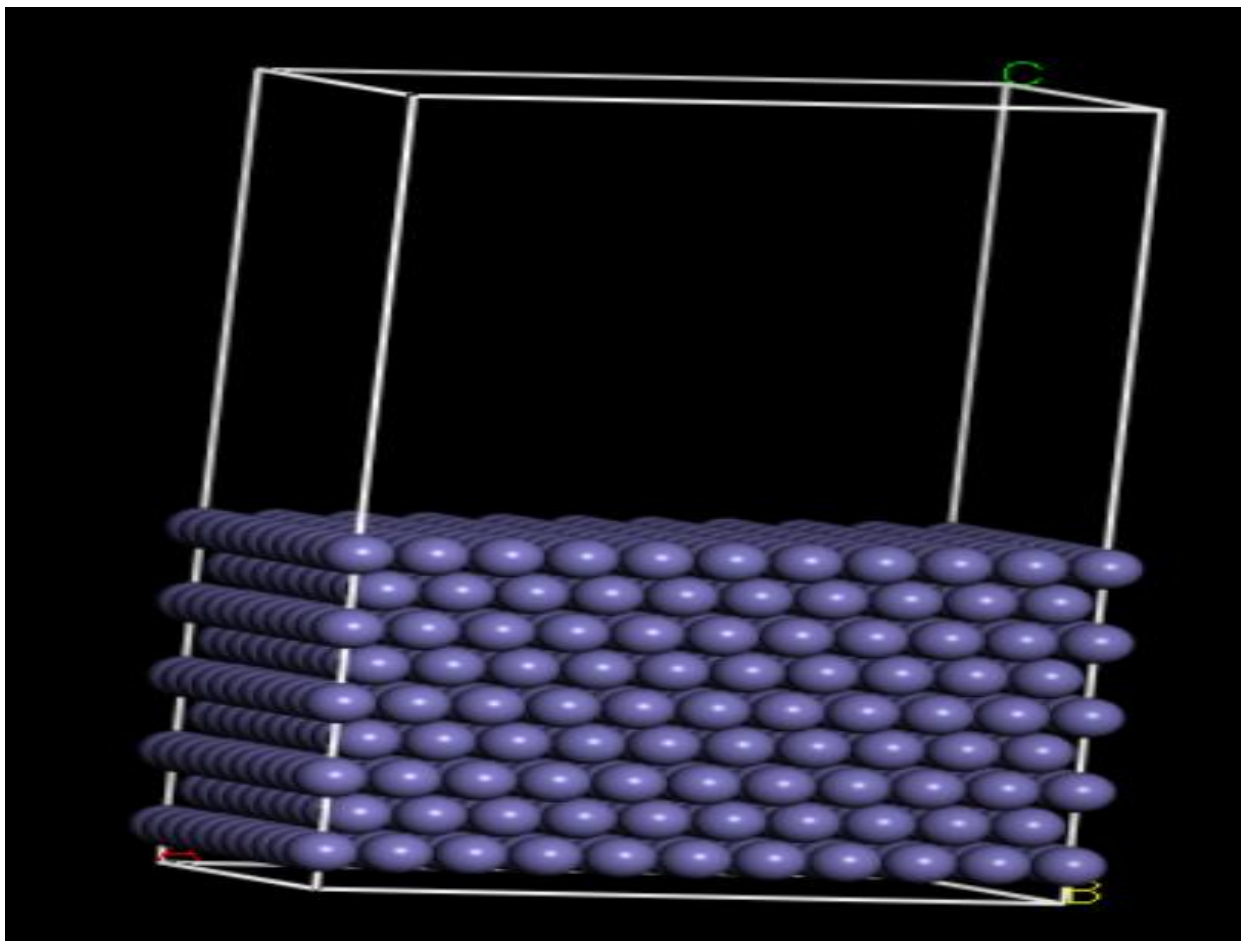
Figure 3.23: Symmetry Supercell calculation dialog, setup tab



**Figure 3.24: Build Fe-crystal Symmetry Supercell**



**Figure 3.25: Build Vacuum Slab Crystal calculation dialog, setup tab**




**Figure 3.26: Built Fe-Crystal in a Vacuum Slab**

In the first method, the Construction task, predefined quantities solvent and counterions were used to construct a cell. The cells were set to have periodic boundary conditions to simulate a bulk substance. After construction the cell were set to have cubic structure which contains all the solvent molecules (Figure 3.30) and the geometry optimization was run.

#### 3.4.3 Importing inhibitor and Molecular optimization

3D atomistic document was created on the material studio interface and the chemical structure of the inhibitor drawn with chemDraw saved in mol (Figure 3.32) was imported.

Materials Studio was started and a 3D Atomistic Document was created. The chemical structure of the inhibitor molecule drawn with chemDraw saved in mol (Figure 3.32) was imported. The molecule was then optimized using a classical simulation tool. Classical simulation tools require a forcefield which describes the forces between atoms in terms of a sum of functions in the distances, angles, etc. between atoms of various types. The Forcite button  on the Modules toolbar was clicked and calculation from the dropdown list was selected. This opens the Forcite Calculation dialog (Figure 3.31). The Task was changed to Geometry Optimization. On the Energy tab the Forcefield was changed to COMPASS. COMPASS is a well validated forcefield with its own charges. Hence, when COMPASS was closed, the charges selection automatically changes to Forcefield assigned. The non-bond settings default to Atom based the Run button was clicked.

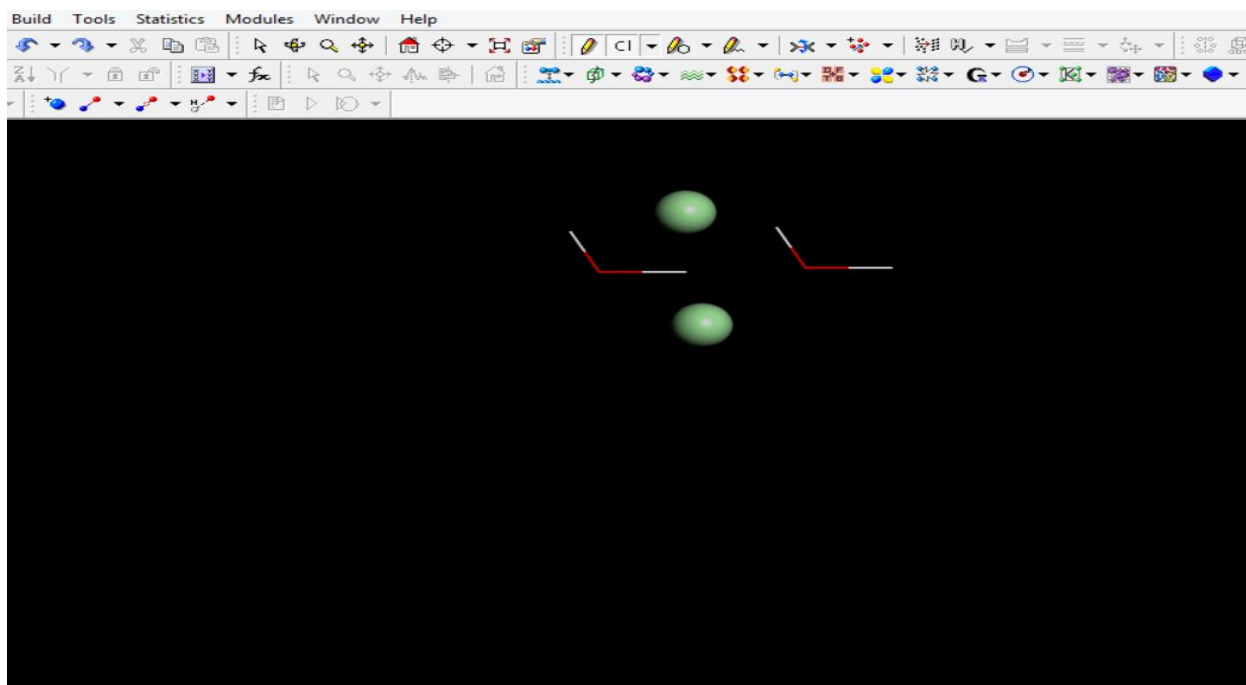


Figure 3.27: Material Studio 3D-atomistic interface for drawing molecules/ions/atoms

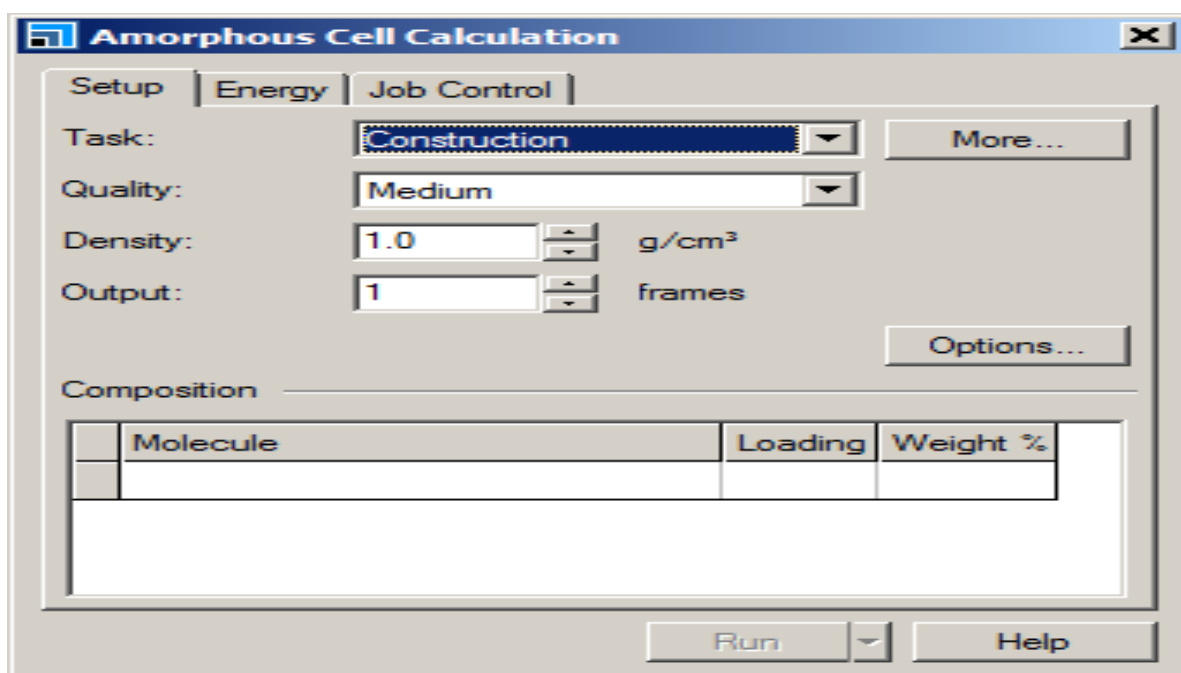
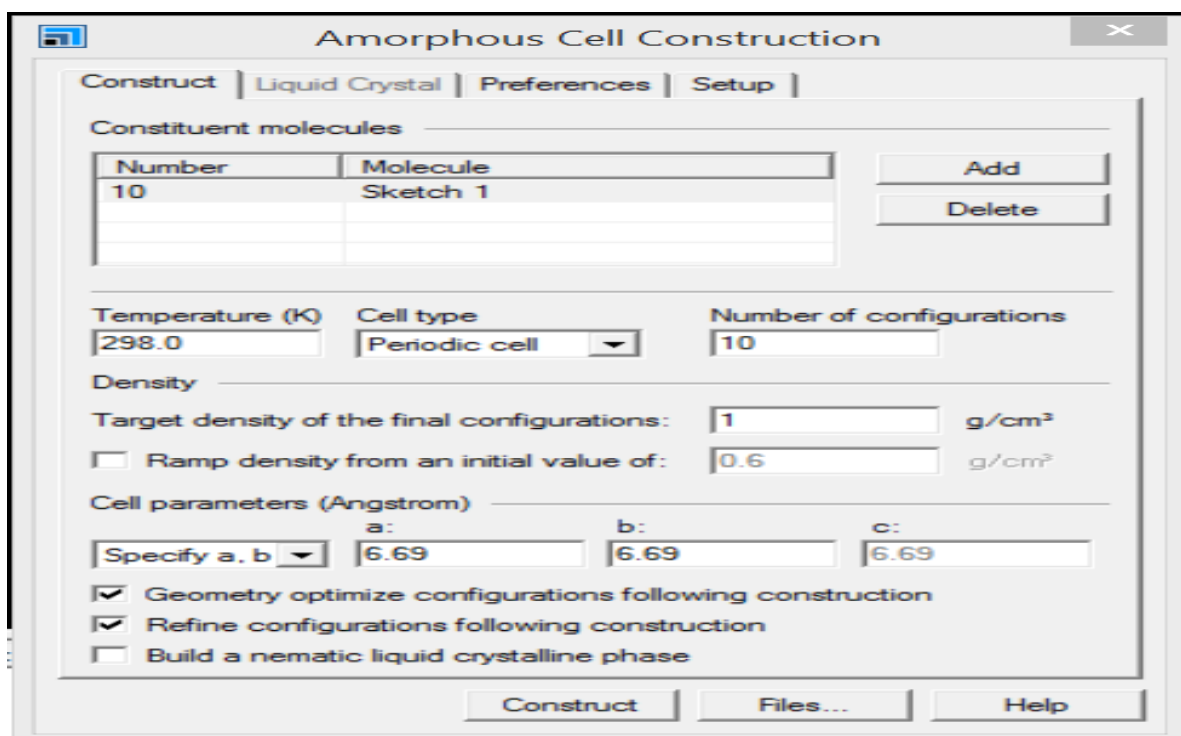
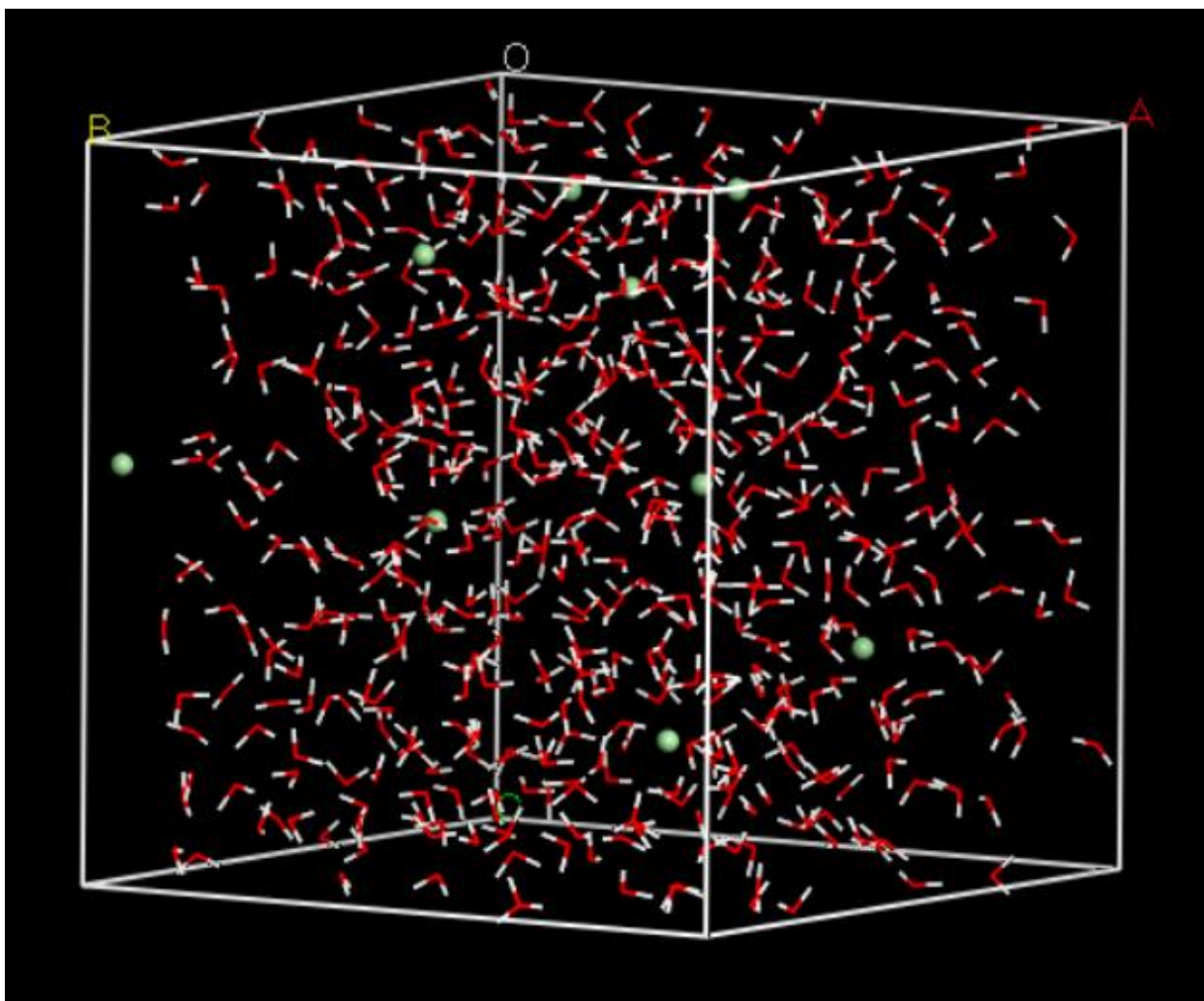


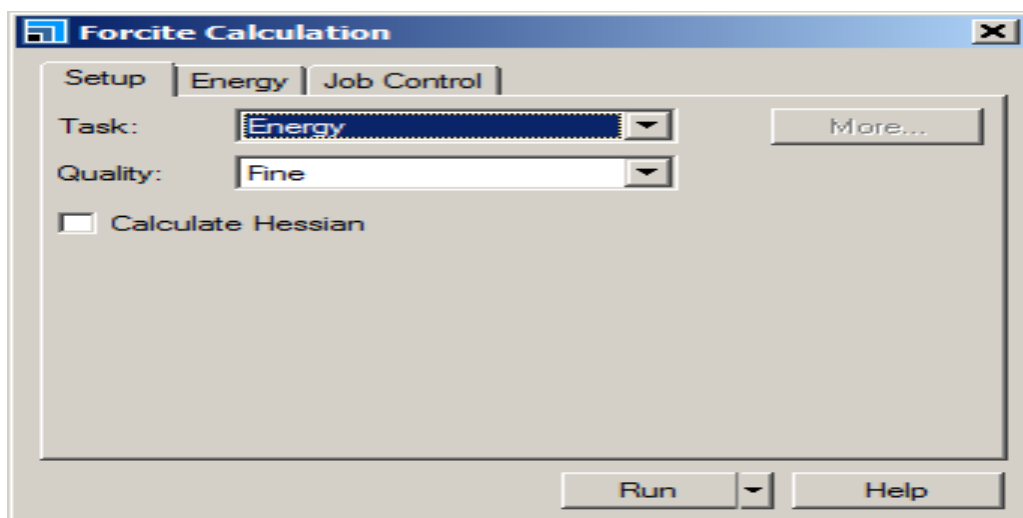
Figure 3.28: Amorphous Cell calculation dialog, setup tab



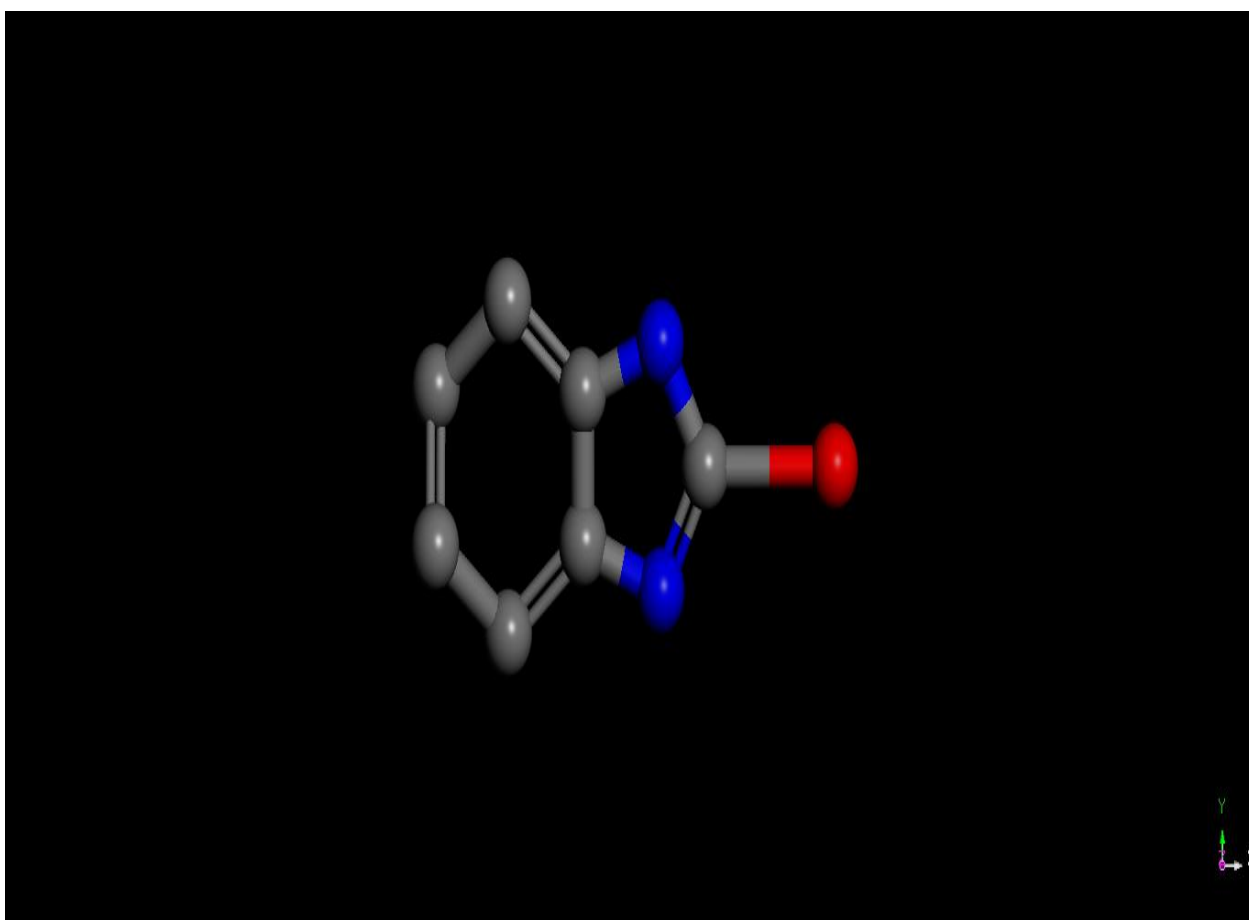
**Figure 3.29: Amorphous Cell construction dialog**



**Figure 3.30: solvent molecules**



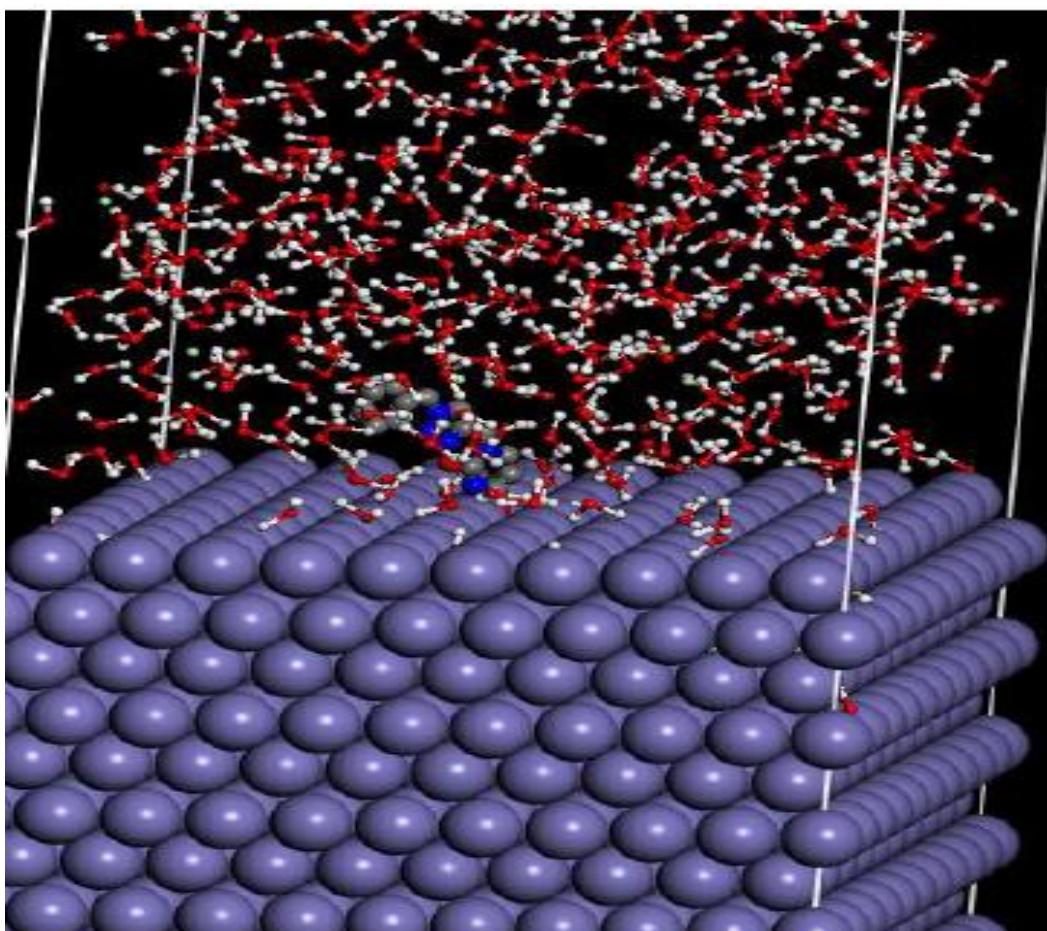
**Figure 3.31:** Forcite Calculation dialog, Setup tab



**Figure 3.32:** Imported inhibitor molecule

#### 3.4.4 Building corrosion system

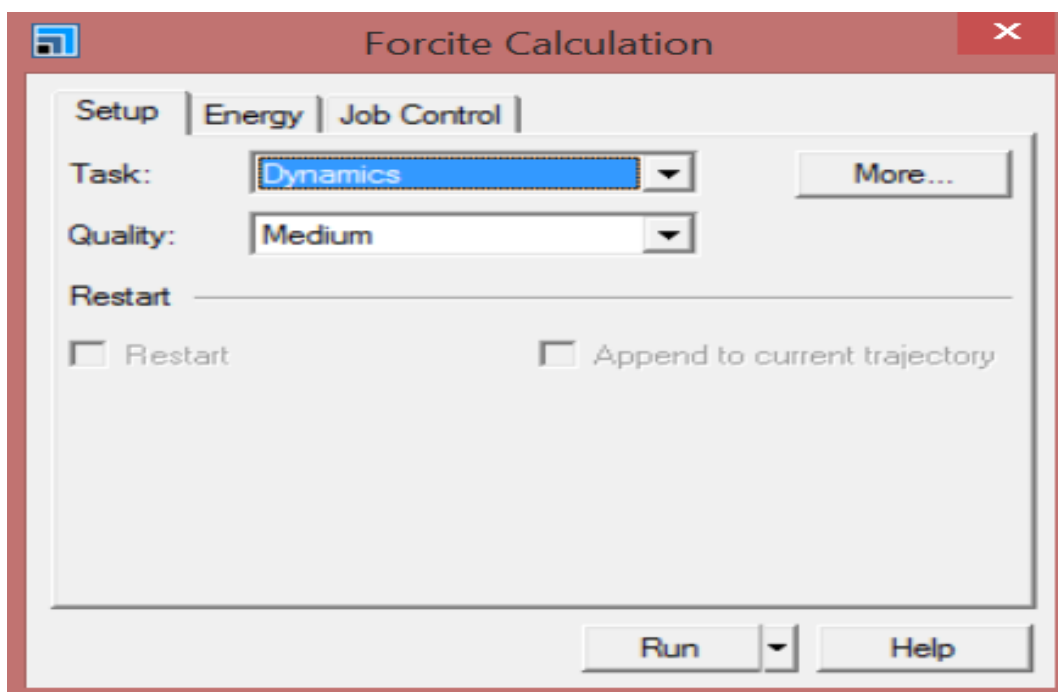
Before running the molecular dynamic simulation the solution and the inhibitor had to be placed on the steel surface. A slab containing solvent and inhibitor molecules was added to the Fe (1 1 0) surface by the “build layers” tool and a geometry optimization was performed. This was done to find the lowest possible starting energy. This optimization uses classical molecular mechanics compared to quantum mechanics for DFT. Geometry optimizations were started by going to the Forcite Calculation tab in the Forcite module and setting the task to “Geometry Optimization”.



**Figure 3.33: Built Corrosion system**

#### 3.4.5 Molecular dynamic simulation

Molecular dynamics simulations were started by going to the Forcite module, selecting Forcite Calculation and changing the task to “Dynamics” as in Figure 3.34. Additional parameters were set depending on the specific requirements of the simulation and the goals of the project. This gives access to the basic dynamic options. However, one will need to open the Dynamics options to set the temperature etc as shown in Figure 3.35. The More... button for Dynamics options was clicked. This opens the Forcite Dynamics dialog. The Temperature was set to 298 K. This temperature represents a trade-off between a system with too much kinetic energy, where the molecule desorbs from the surface, and a system with not enough kinetic energy for the molecule to move around the surface. 5000 steps was used to run the dynamics at 298K which give 50ps of simulation time. On the Forcite Calculation dialog, the Run button was clicked and the dialog was closed.



**Figure 3.34: Forcite Dynamics dialog**

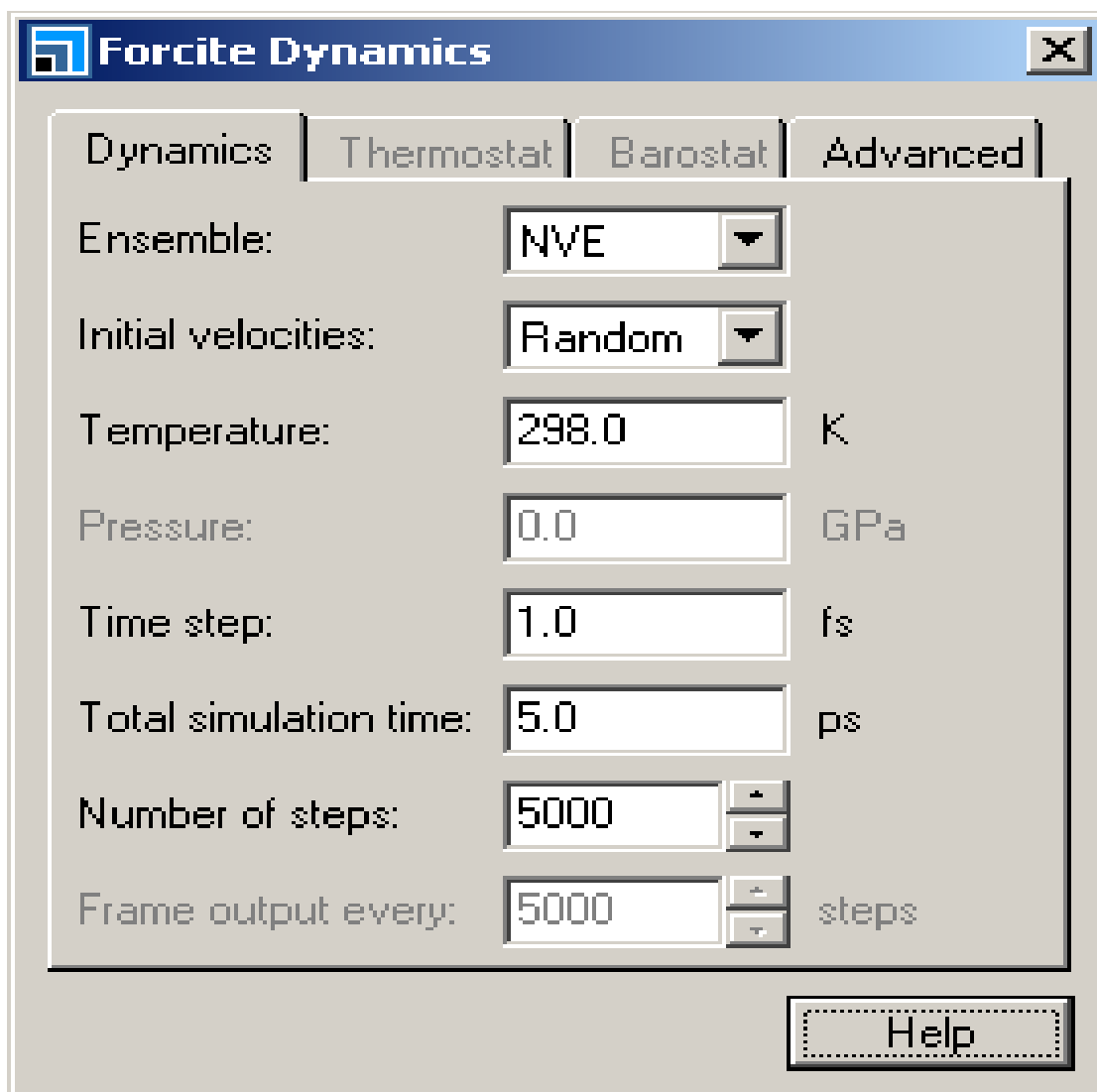


Figure 3.35: Forcite Dynamics dialog, Dynamics tab

## CHAPTER FOUR

### 4.0 RESULTS

#### 4.1 Quantum Chemical studies, GFA Derived models for %IE and molecular dynamics simulation studies of amino acids/analogous derivatives

To investigate the influence of the structure of the inhibitors (amino acids/analogous derivatives) on their inhibition efficiencies, quantum chemical parameters related to the structure were calculated at the B3LYP/6-311+G(d,p) level of theory. The results of quantum chemical parameters were listed in Table 4.1. The optimized molecular structures, HOMO and LUMO electronic density distributions of the first three inhibitors are shown in Table 4.2. Three QSAR models were developed and presented in scheme 4.1 as model (4.1, 4.2, and 4.3 respectively) on the basis of the training set out of which model 4.1 was chosen as the best model for predicting the %IE of the studied corrosion inhibitors based on statistical significance. Figure 4.1 shows a plot of the comparison of the experimental and predicted %IE inhibition efficiency (%IE) for both training and test sets inhibitors.

The external validation of the test set inhibitors showing the experimental and predicted %IEs with residuals for model 4.1 are presented in the Tables 4.3. The stability, reliability, and robustness of the generated model 4.1 were confirmed by predictive  $R^2$  (Table 4.4). The experimental predicted and residual %IE values for the training set of the developed model 4.1 are presented in Tables 4.5, while the applicability domain for Model 4.1 is presented in Figure 4.2. The adsorption of the studied inhibitor molecules on steel surface was simulated by modeling the interactions between the inhibitor molecules (AM-inhibitors) and Fe(110) crystal surface. The equilibrium configurations of the simulated systems are shown in Figure 4.3, while the relevant energy parameters of the systems are listed in Table 4.6.

**Table 4.1. Selected quantum chemical parameters for the studied inhibitors (Amino acids derives)**

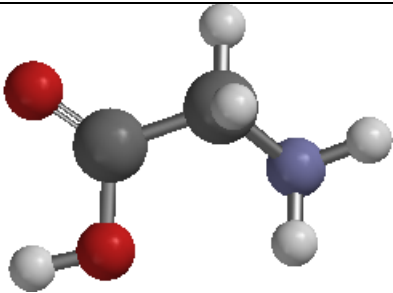
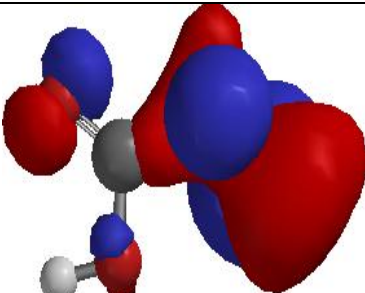
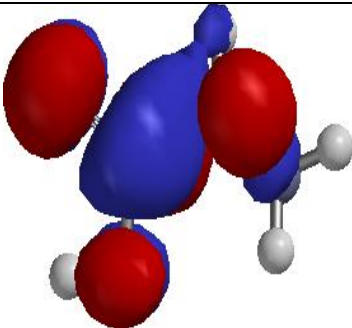
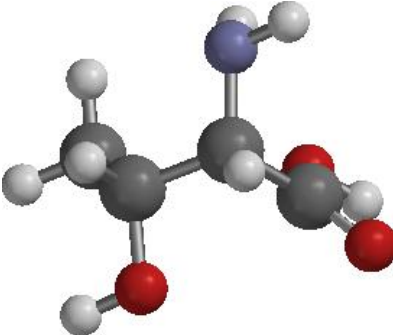
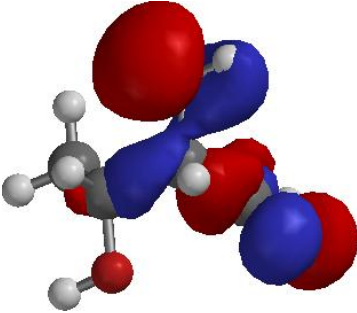
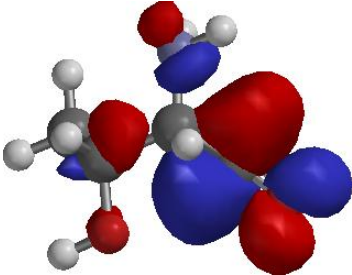
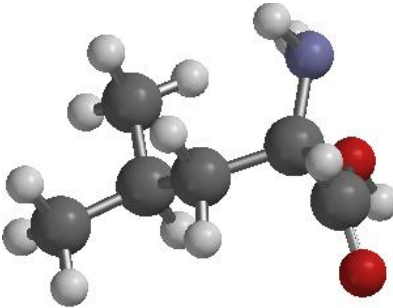
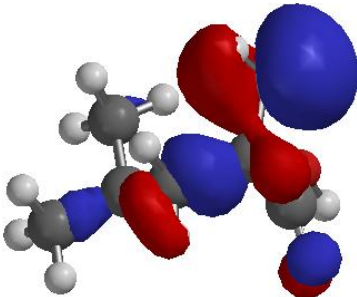
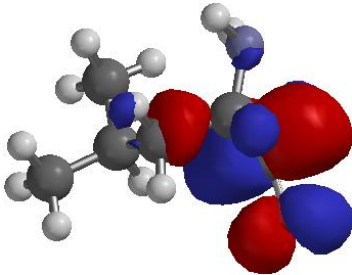
Inhibitors	E HOMO(eV)	E LUMO(eV)	Dipole Moment	$\Delta E$	$\eta$	$\sigma$	$\omega$	$\chi$	$\Delta N$
AM-1	-6.61	0.22	2.45	6.83	3.42	0.29283	17.4302	6.50	0.85375
AM-2	-6.55	0.21	2.47	6.76	3.38	0.29586	16.9826	6.45	0.93795
AM-3	-6.40	0.24	2.33	6.64	3.32	0.30121	15.7474	6.28	1.1952
AM-4	-6.45	0.12	1.58	6.57	3.29	0.30441	16.4533	6.39	1.001925
AM-5	-6.07	0.06	1.38	6.13	3.07	0.32626	13.8385	6.04	1.4712
AM-6	-6.44	0.08	0.46	6.52	3.26	0.30675	16.4832	6.40	0.9780
AM-7	-5.92	-0.19	2.49	5.73	2.87	0.34904	13.3696	6.015	1.411013
AM-8	-6.20	0.34	2.10	6.54	3.27	0.30581	14.0363	6.03	1.58595
AM-9	-6.64	-0.20	1.98	6.44	3.22	0.31056	18.8312	6.74	0.4186
AM-10	-6.47	0.16	1.71	6.63	3.32	0.30166	16.4988	6.39	1.011075
AM-11	-6.29	-1.61	3.09	4.68	2.34	0.42735	18.2549	7.09	-0.11115
AM-12	-6.57	0.15	4.11	6.72	3.36	0.29762	17.3109	6.49	0.8484
AM-13	-5.89	0.97	4.14	6.86	3.43	0.29155	10.3785	5.41	2.735425
AM-14	-5.85	0.15	1.63	6.00	3.00	0.33333	12.1838	5.78	1.8375
AM-15	-6.41	-0.02	3.78	6.39	3.19	0.31299	16.5121	6.42	0.92655
AM-16	-7.82	-2.23	4.73	5.59	2.79	0.35778	35.2878	8.94	-2.70416
AM-17	-7.67	-0.57	3.71	7.10	3.55	0.28169	30.1296	7.96	-1.69513
AM-18	-6.11	0.41	5.21	6.52	3.26	0.30675	13.2397	5.91	1.78485
AM-19	-6.34	0.25	2.47	6.59	3.29	0.30349	15.2757	6.22	1.293288

**Table 4.1. Selected quantum chemical parameters for the studied inhibitors (Amino acids derives) (Continued)**

Inhibitors	E HOMO(eV)	E LUMO(eV)	Dipole Moment	$\Delta E$	$\eta$	$\sigma$	$\omega$	$\chi$	$\Delta N$
AM-20	-5.49	-0.19	2.03	5.30	2.650	0.37736	10.6869	5.585	1.874875
AM-21	-5.54	0.13	1.68	5.67	2.835	0.35273	10.3719	5.475	2.161688
AM-22	-5.33	0.30	1.68	5.63	2.815	0.35524	8.90275	5.18	2.56165
AM-23	-5.36	0.27	1.00	5.63	2.815	0.35524	9.11641	5.225	2.498313
AM-24	-4.85	0.48	1.85	5.33	2.665	0.37524	6.36166	4.61	3.184675
AM-25	-5.33	0.36	1.74	5.69	2.845	0.35149	8.78426	5.15	2.631625

*Energy band gap ( $\Delta E$ ), chemical hardness ( $\eta$ ), chemical softness ( $\sigma$ ), electrophilicity index ( $\omega$ ), global electronegativity ( $\chi$ ), number of transferred electrons ( $\Delta N$ )*

**Table 4.2: Optimized Structures, E-HOMO and E-LUMO and of the studied inhibitors (AM).**

Inhibitor	Optimized	E-HOMO	E-LUMO
AM-1			
AM-2			
AM-3			

Model

4.1

$$\begin{aligned} \%IE = & -0.522168535 * \text{Energy(Solv)} - 12.740565608 * \text{Polarizability} + 4.393211776 * \text{Molecular refractivity} \\ & + 22.867080474 * \text{Balaban index JY} - 0.068768654 * \text{Vertex distance / equality} \\ & + 481.210651872 \end{aligned}$$

$$R^2 = 0.871, R_{adj.}^2 = 0.818, Q_{CV}^2 = 0.750, R_{pred.}^2 = 0.857039$$

4.2

$$\begin{aligned} \%IE = & -0.562150592 * \text{Energy(Solv)} - 13.861849848 * \text{Polarizability} + 4.417855773 * \text{Molecular refractivity} \\ & + 24.998130959 * \text{Balaban index JX} - 0.099320245 * \text{Wiener index} + 528.820786713 \end{aligned}$$

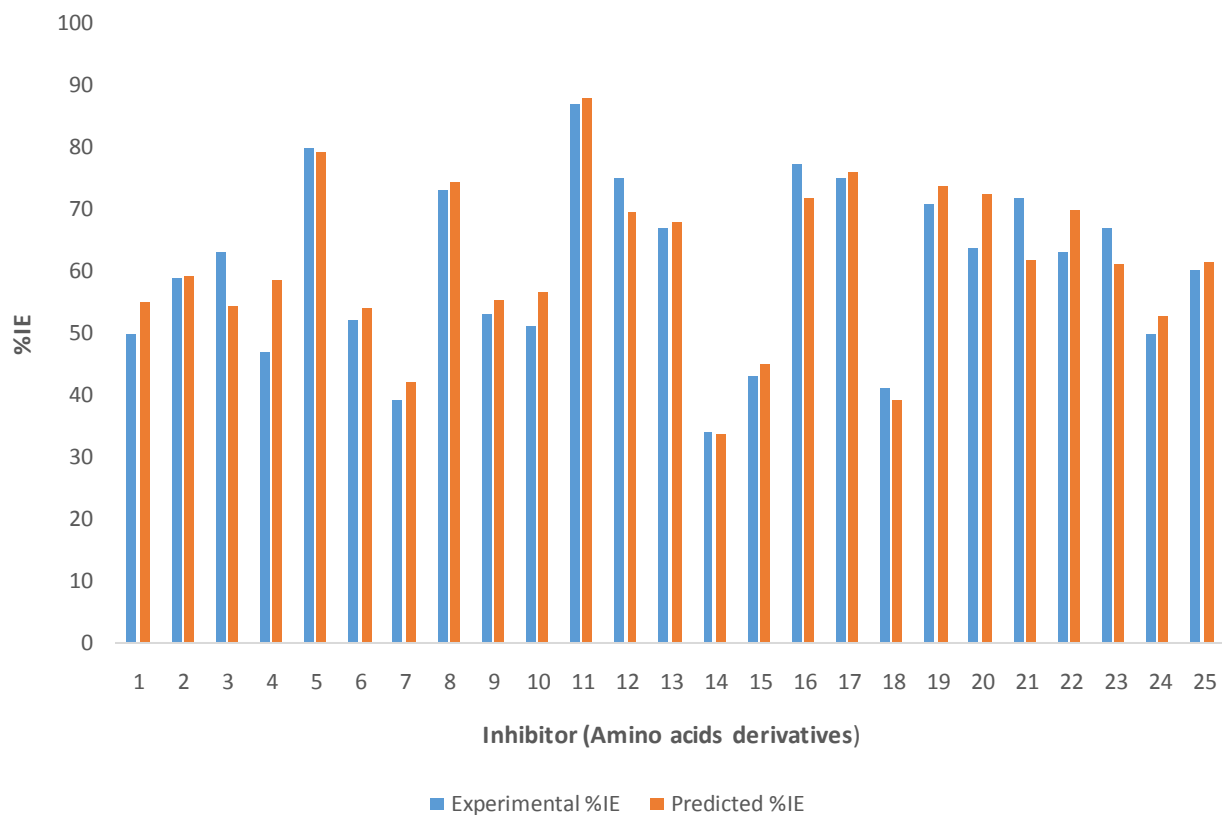
$$R^2 = 0.873, R_{adj.}^2 = 0.817, Q_{CV}^2 = 0.748, R_{pred.}^2 = 0.646$$

4.3

$$\begin{aligned} \%IE = & -0.485526799 * \text{Energy(Solv)} - 11.344160007 * \text{Polarizability} + 3.901129778 * \text{Molecular refractivity} \\ & + 29.698280527 * \text{Balaban index JY} + 4.036638729 * \text{Kappa} - 1(\text{alpha modified}) \\ & + 528.820786713 + 420.964429357 \end{aligned}$$

$$R^2 = 0.870, R_{adj.}^2 = 0.816, Q_{CV}^2 = 0.722, R_{pred.}^2 = 0.635$$

**Scheme 4.1: GFA Derived QSAR models for %IE of Amino acids derivatives**



**Figure 4.1: Experimental against predicted inhibition efficiency (%IE) for Amino acids derivatives**

**Table 4.3: External Validation for model 4.1**

Inhibitors	Experimental %IE	Energy(Solv)(kJ/mol)	Polarizability	Molecular refractivity	Balaban indexJY	Vertex distance/equality	Predicted %IE	Residuals
AM-2	59	-47.4	49.23	26.12639	2.870458	143.6384	59.09246	-0.09246
AM-6	52	-51.87	49.42	25.8671	2.705434	203.5404	54.09308	-2.09308
AM-10	51	-32.13	47.17	20.1639	3.11201	70.36869	56.69358	-5.69358
AM-15	43	-51.83	48.88	25.3979	2.101301	136.5895	45.07604	-2.07604
AM-19	71	-54.56	52.53	36.4759	3.203069	286.3716	73.86074	-2.86074
AM-22	63.24	-15.68	51.9	40.40061	2.812531	190.1745	69.89698	-6.65698
AM-25	60.09	-18.49	50.38	35.7996	2.41688	137.5614	61.46936	-1.37936

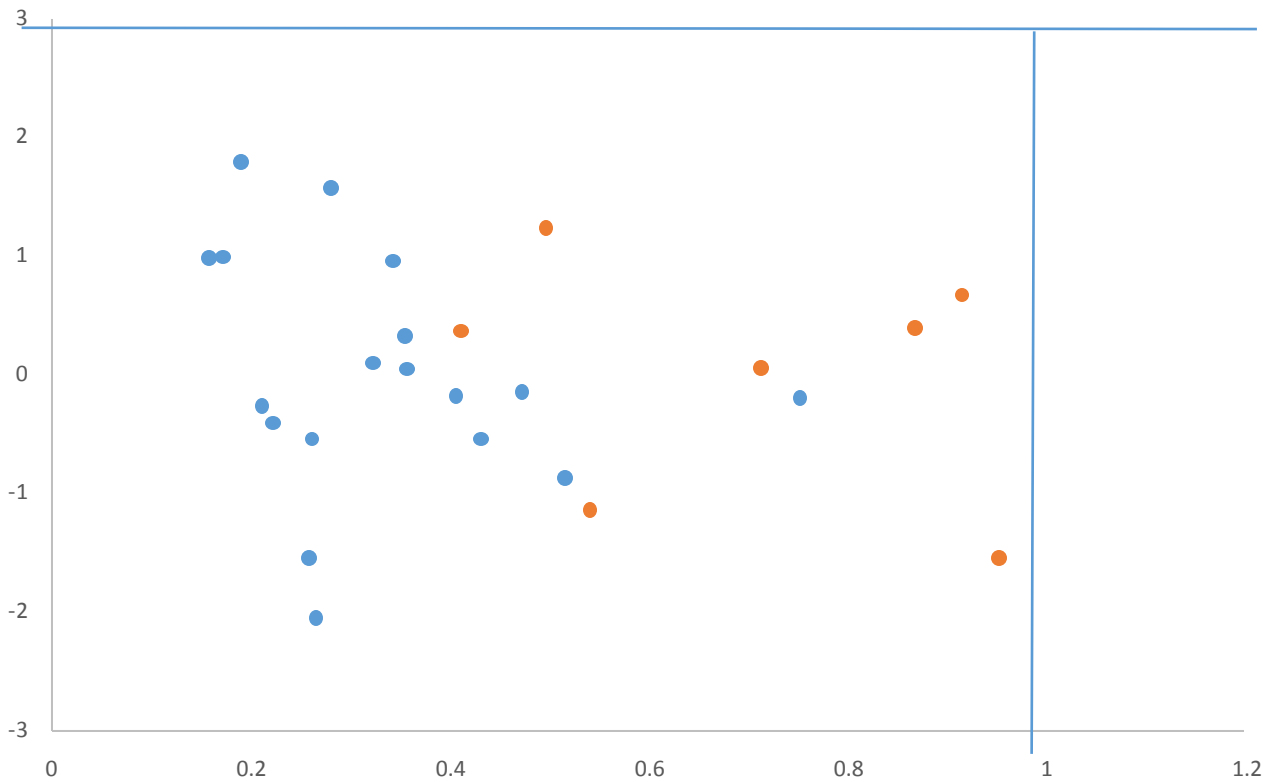
**Table 4.4: Calculation of Predictive  $R^2_{pred}$  of Model 4.1**

Inhibitors	%IE	Yp	Yp-Ye	Ye-Ytrng	(Ye-Yp)^2	(Ye-Ytrng)^2
AM-2	59	59.09246	-0.09246	-2.86778	0.008548	8.224149
AM-6	52	54.09308	-2.09308	-9.86778	4.380973	97.37304
AM-10	51	56.69358	-5.69358	-10.8678	32.41687	118.1086
AM-15	43	45.07604	-2.07604	-18.8678	4.309956	355.993
AM-19	71	73.86074	-2.86074	9.132222	8.183824	83.39748
AM-22	63.24	69.89698	-6.65698	1.372222	44.31536	1.882994
AM-25	60.09	61.46936	-1.37936	-1.77778	1.902632	3.160494
					<b><math>\Sigma=95.51817</math></b>	<b><math>\Sigma=668.1398</math></b>

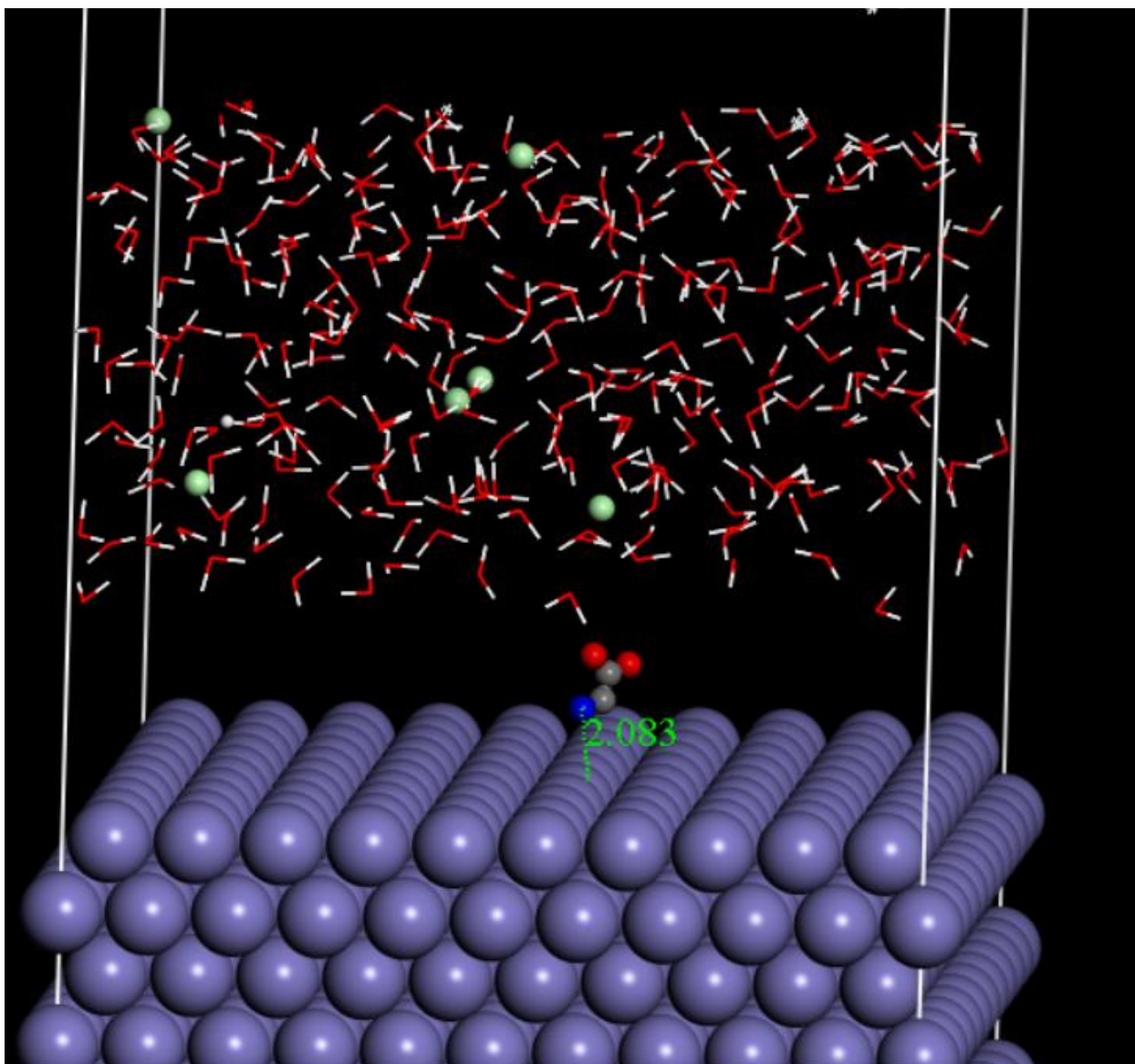
$$R^2_{pred} = 1 - \left( \frac{95.51817}{668.1398} \right)$$
$$= 0.857$$

**Table 4.5: Comparison of Experimental, Predicted and Residual %IE of Model 4.1**

Inhibitors	Experimental %IE	Predicted %IE	Residuals Values
AM-1	50	54.93	-4.93
AM-3	63	54.23	8.77
AM-4	47	58.525	-11.525
AM-5	80	79.4	0.6
AM-7	39	42.01	-3.01
AM-8	73	74.53	-1.53
AM-9	53	55.22	-2.22
AM-11	87	88.15	-1.15
AM-12	75	69.5	5.5
AM-13	67	67.84	-0.84
AM-14	34	33.68	0.32
AM-16	77.4	71.97	5.43
AM-17	75.1	76.12	-1.02
AM-18	41	39.2	1.8
AM-20	63.62	72.33	-8.71
AM-21	71.79	61.79	10
AM-23	66.83	61.24	5.59
AM-24	49.88	52.87	-2.99



**Figure 4.2: The Williams plot, the plot of standardized Residuals versus the leverage value for Amino acids derivatives.**



**Figure 4.3: Molecular dynamic system of Fe, inhibitor molecule and acidic layer**

**Table 4.6: Adsorption Energy, Binding Energy, shortest bond distances and inhibition efficiencies (%IE) of the AM-studied inhibitors**

Inhibitors	Adsorption Energy(kcal/mol)	Binding Energy(kcal/mol)	shortest bond distance(Å)	Experimental %IE
AM-1	-114.20	114.20	2.083	50
AM-2	-116.80	116.80	2.27	59
AM-3	-256.72	256.72	3.07	63
AM-4	-214.82	214.82	2.61	47
AM-5	-399.12	399.12	2.95	80
AM-6	-229.23	229.23	3.10	52
AM-7	-244.21	244.21	3.18	39
AM-8	-297.50	297.50	3.00	73
AM-9	-234.58	234.58	3.20	53
AM-10	-227.71	227.71	2.87	51
AM-11	-651.70	651.70	2.16	87
AM-12	-290.94	290.94	2.95	75
AM-13	-257.21	257.21	3.01	67
AM-14	-181.67	181.67	3.70	34
AM-15	-197.00	197.00	2.86	43
AM-16	-280.41	280.41	2.72	77.4
AM-17	-259.21	259.21	2.87	75.1
AM-18	-128.24	128.24	3.60	41
AM-19	-227.37	227.37	2.98	71
AM-20	-285.05	285.05	3.06	63.62
AM-21	-126.58	126.58	2.87	71.79
AM-22	-467.95	467.95	3.30	63.24
AM-23	-253.35	253.35	3.20	66.83
AM-24	-380.73	380.73	2.77	49.88
AM-25	-346.24	346.24	2.66	60.09

#### **4.2 Quantum Chemical studies, GFA Derived models for %IE and Molecular dynamics Simulation studies of Imidazole derivatives**

The results of quantum chemical parameters were listed in Table 4.7. The optimized molecular structures, HOMO and LUMO electronic density distributions of the first three inhibitors are shown in Table 4.8. Three developed GFA-QSAR models (4.4, 4.5 and 4.6) were recorded and presented in scheme 4.2 out of which model 4.4 was chosen as the best model for predicting the %IE of IM-corrosion inhibitors due to its statistical significance.

Figure 4.4 gives the plot of predicted %IE of both training and test sets against experimental %IE, the comparison of the experimental, predicted and residuals %IE for the test set inhibitors of model 4.4 is presented in Tables 4.9. The stability, reliability, and robustness of the generated model 4.4 were confirmed by predictive  $R^2$  (Table 4.10). The experimental, predicted and residual %IE values of the training set inhibitors are presented in the Tables 4.11 while the applicability domain of the model 4.4 is presented in Figure 4.8 (the danger  $h_i$ , leverage limit is 1.2).

Furthermore, the equilibrium configurations of the simulated systems are shown in Figure 4.6, while the relevant energy parameters of the systems are listed in Table 4.12.

#### **4.3 Quantum Chemical studies, GFA Derived models for %IE and molecular dynamics simulation studies of Triazole derivatives (Steel corrosion inhibitors)**

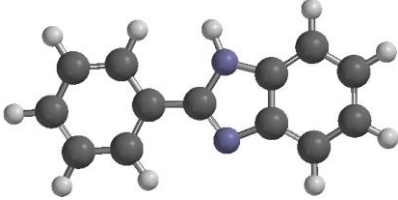
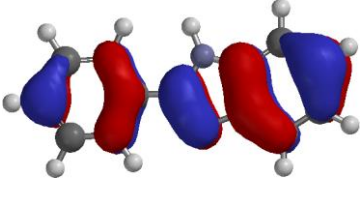
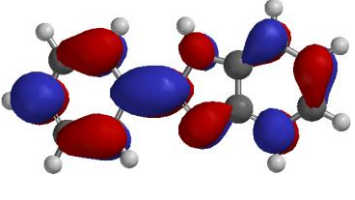
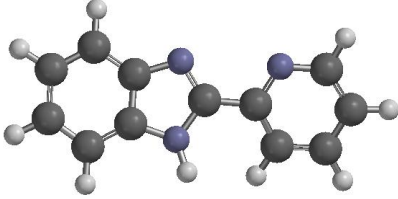
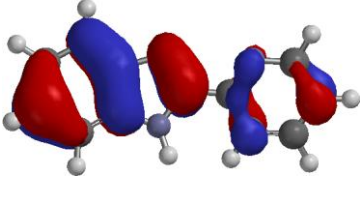
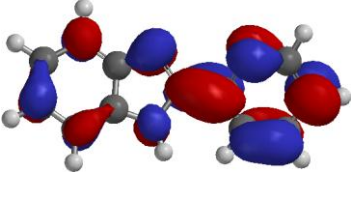
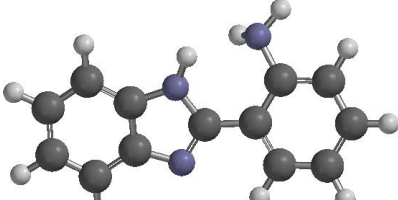
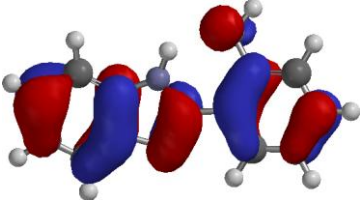
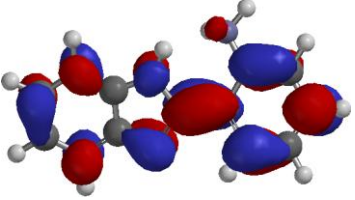
The results of quantum chemical parameters were listed in Table 4.13. The optimized molecular structures, HOMO and LUMO electronic density distributions of the first three inhibitors are shown in Table 4.14.

**Table 4.7: Selected quantum chemical parameters for the studied inhibitors IM- (Imidazole derives)**

Inhibitors	E HOMO(eV)	E LUMO(eV)	Dipole Moment	$\Delta E$	$\eta$	$\sigma$	$\omega$	$\chi$	$\Delta N$
IM-1	-5.70	-1.17	3.09	4.53	2.265	0.4415	13.3626	6.285	0.809738
IM-2	-5.87	-1.37	4.83	4.5	2.25	0.44444	14.7425	6.555	0.500625
IM-3	-5.50	-1.00	4.13	4.5	2.25	0.44444	11.8828	6	1.125
IM-4	-5.86	-0.42	3.6	5.44	2.72	0.36765	13.4091	6.07	1.2648
IM-5	-5.87	-0.43	3.68	5.44	2.72	0.36765	13.4946	6.085	1.2444
IM-6	-5.81	-0.33	3.56	5.48	2.74	0.36496	12.9121	5.975	1.40425
IM-7	-6.07	-0.34	3.44	5.73	2.865	0.34904	14.7147	6.24	1.0887
IM-8	-5.89	-0.22	3.5	5.67	2.835	0.35273	13.2296	6	1.4175
IM-9	-5.83	-0.36	2.26	5.47	2.735	0.36563	13.0993	6.01	1.353825
IM-10	-5.45	0.1	3.75	5.55	2.775	0.36036	9.92843	5.4	2.22
IM-11	-5.87	-1.37	4.83	4.5	2.25	0.44444	14.7425	6.555	0.500625
IM-12	-6.01	-0.31	2.9	5.7	2.85	0.35088	14.2295	6.165	1.189875
IM-13	-5.74	0.00	2.21	5.74	2.87	0.34843	11.82	5.74	1.8081
IM-14	-6.07	-0.34	3.44	5.73	2.865	0.34904	14.7147	6.24	1.0887
IM-15	-5.79	-0.18	3.62	5.61	2.805	0.35651	12.4966	5.88	1.5708
IM-16	-6.04	-0.58	3.47	5.46	2.73	0.3663	14.9551	6.33	0.91455
IM-17	-5.40	-0.93	4.33	4.47	2.235	0.44743	11.1943	5.865	1.268363
IM-18	-5.90	-1.01	5.38	4.89	2.445	0.409	14.593	6.405	0.727388
IM-19	-5.89	-0.92	5.62	4.97	2.485	0.40241	14.4056	6.35	0.807625
IM-20	-5.68	-0.99	7.32	4.69	2.345	0.42644	13.0408	6.175	0.967313

*Energy band gap ( $\Delta E$ ), chemical hardness ( $\eta$ ), chemical softness ( $\sigma$ ), electrophilicity index ( $\omega$ ), global electronegativity ( $\chi$ ), number of transferred electrons ( $\Delta N$ )*

**Table 4.8: Optimized Structures, E-HOMO and E-LUMO of the studied inhibitors (IM).**

Inhibitor	Optimized	E-HOMO	E-LUMO
IM-1			
IM-2			
IM-3			

Model

4.4

$$\%IE = 53.250057429 * E - \text{HOMO(eV)} - 1.167830197 * \text{Polar surface area} + 652.158586289 * \text{Ovality} \\ - 9.872435953 * \text{Polarizability} - 5.645379027 * \text{Log P} + 126.822103851$$

$$R^2 = 0.942, R_{adj.}^2 = 0.908, Q_{CV}^2 = 0.795, R_{pred.}^2 = 0.983$$

4.5

$$\%IE = -3.648913972 * \text{Dipole Moment} - 46.260136323 * \text{Ionization energy} - 0.664503569 * \text{Polar surface area} \\ + 512.505239261 * \text{Ovality} - 7.511931371 * \text{Polarizability} + 135.178755055$$

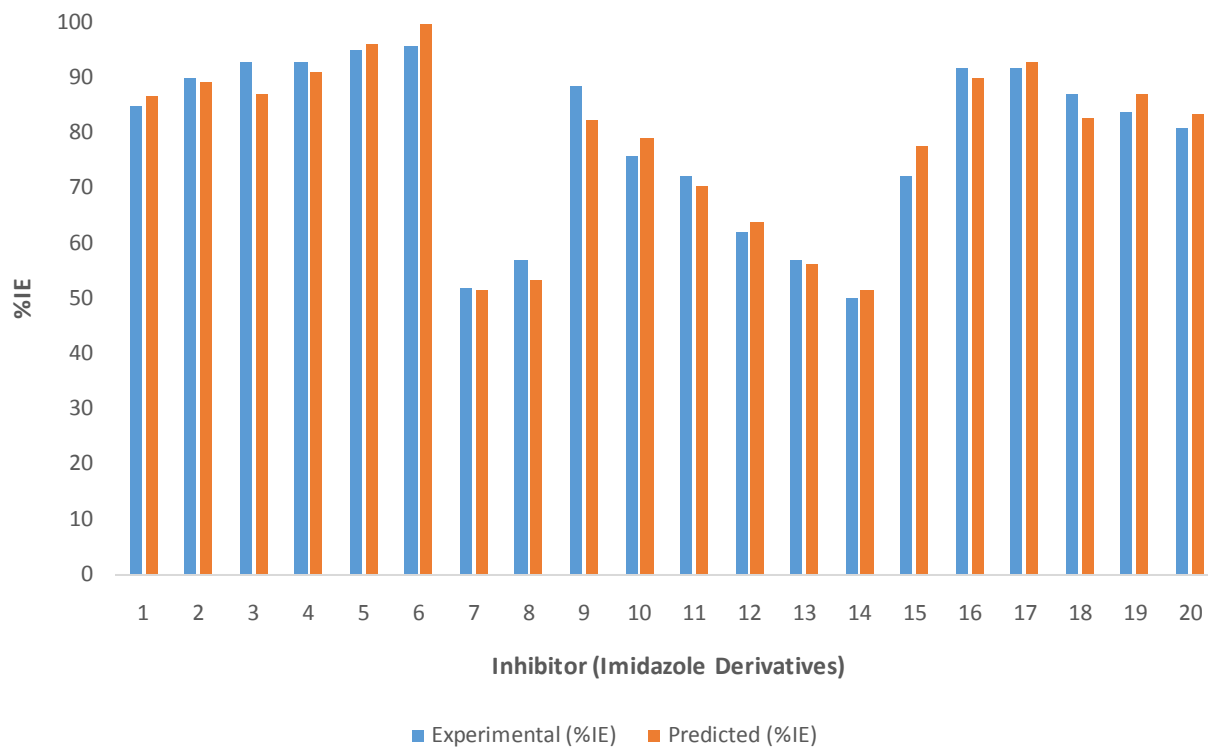
$$R^2 = 0.909, R_{adj.}^2 = 0.859, Q_{CV}^2 = 0.648, R_{pred.}^2 = 0.879$$

4.6

$$\%IE = 46.260136323 * E - \text{HOMO(eV)} - 3.648913972 * \text{Dipole Moment} - 0.664503569 * \text{Polar surface area} \\ + 512.505239261 * \text{Ovality} - 7.511931371 * \text{Polarizability} + 135.178755055$$

$$R^2 = 0.909, R_{adj.}^2 = 0.859, Q_{CV}^2 = 0.650, R_{pred.}^2 = 0.843$$

**Scheme 4.2: GFA Derived QSAR models for %IE of Imidazole derivatives**



**Figure 4.4: Experimental against predicted inhibition efficiency (%IE) for Imidazole derivatives**

**Table 4.9: External Validation for model 4.4**

Inhibitors	Experimental (%IE)	E HOMO(eV)	Polar surface area	Ovality	Polarizability	Log P	Predicted %IE	Residual Values
IM-2	90	-5.87	26.881	1.31	54.879	1.04	89.51896	0.481039
IM-8	57.1	-5.89	20.54	1.22	54.154	-0.55	53.29857	3.801433
IM-13	57.07	-5.74	40.697	1.2	50.75	-0.22	56.44575	0.624253
IM-17	92	-5.4	51.474	1.56	72.35	-1.91	93.03823	-1.03823
IM-20	81.1	-5.68	36.72	1.51	68.97	0.34	83.41718	-2.31718

**Table 4.10: Calculation of Predictive  $R^2_{pred}$  of Model 4.4**

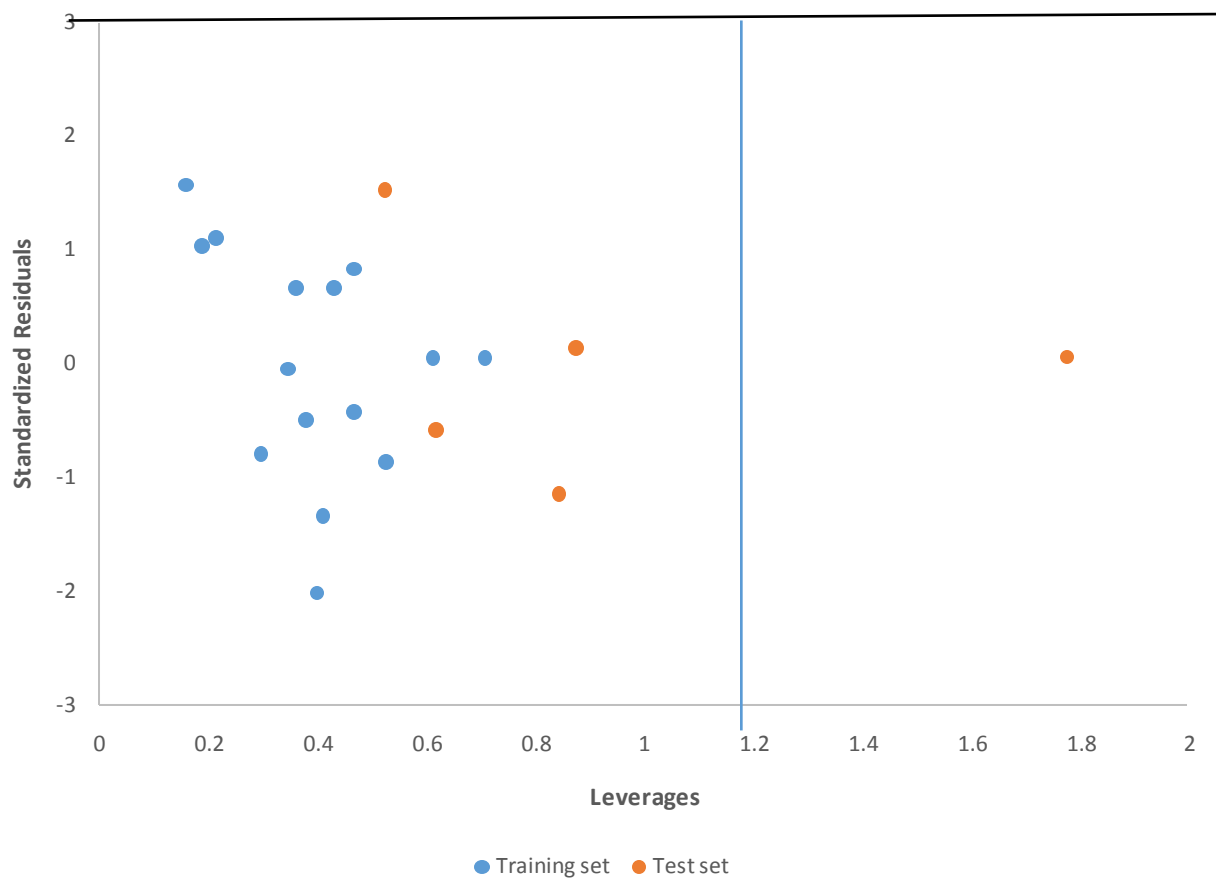
Inhibitors	Ye	Yp	Ye-Yp	Ytrng	Ye-Ytrng	(Ye-Yp) <sup>2</sup>	(Ye-Ytrng) <sup>2</sup>
IM-2	90	89.51896	0.481039	79.93	10.07	0.231399	101.4049
IM-8	57.1	53.29857	3.801433	79.93	-22.83	14.4509	521.2089
IM-13	57.07	56.44575	0.624253	79.93	-22.86	0.389692	522.5796
IM-17	92	93.03823	-1.03823	79.93	12.07	1.077913	145.6849
IM-20	81.1	83.41718	-2.31718	79.93	1.17	5.369313	1.3689
						<b><math>\Sigma=21.51921</math></b>	<b><math>\Sigma=1292.247</math></b>

$$R^2_{pred} = 1 - \left( \frac{21.51921}{1292.247} \right)$$

$$= 0.983$$

**Table 4.11: Comparison of Experimental, Predicted and Residual %IE of Model 4.4**

Inhibitors	Experimental %IE	Predicted %IE	Residuals Values
IM-1	85	86.75	-1.75
IM-3	93	87.05	5.95
IM-4	93	91.24	1.76
IM-5	95	96.1	-1.1
IM-6	96	100.68	-4.68
IM-7	52.2	51.61	0.59
IM-9	88.7	82.49	6.21
IM-10	75.99	79.33	-3.34
IM-11	72.4	70.65	1.75
IM-12	62.32	63.84	-1.52
IM-14	50.34	51.61	-1.27
IM-15	72.2	77.78	-5.58
IM-16	91.8	89.92	1.88
IM-18	87.1	82.66	4.44
IM-20	81.1	87.18	-6.08



**Figure 4.5: The Williams plot, the plot of standardized Residuals versus the leverage value for Imidazole derivatives.**

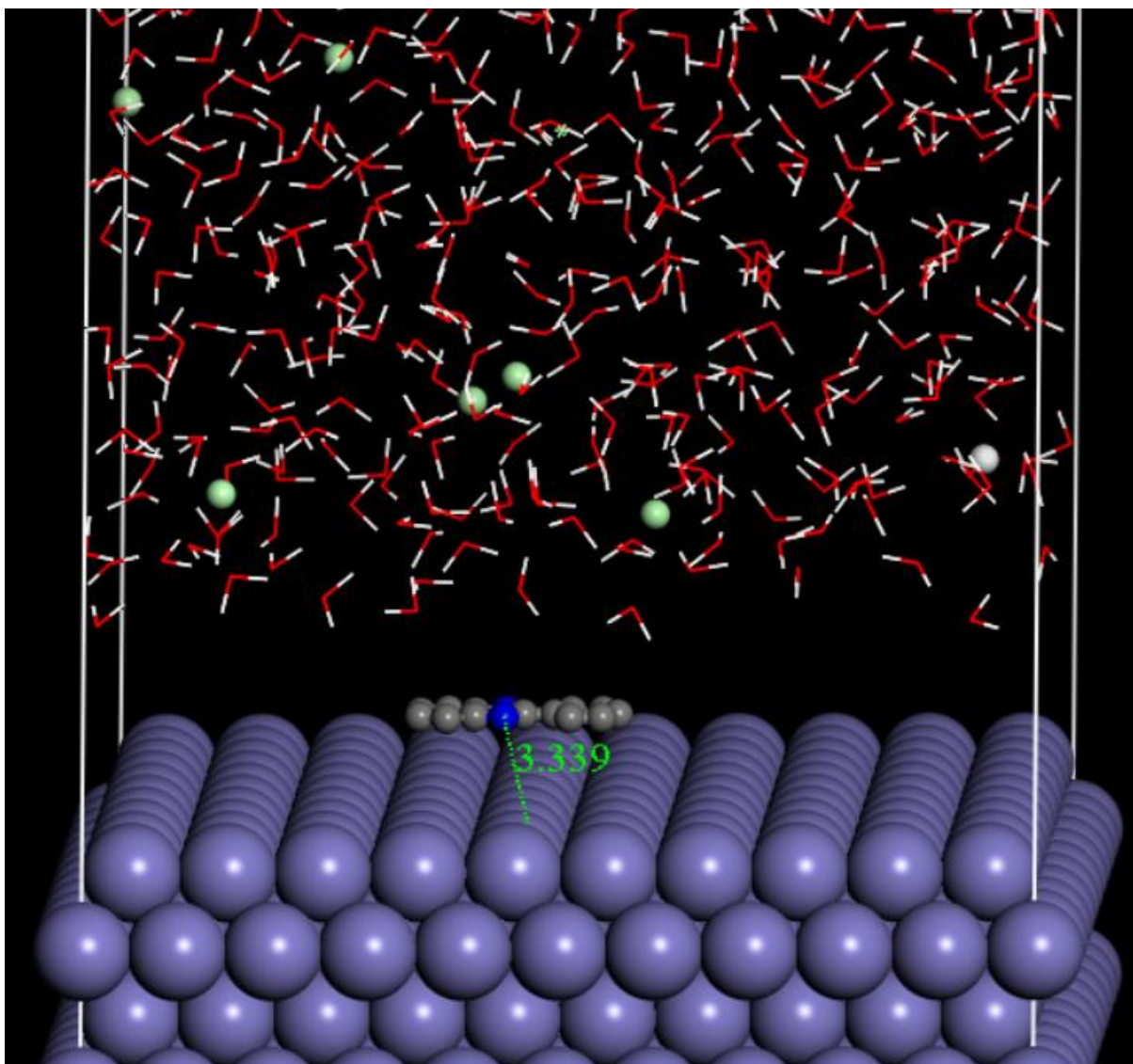


Figure 4.6: Equilibrium adsorption configurations of inhibitor, IM-1 on Fe (1 1 0) surface

**Table 4.12: Adsorption Energy, Binding Energy, shortest bond distances and inhibition efficiencies (%IE) of the IM-inhibitors**

Inhibitors	Adsorption Energy(kcal/mol)	Binding Energy(kcal/mol)	shortest bond distance(Å)	Experimental % IE
IM-1	-142.82	142.82	3.339	85
IM-2	-231.16	231.16	2.78	90
IM-3	-256.72	256.72	2.80	93
IM-4	-214.82	214.82	2.78	93
IM-5	-329.12	329.12	3.03	95
IM-6	-359.23	359.23	2.988	96
IM-7	-144.21	144.21	3.13	52.2
IM-8	-197.50	197.50	3.27	57.1
IM-9	-234.58	234.58	3.10	88.7
IM-10	-227.71	227.71	3.05	75.99
IM-11	-215.70	215.70	2.87	72.4
IM-12	-190.94	190.94	4.39	62.32
IM-13	-157.21	157.21	3.42	57.07
IM-14	-181.67	181.67	3.34	50.34
IM-15	-197.00	197.00	3.17	72.2
IM-16	-280.41	280.41	2.67	91.8
IM-17	-259.21	259.21	2.71	92
IM-18	-228.24	228.24	2.89	87.1
IM-19	-227.37	227.37	3.00	83.9
IM-20	-218.05	218.05	2.86	81.1

All the Three developed GFA-QSAR models (4.7, 4.8 and 4.9) were reported and presented in scheme 4.3 out of which model 4.7 was chosen as the best model for predicting the %IE of Steel anticorrosion molecules (Trizole derivatives) due to its statistical significance. Figure 4.7 gives the plot of experimental %IE for both training and test sets against predicted %IE. The comparison of the experimental, predicted and residual %IE values for the test set inhibitors of model 4.7 is presented in Tables 4.15, the stability, reliability and robustness of the generated model 4.7 were confirmed by predictive  $R^2$  (Tables 4.16). The experimental, predicted and residuals %IE values of the training set inhibitors are presented in the Table 4.17, while the corresponding Williams plot of the leverages against standardized residuals for both the training and test sets are presented in Figure 4.8(warning leverage  $h^*= 0.783$ )

Furthermore, Figure 4.9 shows the adorable configuration of the first inhibitor in the series, while Table 4.18 shows molecular dynamics results.

**Table 4.13: Selected quantum chemical parameters for the studied inhibitors, TR (Triazole derivatives)**

Inhibitors	E HOMO(eV)	E LUMO(eV)	Dipole Moment	$\Delta E$	$\eta$	$\sigma$	$\omega$	$\chi$	$\Delta N$
TR-1	-6.50	-2.08	6.04	4.42	2.21	-0.45249	-20.3365	4.29	2.99455
TR-2	-6.28	-2.02	5.87	4.26	2.13	-0.46948	-18.342	4.15	3.03525
TR-3	-6.27	-2.03	5.84	4.24	2.12	-0.4717	-18.2559	4.15	3.021
TR-4	-5.94	-2.09	5.87	3.85	1.925	-0.51948	-15.5157	4.015	2.873063
TR-5	-5.83	-0.92	5.36	4.91	2.455	-0.40733	-13.982	3.375	4.449688
TR-6	-5.53	-0.86	5.89	4.67	2.335	-0.42827	-11.9179	3.195	4.442338
TR-7	-5.90	-0.98	5.26	4.92	2.46	-0.4065	-14.5553	3.44	4.3788
TR-8	-6.00	-1.00	5.45	5.00	2.50	-0.4000	-15.3125	3.5	4.375
TR-9	-6.03	-1.53	2.65	4.50	2.25	-0.44444	-16.0745	3.78	3.6225
TR-10	-6.09	-1.58	2.70	4.51	2.255	-0.44346	-16.5824	3.835	3.568538
TR-11	-5.93	-0.90	4.30	5.03	2.515	-0.39761	-14.6652	3.415	4.508138
TR-12	-5.68	-0.94	5.46	4.74	2.37	-0.42194	-12.983	3.31	4.37265
TR-13	-5.58	-1.46	4.27	4.12	2.06	-0.48544	-12.7621	3.52	3.5844
TR-14	-5.70	-0.94	5.94	4.76	2.38	-0.42017	-13.1167	3.32	4.3792
TR-15	-5.90	-1.03	2.72	4.87	2.435	-0.41068	-14.6176	3.465	4.303863
TR-16	-5.86	-1.11	4.45	4.75	2.375	-0.42105	-14.4225	3.485	4.174063
TR-17	-6.59	-1.04	3.38	5.55	2.775	-0.36036	-20.194	3.815	4.419188
TR-18	-6.63	-1.07	3.85	5.56	2.78	-0.35971	-20.6033	3.85	4.3785
TR-19	-6.66	-1.10	4.05	5.56	2.78	-0.35971	-20.9256	3.88	4.3368
TR-20	-6.66	-1.09	4.03	5.57	2.785	-0.35907	-20.9093	3.875	4.351563
TR-21	-6.65	-1.08	3.79	5.57	2.785	-0.35907	-20.8015	3.865	4.365488
TR-22	-6.32	-0.90	3.99	5.42	2.71	-0.369	-17.6585	3.61	4.59345

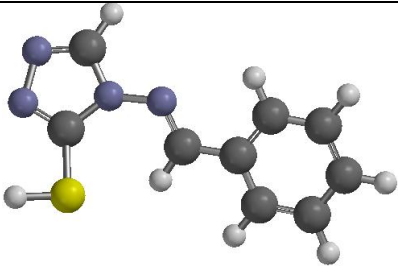
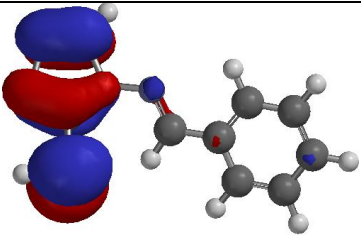
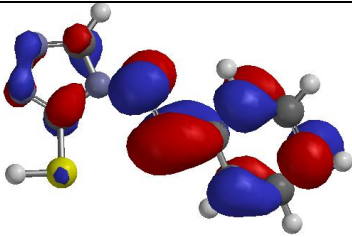
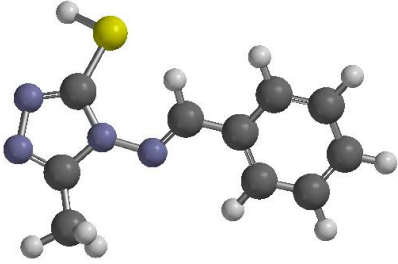
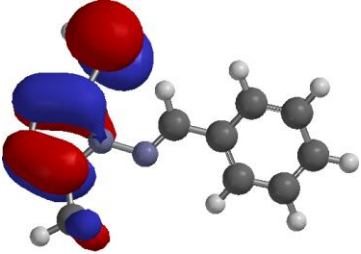
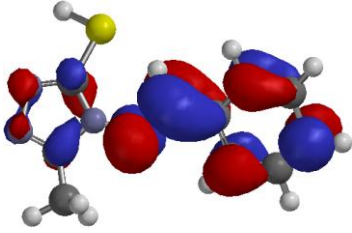
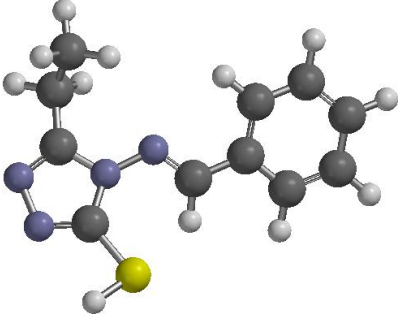
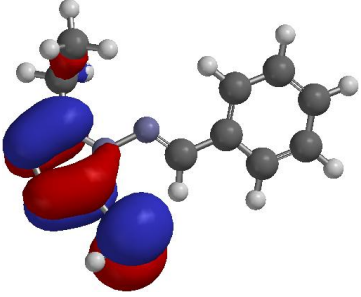
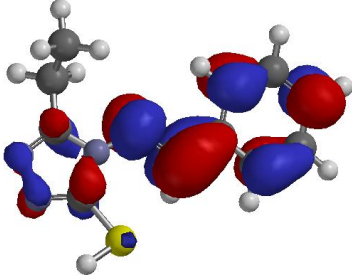
*Energy band gap ( $\Delta E$ ), chemical hardness ( $\eta$ ), chemical softness ( $\sigma$ ), electrophilicity index ( $\omega$ ), global electronegativity ( $\chi$ ), number of transferred electrons ( $\Delta N$ )*

**Table 4.13: Selected quantum chemical parameters for the studied inhibitors, TR (Triazole derivatives) (Continued)**

Inhibitors	E HOMO(eV)	E LUMO(eV)	Dipole Moment	$\Delta E$	$\eta$	$\sigma$	$\omega$	$\chi$	$\Delta N$
TR-23	-6.38	-0.95	3.13	5.43	2.715	-0.36832	-18.2342	3.665	4.527263
TR-24	-6.39	-0.96	2.01	5.43	2.715	-0.36832	-18.3339	3.675	4.513688
TR-25	-6.41	-0.98	1.92	5.43	2.715	-0.36832	-18.534	3.695	4.486538
TR-26	-6.40	-1.09	2.06	5.31	2.655	-0.37665	-18.6182	3.745	4.321013
TR-27	-6.89	-0.57	5.02	6.32	3.16	-0.31646	-21.9824	3.73	5.1666
TR-28	-6.98	-1.09	2.83	5.89	2.945	-0.33956	-23.9741	4.035	4.365963
TR-29	-5.93	-1.48	5.59	4.45	2.225	-0.44944	-15.2713	3.705	3.665688
TR-30	-6.04	-1.53	4.58	4.51	2.255	-0.44346	-16.1528	3.785	3.624913
TR-31	-6.08	-1.52	6.30	4.56	2.28	-0.4386	-16.4616	3.8	3.648

*Energy band gap ( $\Delta E$ ), chemical hardness ( $\eta$ ), chemical softness ( $\sigma$ ), electrophilicity index ( $\omega$ ), global electronegativity ( $\chi$ ), number of transferred electrons ( $\Delta N$ )*

**Table 4.14: Optimized Structures, E-HOMO and E-LUMO and of the studied inhibitors (TR).**

Inhibitor	Optimized	E-HOMO	E-LUMO
TR-1			
TR-2			
TR-3			

Model

4.7

$$\begin{aligned} \%IE = & 4.497478061 * \text{Electrophilicity index} - 0.601205053 * \text{Polar surface area} - 4.986481686 \\ & * \text{Subgraph counts (3): path} + 52.210335323 * \text{Chi (1)} - 17.196865152 * \text{Element count} \\ & + 114.610286656 \end{aligned}$$

$$R^2 = 0.862, R_{adj.}^2 = 0.822, Q_{CV}^2 = 0.706, R_{pred.}^2 = 0.835$$

4.8

$$\begin{aligned} \%IE = & 3.720636605 * \text{Electrophilicity index} - 0.722348241 * \text{Polar surface area} + 20.991745733 \\ & * \text{Subgraph counts (0): path} - 4.030974701 * \text{Subgraph counts (3): path} - 14.365673794 \\ & * \text{Element count} + 119.220231477 \end{aligned}$$

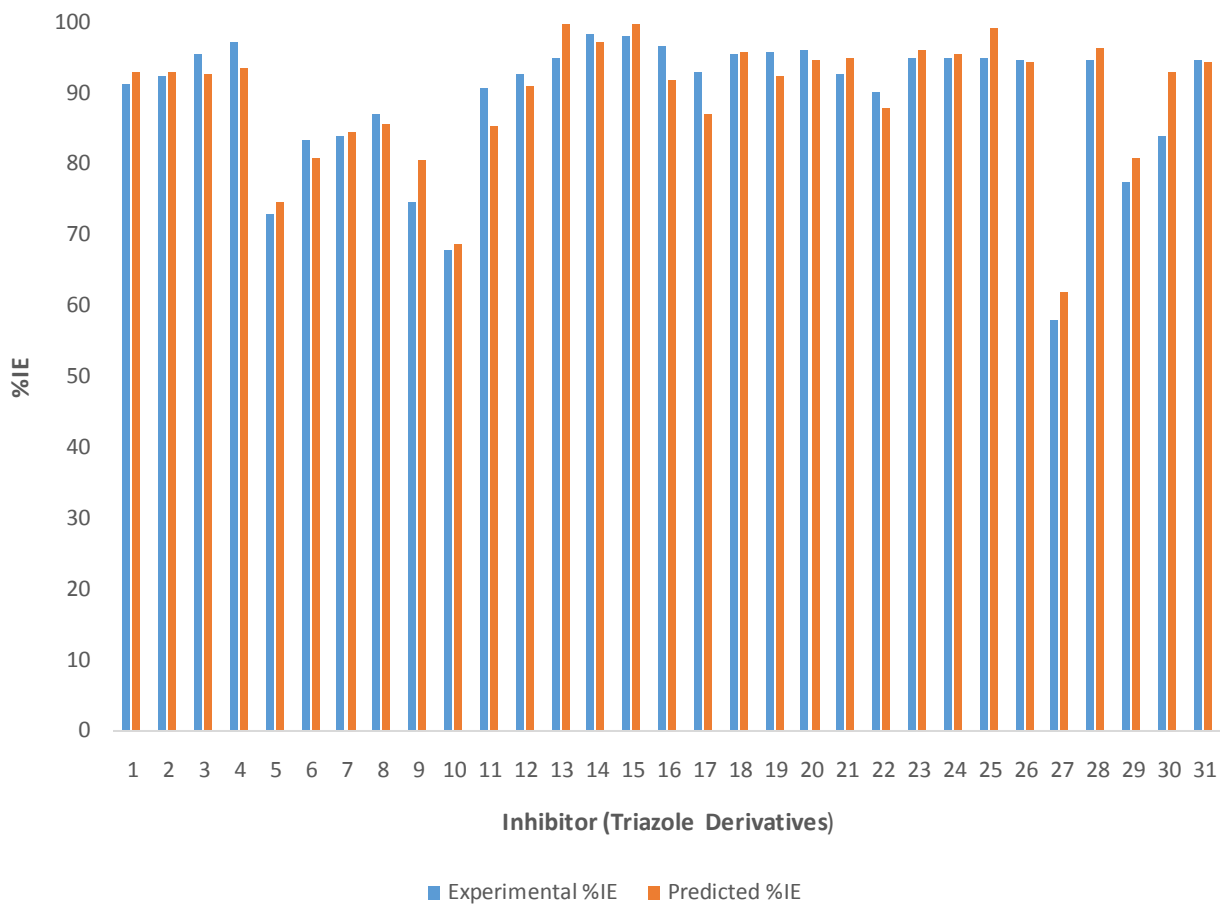
$$R^2 = 0.856, R_{adj.}^2 = 0.813, Q_{CV}^2 = 0.791, R_{pred.}^2 = 0.617$$

4.9

$$\begin{aligned} \%IE = & 4.208210583 * \text{Electrophilicity index} - 0.730392720 * \text{Polar surface area} + 25.925790261 * \text{Kappa} \\ & - 3 + 6.296887586 * \text{Subgraph counts (1): path} - 14.931174364 * \text{Element count} \\ & + 164.744476474 \end{aligned}$$

$$R^2 = 0.854, R_{adj.}^2 = 0.811, Q_{CV}^2 = 0.689, R_{pred.}^2 = 0.658$$

**Scheme 4.3: GFA Derived QSAR models for %IE of Triazole derivatives**



**Figure 4.7: Experimental against predicted inhibition efficiency (%IE) for Triazole derivatives**

**Table 4.15: External Validation for model 4.7**

Inhibitors	Experimental %IE	Electrophilicity index	Polar surface area	Subgraph counts (3): path	Chi (1)	Element count	Predicted %IE	Residuals
TR-2	92.63	-18.342	30.678	26	7.210857	10	93.14808	0.51808
TR-7	84.2	-14.5553	21.659	37	8.987602	14	84.72639	0.526388
TR-10	68.1	-16.5824	46.586	33	8.102653	12	68.75961	0.659615
TR-14	98.36	-13.1167	35.367	26	6.567886	9	97.45687	-0.90313
TR-19	95.9	-20.9256	64.744	40	10.46736	14	92.47236	-3.42764
TR-25	95	-18.534	64.56	43	11.00804	15	99.41225	4.412253
TR-28	94.7	-23.9741	51.947	23	7.388134	9	96.44262	1.742617
TR-30	84.11	-16.1528	43.697	58	12.20271	16	93.04426	8.934257

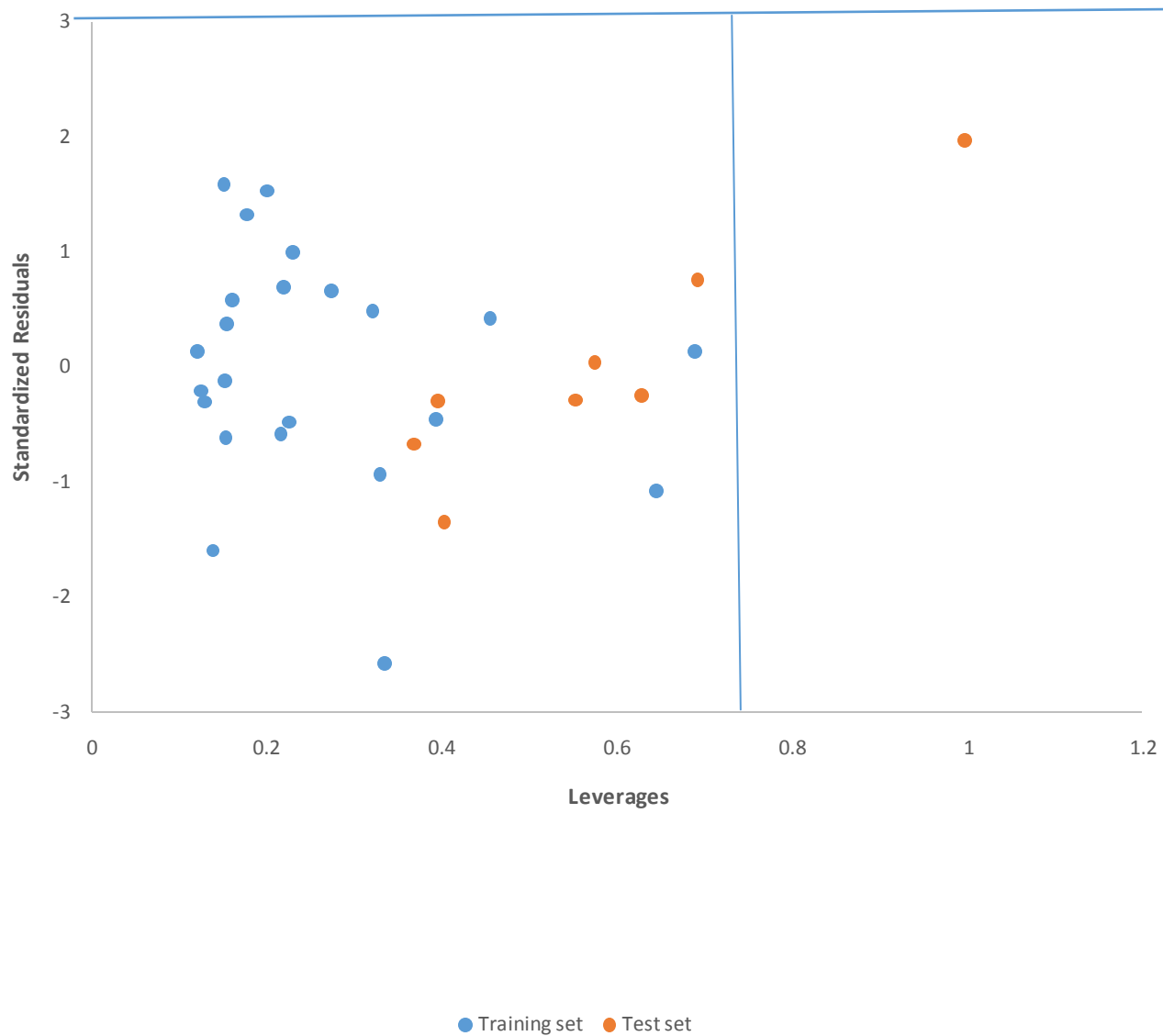
**Table 4.16: Calculation of Predictive  $R^2_{pred}$  of Model 4.7**

Inhibitors	Ye	Yp	Yp-Ye	Ytrng	Ye-Ytrng	(Ye-Yp)^2	(Ye-Ytrng)^2
2	92.63	93.14808	0.51808	89.57913	3.05087	0.268407	9.307805
7	84.2	84.72639	0.526388	89.57913	-5.37913	0.277085	28.93504
10	68.1	68.75961	0.659615	89.57913	-21.4791	0.435091	461.353
14	98.36	97.45687	-0.90313	89.57913	8.78087	0.815649	77.10367
19	95.9	92.47236	-3.42764	89.57913	6.32087	11.74869	39.95339
25	95	99.41225	4.412253	89.57913	5.42087	19.46798	29.38583
28	94.7	96.44262	1.742617	89.57913	5.12087	3.036713	26.22331
30	84.11	93.04426	8.934257	89.57913	-5.46913	79.82095	29.91139
						<b><math>\Sigma=115.8706</math></b>	<b><math>\Sigma=702.1735</math></b>

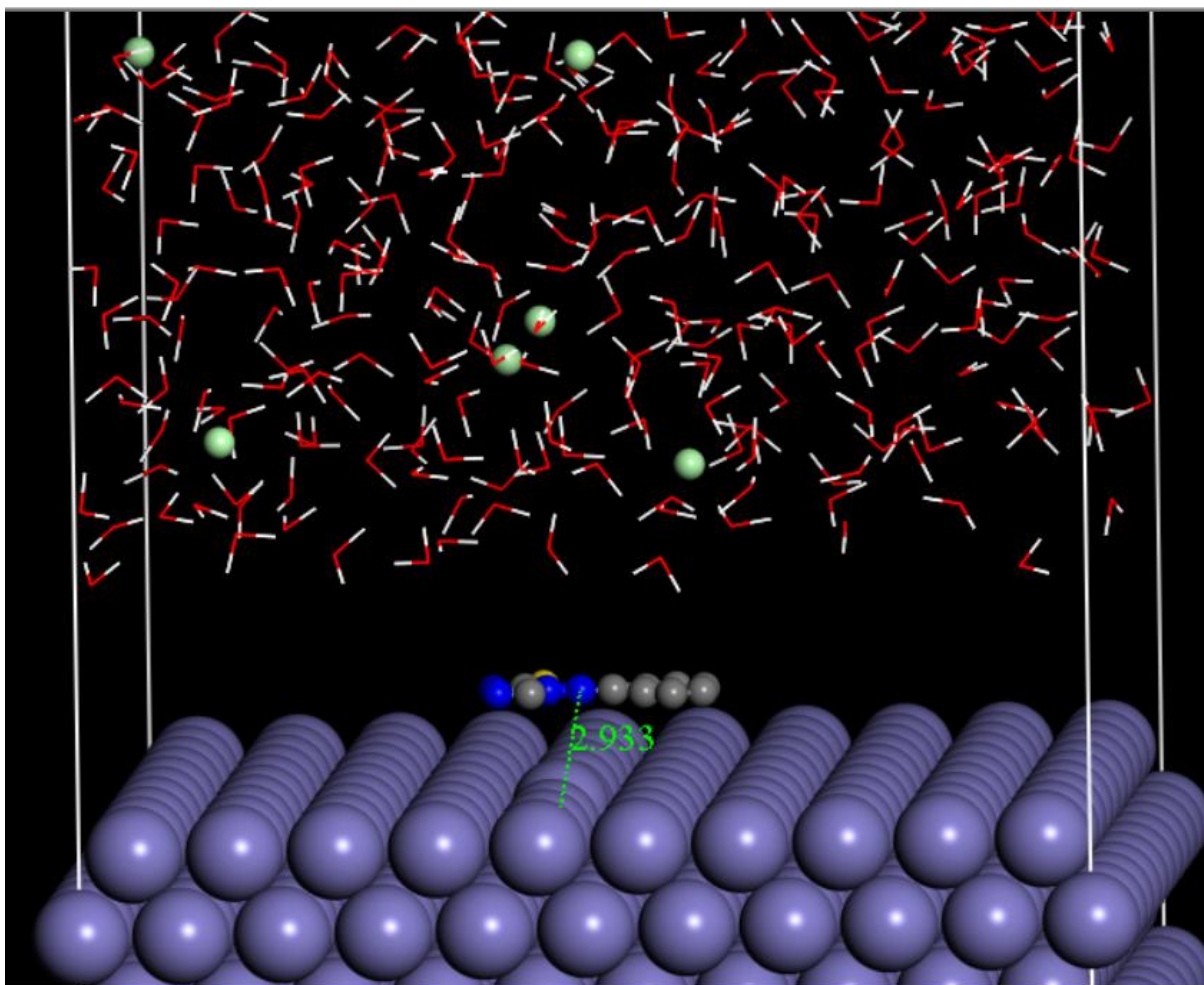
$$R^2_{pred} = 1 - \left( \frac{115.8706}{702.1735} \right)$$
$$= 0.835$$

**Table 4.17: Comparison of Experimental, Predicted and Residual %IE of Model 4.7**

Inhibitors	Experimental % IE	Predicted % IE	Residuals Values
TR-1	91.43	93.08	-1.65
TR-3	95.53	92.97	2.56
TR-4	97.48	93.81	3.67
TR-5	73	74.75	-1.75
TR-6	83.4	80.96	2.44
TR-8	87.3	85.75	1.55
TR-9	74.7	80.56	-5.86
TR-11	91	85.37	5.63
TR-12	92.9	91.09	1.81
TR-13	95.2	104.67	-9.47
TR-15	98.16	100.31	-2.15
TR-16	96.73	91.86	4.87
TR-17	93.1	87.25	5.85
TR-18	95.6	96.03	-0.43
TR-20	96.1	94.71	1.39
TR-21	92.9	95.16	-2.26
TR-22	90.2	88.04	2.16
TR-23	95	96.1	-1.1
TR-24	95	95.76	-0.76
TR-26	94.9	94.41	0.49
TR-27	58.2	62.16	-3.96
TR-29	77.57	80.98	-3.41
TR-31	94.92	94.42	0.5



**Figure 4.8: The Williams plot, the plot of standardized Residuals versus the leverage value for Triazole derivatives.**



**Figure 4.9: Equilibrium adsorption configurations of TR-1 on Fe (1 1 0) surface**

**Table 4.18: Adsorption Energy, Binding Energy, shortest bond distances and inhibition efficiencies (%IE) of the studied inhibitors, Triazoles Derivatives, (TR)**

Inhibitors	Adsorption Energy(kcal/mol)	Binding Energy(kcal/mol)	shortest bond distance(Å)	Experimental %IE
TR-1	-328.63	328.63	2.933	91.43
TR-2	-333.72	333.72	2.78	92.63
TR-3	-337.16	337.16	2.8	95.53
TR-4	-436.45	436.45	2.78	97.48
TR-5	-257.23	257.23	3.03	73
TR-6	-282.26	282.26	2.988	83.4
TR-7	-284.4	284.4	3.13	84.2
TR-8	-272	272	3.27	87.3
TR-9	-289.68	289.68	3.1	74.7
TR-10	-183.31	183.31	3.05	68.1
TR-11	-289.37	289.37	2.87	91
TR-12	-343.56	343.56	4.39	92.9
TR-13	-361.4	361.4	3.42	95.2
TR-14	-352.23	352.23	3.34	98.36
TR-15	-419.28	419.28	3.17	98.16
TR-16	-473.42	473.42	2.67	96.73
TR-17	-480.2	480.2	2.71	93.1
TR-18	-488.07	488.07	2.89	95.6

**Table 4.18: Adsorption Energy, Binding Energy, shortest bond distances and inhibition efficiencies (%IE) of the studied inhibitors, Triazoles Derivatives, (TR) (Continued)**

Inhibitors	Adsorption Energy(kcal/mol)	Binding Energy(kcal/mol)	shortest bond distance(Å)	Experimental %IE
TR-19	-443.69	443.69	2.96	95.9
TR-20	-438.95	438.95	2.86	96.1
TR-21	-465.99	465.99	3	92.9
TR-22	-481.69	481.69	2.92	90.2
TR-23	-477.92	477.92	2.78	95
TR-24	-450.01	450.01	2.8	95
TR-25	-388.4	388.4	2.78	95
TR-26	-397.09	397.09	3.03	94.9
TR-27	-230.23	230.23	2.988	58.2
TR-28	-371.07	371.07	3.13	94.7
TR-29	-286.21	286.21	3.27	77.57
TR-30	-290.23	290.23	3.1	84.11
TR-31	-373.25	373.25	3.05	94.92

## CHAPTER FIVE

### 5.0 DISCUSSION OF RESULTS

#### 5.1 Quantum Chemical studies, GFA-QSAR Derived models for %IE and molecular dynamics simulation studies of amino acids derivatives (Steel corrosion inhibitors)

Quantum chemical calculations were performed on the AM-inhibitors in order to relate their inhibition potentials to molecular structures. According to the frontier orbital approximation, donor-acceptor interactions do occur between frontiers molecular orbitals (HOMO and LUMO) of reacting species (Bereket *et al.*, 2003). The adsorption process of a corrosion inhibitor molecule onto a metal surface increases with increase of the HOMO energy (E-HOMO) and a decrease of the LUMO energy (E-LUMO). This is because, from the HOMO orbital the inhibitor molecule will donate the electrons to the *d*-orbital of the metal molecule, and the LUMO orbital of the inhibitor will receive the electrons from the *d*-orbital of the metal molecule, in-electron-donation and electron-back-donation process. Thus, E-HOMO is often associated with the electron donating ability of a molecule; high value of E-HOMO indicates the tendency of the inhibitor to donate electrons to the acceptor metal.

The optimized structures of first three AM-inhibitors by DFT calculations are displayed in Table 4.2 and both the highest occupied molecular orbital (HOMO) and lowest unoccupied molecular orbital (LUMO) were also analyzed. It can be observed from Table 4.2 that HOMOs are much more concentrated on the NH<sub>2</sub> –functional group. This suggests that the N-atom of the amino group play the more important role in donating electrons to the metal atoms when the inhibitor adsorbed on iron.

For the LUMOs are dominantly concentrated on the carboxylic part of the molecule. That is to say, the carboxylic segment of the studied AM-inhibitors has stronger electron-accepting ability than the amino group segment. All the other inhibitors of AM-series were expected to follow the same trend.

From Table 4.1 (AM-inhibitors) it can be seen that E-HOMO value decreased in the order of AM-24 > AM-22 , AM-25 > AM-23 > AM-20 > AM-21 > AM-14 > AM-13 > AM-7 > AM-5 > AM-18 > AM-8 > AM-11 > AM-19 > AM-3 > AM-6 > AM-15 > AM-4 > AM-10 > AM-2 > AM-12 > AM-1 > AM-9 > AM-17 > AM-16. Thus, AM-24 with higher HOMO energy will be the best electron donor.

On the other hand, E-LUMO indicates the ability of the inhibitor to receive electrons, lower value of E-LUMO indicates more tendency of the inhibitor to receive electrons from the donor metal (Gece and Bilgiç, 2009; Obot *et al.*, 2015). The trend at which the LUMO energies decrease follow the order AM-13 > AM-24 > AM-18 > AM-25 > AM-22 > AM-23 > AM-19 > AM-3 > AM-1 > AM-2 > AM-10 > AM-4 > AM-21 > AM-12 , 14 > AM-21 > AM-5 > AM-6 > AM-15 > AM-7, AM-20 > AM-9 > AM-17 > AM-16 > AM-11, and is consistent with the inhibition efficiencies, since as the LUMO energies decreases the %IEs increases. Based on this parameter it suggests that AM-11 is the best inhibitor with the lowest LUMO energy among the series which strongly agrees with the experimental findings as the inhibitor has the highest %IE. This suggests that the electron-donating process from the inhibitor to the metal surface is predominant over the electron-back-donation from the Fe surface to the inhibitor molecule.

Energy gap  $\Delta E$  (E-LUMO - E-HOMO) is an important parameter of a reactive inhibitor toward the adsorption on the steel surface; efficient inhibitor is characterized by a small energy gap (Ebenso *et al.*, 2012). From Table 4.1, the trend of decreasing the energy

gap with increasing % IEs is consistent with experiment, *i.e.* the energy gaps decrease as the %IEs increase from AM-1 to AM-25 in the order, AM-17 > AM-13 > AM-1 > AM-2 > AM-12 > AM-3 > AM-10 > AM-19 > AM-4 > AM-8 > AM-18 > AM-6 > AM-9 > AM-15 > AM-5 > AM-14 > AM-7 > AM-25 > AM-21 > AM-22 > AM-23 > AM-16 > AM-24 > AM-20 > AM-11. This suggest that AM-11 with the lowest energy gap of 4.68eV is the best inhibitor among the series which agrees with its high %IE of 87% obtained from the experimental observation.

Dipole moment ( $\mu$ ):The dipole moment is a descriptor of the polarity of inhibitors. Abdallah and his co-researchers in 2013 reported that dipole moment is an indicator of the electronic distribution in a molecule and is one of the properties used to rationalize molecular structure (Abdallah *et al.*, 2013). However, there is lack of general consensus on the correlation between the dipole moment and corrosion inhibition efficiency (Gao and Liang, 2007). There is an opinion that high dipole moment favors high inhibition efficiency (Tanak *et al.*, 2010), while a dissenting opinion infers conversely (Verma *et al.*, 2016). There is no general trend of relationship between the dipole moments of the studied inhibitors and experimental inhibition efficiencies. However the order of increase in dipole moment are:AM-18 > AM-16 > AM-13 > AM-12 > AM-15 > AM-17 > AM-11 > AM-7 > AM-19 > AM-2 > AM-1 > AM-3 > AM-8 > AM-20 > AM-9 > AM-24 > AM-25 > AM-10 > AM-22 > AM-21 > AM-14 > AM-4 > AM-5 > AM-28 > AM-6.

Inhibitor with the large hardness ( $\eta$ ) value is expected to be a weaker inhibitor compared to the inhibitors with lower values(Nwankwo *et al.*, 2017). From the results in table 4.1, inhibitors are arranged in descending order of hardness as: AM-17 > AM-13 > AM-1 > AM-2 > AM-12 > AM-3 > AM-10 > AM-19 > AM-4 > AM-8 > AM-6 > AM-18 > AM-9 > AM-15 > AM-5 > AM-14 > AM-7 > AM-25 > AM-21 > AM-23 > AM-22 >

AM-16 > AM-24 > AM-20 > AM-11. This suggests that AM-11 with the lowest hardness value will be the best inhibitor which may be the reason for its high %IE observed from the experiment. The ordering is in good agreement with the experimental %IEs.

Additionally, Adsorption usually occurs in the region of the molecule where chemical softness ( $\sigma$ ) has the highest value. The order across structures in the  $\sigma$  values as reported in Table 4.1 suggests that Inhibitor-11 has the highest value and therefore the most reactive inhibitor which strongly agrees with the experimental findings as the inhibitor has the highest %IE.

Global electrophilicity index ( $\omega$ ): The tendency of the inhibitor molecule to accept electron/s is also measured by this parameter. Thus, for the series AM-1 to AM-25 this parameter decreases in the following order; AM-16 > AM-17 > AM-9 > AM-11 > AM-1 > AM-12 > AM-2 > AM-15 > AM-10 > AM-6 > AM-4 > AM-3 > AM-19 > AM-8 > AM-5 > AM-7 > AM-18 > AM-14 > AM-20 > AM-13 > AM-21 > AM-23 > AM-22 > AM-25 > AM-24. We find that the inhibitor (AM-16) with relatively high inhibition efficiency exhibits higher electrophilicity index, this is in agreement with the donation and back-donation processes. These donation and back-donation processes strengthen the adsorption of the inhibitor onto the metal surface (Fuentelba *et al.*, 2000). These results are in good agreement with experimental results.

Global electronegativity ( $\chi$ ): When the AM-inhibitor is adsorbed onto an iron surface, a current of electrons will flow from the AM-inhibitor because of their lower electronegativity as compared to that of iron ( $\chi_{\text{Fe}} = 7.0 \text{ eV/mol}$ ), until the chemical potentials become equal (Lukovits *et al.*, 2001). According to Sanderson's electronegativity equalization principle, the inhibitor with high electronegativity and hence

low electronegativity difference (between the Fe and the inhibitor) will quickly reaches equalization and hence will have a low reactivity which in turn means low inhibition efficiency (Wazzan *et al.*, 2016). AM-16 > AM-17 > AM-11 > AM-9 > AM-1 > AM-12 > AM-2 > AM-15 > AM-6 > AM-10 > AM-4 > AM-3 > AM-19 > AM-5 > AM-8 > AM-7 > AM-18 > AM-14 > AM-20 > AM-21 > AM-13 > AM-23 > AM-22 > AM-25 > AM-24. Thus, AM-16 has the largest electronegativity value of 8.935eV as seen in Table (4.1), greater than that of iron. Again the inhibition efficiency of these inhibitors compared to its members of the same series is expected to be lower. Therefore, the trend of decreasing the electronegativity values totally disagree with the experimental %IEs.

Fraction of electrons transferred ( $\Delta N$ ): This value showed inhibition effect resulting from electrons donation. If  $\Delta N < 3.6$ , the inhibition efficiency increased with the increasing electron-releasing ability at the metal surface(Saha and Banerjee, 2015; Wazzan, 2015). The calculated  $\Delta N$  values for the AM-inhibitors are summarized in Table 4.1. The descending order arrangement are: AM-24 > AM-13 > AM-25 > AM-22 > AM-23 > AM-21 > AM-20 > AM-14 > AM-18 > AM-8 > AM-5 > AM-7 > AM-19 > AM-3 > AM-10 > AM-4 > AM-6 > AM-2 > AM-15 > AM-1 > AM-12 > AM-9 > AM-11 > AM-17 > AM-16. For all AM-inhibitors,  $\Delta N$  values are smaller than 3.6. This suggest that all the twenty-five inhibitors are electrons donors with varying degrees, and the steel surface is the acceptor thereby binding the inhibitor to the Fe surface resulting in inhibition adsorption layer that prevent the corrosion process.

The trends across structures in the individual quantum chemical properties discussed so far such as E-LUMO, dipole moment, energy band gap ( $\Delta E = E-LUMO - E-HOMO$ ), chemical hardness ( $\eta$ ), chemical softness ( $\sigma$ ) and electronegativity ( $\chi$ )show good

correlation with experimentally determined inhibition efficiencies of the inhibitors. So also, *E-HOMO*, global and the number of transferred electrons ( $\Delta N$ ) agree with each other.

#### 5.1.2 Quantitative structure–activity relationship (QSAR) Studies for Amino Acids Derivatives

Genetic function approximation was used on the training set to select the significant descriptors and it was found that among all the computed descriptors, Solvation Energy, Polarizability, Molecular refractivity, Balaban index  $JY$  and Vertex distance/equality construct the best model. The selected descriptors were subjected to regression analysis with the experimentally determined inhibition efficiencies as the dependent variable and the selected descriptors as the independent variables using Genetic function approximation (GFA) method in Material studio software, three new GFA equations as shown in Scheme 4.1 as model (4.1, 4.2 and 4.3) were developed on the basis of the training set.

Based on the model with the best statistical parameters identified using the parameters in Table 3.1 as standard, Model 4.1 was chosen as the best model for predicting the %IE of steel corrosion inhibitors. Model 4.1 was developed to predict the inhibition efficiency of the studied inhibitors against steel corrosion.

Furthermore, the built model from the training set was used to evaluate the predictive ability of the produced model by predicting the %IE values in the prediction set (test set). The results are given in Table 4.3 the predicted inhibition efficiency were plotted against the experimental inhibition efficiency for the training and test sets in Figure 4.1. The inhibition efficiency results obtained for both the training set (Table 4.5) and test set

(Table 4.3) are in good agreements with the experimental data obtained. The differences between predicted and experimental inhibition efficiencies (%), was minimal.

The result of the GFA QSAR model is in conformity with the standard shown in Table 3.1 as seen in model 4.1. The closeness of coefficient of determination ( $R^2$ ) to its absolute value of 1.0 is an indication that the model explained a very high percentage of the response variable (descriptor) variation, high enough for a robust QSAR model. The high adjusted  $R^2$  ( $R^2_{adj}$ ) value as seen in Scheme 4.1 and its closeness in value to the value of  $R^2$  implies that the model has excellent explanatory power to the descriptors in it. Also, the high and closeness of  $Q^2$  value to  $R^2$  revealed that the model was not over fitted. The high  $R^2_{pred}$  as calculated in Table 4.4, is an indication that the model is capable of providing valid predictions for new molecules that fall within its applicability domain.

Furthermore, the equation contains five descriptors and each descriptor has a positive or negative coefficient attached to it. These coefficients along with the value of descriptor have a significant role in deciding the overall inhibition efficiency of the inhibitor molecules. Examination of model 4.1 shows that coefficients of each descriptor play an important role in deriving the inhibition efficiency. From the point of view of inhibition of the molecules in terms of %IE values, the weight of positive coefficient is very significant because it contributes towards the increased value of %IE. So the descriptors with high weight positive coefficients are most important followed by descriptors with the low weight negative coefficient and lastly the descriptors with high weight negative coefficients (Y Wong *et al.*, 2012). On the basis of values of the coefficients on the model, the associated descriptors are arranged in a sequence pertaining

to their contribution towards overall inhibition efficiency of the inhibitors, in the following increasing order of inhibition efficiency of inhibitors towards corrosion of steel.

Balaban index  $JY$  > Molecular refractivity > Vertex distance/equality  
> Energy(Solv) > Polarizability

The leverages for each inhibitor in the dataset were plotted against their standardized residuals, leading to discovery of outliers and influential inhibitors in the model. Figure 4.2 shows the Williams plot of standardized residuals against calculated leverages for both the training and test set. The warning leverage ( $h^*$ ), was found to be 1.0 ( $N = 18$  and  $p=5$ ) for the developed QSAR model (Roy *et al.*, 2015). The inhibitors that had a standardized residual more than the standard deviation units were considered to be outliers while inhibitors with a leverage value higher than  $h^*$  were considered to be influential or high leverage inhibitors. Based on the leverages none of the inhibitors were found to be outside of the defined AD (Figure 4.2) of the QSAR model. In addition, no outlier compounds with standardized residuals  $> \pm 3d$  for the dataset were identified.

### 5.1.3 Molecular Dynamic Simulation Studies for Amino Acids Derivatives

Electronic properties alone are not sufficient to predict the trend of the inhibition performance of the investigated inhibitors in spite of its success in exploring the mechanism of inhibitors. Therefore, it is imperative to carry out rigorous modelling of the direct interaction of the inhibitors with Fe. It is generally believed that the primary mechanism of corrosion inhibition is by adsorption. The adsorption of the studied inhibitors

on the steel surface was simulated by modeling the interactions between the inhibitors and Fe(110) crystal surface in 1M HCl.

The first step of this investigation was the geometry optimization of the studied inhibitors, solvent molecules ( $\text{H}_2\text{O}$ ), hydronium ions ( $\text{H}_3\text{O}^+$ ) and chloride ions ( $\text{Cl}^-$ ). The geometry optimization of the system was performed until the total energy reached a local minimum on the potential energy surface. During the course of the geometry optimization process, atomic coordinates were adjusted based on COMPASS force field until the total energy of the individual structure reached the minimum energy, afterward, a simulation box was created by the all concerned species. Then the dynamics process was carried out, and the whole system reached equilibrium when both temperature and energy of the system were balanced. The equilibrium configurations of the simulated system for AM-1 are shown in Figure 4.3, all the other inhibitors were examined similarly. After the system reaches equilibrium adsorption and binding energy values of the surface adsorbed inhibitor molecules was calculated according to equation (3.15) and (3.16) respectively and are tabulated in Table 4.6.

It can be observed from the molecular structures of the examined inhibitors that these molecules contain various lone pair electrons on N and O atoms, as well as  $\pi$ -aromatic systems. Therefore, the lone pair electrons on heteroatoms will be donated to the empty d orbitals of iron Metal. It can be seen from Figure 4.3 that inhibitor molecule adsorb almost flatly in orientation with respect to the iron surface. This flat orientation can be explained in terms of chemical bond formation between the inhibitors and iron surface.

Generally, the bond distance within  $3.5\text{\AA}$  indicates the formation of strong chemical bond between the atoms and the bond distance above  $3.5\text{\AA}$  signifies interaction between the atoms are of Van der Waals type (Shi *et al.*, 2013; Zeng *et al.*, 2011). Figure 4.7 show the

shortest bond distance between the heteroatoms of the inhibitor and Fe atom. The measured shortest bond distances for all the studied inhibitors and Fe-surface are presented in table 4.6. From the mentioned values (Table 4.6) it is seen that all the shortest bond distances are within the range of 3.5Å, it indicates that a chemical bond is formed between the inhibitor molecule and Fe surface atom. Hence, a chemical adsorption will occur on Fe surfaces.

Additionally, it could be seen from Table 4.6 that the calculated adsorption energy values of the adsorption systems at 298 K are large and negative. These larger negative values of adsorption energies can be ascribed to the strong interaction between the studied inhibitors molecules and iron surfaces. Thus calculated adsorption energy values reveal that Am11 inhibitor molecule adsorb on the iron surface more spontaneously than any inhibitor among AM-1 to AM-25 inhibitors.

Moreover, the adsorption ability of the molecule on the iron surface can also be measured from the binding energy values. The higher is the binding energy is, the more will be the adsorption. Thus, it is further confirmed from the MD simulations that adsorption of the inhibitor molecules on the metallic surfaces mainly occurred by the chemical adsorption phenomenon, since magnitude of the binding energies is actually in the range of chemisorptive interactions ( $>100 \text{ kcal mol}^{-1}$ ) (Akalezi *et al.*, 2012). These outcomes are in good agreement with the results obtained from wet chemical experimentation as well as from quantum chemical calculations (Tang *et al.*, 2013).

## **5.2 Quantum Chemical studies, GFA Derived models for %IE and molecular dynamics simulation studies of Imidazole derivatives (Steel corrosion inhibitors)**

The results from the Table 4.8 indicate that the HOMO and LUMO orbitals are largely distributed evenly throughout molecular structure. It seems that the presence of the

benzene ring in IM molecule has a notable influence on the donor-acceptor interactions during the adsorption process.

Frontier molecular orbital energies of the studied imidazole inhibitors (E-HOMO and E-LUMO) are listed in Table 4.7. According to the frontier molecular orbital theory, a high E-HOMO value for a molecule implies the tendency of the molecule to donate electrons to the appropriate vacant d-orbital of the metal atoms (Saha and Banerjee, 2015). The higher the HOMO energy the more the probability of a molecule to donate electron to the metal. Thus, E-HOMO decreases in the order, IM-17 > IM-10 > IM-3 > IM-20 > IM-1 > IM-13 > IM-15 > IM-6 > IM-9 > IM-4 > IM-2 > IM-5 > IM-11 > IM-6 > IM-19 > IM-18 > IM-12 > IM-16 > IM-7 > IM-14. A comparison of the E-HOMO of the studied inhibitors shows that IM-17 has the highest while IM-14 has the lowest which indicates that IM-17 would be the most preferred electron donor while IM-14 would be the least preferred.

On the other hand, a low E-LUMO value for a molecule indicates the relative tendency of the molecule to accept electrons from metallic orbital during back-donation. From Table 4.7, the E-LUMO value in the descending order are: IM-10 > IM-13 > IM-15 > IM-8 > IM-12 > IM-6 > IM-7 > IM-14 > IM-9 > IM-4 > IM-5 > IM-16 > IM-19 > IM-17 > IM-20 > IM-3 > IM-18 > IM-1 > IM-2, IM-11, indicating that IM-11 has a stronger tendency to accept electrons from metallic orbital as they adsorb on iron. Therefore, IM-11 can more powerfully adsorb on the metallic surface to achieve better corrosion inhibition effectiveness.

Energy gap  $\Delta E$  (E-LUMO - E-HOMO) is an important parameter as efficient inhibitor is characterized by a small energy gap (Ebenso *et al.*, 2012). From Table 4.7, the trend of decreasing the energy gap is consistent with increasing experimental %IEs of the

studied IM-inhibitors, *i.e.* the energy gaps decrease as the %IEs increase from IM-1 to IM-20. Thus, IM-13 > IM-7 > IM-14 > IM-12 > IM-8 > IM-15 > IM-10 > IM-6 > IM-9 > IM-16 > IM-5 > IM-4 > IM-19 > IM-18 > IM-20 > IM-1 > IM-2 > IM-11 > IM-3 > IM-17. This suggest that IM-17 with the lowest energy gap of 4.47eV is the best inhibitor in term of this parameter among the series.

Dipole moment ( $\mu$ ) can give information on the polarity of a molecule. Molecules with higher value of the dipole moment have a greater tendency to interact with other molecule through electrostatic interactions (Wazzan *et al.*, 2016). Based on this parameter presented in Table 4.7., the trend of increase in the  $\mu$  follow the order: IM-20 > IM-19 > IM-18 > IM-2 > IM-11 > IM-17 > IM-3 > IM-10 > IM-5 > IM-15 > IM-4 > IM-6 > IM-8 > IM-16 > IM-7 > IM-14 > IM-1 > IM-12 > IM-9 > IM-13. IM-20 has the highest and there for the best to be adsorbed on the metallic surface.

Inhibitor with the large hardness ( $\eta$ ) value is expected to be a weaker inhibitor compared to the inhibitors with lower values. From the results in Table 4.7 the hardness value decreases in the order IM-13 > IM-7 > IM-14 > IM-12 > IM-8 > IM-15 > IM-10 > IM-6 > IM-9 > IM-16 > IM-5 > IM-4 > IM-19 > IM-18 > IM-20 > IM-1 > IM-2 > IM-11 > IM-3 > IM-17, this shows that IM-17 with the lowest value of 2.235 will be the best inhibitor and this inhibitor was found to have relatively high %IE from the experiment.

Additionally, Adsorption usually occurs in the region of the molecule where chemical softness ( $\sigma$ ) has the highest value. The order across structures in the  $\sigma$  values as reported in Table 6 decreases in the order, IM-17 > IM-2 > IM-11 > IM-3 > IM-1 > IM-20 > IM-18 > IM-19 > IM-5 > IM-4 > IM-16 > IM-9 > IM-6 > IM-10 > IM-15 > IM-18 > IM-12 > IM-7 > IM-14 > IM-10. This suggests that IM-17 has the highest and therefore the

most reactive inhibitor molecule. This observation partially agree with the trend in the inhibition efficiencies of the inhibitors.

Moreover, the tendency of the inhibitor molecule to accept electron/s is measured by global electrophilicity index ( $\omega$ ), thus, for the series IM-1 to IM-20, the values for this parameter decreases as IM-16 > IM-2 > IM-11 > IM-7 > IM-14 > IM-18 > IM-19 > IM-12 > IM-5 > IM-4 > IM-1 > IM-8 > IM-9 > IM-20 > IM-6 > IM-15 > IM-3 > IM-13 > IM-17 > IM-10. According to this parameter IM-10 with lower electrophilicity index should exhibits higher inhibition efficiency.

Furthermore, the inhibitor with high electronegativity and hence low electronegativity difference (between the Fe and the inhibitor) will quickly reaches equalization and hence will have a low reactivity which in turn means low inhibition efficiency (Saha and Banerjee, 2015). From Table 4.7 it is observed that this value decreases in the order, IM-2 > IM-11 > IM-18 > IM-19 > IM-16 > IM-1 > IM-7 > IM-14 > IM-20 > IM-12 > IM-5 > IM-4 > IM-9 > IM-8 > IM-3 > IM-6 > IM-15 > IM-17 > IM-13 > IM-10. This indicate that IM-10 with the lowest electronegativity value is the best inhibitor among the series.

$\Delta N$  value showed inhibition effect resulting from electrons donation. If  $\Delta N < 3.6\text{\AA}$ , the inhibition efficiency increases with the increasing electron-releasing ability at the metal surface (Saha and Banerjee, 2015). The calculated  $\Delta N$  values for the IM-inhibitors are summarized in Table 4.7. For all IM-inhibitors,  $\Delta N$  values are smaller than  $3.6\text{\AA}$ . It decreases in the order: IM-10 > IM-13 > IM-15 > IM-8 > IM-6 > IM-9 > IM-17 > IM-4 > IM-5 > IM-12 > IM-3 > IM-7 > IM-14 > IM-20 > IM-16 > IM-1 > IM-19 > IM-18 > IM-2 > IM-11. This suggest that of all the twenty inhibitors are electrons donors with varying

degrees, and the steel surface is the acceptor thereby binding the inhibitor to the Fe surface resulting in inhibition adsorption layer that prevent the corrosion process.

### 5.2.2 Quantitative structure–activity relationship (QSAR) Studies for Imidazole Derivatives

Three QSAR models was built and reported on the basis of the training set inhibitors, the developed models are shown in scheme 4.2 as model 4.4, 4.5 and 4.6 respectively. Based on the model with the best statistical parameters identified using the parameters in Table 3.1 as standard, Model 4.4 was chosen as the best model for predicting the %IE of steel corrosion inhibitors. The result obtained is in conformity with the standard shown in Table 3.1 as  $R^2 = 0.942$ ,  $R^2_{\text{adj}} = 0.908$ ,  $Q^2 = 0.795$ ,  $R^2_{\text{pred.}} = 0.985$ . This confirms the robustness of the model.

The closeness of coefficient of determination ( $R^2$ ) to its absolute value of 1.0 is an indication that the model has a very high percentage of the response variable (descriptor) variation, high enough for a robust QSAR model. The high adjusted  $R^2$  ( $R^2_{\text{adj}}$ ) value and its closeness in value to the value of  $R^2$  implies that the model has excellent explanatory power to the descriptors in it. Also, the high and closeness of  $Q^2$  value to  $R^2$  revealed that the model was not over fitted. The high  $R^2_{\text{pred.}}$  is an indication that the model is capable of providing valid predictions for new molecules that falls within its applicability domain.

The comparison of experimental and predicted %IEs of the test and training set inhibitors with residuals are presented in Table 4.9 and Table 4.11 respectively. Also, the high linearity of the plot of experimental against predicted %IE (Figure 4.4) also shows the high predictability of the model.

Additionally, On the basis of values of the coefficients on the model, the associated descriptors are arranged in a sequence pertaining to their contribution towards overall

inhibition efficiency of the inhibitors, in the following increasing order of inhibition efficiency of inhibitors

Ovality > E – HOMO > Polarizability > Polar surface area > Log P

Furthermore, Figure 4.5 shows the Williams plot of standardized residuals against calculated leverages for both the training and test set. The warning leverage ( $h^*$ ) = 1.2. Based on the leverages one of the inhibitor (IM-9) were found to be outside of the defined AD (Figure 4.5) of the QSAR model which is considered as influential compound. In addition, no outlier compounds with standardized residuals  $> \pm 3d$  for the dataset were identified.

### 5.2.3 Molecular Dynamic Simulation Studies for Imidazole Derivatives

Geometry optimization of the studied inhibitors, solvent molecules ( $H_2O$ ), hydronium ions ( $H_3O^+$ ) and chloride ions ( $Cl^-$ ) was carried out until the total energy reached a local minimum on the potential energy surface. During the course of the geometry optimization process, atomic coordinates were adjusted based on COMPASS force field until the total energy of the individual structure reaches the minimum energy, afterward, a simulation box was created by the all concerned species. Then the dynamics process was performed, and the whole system reached equilibrium when both temperature and energy of the system were balanced. The best adsorption configurations of the best inhibitor molecules over the Fe (1 1 0) surface are depicted in Figure 4.6. All the other

inhibitors were studied in the same way. The adsorption and binding energy values were calculated according to equation 3.15 and 3.16 and was listed in Table 4.12.

It can be observed from the molecular structures of the examined inhibitors that these molecules contain various lone pair of electrons on N and O atoms, as well as  $\pi$ -aromatic systems. Therefore, the lone pair of electrons on heteroatoms will be donated to the empty d orbitals of iron Metal. It can be seen from Figure 1 that the inhibitor adsorb almost flatly. Additionally, it could be seen in Table 4.12 that the calculated adsorption energy values of the adsorption systems at 298 K are large and negative. These larger negative values of adsorption energies can be ascribed to the strong interaction between the studied inhibitors and iron surfaces. Thus calculated adsorption energy values revealed that inhibitor (IM-6) adsorb on the iron surface more spontaneously than any other inhibitor of the series. These outcomes are in good agreement with the results obtained from wet chemical experimentation as the inhibitor has the higher inhibition efficiency(Aljourani *et al.*, 2009).

The measured short bond distances and the larger binding energy values for the studied inhibitors indicates that a chemical bond was formed between the inhibitor molecule and Fe surface atom. Thus, it is further confirmed from the MD simulations that adsorption of the inhibitor molecules on the metallic surfaces mainly occurred by the chemical adsorption phenomenon since the bond distances ( $< 3.5\text{\AA}$ ) and the magnitude of the binding energy ( $> 100\text{kcal/mol}$ ) are all within the range of chemisorptive interaction(Akalezi *et al.*, 2012).

### **5.3 Quantum Chemical studies, GFA Derived models for %IE and molecular dynamics simulation studies of Triazole derivatives (Steel corrosion inhibitors)**

Table 4.17 shows the HOMO and the LUMO for the studied TR-inhibitors. The results shows that the HOMO is spread throughout the azole moiety while the LUMO energy was concentrated on the heteroatom (N), carbon that link the azole ring to the benzene ring and on the benzene ring itself. This suggested that the nitrogen atom in the azole moiety and the benzene ring were the active sites.

From Table 4.13 it can be seen that E-HOMO value decreased in the order TR-6 > TR-13 > TR-12 > TR-14 > TR-5 > TR-16 > TR-7 > TR-15 > TR-11 > TR-29 > TR-4 > TR-8 > TR-9 > TR-30, 31 > TR-10, TR-3 > TR-2 > TR-22 > TR-23 > TR-24 > TR-26 > TR-25 > TR-1 > TR-17 > TR-18 > TR-29 > TR-19 > TR-20 > TR-27 > TR-28. This means TR-6 have the ability to donate electron to the metallic surface more than any inhibitor in the series.

The calculated E-LUMO value exemplifies that the electron acceptance capability decreased in the order TR-27 > TR-6 > TR-11 > TR-22 > TR-5 > TR-12 > TR-14 > TR-23 > TR-24 > TR-7 > TR-25 > TR-8 > TR-15 > TR-17 > TR-18 > TR-21 > TR-26 > TR-20 > TR-28 > TR-19 > TR-16 > TR-13 > TR-29 > TR-31 > TR-9 > TR-30 > TR-10 > TR-2 > TR-3 > TR-1 > TR-4. Hence, TR-4 will accept electron from the metal than any inhibitor in the series. This observation is in good agreement with the experimental findings(Wang *et al.*, 2004).

Energy gap ( $\Delta E$ ) is also an important parameter in determining adsorption of organic molecule on the metallic surface. As  $\Delta E$  decreased, reactivity of the molecule will definitely increase, which in turn would lead to an increase in adsorption onto a metallic surface. It can be seen in Table 4.13 that the decrease in  $\Delta E$  value follows the trend TR-27 > TR-28 > TR-20 > TR-21 > TR-19 > TR-18 > TR-17 > TR-23 > TR-24 > TR-25 > TR-22

> TR-26 > TR-11 > TR-8 > TR-7 > TR-5 > TR-15 > TR-14 > TR-16 > TR-12 > TR-6 > TR-31 > TR-30 > TR-10 > TR-9 > TR-29 > TR-1 > TR-2 > TR-3 > TR-13 > TR-4. This further confirmed the high inhibitive performance of TR-4 compared to other inhibitors in the series.

Dipole moment of a molecule is also an important parameter to elucidate chemical reactivity of a molecule. For this series it can be observed from Table 4.13 that dipole moment values decreased in the order TR-31 > TR-1 > TR-14 > TR-6 > TR-2 > TR-4 > TR-3 > TR-29 > TR-12 > TR-8 > TR-5 > TR-7 > TR-27 > TR-30 > TR-16 > TR-11 > TR-13 > TR-19 > TR-20 > TR-22 > TR-18 > TR-21 > TR-17 > TR-23 > TR-28 > TR-15 > TR-10 > TR-9 > TR-26 > TR-24 > TR-25. This suggest that TR-31 will be adsorbed more.

Adsorption of inhibitor molecule on the metallic surfaces also has been reported to be associated with the softness ( $\sigma$ ) of the inhibitor molecule. It can be seen from Table 4.13, that the calculated values of softness follows the trend: TR-27 > TR-28 > TR-20 > TR-21 > TR-19 > TR-18 > TR-17 TR-> 23 TR-> TR-24 > TR-25 > 22 TR-> TR-26 > TR-11 > TR-8 > TR-7 > TR-5 > TR-15 > TR-14 > 16 > TR-12 > TR-6 > TR-31 > TR-30 > TR-10 > TR-9 > TR-29 > TR-1 > TR-2 > TR-3 > TR-13 > TR-4 . This observation supports the better adsorption proficiency of TR-4 on the metal surface.

Electron transfer will happen from molecule to metal surface if  $\Delta N > 0$  and vice versa if  $\Delta N < 0$ . According to Awadet *al.* (2010), electron-donating ability of the molecule increases if  $\Delta N < 3.6$ . According to this criterion, it was observed from Table 4.13 that all the TR-inhibitors will donate electron to the metal surface since they all have  $\Delta N > 0$ . TR-4 has higher tendency to donate electrons to a metal surface among the inhibitors, because it has  $\Delta N < 3.6$ , followed by TR-1, TR-2 and TR-3. While for the other inhibitors in the

series they all have  $\Delta N$  value  $> 3.6$ . The  $\Delta N$  decreases in the order: TR-27  $>$  TR-22  $>$  TR-23  $>$  TR-24  $>$  TR-11  $>$  TR-25  $>$  TR-5  $>$  TR-6  $>$  TR-17  $>$  TR-14  $>$  TR-7  $>$  TR-18  $>$  TR-8  $>$  TR-12  $>$  TR-28  $>$  TR-21  $>$  TR-20  $>$  TR-19  $>$  TR-26  $>$  TR-15  $>$  TR-16  $>$  TR-29  $>$  TR-31  $>$  TR-30  $>$  TR-9  $>$  TR-13  $>$  TR-10  $>$  TR-2  $>$  TR-3  $>$  TR-1  $>$  TR-4. This result indicates that TR-4 inhibitor donates its electron in higher fraction than any other inhibitor of among the series and this outcomes correlate partially with the experimentally obtained inhibition efficiency.

It can be observed that TR-4 has been consistently tallying with most of this parameters and it has a very high %IE from the experiment. This suggest that TR-4 will be the best inhibitor candidate to be chose when designing new inhibitor with better inhibitive performance.

### 5.3.2 Quantitative structure–activity relationship (QSAR) Studies for Triazole Derivatives

The QSAR model 4.7 among the three models (model 4.7, 4.8 and 4.9) presented in scheme 4.3 for Triazole derivatives has good validation parameter for predictive model having squared correlation coefficient ( $R^2$ ) of 0.862, adjusted squared correlation coefficient ( $R^2_{adj}$ ) value of 0.822, Leave one out (LOO) cross validation coefficient ( $Q^2$ ) value of 0.706 and the external validation ( $R^2_{pred}$ ) of 0.835 as shown in Table 4.16.

Moreover in Tables 4.15 and 4.17, the relatively low residual, experimental and predicted inhibition efficiencies shows the high reliability and predictability of model 4.7. Also, Figure 4.7 gives the plot of experimental %IEs of both training and test sets against predicted %IEs. The linearity of the plot further confirms the reliability and predictability of the model.

The Williams plot (Figure 4.8) was exploited to visualize the model's applicability domain (AD). From the plot, it is obvious that all the inhibitors used in this work are within the domain of the model (warning leverage  $h^* = 0.783$ ) with the exception of TR-30 this is considered as an influential inhibitor. Therefore, the model gave good prediction.

On the basis of values of the coefficients on the model, the associated descriptors are arranged in a sequence pertaining to their contribution towards overall inhibition efficiency of the inhibitors, in the following increasing order of inhibition efficiency of inhibitors towards corrosion of steel.

Chi (1) > Electrophilicity index > Polar surface area  
> Subgraph counts (3): path > Element count

### 5.3.3 Molecular Dynamic Simulation Studies for Imidazole Derivatives

In order to get more suitable and adorable adsorption configuration of the studied inhibitors molecules geometry optimization was carried out on all the individual species in the system. In the course of the geometry optimization process atomic coordinates were adjusted based on COMPASS force field until the total energy of the individual structure reached the minimum energy. Afterwards a simulation box is created by the all concerned species. In this context, simulation would be completed when the temperature and energy of the system reached equilibrium.

After the system reaches equilibrium, adsorption and binding energy values of the surface adsorbed inhibitor molecules were calculated according to equation 3.15 and 3.16 respectively. The obtained E-adsorption and E-binding values are tabulated in Table 4.18.

The best adsorption configurations of the inhibitor molecules over the Fe (1 1 0) surface is depicted in Figure 4.9. It can be seen from this Figure that inhibitor molecules adsorb almost flatly in orientation with respect to the iron surface. This flat orientation can be explained in terms of chemical bond formation between the inhibitors and iron surface.

Additionally, it could be seen from Table 4.18 that the calculated adsorption energy values of the adsorption systems at 298 K are very large. These larger negative values of interaction energies can be ascribed to the strong interaction between the studied inhibitor molecules and iron surfaces. Thus calculated adsorption energy values reveal that TR-3 inhibitor adsorb on the iron surface more spontaneously than that any other inhibitor in the series.

Moreover, the adsorption ability of the molecule on the iron surface was also measured from the binding energy values and bond distances between the inhibitor and the metallic surface. The higher the binding energy, the more will be the adsorption. Thus, it can be seen from the binding energy values that the adsorption ability of the inhibitor molecules on the iron surface at 298 K follows the order of decrease in the bond distance. These outcomes are in good agreement with the results obtained from wet chemical experimentation. Hence, a chemical adsorption will occur on Fe surfaces as the binding energies are in the range of chemisorptive interaction ( $>100\text{kcal/mol}$ ) (Akalezi *et al.*, 2012). It is further confirmed from the shortest bond distances observed which are all within the range of  $3.5\text{\AA}$ , indicating a chemical bond formation between the inhibitor molecule and Fe surface atom.

#### **5.4 Comparison of the Effectiveness of AM, IM and TR in Inhibiting Corrosion of Steel**

A comparison of the inhibition effectiveness of the AM, IM and TR inhibitors indicated that their inhibition effect has been closely related to orbital energies E-HOMO, E-LUMO, dipole moment, energy band gap ( $\Delta E = E-LUMO - E-HOMO$ ), chemical hardness ( $\eta$ ), chemical softness ( $\sigma$ ), electrophilicity index ( $\omega$ ), global electronegativity ( $\chi$ ) and the number of transferred electrons ( $\Delta N$ ). Inhibition efficiency of these inhibitors show good correlation with some of these parameters as discussed in section (5.1, 5.2 and 5.3). However, TR-inhibitors show more correlation followed by AM-inhibitors with IM-inhibitors having the least correlated. Furthermore, HOMOs for all the inhibitors are much more concentrated on N-atom of the amino group, Imidazolic ring and the triazole rings. This suggests that the N-atom segments play the more important role in donating electrons to the metal atoms when the inhibitor adsorb on iron.

Correlation between experimental efficiencies obtained from the literature and the predicted QSAR model gave good correlation coefficients for all the three series. Highly significant multiple correlation coefficient ( $R^2 > 0.6$ ) was obtained between experimental and predicted efficiencies for all the proposed models. The prediction of corrosion efficiencies of these inhibitors nicely matched the experimental measurements. The differences between predicted and experimental inhibition efficiencies (%) are ranged between 1-10%, which represent the applicability of all the proposed models. The above results can be used to predict the corrosion inhibition of some analogues of the AM, IM and TR derivatives respectively. Consequently, the inhibition efficiency can be treated as a controlled property via the change of electronic properties of compounds by changing their functional groups. These correlations may be useful in designing new inhibitors by selecting the substituents on the parent molecules. QSAR approach may be used to find the

optimal group of descriptors that might predict the structure and molecule suitability to be an inhibitor.

MD simulations give a better overview on the reactivity of the studied inhibitors towards steel and are in good correlation with the experimental results obtained from the literatures for all the three series as they all prove chemical bond formation. The interaction energies between TR-inhibitors and Fe (1 1 0) plane is more negative than that between AM-Inhibitors and Fe (1 1 0) plane and IM-Inhibitors and Fe (1 1 0) plane, indicating that TR-Inhibitors can more tightly adsorb on iron surface and further that TR-Inhibitors can achieve a better corrosion inhibition effectiveness than AM-Inhibitors and IM-Inhibitors. This may be due to the large number of the heteroatoms presence in TR-inhibitors. Therefore Computational calculations using quantum chemical calculations, QSAR analysis and MD simulations approach may well be able to foretell molecule structures that are better for corrosion inhibition purposes if it is taken into account that the effect depends only on the inhibitor molecule properties.

## CHAPTER SIX

### 6.0 SUMMARY, CONCLUSION AND RECOMMENDATIONS

#### 6.1 Summary of the Findings

Quantum chemical Studies, quantitative structure–activity relationship (QSAR) analysis and molecular dynamics simulation was used to evaluate the structural, electronic and reactivity parameters of Amino acids, Imidazole and Triazole derivatives in relation to their effectiveness as corrosion inhibitors. Quantum chemical parameters such as energy of the highest occupied molecular orbital (E-HOMO), the energy of the lowest unoccupied molecular orbital (E-LUMO), energy band gap  $\Delta E$ , Dipole Moment, electrophilicity index ( $\omega$ ), chemical softness ( $\sigma$ ), chemical hardness ( $\eta$ ) and fraction of electron transfer from the inhibitors molecule to the metallic surface ( $\Delta N$ ) were obtained. QSAR model between the inhibition efficiencies and structural properties was built by the Generic function algorithm. The predictive ability of the models was judged from the prediction of the %IE of the test set inhibitors.

A comparison of statistical quality of different models indicates that model 4.1, 4.4 and 4.7 are the most significant statistically. The best linear models (model 4.1, 4.4 and 4.7 based on external validation parameter  $R^2_{pred}$ ) showed good internal and external prediction power. Furthermore, molecular dynamics simulations were performed to study

the adsorption behavior of the studied inhibitors on the Fe (1 1 0) surface and it was observed that the adsorption occurs mostly through the lone pair of electrons of the hetero-atoms (mainly N-atom for both AM, IM and TR-inhibitors) and p-electrons of the azole moiety. All values of adsorption energies, ( $E_{\text{ads}}$ ), are negative, which means that the adsorption could occur spontaneously.

## 6.2 Conclusion

A Molecular modelling approach was performed to study the corrosion inhibition performance of amino acids, imidazole and triazole derivatives on steel surface. It was evident from this investigation that theoretical studies can provide an insight into the chemical reactivity of the studied inhibitors. It also offers atomic level investigation of the experimental findings. The followings outcomes can be concluded from this study:

- i. Quantum chemical calculation reveals that electron donation and electron acceptance capability of the studied inhibitors is in good agreement with the results obtained from previously performed experimental findings.
- ii. The prediction of corrosion efficiencies of the studied inhibitors by the built QSAR models gave a very good correlation coefficients for all the three series. The robustness and applicability of the QSAR models has been established by internal and external validation techniques.
- iii. The interaction energies ( $E_{\text{ads}}$  and  $E_{\text{bind}}$ ) between the studied inhibitors and Fe (1 1 0) plane via MD-simulation were large indicating chemical bond formation and that the inhibitors can more tightly adsorb on iron surface. The order of an adsorption energy and binding energy values are in good agreement with the

experimental findings. Furthermore, MD simulation reveals that the all the shortest bond distances between the heteroatoms of the inhibitors and Fe atoms are lying within a range of  $3.5\text{\AA}$ , which indicate the formation of a chemical bond between the inhibitors and Fe atoms.

### **6.3 Recommendations**

In future design of novel corrosion inhibitors against steel, the following recommendations are made:

- i. From the results obtained in this study, it is good to carry out more computational calculations on other organic inhibitors that are less harmful to the environment to evaluate their efficiencies based on their molecular properties.
- ii. The quantum chemical calculations, QSAR analysis and MD simulations techniques used in this study should be extended to corrosion inhibition studies involving other inhibitors and metals / alloys. This is because the method is simple and effective in determining corrosion inhibition and protection.
- iii. Further work is needed to design and synthesize more efficient inhibitor against steel corrosion that will be more acceptable to the environment than the existing ones.

## References

Abdallah, M., Atwa, S., Salem, M., and Fouda, A. (2013). Synergistic effect of some halide ions on the inhibition of zinc corrosion in hydrochloric acid by tetrahydro carbazole derivatives compounds. *International Journal of Electrochemical Science*, **8**: 10001-10021.

Abdulfatai, U., Uzairu, A., and Uba, S. (2017). Quantitative structure-activity relationship and molecular docking studies of a series of quinazolinonyl analogues as inhibitors of gamma amino butyric acid aminotransferase. *Journal of advanced research*, **8(1)**: 33-43.

Accelrys, Inc., San Diego, CA, 2007.

Ahamad, I., and Quraishi, M. (2009). Bis (benzimidazol-2-yl) disulphide: an efficient water soluble inhibitor for corrosion of mild steel in acid media. *Corrosion Science*, **51(9)**: 2006-2013.

Akalezi, C. O., Enenebaku, C. K., and Oguzie, E. E. (2012). Application of aqueous extracts of coffee senna for control of mild steel corrosion in acidic environments. *International Journal of Industrial Chemistry*, **3(1)**: 13.

Al Hashem, A. (2011). Corrosion in the Gulf Cooperation Council (GCC) states: statistics and figures

Alder, B. J., and Wainwright, T. E. (1959). Studies in molecular dynamics. I. General method. *The Journal of Chemical Physics*, **31(2)**: 459-466.

Aljourani, J., Raeissi, K., and Golozar, M. (2009). Benzimidazole and its derivatives as corrosion inhibitors for mild steel in 1M HCl solution. *Corrosion Science*, **51(8)** 1836-1843.

Amin, M. A., and Ibrahim, M. M. (2011). Corrosion and corrosion control of mild steel in concentrated H<sub>2</sub>SO<sub>4</sub> solutions by a newly synthesized glycine derivative. *Corrosion Science*, **53(3)**: 873-885.

Anonymous, (2017), Word consumption of corrosion inhibitors.

www.ihsmarkit.com/products/chemical-corrosion-inhibitors-scup.html.  
Retrieved date 23<sup>rd</sup> February, 2017

- Asadollahi, T., Dadfarnia, S., Shabani, A. M. H., Ghasemi, J. B., and Sarkhosh, M. (2011). QSAR models for CXCR2 receptor antagonists based on the genetic algorithm for data preprocessing prior to application of the PLS linear regression method and design of the new compounds using in silico virtual screening. *Molecules*, **16(3)**: 1928-1955.
- Ashassi-Sorkhabi, H., Majidi, M., and Seyyedi, K. (2004). Investigation of inhibition effect of some amino acids against steel corrosion in HCl solution. *Applied surface science*, **225(1-4)**: 176-185.
- Atalay, Y., Yakuphanoglu, F., Sekerci, M., Avcı, D., and Başoğlu, A. (2006). Theoretical studies of molecular structure and vibrational spectra of 2-amino-5-phenyl-1, 3, 4-thiadiazole. *Spectrochimica Acta Part A: Molecular and Biomolecular Spectroscopy*, **64(1)**: 68-72.
- Awad, M. K., Mustafa, M. R., and Elnga, M. M. A. (2010). Computational simulation of the molecular structure of some triazoles as inhibitors for the corrosion of metal surface. *Journal of Molecular Structure: THEOCHEM*, **959(1-3)**: 66-74.
- Babić-Samardžija, K., Lupu, C., Hackerman, N., Barron, A. R., and Lutge, A. (2005). Inhibitive properties and surface morphology of a group of heterocyclic diazoles as inhibitors for acidic iron corrosion. *Langmuir*, **21(26)**: 12187-12196.
- Bazzi, L., Kertit, S., and Hamdani, M. (1995). Some organic compounds as inhibitors for the corrosion of aluminum alloy 6063 in deaerated carbonate solution. *Corrosion*, **51(11)**: 811-817.
- Becke, A. D. (1993). Density-functional thermochemistry. III. The role of exact exchange. *The Journal of Chemical Physics*, **98(7)**: 5648-5652.
- Bentiss, F., Lagrenee, M., Traisnel, M., and Hornez, J. (1999). The corrosion inhibition of mild steel in acidic media by a new triazole derivative. *Corrosion Science*, **41(4)**: 789-803.
- Bentiss, F., Traisnel, M., Vezin, H., and Lagrenée, M. (2003). Linear resistance model of the inhibition mechanism of steel in HCl by triazole and oxadiazole derivatives: structure–activity correlations. *Corrosion Science*, **45(2)**: 371-380.
- Bereket, G., Öğretir, C., and Özşahin, Ç. (2003). Quantum chemical studies on the inhibition efficiencies of some piperazine derivatives for the corrosion of steel in acidic medium. *Journal of Molecular Structure: THEOCHEM*, **663(1-3)**: 39-46.

- Brandon K., Aline O (2015). Comprehensive R archive network (CRAN). Retrieved 03, July 2015 from [http:// CRAN.R-project.org](http://CRAN.R-project.org).
- Brondel, D., Edwards, R., Hayman, A., Hill, D., Mehta, S., and Semerad, T. (1994). Corrosion in the oil industry. *Oilfield review*, **6(2)**: 4-18.
- Clark, D. S., and Varney, W. R. (1962). *Physical metallurgy for engineers*: Van Nostrand Princeton, New Jersey.
- Collins, W., Weyers, R., and Al-Qadi, I. (1993). Chemical treatment of corroding steel reinforcement after removal of chloride-contaminated concrete. *Corrosion*, **49(1)**: 74-88.
- Dafali, A., Hammouti, B., Mokhlisse, R., and Kertit, S. (2003). Substituted uracils as corrosion inhibitors for copper in 3% NaCl solution. *Corrosion Science*, **45(8)**: 1619-1630.
- de Queiroz Baddini, A. L., Cardoso, S. P., Hollauer, E., and Gomes, J. A. d. C. P. (2007). Statistical analysis of a corrosion inhibitor family on three steel surfaces (duplex, super-13 and carbon) in hydrochloric acid solutions. *Electrochimica Acta*, **53(2)**: 434-446.
- Deng, Q., Shi, H.-W., Ding, N.-N., Chen, B.-Q., He, X.-P., Liu, G., Tang, Y., Long, Y.-T., and Chen, G.-R. (2012). Novel triazolyl bis-amino acid derivatives readily synthesized via click chemistry as potential corrosion inhibitors for mild steel in HCl. *Corrosion Science*, **57**: 220-227.
- El Ashry, E. S. H., El Nemr, A., Esawy, S. A., and Ragab, S. (2006). Corrosion inhibitors- Part II: Quantum chemical studies on the corrosion inhibitions of steel in acidic medium by some triazole, oxadiazole and thiadiazole derivatives. *Electrochimica Acta*, **51(19)**, 3957-3968.
- Ebenso, E. E., Arslan, T., Kandemirli, F., Caner, N., and Love, I. (2010). Quantum chemical studies of some rhodanine azosulpha drugs as corrosion inhibitors for mild steel in acidic medium. *International Journal of Quantum Chemistry*, **110(5)**: 1003-1018.
- Ebenso, E. E., Khaled, K., Shukla, S. K., Singh, A. K., Eddy, N., Saracoglu, M., Murulana, L. C., Kandemirli, F., Arslan, T., and Obot, I. (2012). Quantum chemical investigations on quinoline derivatives as effective corrosion inhibitors for mild steel in acidic medium. *International Journal of Electrochemical Science*, **7**, 5643 - 5676
- Eddy, N., and Mamza, P. (2009). Inhibitive and adsorption properties of ethanol extract of seeds and leaves of *Azadirachta indica* on the corrosion of mild steel in H<sub>2</sub>SO<sub>4</sub>. *Portugaliae Electrochimica Acta*, **27(4)**: 443-456.

- Eddy, N. O., Awe, F. E., Gimba, C. E., Ibisi, N. O., and Ebenso, E. E. (2011). QSAR, experimental and computational chemistry simulation studies on the inhibition potentials of some amino acids for the corrosion of mild steel in 0.1 M HCl. *Int. J. Electrochem. Sci*, **6(4)**: 931-957.
- El-Haddad, M. N. (2013). Chitosan as a green inhibitor for copper corrosion in acidic medium. *International journal of biological macromolecules*, **55**, 142-149.
- El Sayed, H., El Nemr, A., Essawy, S. A., and Ragab, S. (2008). Corrosion inhibitors part V: QSAR of benzimidazole and 2-substituted derivatives as corrosion inhibitors by using the quantum chemical parameters. *Progress in Organic Coatings*, **61(1)**: 11-20.
- El Sayed, H., El Nemr, A., and Ragab, S. (2012). Quantitative structure activity relationships of some pyridine derivatives as corrosion inhibitors of steel in acidic medium. *Journal of molecular modeling*, **18(3)**: 1173-1188.
- El-Salah, K., Keddami, M., Rahmouni, K., Srhiri, A., and Takenouti, H. (2004). Aminotriazole as corrosion inhibitor of Cu<sub>30</sub>Ni alloy in 3% NaCl in presence of ammoniac. *Electrochimica Acta*, **49(17-18)**: 2771-2778.
- Ezeoke, A. U., Adeyemi, O. G., Akerele, O. A., and Obi-Egbedi, N. O. (2012). Computational and experimental studies of 4-Aminoantipyrine as corrosion inhibitor for mild steel in sulphuric acid solution. *Int. J. Electrochem. Sci*, **7**, 534-553.
- Fermi, I., Pasta, P., Ulam, S., and Tsingou, M. (1955). Studies of the nonlinear problems: Los Alamos Scientific Lab., N. Mex. pp 34
- Ferreira, E., Giacomelli, C., Giacomelli, F., and Spinelli, A. (2004). Evaluation of the inhibitor effect of L-ascorbic acid on the corrosion of mild steel. *Materials Chemistry and Physics*, **83(1)**: 129-134.
- Finšgar, M., and Jackson, J. (2016). Electrochemical Study of AISI C1018 Steel in Methanesulfonic Acid Containing an Acetylenic Alcohol-Based Corrosion Inhibitor Formulation. *Journal of laboratory automation*, **21(5)**: 632-641.
- Finšgar, M., and Milošev, I. (2010). Inhibition of copper corrosion by 1, 2, 3-benzotriazole: a review. *Corrosion Science*, **52(9)**: 2737-2749.
- Fu, J.-j., Li, S.-n., Wang, Y., and Cao, L.-h. (2010). Computational and electrochemical studies of some amino acid compounds as corrosion inhibitors for mild steel in hydrochloric acid solution. *Journal of materials science*, **45(22)**: 6255-6265.

- Fuentealba, P., Pérez, P., and Contreras, R. (2000). On the condensed Fukui function. *The Journal of Chemical Physics*, **113**(7): 2544-2551.
- Gao, G., and Liang, C. (2007). Electrochemical and DFT studies of  $\beta$ -amino-alcohols as corrosion inhibitors for brass. *Electrochimica Acta*, **52**(13): 4554-4559.
- Garcia-Arriaga, V., Alvarez-Ramirez, J., Amaya, M., and Sosa, E. (2010). H<sub>2</sub>S and O<sub>2</sub> influence on the corrosion of carbon steel immersed in a solution containing 3 M diethanolamine. *Corrosion Science*, **52**(7): 2268-2279.
- Gece, G. (2008). The use of quantum chemical methods in corrosion inhibitor studies. *Corrosion Science*, **50**(11): 2981-2992.
- Gece, G., and Bilgiç, S. (2009). Quantum chemical study of some cyclic nitrogen compounds as corrosion inhibitors of steel in NaCl media. *Corrosion Science*, **51**(8): 1876-1878.
- Gece, G., and Bilgiç, S. (2010). A theoretical study on the inhibition efficiencies of some amino acids as corrosion inhibitors of nickel. *Corrosion Science*, **52**(10): 3435-3443.
- Gholami, M., Danaee, I., Maddahy, M. H., and RashvandAvei, M. (2013). Correlated ab initio and electroanalytical study on inhibition behavior of 2-mercaptobenzothiazole and its thiole–thione tautomerism effect for the corrosion of steel (API 5L X52) in sulphuric acid solution. *Industrial & Engineering Chemistry Research*, **52**(42): 14875-14889.
- González-Olvera, R., Espinoza-Vázquez, A., Negrón-Silva, G. E., Palomar-Pardavé, M. E., Romero-Romo, M. A., and Santillan, R. (2013). Multicomponent click synthesis of new 1, 2, 3-triazole derivatives of pyrimidine nucleobases: Promising acidic corrosion inhibitors for steel. *Molecules*, **18**(12): 15064-15079.
- Gurudatt, D. M., Mohana, K. N., and Tandon, H. C. (2015). Synthesis of new 1, 2, 4-triazole derivatives and their anticorrosion properties on mild steel in hydrochloric acid medium. *Journal of Molecular Liquids*, **211**, 275-287.
- Hansch, C., and Fujita, T. (1964).  $p$ - $\sigma$ - $\pi$  Analysis. A method for the correlation of biological activity and chemical structure. *Journal of the American Chemical Society*, **86**(8): 1616-1626.
- Hluchan, V., Wheeler, B., and Hackerman, N. (1988). Amino acids as corrosion inhibitors in hydrochloric acid solutions. *Materials and Corrosion*, **39**(11): 512-517.
- Hu, P., and Dai, W. (2012). Computer simulation and density functional theory study on relationship between structure of amino acid and inhibition performance. *Materials Research Innovations*, **16**(1): 67-72.

- Jones, D. A. (1996). *Principles and prevention of corrosion*: Prentice Hall.C.P. edited. NACE, Houston. Reprinted by permission of the National Association of Corrosion Engineers. Pp 197
- Karelson, M., Lobanov, V. S., and Katritzky, A. R. (1996). Quantum-chemical descriptors in QSAR/QSPR studies. *Chemical reviews*, **96(3)**: 1027-1044.
- Kennard, R. W., and Stone, L. A. (1969). Computer aided design of experiments. *Technometrics*, **11(1)**: 137-148.
- Khaled, K. (2003). The inhibition of benzimidazole derivatives on corrosion of iron in 1 M HCl solutions. *Electrochimica Acta*, **48(17)**: 2493-2503.
- Khaled, K. (2008). Molecular simulation, quantum chemical calculations and electrochemical studies for inhibition of mild steel by triazoles. *Electrochimica Acta*, **53(9)**: 3484-3492.
- Khaled, K. (2011). Modeling corrosion inhibition of iron in acid medium by genetic function approximation method: A QSAR model. *Corrosion Science*, **53(11)**: 3457-3465.
- Khaled, K., and Hackerman, N. (2003). Investigation of the inhibitive effect of ortho-substituted anilines on corrosion of iron in 1 M HCl solutions. *Electrochimica Acta*, **48(19)**: 2715-2723.
- Kiani, M., Mousavi, M., Ghasemi, S., Shamsipur, M., and Kazemi, S. (2008). Inhibitory effect of some amino acids on corrosion of Pb–Ca–Sn alloy in sulfuric acid solution. *Corrosion Science*, **50(4)**: 1035-1045.
- Kokalj, A. (2010). Is the analysis of molecular electronic structure of corrosion inhibitors sufficient to predict the trend of their inhibition performance. *Electrochimica Acta*, **56(2)**: 745-755.
- Kraka, E., and Cremer, D. (2000). Computer design of anticancer drugs. A new enediyne warhead. *Journal of the American Chemical Society*, **122(34)**: 8245-8264.
- Kuznetsov, Y. I., and Kazansky, L. (2008). Physicochemical aspects of metal protection by azoles as corrosion inhibitors. *Russian Chemical Reviews*, **77(3)**: 219-232.
- Larif, M., Chtita, S., Adad, A., Hmamouchi, R., Bouachrine, M., and Lakhliifi, T. (2013). Predicting biological activity of Anticancer Molecules 3-ary 1-4-hydroxyquinolin-2-(1H)-one by DFT-QSAR models. *International Journal*, **3(12)**: 32-42.
- Lebrini, M., Robert, F., and Roos, C. (2011). Alkaloids extract from *Palicourea guianensis* plant as corrosion inhibitor for C38 steel in 1 M hydrochloric acid medium. *International journal of electrochemical science*, **6(3)**: 847-859.

- Levine, I. N., Busch, D. H., and Shull, H. (2000). *Quantum chemistry* (Vol. 5): Prentice Hall Upper Saddle River, NJ. 7<sup>th</sup> edition, Pp. 180.
- Li, W., Hu, L., Tao, Z., Tian, H., and Hou, B. (2011). Experimental and quantum chemical studies on two triazole derivatives as corrosion inhibitors for mild steel in acid media. *Materials and Corrosion*, **62(11)**: 1042-1050.
- Lukovits, I., Kalman, E., and Zucchi, F. (2001). Corrosion inhibitors—correlation between electronic structure and efficiency. *Corrosion*, **57(1)**: 3-8.
- Lyon, S. (2004). Materials science: A natural solution to corrosion. *Nature*, **427(6973)**: 406.
- Ma, Q., Qi, S., He, X., Tang, Y., and Lu, G. (2017). 1, 2, 3-Triazole derivatives as corrosion inhibitors for mild steel in acidic medium: Experimental and computational chemistry studies. *Corrosion Science*, **129**, 91-101.
- Martinez, S., and Metikoš-Huković, M. (2003). A nonlinear kinetic model introduced for the corrosion inhibitive properties of some organic inhibitors. *Journal of Applied Electrochemistry*, **33(12)**: 1137-1142.
- Masoud, M., Awad, M., Shaker, M., and El-Tahawy, M. (2010). The role of structural chemistry in the inhibitive performance of some aminopyrimidines on the corrosion of steel. *Corrosion Science*, **52(7)**: 2387-2396.
- Matheswaran, P., and Ramasamy, A. (2010). Influence of benzotriazole on corrosion inhibition of mild steel in citric acid medium. *Journal of Chemistry*, **7(3)**: 1090-1094.
- Moniz, B., Pollock, W. I., Gutzeit, J., Herbert, R., Schluter, J., and Siebert, O. (1986). Process industries corrosion Moniz, B.J. and Pollock edited. NACE. Houston. Reprinted by permission of the National Association of Corrosion Engineers. Pp. 312
- Moore, J. J. (2013). Chemical metallurgy. Elsevier. London. Butterworths. 7th edition, Pp 378.
- Moretti, G., Guidi, F., and Grion, G. (2004). Tryptamine as a green iron corrosion inhibitor in 0.5 M deaerated sulphuric acid. *Corrosion Science*, **46(2)**: 387-403.
- Muralidharan, S., Quraishi, M., and Iyer, S. (1995). The effect of molecular structure on hydrogen permeation and the corrosion inhibition of mild steel in acidic solutions. *Corrosion Science*, **37(11)**: 1739-1750.

- Murulana, L. C., Singh, A. K., Shukla, S. K., Kabanda, M. M., and Ebenso, E. E. (2012). Experimental and quantum chemical studies of some bis (trifluoromethyl-sulfonyl) imide imidazolium-based ionic liquids as corrosion inhibitors for mild steel in hydrochloric acid solution. *Industrial & Engineering Chemistry Research*, **51(40)**: 13282-13299.
- Musa, A. Y., Jalgham, R. T., and Mohamad, A. B. (2012). Molecular dynamic and quantum chemical calculations for phthalazine derivatives as corrosion inhibitors of mild steel in 1 M HCl. *Corrosion Science*, **56**, 176-183.
- Nimmo, B., and Hinds, G. (2003). Beginners guide to corrosion. *National Physical Library*, Pp. 200-201.
- Nwankwo, H. U., Ateba, C. N., Olasunkanmi, L. O., Adekunle, A. S., Isabirye, D. A., Onwudiwe, D. C., and Ebenso, E. E. (2016). Synthesis, characterization, antimicrobial studies and corrosion inhibition potential of 1, 8-dimethyl-1, 3, 6, 8, 10, 13-hexaazacyclotetradecane: experimental and quantum chemical studies. *Materials*, **9(2)**, 107.
- Obot, I., and Gasem, Z. (2014). Theoretical evaluation of corrosion inhibition performance of some pyrazine derivatives. *Corrosion Science*, **83**, 359-366.
- Obot, I., Macdonald, D., and Gasem, Z. (2015). Density functional theory (DFT) as a powerful tool for designing new organic corrosion inhibitors. Part 1: an overview. *Corrosion Science*, **99**, 1-30.
- Obot, I., and Obi-Egbedi, N. (2010). An interesting and efficient green corrosion inhibitor for aluminium from extracts of *Chlomolaena odorata* L. in acidic solution. *Journal of Applied Electrochemistry*, **40(11)**: 1977-1984.
- Obot, I. B. (2014). Recent advances in computational design of organic materials for corrosion protection of steel in aqueous media *Developments in corrosion protection*: InTech. Retrived may 2015 at <http://dx.doi.org/10.5772/57245>
- Osman, M., and Shalaby, M. (2003). Some ethoxylated fatty acids as corrosion inhibitors for low carbon steel in formation water. *Materials Chemistry and Physics*, **77(1)**: 261-269.
- Ouici, H., Benali, O., and Guendouzi, A. (2015). *Corrosion inhibition of mild steel in acidic media using newly synthesized heterocyclic organic molecules: Correlation between inhibition efficiency and chemical structure*. Paper presented at the AIP Conference Proceedings. Pp. 55.
- Palomar-Pardavé, M., Romero-Romo, M., Herrera-Hernández, H., Abreu-Quijano, M., Likhanova, N. V., Uruchurtu, J., and Juárez-García, J. (2012). Influence of the alkyl chain length of 2 amino 5 alkyl 1, 3, 4 thiadiazole compounds on the corrosion

- inhibition of steel immersed in sulfuric acid solutions. *Corrosion Science*, **54**, 231-243.
- Popova, A., Christov, M., and Deligeorgiev, T. (2003). Influence of the molecular structure on the inhibitor properties of benzimidazole derivatives on mild steel corrosion in 1 M hydrochloric acid. *Corrosion*, **59(9)**: 756-764.
- Popova, A., Christov, M., Raicheva, S., and Sokolova, E. (2004). Adsorption and inhibitive properties of benzimidazole derivatives in acid mild steel corrosion. *Corrosion Science*, **46(6)**: 1333-1350.
- Popova, A., Christov, M., and Zwetanova, A. (2007). Effect of the molecular structure on the inhibitor properties of azoles on mild steel corrosion in 1 M hydrochloric acid. *Corrosion Science*, **49(5)**: 2131-2143.
- Popova, A., Sokolova, E., Raicheva, S., and Christov, M. (2003). AC and DC study of the temperature effect on mild steel corrosion in acid media in the presence of benzimidazole derivatives. *Corrosion Science*, **45(1)**: 33-58.
- Pourbasheer, E., Aalizadeh, R., Ganjali, M. R., Norouzi, P., and Banaei, A. (2014). QSAR study of mGlu5 inhibitors by genetic algorithm-multiple linear regressions. *Medicinal Chemistry Research*, **23(6)**: 3082-3091.
- Quraishi, M. (2013). Electrochemical and theoretical investigation of triazole derivatives on corrosion inhibition behavior of copper in hydrochloric acid medium. *Corrosion Science*, **70**, 161-169.
- Quraishi, M., and Jamal, D. (2000). Fatty acid triazoles: novel corrosion inhibitors for oil well steel (N-80) and mild steel. *Journal of the American Oil Chemists' Society*, **77(10)**: 1107-1111.
- Quraishi, M., and Sardar, R. (2002). Aromatic triazoles as corrosion inhibitors for mild steel in acidic environments. *Corrosion*, **58(9)**: 748-755.
- Quraishi, M., Sudheer, Ansari, K., and Ebenso, E. E. (2012). 3-Aryl substituted triazole derivatives as new and effective corrosion inhibitors for mild steel in hydrochloric acid solution. *International journal of electrochemical science*, **7(8)**: 7476-7492.
- Roberge, P. R. (1999). Corrosion inhibitors. *Handbook of Corrosion Engineering*, McGraw-Hill, New York, Pp. 833.
- Roy, K., Kar, S., Das, R.N. (2015). A Primer on QSAR/QSPR Modeling Fundamental Concepts. *Springer Briefs in Molecular Science*. DOI 10.1007/978-3-319-17281.
- Saha, S. K., and Banerjee, P. (2015). A theoretical approach to understand the inhibition mechanism of steel corrosion with two aminobenzonitrile inhibitors. *RSC Advances*, **5(87)**: 71120-71130.

- Sanyal, B. (1981). Organic compounds as corrosion inhibitors in different environments—a review. *Progress in Organic Coatings*, **9(2)**: 165-236.
- Sastri, V. S. (1998). *Corrosion Inhibitors: Principles and Applications*. New York: John Wiley & Sons Ltd. West Sussex. Pp. 87-93
- Sastri, V. S. (2011). *Green Corrosion Inhibitors: Theory and Practice*. John Wiley & Sons, Inc., Hoboken, New Jersey. Pp. 173-177
- Sherif, E.-S. M. (2006). Effects of 2-amino-5-(ethylthio)-1, 3, 4-thiadiazole on copper corrosion as a corrosion inhibitor in 3% NaCl solutions. *Applied surface science*, **252(24)**: 8615-8623.
- Shi, W., Xia, M., Lei, W., and Wang, F. (2013). Molecular dynamics study of polyether polyamino methylene phosphonates as an inhibitor of anhydrite crystal. *Desalination*, **322**, 137-143.
- Silva, A., Agostinho, S., Barcia, O., Cordeiro, G., and D'elia, E. (2006). The effect of cysteine on the corrosion of 304L stainless steel in sulphuric acid. *Corrosion Science*, **48(11)**: 3668-3674.
- Singh, P., Ebenso, E. E., Olasunkanmi, L. O., Obot, I., and Quraishi, M. (2016). Electrochemical, theoretical, and surface morphological studies of corrosion inhibition effect of green naphthyridine derivatives on mild steel in hydrochloric acid. *The Journal of Physical Chemistry C*, **120(6)**: 3408-3419.
- Sun, S., Geng, Y., Tian, L., Chen, S., Yan, Y., and Hu, S. (2012). Density functional theory study of imidazole, benzimidazole and 2-mercaptobenzimidazole adsorption onto clean Cu (1 1 1) surface. *Corrosion Science*, **63**, 140-147.
- Szklarska-Smialowska, Z., and ZS-Smialowska. (2005). *Pitting and crevice corrosion*: NACE International 15835 Park Ten Pl, Houston, TX 77084, USA. Pp. 165
- Tanak, H., Ađar, A., and Yavuz, M. (2010). Experimental and quantum chemical calculational studies on 2-[(4-Fluorophenylimino) methyl]-3, 5-dimethoxyphenol. *Journal of molecular modeling*, **16(3)**: 577-587.
- Tang, Y., Zhang, F., Hu, S., Cao, Z., Wu, Z., and Jing, W. (2013). Novel benzimidazole derivatives as corrosion inhibitors of mild steel in the acidic media. Part I: gravimetric, electrochemical, SEM and XPS studies. *Corrosion Science*, **74**, 271-282.
- Taylor, C., Chandra, A., Vera, J., and Sridhar, N. (2015). Multiphysics modelling, quantum chemistry and risk analysis for corrosion inhibitor design and lifetime prediction. *Faraday discussions*, **180**, 459-477.

- Tong, W., Hong, H., Xie, Q., Shi, L., Fang, H., and Perkins, R. (2005). Assessing QSAR limitations-A regulatory perspective. *Current Computer-Aided Drug Design*, **1(2)**: 195-205.
- Tropsha, A., Gramatica, P., and Gombar, V. K. (2003). The importance of being earnest: validation is the absolute essential for successful application and interpretation of QSPR models. *Molecular Informatics*, **22(1)**: 69-77.
- Veerasingh, R., Rajak, H., Jain, A., Sivadasan, S., Varghese, C. P., and Agrawal, R. K. (2011). Validation of QSAR models-strategies and importance. *International Journal of Drug Design & Discovery*, **3**, 511-519.
- Verma, C., Olasunkanmi, L. O., Ebenso, E. E., Quraishi, M. A., and Obot, I. B. (2016). Adsorption behavior of glucosamine-based, pyrimidine-fused heterocycles as green corrosion inhibitors for mild steel: experimental and theoretical studies. *The Journal of Physical Chemistry C*, **120(21)**: 11598-11611.
- Vosta, J., and Eliasek, J. (1971). Study on corrosion inhibition from aspect of quantum chemistry. *Corrosion Science*, **11(4)**: 223-229.
- Wang, H.-L., Liu, R.-B., and Xin, J. (2004). Inhibiting effects of some mercapto-triazole derivatives on the corrosion of mild steel in 1.0 M HCl medium. *Corrosion Science*, **46(10)**: 2455-2466.
- Wazzan, N. A. (2015). DFT calculations of thiosemicarbazide, arylisothiocyanates, and 1-aryl-2, 5-dithiohydrazodicarbonamides as corrosion inhibitors of copper in an aqueous chloride solution. *Journal of Industrial and Engineering Chemistry*, **26**, 291-308.
- Wazzan, N. A., Obot, I., and Kaya, S. (2016). Theoretical modeling and molecular level insights into the corrosion inhibition activity of 2-amino-1, 3, 4-thiadiazole and its 5-alkyl derivatives. *Journal of Molecular Liquids*, **221**, 579-602.
- Wu, W., Zhang, C., Lin, W., Chen, Q., Guo, X., Qian, Y., and Zhang, L. (2015). Quantitative structure-property relationship (QSPR) modeling of drug-loaded polymeric micelles via genetic function approximation. *PloS one*, **10(3)**: e0119575.
- Wymysłowski, A., Iwamoto, N., Yuen, M. M. F., and Fan, H. (2014). *Molecular Modeling and Multiscaling Issues for Electronic Material Applications*, Springer, Spring Street, New York, 2, 234
- Xia, S., Qiu, M., Yu, L., Liu, F., and Zhao, H. (2008). Molecular dynamics and density functional theory study on relationship between structure of imidazoline derivatives and inhibition performance. *Corrosion Science*, **50(7)**: 2021-2029.

- Y Wong, K., R Duchowicz, P., G Mercader, A., and A Castro, E. (2012). QSAR applications during last decade on inhibitors of acetylcholinesterase in Alzheimer's disease. *Mini reviews in medicinal chemistry*, **12(10)**: 936-946.
- Yaro, A. S., Khadom, A. A., and Wael, R. K. (2013). Apricot juice as green corrosion inhibitor of mild steel in phosphoric acid. *Alexandria Engineering Journal*, **52(1)**: 129-135.
- Zeng, J., Zhang, J., and Gong, X. (2011). Molecular dynamics simulation of interaction between benzotriazoles and cuprous oxide crystal. *Computational and Theoretical Chemistry*, **963(1)**: 110-114.
- Zerfaoui, M., Oudda, H., Hammouti, B., Kertit, S., and Benkaddour, M. (2004). Inhibition of corrosion of iron in citric acid media by aminoacids. *Progress in Organic Coatings*, **51(2)**: 134-138.
- Zhang, S., Lei, W., Xia, M., and Wang, F. (2005). QSAR study on N-containing corrosion inhibitors: quantum chemical approach assisted by topological index. *Journal of Molecular Structure: THEOCHEM*, **732(1-3)**: 173-182.
- Zhao, H., Zhang, X., Ji, L., Hu, H., and Li, Q. (2014). Quantitative structure–activity relationship model for amino acids as corrosion inhibitors based on the support vector machine and molecular design. *Corrosion Science*, **83**, 261-271.

# ***THE END***

Abdallah, M., Atwa, S., Salem, M., and Fouda, A. (2013). Synergistic effect of some halide ions on the inhibition of zinc corrosion in hydrochloric acid by tetrahydro carbazole derivatives compounds. *International Journal of Electrochemical Science*, **8**: 10001-10021.

Abdulfatai, U., Uzairu, A., and Uba, S. (2017). Quantitative structure-activity relationship and molecular docking studies of a series of quinazolinonyl analogues as inhibitors of gamma amino butyric acid aminotransferase. *Journal of advanced research*, **8**(1): 33-43.

Accelrys, Inc., San Diego, CA, 2007.

Ahamad, I., and Quraishi, M. (2009). Bis (benzimidazol-2-yl) disulphide: an efficient water soluble inhibitor for corrosion of mild steel in acid media. *Corrosion Science*, **51**(9): 2006-2013.

Akalezi, C. O., Enenebaku, C. K., and Oguzie, E. E. (2012). Application of aqueous extracts of coffee senna for control of mild steel corrosion in acidic environments. *International Journal of Industrial Chemistry*, **3**(1): 13.

Al Hashem, A. (2011). Corrosion in the Gulf Cooperation Council (GCC) states: statistics and figures

Alder, B. J., and Wainwright, T. E. (1959). Studies in molecular dynamics. I. General method. *The Journal of Chemical Physics*, **31**(2): 459-466.

Aljourani, J., Raeissi, K., and Golozar, M. (2009). Benzimidazole and its derivatives as corrosion inhibitors for mild steel in 1M HCl solution. *Corrosion Science*, **51**(8) 1836-1843.

Amin, M. A., and Ibrahim, M. M. (2011). Corrosion and corrosion control of mild steel in concentrated H<sub>2</sub>SO<sub>4</sub> solutions by a newly synthesized glycine derivative. *Corrosion Science*, **53**(3): 873-885.

Anonymous, (2017): [www.ihsmarket.com/products/chemical-corrosion-inhibitors-scup.html](http://www.ihsmarket.com/products/chemical-corrosion-inhibitors-scup.html). Retrieved date 23<sup>rd</sup> February, 2017

- Asadollahi, T., Dadfarnia, S., Shabani, A. M. H., Ghasemi, J. B., and Sarkhosh, M. (2011). QSAR models for CXCR2 receptor antagonists based on the genetic algorithm for data preprocessing prior to application of the PLS linear regression method and design of the new compounds using in silico virtual screening. *Molecules*, **16(3)**: 1928-1955.
- Ashassi-Sorkhabi, H., Majidi, M., and Seyyedi, K. (2004). Investigation of inhibition effect of some amino acids against steel corrosion in HCl solution. *Applied surface science*, **225(1-4)**: 176-185.
- Atalay, Y., Yakuphanoglu, F., Sekerci, M., Avcı, D., and Başoğlu, A. (2006). Theoretical studies of molecular structure and vibrational spectra of 2-amino-5-phenyl-1, 3, 4-thiadiazole. *Spectrochimica Acta Part A: Molecular and Biomolecular Spectroscopy*, **64(1)**: 68-72.
- Awad, M. K., Mustafa, M. R., and Elnga, M. M. A. (2010). Computational simulation of the molecular structure of some triazoles as inhibitors for the corrosion of metal surface. *Journal of Molecular Structure: THEOCHEM*, **959(1-3)**: 66-74.
- Babić-Samardžija, K., Lupu, C., Hackerman, N., Barron, A. R., and Luttge, A. (2005). Inhibitive properties and surface morphology of a group of heterocyclic diazoles as inhibitors for acidic iron corrosion. *Langmuir*, **21(26)**: 12187-12196.
- Bazzi, L., Kertit, S., and Hamdani, M. (1995). Some organic compounds as inhibitors for the corrosion of aluminum alloy 6063 in deaerated carbonate solution. *Corrosion*, **51(11)**: 811-817.
- Becke, A. D. (1993). Density-functional thermochemistry. III. The role of exact exchange. *The Journal of Chemical Physics*, **98(7)**: 5648-5652.
- Bentiss, F., Lagrenée, M., Traisnel, M., and Hornez, J. (1999). The corrosion inhibition of mild steel in acidic media by a new triazole derivative. *Corrosion Science*, **41(4)**: 789-803.
- Bentiss, F., Traisnel, M., Vezin, H., and Lagrenée, M. (2003). Linear resistance model of the inhibition mechanism of steel in HCl by triazole and oxadiazole derivatives: structure–activity correlations. *Corrosion Science*, **45(2)**: 371-380.
- Bereket, G., Öğretir, C., and Özşahin, Ç. (2003). Quantum chemical studies on the inhibition efficiencies of some piperazine derivatives for the corrosion of steel in acidic medium. *Journal of Molecular Structure: THEOCHEM*, **663(1-3)**: 39-46.
- Brandon K., Aline O (2015). Comprehensive R archive network (CRAN). Retrieved 03, July 2015 from <http://CRAN.R-project.org>.

- Brondel, D., Edwards, R., Hayman, A., Hill, D., Mehta, S., and Semerad, T. (1994). Corrosion in the oil industry. *Oilfield review*, **6(2)**: 4-18.
- Clark, D. S., and Varney, W. R. (1962). *Physical metallurgy for engineers*: Van Nostrand Princeton, New Jersey.
- Collins, W., Weyers, R., and Al-Qadi, I. (1993). Chemical treatment of corroding steel reinforcement after removal of chloride-contaminated concrete. *Corrosion*, **49(1)**: 74-88.
- Dafali, A., Hammouti, B., Mokhlisse, R., and Kertit, S. (2003). Substituted uracils as corrosion inhibitors for copper in 3% NaCl solution. *Corrosion Science*, **45(8)**: 1619-1630.
- de Queiroz Baddini, A. L., Cardoso, S. P., Hollauer, E., and Gomes, J. A. d. C. P. (2007). Statistical analysis of a corrosion inhibitor family on three steel surfaces (duplex, super-13 and carbon) in hydrochloric acid solutions. *Electrochimica Acta*, **53(2)**: 434-446.
- Deng, Q., Shi, H.-W., Ding, N.-N., Chen, B.-Q., He, X.-P., Liu, G., Tang, Y., Long, Y.-T., and Chen, G.-R. (2012). Novel triazolyl bis-amino acid derivatives readily synthesized via click chemistry as potential corrosion inhibitors for mild steel in HCl. *Corrosion Science*, **57**: 220-227.
- El Ashry, E. S. H., El Nemr, A., Esawy, S. A., and Ragab, S. (2006). Corrosion inhibitors-Part II: Quantum chemical studies on the corrosion inhibitions of steel in acidic medium by some triazole, oxadiazole and thiadiazole derivatives. *Electrochimica Acta*, **51(19)**, 3957-3968.
- Ebenso, E. E., Arslan, T., Kandemirli, F., Caner, N., and Love, I. (2010). Quantum chemical studies of some rhodanine azosulpha drugs as corrosion inhibitors for mild steel in acidic medium. *International Journal of Quantum Chemistry*, **110(5)**: 1003-1018.
- Ebenso, E. E., Khaled, K., Shukla, S. K., Singh, A. K., Eddy, N., Saracoglu, M., Murulana, L. C., Kandemirli, F., Arslan, T., and Obot, I. (2012). Quantum chemical investigations on quinoline derivatives as effective corrosion inhibitors for mild steel in acidic medium. *International Journal of Electrochemical Science*, **7**, 5643 - 5676
- Eddy, N., and Mamza, P. (2009). Inhibitive and adsorption properties of ethanol extract of seeds and leaves of *Azadirachta indica* on the corrosion of mild steel in H<sub>2</sub>SO<sub>4</sub>. *Portugaliae Electrochimica Acta*, **27(4)**: 443-456.
- Eddy, N. O., Awe, F. E., Gimba, C. E., Ibisi, N. O., and Ebenso, E. E. (2011). QSAR, experimental and computational chemistry simulation studies on the inhibition

- potentials of some amino acids for the corrosion of mild steel in 0.1 M HCl. *Int. J. Electrochem. Sci*, **6(4)**: 931-957.
- El-Haddad, M. N. (2013). Chitosan as a green inhibitor for copper corrosion in acidic medium. *International journal of biological macromolecules*, **55**, 142-149.
- El Sayed, H., El Nemr, A., Essawy, S. A., and Ragab, S. (2008). Corrosion inhibitors part V: QSAR of benzimidazole and 2-substituted derivatives as corrosion inhibitors by using the quantum chemical parameters. *Progress in Organic Coatings*, **61(1)**: 11-20.
- El Sayed, H., El Nemr, A., and Ragab, S. (2012). Quantitative structure activity relationships of some pyridine derivatives as corrosion inhibitors of steel in acidic medium. *Journal of molecular modeling*, **18(3)**: 1173-1188.
- El-Salah, K., Keddam, M., Rahmouni, K., Srhiri, A., and Takenouti, H. (2004). Aminotriazole as corrosion inhibitor of Cu<sub>30</sub>Ni alloy in 3% NaCl in presence of ammoniac. *Electrochimica Acta*, **49(17-18)**: 2771-2778.
- Ezeoke, A. U., Adeyemi, O. G., Akerele, O. A., and Obi-Egbedi, N. O. (2012). Computational and experimental studies of 4-Aminoantipyrine as corrosion inhibitor for mild steel in sulphuric acid solution. *Int. J. Electrochem. Sci*, **7**, 534-553.
- Fermi, I., Pasta, P., Ulam, S., and Tsingou, M. (1955). Studies of the nonlinear problems: Los Alamos Scientific Lab., N. Mex.
- Ferreira, E., Giacomelli, C., Giacomelli, F., and Spinelli, A. (2004). Evaluation of the inhibitor effect of L-ascorbic acid on the corrosion of mild steel. *Materials Chemistry and Physics*, **83(1)**: 129-134.
- Finšgar, M., and Jackson, J. (2016). Electrochemical Study of AISI C1018 Steel in Methanesulfonic Acid Containing an Acetylenic Alcohol-Based Corrosion Inhibitor Formulation. *Journal of laboratory automation*, **21(5)**: 632-641.
- Finšgar, M., and Milošev, I. (2010). Inhibition of copper corrosion by 1, 2, 3-benzotriazole: a review. *Corrosion Science*, **52(9)**: 2737-2749.
- Fu, J.-j., Li, S.-n., Wang, Y., and Cao, L.-h. (2010). Computational and electrochemical studies of some amino acid compounds as corrosion inhibitors for mild steel in hydrochloric acid solution. *Journal of materials science*, **45(22)**: 6255-6265.
- Fuentealba, P., Pérez, P., and Contreras, R. (2000). On the condensed Fukui function. *The Journal of Chemical Physics*, **113(7)**: 2544-2551.

- Gao, G., and Liang, C. (2007). Electrochemical and DFT studies of  $\beta$ -amino-alcohols as corrosion inhibitors for brass. *Electrochimica Acta*, **52(13)**: 4554-4559.
- Garcia-Arriaga, V., Alvarez-Ramirez, J., Amaya, M., and Sosa, E. (2010). H<sub>2</sub>S and O<sub>2</sub> influence on the corrosion of carbon steel immersed in a solution containing 3 M diethanolamine. *Corrosion Science*, **52(7)**: 2268-2279.
- Gece, G. (2008). The use of quantum chemical methods in corrosion inhibitor studies. *Corrosion Science*, **50(11)**: 2981-2992.
- Gece, G., and Bilgiç, S. (2009). Quantum chemical study of some cyclic nitrogen compounds as corrosion inhibitors of steel in NaCl media. *Corrosion Science*, **51(8)**: 1876-1878.
- Gece, G., and Bilgiç, S. (2010). A theoretical study on the inhibition efficiencies of some amino acids as corrosion inhibitors of nickel. *Corrosion Science*, **52(10)**: 3435-3443.
- Gholami, M., Danaee, I., Maddahy, M. H., and RashvandAvei, M. (2013). Correlated ab initio and electroanalytical study on inhibition behavior of 2-mercaptobenzothiazole and its thiole–thione tautomerism effect for the corrosion of steel (API 5L X52) in sulphuric acid solution. *Industrial & Engineering Chemistry Research*, **52(42)**: 14875-14889.
- González-Olvera, R., Espinoza-Vázquez, A., Negrón-Silva, G. E., Palomar-Pardavé, M. E., Romero-Romo, M. A., and Santillan, R. (2013). Multicomponent click synthesis of new 1, 2, 3-triazole derivatives of pyrimidine nucleobases: Promising acidic corrosion inhibitors for steel. *Molecules*, **18(12)**: 15064-15079.
- Gurudatt, D. M., Mohana, K. N., and Tandon, H. C. (2015). Synthesis of new 1, 2, 4-triazole derivatives and their anticorrosion properties on mild steel in hydrochloric acid medium. *Journal of Molecular Liquids*, **211**, 275-287.
- Hansch, C., and Fujita, T. (1964).  $\rho$ - $\sigma$ - $\pi$  Analysis. A method for the correlation of biological activity and chemical structure. *Journal of the American Chemical Society*, **86(8)**: 1616-1626.
- Hluchan, V., Wheeler, B., and Hackerman, N. (1988). Amino acids as corrosion inhibitors in hydrochloric acid solutions. *Materials and Corrosion*, **39(11)**: 512-517.
- Hu, P., and Dai, W. (2012). Computer simulation and density functional theory study on relationship between structure of amino acid and inhibition performance. *Materials Research Innovations*, **16(1)**: 67-72.
- Jones, D. A. (1996). *Principles and prevention of corrosion*: Prentice Hall.

- Karelson, M., Lobanov, V. S., and Katritzky, A. R. (1996). Quantum-chemical descriptors in QSAR/QSPR studies. *Chemical reviews*, **96(3)**: 1027-1044.
- Kennard, R. W., and Stone, L. A. (1969). Computer aided design of experiments. *Technometrics*, **11(1)**: 137-148.
- Khaled, K. (2003). The inhibition of benzimidazole derivatives on corrosion of iron in 1 M HCl solutions. *Electrochimica Acta*, **48(17)**: 2493-2503.
- Khaled, K. (2008). Molecular simulation, quantum chemical calculations and electrochemical studies for inhibition of mild steel by triazoles. *Electrochimica Acta*, **53(9)**: 3484-3492.
- Khaled, K. (2011). Modeling corrosion inhibition of iron in acid medium by genetic function approximation method: A QSAR model. *Corrosion Science*, **53(11)**: 3457-3465.
- Khaled, K., and Hackerman, N. (2003). Investigation of the inhibitive effect of ortho-substituted anilines on corrosion of iron in 1 M HCl solutions. *Electrochimica Acta*, **48(19)**: 2715-2723.
- Kiani, M., Mousavi, M., Ghasemi, S., Shamsipur, M., and Kazemi, S. (2008). Inhibitory effect of some amino acids on corrosion of Pb–Ca–Sn alloy in sulfuric acid solution. *Corrosion Science*, **50(4)**: 1035-1045.
- Kokalj, A. (2010). Is the analysis of molecular electronic structure of corrosion inhibitors sufficient to predict the trend of their inhibition performance. *Electrochimica Acta*, **56(2)**: 745-755.
- Kraka, E., and Cremer, D. (2000). Computer design of anticancer drugs. A new enediyne warhead. *Journal of the American Chemical Society*, **122(34)**: 8245-8264.
- Kuznetsov, Y. I., and Kazansky, L. (2008). Physicochemical aspects of metal protection by azoles as corrosion inhibitors. *Russian Chemical Reviews*, **77(3)**: 219-232.
- Larif, M., Chtita, S., Adad, A., Hmamouchi, R., Bouachrine, M., and Lakhlifi, T. (2013). Predicting biological activity of Anticancer Molecules 3-ary 1-4-hydroxyquinolin-2-(1H)-one by DFT-QSAR models. *International Journal*, **3(12)**: 32-42.
- Lebrini, M., Robert, F., and Roos, C. (2011). Alkaloids extract from *Palicourea guianensis* plant as corrosion inhibitor for C38 steel in 1 M hydrochloric acid medium. *International journal of electrochemical science*, **6(3)**: 847-859.
- Levine, I. N., Busch, D. H., and Shull, H. (2000). *Quantum chemistry* (Vol. 5): Prentice Hall Upper Saddle River, NJ.

- Li, W., Hu, L., Tao, Z., Tian, H., and Hou, B. (2011). Experimental and quantum chemical studies on two triazole derivatives as corrosion inhibitors for mild steel in acid media. *Materials and Corrosion*, **62(11)**: 1042-1050.
- Lukovits, I., Kalman, E., and Zucchi, F. (2001). Corrosion inhibitors—correlation between electronic structure and efficiency. *Corrosion*, **57(1)**: 3-8.
- Lyon, S. (2004). Materials science: A natural solution to corrosion? *Nature*, **427(6973)**: 406.
- Ma, Q., Qi, S., He, X., Tang, Y., and Lu, G. (2017). 1, 2, 3-Triazole derivatives as corrosion inhibitors for mild steel in acidic medium: Experimental and computational chemistry studies. *Corrosion Science*, **129**, 91-101.
- Martinez, S., and Metikoš-Huković, M. (2003). A nonlinear kinetic model introduced for the corrosion inhibitive properties of some organic inhibitors. *Journal of Applied Electrochemistry*, **33(12)**: 1137-1142.
- Masoud, M., Awad, M., Shaker, M., and El-Tahawy, M. (2010). The role of structural chemistry in the inhibitive performance of some aminopyrimidines on the corrosion of steel. *Corrosion Science*, **52(7)**: 2387-2396.
- Matheswaran, P., and Ramasamy, A. (2010). Influence of benzotriazole on corrosion inhibition of mild steel in citric acid medium. *Journal of Chemistry*, **7(3)**: 1090-1094.
- Moniz, B., Pollock, W. I., Gutzeit, J., Herbert, R., Schluter, J., and Siebert, O. (1986). Process industries corrosion Moniz, B.J. and Pollock edited. NACE. Houston. Reprinted by permission of the National Association of Corrosion Engineers.
- Moore, J. J. (2013). *Chemical metallurgy*: Elsevier.
- Moretti, G., Guidi, F., and Grion, G. (2004). Tryptamine as a green iron corrosion inhibitor in 0.5 M deaerated sulphuric acid. *Corrosion Science*, **46(2)**: 387-403.
- Muralidharan, S., Quraishi, M., and Iyer, S. (1995). The effect of molecular structure on hydrogen permeation and the corrosion inhibition of mild steel in acidic solutions. *Corrosion Science*, **37(11)**: 1739-1750.
- Murulana, L. C., Singh, A. K., Shukla, S. K., Kabanda, M. M., and Ebenso, E. E. (2012). Experimental and quantum chemical studies of some bis (trifluoromethyl-sulfonyl) imide imidazolium-based ionic liquids as corrosion inhibitors for mild steel in hydrochloric acid solution. *Industrial & Engineering Chemistry Research*, **51(40)**: 13282-13299.

- Musa, A. Y., Jalgham, R. T., and Mohamad, A. B. (2012). Molecular dynamic and quantum chemical calculations for phthalazine derivatives as corrosion inhibitors of mild steel in 1 M HCl. *Corrosion Science*, **56**, 176-183.
- Nimmo, B., and Hinds, G. (2003). Beginners guide to corrosion. *National Physical Library*, 200-201.
- Nwankwo, H. U., Ateba, C. N., Olasunkanmi, L. O., Adekunle, A. S., Isabirye, D. A., Onwudiwe, D. C., and Ebenso, E. E. (2016). Synthesis, characterization, antimicrobial studies and corrosion inhibition potential of 1, 8-dimethyl-1, 3, 6, 8, 10, 13-hexaazacyclotetradecane: experimental and quantum chemical studies. *Materials*, **9(2)**, 107.
- Obot, I., and Gasem, Z. (2014). Theoretical evaluation of corrosion inhibition performance of some pyrazine derivatives. *Corrosion Science*, **83**, 359-366.
- Obot, I., Macdonald, D., and Gasem, Z. (2015). Density functional theory (DFT) as a powerful tool for designing new organic corrosion inhibitors. Part 1: an overview. *Corrosion Science*, **99**, 1-30.
- Obot, I., and Obi-Egbedi, N. (2010). An interesting and efficient green corrosion inhibitor for aluminium from extracts of *Chlomolaena odorata* L. in acidic solution. *Journal of Applied Electrochemistry*, **40(11)**: 1977-1984.
- Obot, I. B. (2014). Recent advances in computational design of organic materials for corrosion protection of steel in aqueous media *Developments in corrosion protection*: InTech. Retrived may 2015 at <http://dx.doi.org/10.5772/57245>
- Osman, M., and Shalaby, M. (2003). Some ethoxylated fatty acids as corrosion inhibitors for low carbon steel in formation water. *Materials Chemistry and Physics*, **77(1)**: 261-269.
- Ouici, H., Benali, O., and Guendouzi, A. (2015). *Corrosion inhibition of mild steel in acidic media using newly synthesized heterocyclic organic molecules: Correlation between inhibition efficiency and chemical structure*. Paper presented at the AIP Conference Proceedings.
- Palomar-Pardavé, M., Romero-Romo, M., Herrera-Hernández, H., Abreu-Quijano, M., Likhanova, N. V., Uruchurtu, J., and Juárez-García, J. (2012). Influence of the alkyl chain length of 2 amino 5 alkyl 1, 3, 4 thiadiazole compounds on the corrosion inhibition of steel immersed in sulfuric acid solutions. *Corrosion Science*, **54**, 231-243.
- Popova, A., Christov, M., and Deligeorgiev, T. (2003). Influence of the molecular structure on the inhibitor properties of benzimidazole derivatives on mild steel corrosion in 1 M hydrochloric acid. *Corrosion*, **59(9)**: 756-764.

- Popova, A., Christov, M., Raicheva, S., and Sokolova, E. (2004). Adsorption and inhibitive properties of benzimidazole derivatives in acid mild steel corrosion. *Corrosion Science*, **46(6)**: 1333-1350.
- Popova, A., Christov, M., and Zwetanova, A. (2007). Effect of the molecular structure on the inhibitor properties of azoles on mild steel corrosion in 1 M hydrochloric acid. *Corrosion Science*, **49(5)**: 2131-2143.
- Popova, A., Sokolova, E., Raicheva, S., and Christov, M. (2003). AC and DC study of the temperature effect on mild steel corrosion in acid media in the presence of benzimidazole derivatives. *Corrosion Science*, **45(1)**: 33-58.
- Pourbasheer, E., Aalizadeh, R., Ganjali, M. R., Norouzi, P., and Banaei, A. (2014). QSAR study of mGlu5 inhibitors by genetic algorithm-multiple linear regressions. *Medicinal Chemistry Research*, **23(6)**: 3082-3091.
- Quraishi, M. (2013). Electrochemical and theoretical investigation of triazole derivatives on corrosion inhibition behavior of copper in hydrochloric acid medium. *Corrosion Science*, **70**, 161-169.
- Quraishi, M., and Jamal, D. (2000). Fatty acid triazoles: novel corrosion inhibitors for oil well steel (N-80) and mild steel. *Journal of the American Oil Chemists' Society*, **77(10)**: 1107-1111.
- Quraishi, M., and Sardar, R. (2002). Aromatic triazoles as corrosion inhibitors for mild steel in acidic environments. *Corrosion*, **58(9)**: 748-755.
- Quraishi, M., Sudheer, Ansari, K., and Ebenso, E. E. (2012). 3-Aryl substituted triazole derivatives as new and effective corrosion inhibitors for mild steel in hydrochloric acid solution. *International journal of electrochemical science*, **7(8)**: 7476-7492.
- Roberge, P. R. (1999). Corrosion inhibitors. *Handbook of Corrosion Engineering*, McGraw-Hill, New York, pp 833.
- Roy, K., Kar, S., Das, R.N.** (2015). A Primer on QSAR/QSPR Modeling Fundamental Concepts. *Springer Briefs in Molecular Science*. DOI 10.1007/978-3-319-17281.
- Saha, S. K., and Banerjee, P. (2015). A theoretical approach to understand the inhibition mechanism of steel corrosion with two aminobenzonitrile inhibitors. *RSC Advances*, **5(87)**: 71120-71130.
- Sanyal, B. (1981). Organic compounds as corrosion inhibitors in different environments—a review. *Progress in Organic Coatings*, **9(2)**: 165-236.
- Sastri, V. S. (1998). Corrosion Inhibitors: Principles and Applications. New York: John Wiley & Sons Ltd. West Sussex.

- Sastri, V. S. (2012). *Green corrosion inhibitors: theory and practice* (Vol. 10): John Wiley & Sons.
- Sherif, E.-S. M. (2006). Effects of 2-amino-5-(ethylthio)-1, 3, 4-thiadiazole on copper corrosion as a corrosion inhibitor in 3% NaCl solutions. *Applied surface science*, **252(24)**: 8615-8623.
- Shi, W., Xia, M., Lei, W., and Wang, F. (2013). Molecular dynamics study of polyether polyamino methylene phosphonates as an inhibitor of anhydrite crystal. *Desalination*, **322**, 137-143.
- Silva, A., Agostinho, S., Barcia, O., Cordeiro, G., and D'elia, E. (2006). The effect of cysteine on the corrosion of 304L stainless steel in sulphuric acid. *Corrosion Science*, **48(11)**: 3668-3674.
- Singh, P., Ebenso, E. E., Olasunkanmi, L. O., Obot, I., and Quraishi, M. (2016). Electrochemical, theoretical, and surface morphological studies of corrosion inhibition effect of green naphthyridine derivatives on mild steel in hydrochloric acid. *The Journal of Physical Chemistry C*, **120(6)**: 3408-3419.
- Sun, S., Geng, Y., Tian, L., Chen, S., Yan, Y., and Hu, S. (2012). Density functional theory study of imidazole, benzimidazole and 2-mercaptobenzimidazole adsorption onto clean Cu(1 1 1) surface. *Corrosion Science*, **63**, 140-147.
- Szklarska-Smialowska, Z., and ZS-Smialowska. (2005). *Pitting and crevice corrosion*: NACE International 15835 Park Ten Pl, Houston, TX 77084, USA
- Tanak, H., Ađar, A., and Yavuz, M. (2010). Experimental and quantum chemical calculational studies on 2-[(4-Fluorophenylimino) methyl]-3, 5-dimethoxyphenol. *Journal of molecular modeling*, **16(3)**: 577-587.
- Tang, Y., Zhang, F., Hu, S., Cao, Z., Wu, Z., and Jing, W. (2013). Novel benzimidazole derivatives as corrosion inhibitors of mild steel in the acidic media. Part I: gravimetric, electrochemical, SEM and XPS studies. *Corrosion Science*, **74**, 271-282.
- Taylor, C., Chandra, A., Vera, J., and Sridhar, N. (2015). Multiphysics modelling, quantum chemistry and risk analysis for corrosion inhibitor design and lifetime prediction. *Faraday discussions*, **180**, 459-477.
- Tong, W., Hong, H., Xie, Q., Shi, L., Fang, H., and Perkins, R. (2005). Assessing QSAR limitations-A regulatory perspective. *Current Computer-Aided Drug Design*, **1(2)**: 195-205.
- Tropsha, A., Gramatica, P., and Gombar, V. K. (2003). The importance of being earnest: validation is the absolute essential for successful application and interpretation of QSPR models. *Molecular Informatics*, **22(1)**: 69-77.

- Veerasamy, R., Rajak, H., Jain, A., Sivadasan, S., Varghese, C. P., and Agrawal, R. K. (2011). Validation of QSAR models-strategies and importance. *International Journal of Drug Design & Discovery*, **3**, 511-519.
- Verma, C., Olasunkanmi, L. O., Ebenso, E. E., Quraishi, M. A., and Obot, I. B. (2016). Adsorption behavior of glucosamine-based, pyrimidine-fused heterocycles as green corrosion inhibitors for mild steel: experimental and theoretical studies. *The Journal of Physical Chemistry C*, **120(21)**: 11598-11611.
- Vosta, J., and Eliasek, J. (1971). Study on corrosion inhibition from aspect of quantum chemistry. *Corrosion Science*, **11(4)**: 223-229.
- Wang, H.-L., Liu, R.-B., and Xin, J. (2004). Inhibiting effects of some mercapto-triazole derivatives on the corrosion of mild steel in 1.0 M HCl medium. *Corrosion Science*, **46(10)**: 2455-2466.
- Wazzan, N. A. (2015). DFT calculations of thiosemicarbazide, arylisothiocyanates, and 1-aryl-2, 5-dithiohydrazodicarbonamides as corrosion inhibitors of copper in an aqueous chloride solution. *Journal of Industrial and Engineering Chemistry*, **26**, 291-308.
- Wazzan, N. A., Obot, I., and Kaya, S. (2016). Theoretical modeling and molecular level insights into the corrosion inhibition activity of 2-amino-1, 3, 4-thiadiazole and its 5-alkyl derivatives. *Journal of Molecular Liquids*, **221**, 579-602.
- Wu, W., Zhang, C., Lin, W., Chen, Q., Guo, X., Qian, Y., and Zhang, L. (2015). Quantitative structure-property relationship (QSPR) modeling of drug-loaded polymeric micelles via genetic function approximation. *PloS one*, **10(3)**: e0119575.
- Wymysłowski, A., Iwamoto, N., Yuen, M. M. F., and Fan, H. (2014). *Molecular Modeling and Multiscaling Issues for Electronic Material Applications: Volume 2*.
- Xia, S., Qiu, M., Yu, L., Liu, F., and Zhao, H. (2008). Molecular dynamics and density functional theory study on relationship between structure of imidazoline derivatives and inhibition performance. *Corrosion Science*, **50(7)**: 2021-2029.
- Y Wong, K., R Duchowicz, P., G Mercader, A., and A Castro, E. (2012). QSAR applications during last decade on inhibitors of acetylcholinesterase in Alzheimer's disease. *Mini reviews in medicinal chemistry*, **12(10)**: 936-946.
- Yaro, A. S., Khadom, A. A., and Wael, R. K. (2013). Apricot juice as green corrosion inhibitor of mild steel in phosphoric acid. *Alexandria Engineering Journal*, **52(1)**: 129-135.

- Zeng, J., Zhang, J., and Gong, X. (2011). Molecular dynamics simulation of interaction between benzotriazoles and cuprous oxide crystal. *Computational and Theoretical Chemistry*, **963(1)**: 110-114.
- Zerfaoui, M., Oudda, H., Hammouti, B., Kertit, S., and Benkaddour, M. (2004). Inhibition of corrosion of iron in citric acid media by aminoacids. *Progress in Organic Coatings*, **51(2)**: 134-138.
- Zhang, D.-Q., Cai, Q.-R., He, X.-M., Gao, L.-X., and Zhou, G.-D. (2008). Inhibition effect of some amino acids on copper corrosion in HCl solution. *Materials Chemistry and Physics*, **112(2)**: 353-358.
- Zhang, F., Tang, Y., Cao, Z., Jing, W., Wu, Z., and Chen, Y. (2012). Performance and theoretical study on corrosion inhibition of 2-(4-pyridyl)-benzimidazole for mild steel in hydrochloric acid. *Corrosion Science*, **61**, 1-9.
- Zhang, S., Lei, W., Xia, M., and Wang, F. (2005). QSAR study on N-containing corrosion inhibitors: quantum chemical approach assisted by topological index. *Journal of Molecular Structure: THEOCHEM*, **732(1-3)**: 173-182.
- Zhao, H., Zhang, X., Ji, L., Hu, H., and Li, Q. (2014). Quantitative structure–activity relationship model for amino acids as corrosion inhibitors based on the support vector machine and molecular design. *Corrosion Science*, **83**, 261-271.

## References

- Abdallah, M., Atwa, S., Salem, M., and Fouda, A. (2013). Synergistic effect of some halide ions on the inhibition of zinc corrosion in hydrochloric acid by tetrahydro carbazole derivatives compounds. *Int. J. Electrochem. Sci*, 8, 10001-10021.
- Abdulfatai, U., Uzairu, A., and Uba, S. (2017). Quantitative structure-activity relationship and molecular docking studies of a series of quinazolinonyl analogues as inhibitors of gamma amino butyric acid aminotransferase. *Journal of advanced research*, 8(1), 33-43.
- Ahamad, I., and Quraishi, M. (2009). Bis (benzimidazol-2-yl) disulphide: an efficient water soluble inhibitor for corrosion of mild steel in acid media. *Corrosion Science*, 51(9), 2006-2013.
- Akalezi, C. O., Enenebaku, C. K., and Oguzie, E. E. (2012). Application of aqueous extracts of coffee senna for control of mild steel corrosion in acidic environments. *International Journal of Industrial Chemistry*, 3(1), 13.
- Al Hashem, A. (2011). Corrosion in the Gulf Cooperation Council (GCC) states: statistics and figures. *proceedings of the Corrosion UAE, Abu Dhabi, UAE*.
- Alder, B. J., and Wainwright, T. E. (1959). Studies in molecular dynamics. I. General method. *The Journal of Chemical Physics*, 31(2), 459-466.
- Aljourani, J., Raeissi, K., and Golozar, M. (2009). Benzimidazole and its derivatives as corrosion inhibitors for mild steel in 1M HCl solution. *Corrosion Science*, 51(8), 1836-1843.
- Amin, M. A., and Ibrahim, M. M. (2011). Corrosion and corrosion control of mild steel in concentrated H<sub>2</sub>SO<sub>4</sub> solutions by a newly synthesized glycine derivative. *Corrosion Science*, 53(3), 873-885.
- Asadollahi, T., Dadfarnia, S., Shabani, A. M. H., Ghasemi, J. B., and Sarkhosh, M. (2011). QSAR models for CXCR2 receptor antagonists based on the genetic algorithm for data preprocessing prior to application of the PLS linear regression method and design of the new compounds using in silico virtual screening. *Molecules*, 16(3), 1928-1955.
- Ashassi-Sorkhabi, H., Majidi, M., and Seyyedi, K. (2004). Investigation of inhibition effect of some amino acids against steel corrosion in HCl solution. *Applied surface science*, 225(1-4), 176-185.
- Atalay, Y., Yakuphanoglu, F., Sekerci, M., Avci, D., and Başıoğlu, A. (2006). Theoretical studies of molecular structure and vibrational spectra of 2-amino-5-phenyl-1, 3, 4-thiadiazole. *Spectrochimica Acta Part A: Molecular and Biomolecular Spectroscopy*, 64(1), 68-72.

- Babić-Samardžija, K., Lupu, C., Hackeman, N., Barron, A. R., and Luttge, A. (2005). Inhibitive properties and surface morphology of a group of heterocyclic diazoles as inhibitors for acidic iron corrosion. *Langmuir*, 21(26), 12187-12196.
- Bazzi, L., Kertit, S., and Hamdani, M. (1995). Some organic compounds as inhibitors for the corrosion of aluminum alloy 6063 in deaerated carbonate solution. *Corrosion*, 51(11), 811-817.
- Becke, A. D. (1993). Density-functional thermochemistry. III. The role of exact exchange. *The Journal of Chemical Physics*, 98(7), 5648-5652.
- Bentiss, F., Lagrenée, M., Traisnel, M., and Homez, J. (1999). The corrosion inhibition of mild steel in acidic media by a new triazole derivative. *Corrosion Science*, 41(4), 789-803.
- Bentiss, F., Traisnel, M., Vezin, H., and Lagrenée, M. (2003). Linear resistance model of the inhibition mechanism of steel in HCl by triazole and oxadiazole derivatives: structure-activity correlations. *Corrosion Science*, 45(2), 371-380.
- Bereket, G., Öğretir, C., and Özşahin, Ç. (2003). Quantum chemical studies on the inhibition efficiencies of some piperazine derivatives for the corrosion of steel in acidic medium. *Journal of Molecular Structure: THEOCHEM*, 663(1-3), 39-46.
- Brondel, D., Edwards, R., Hayman, A., Hill, D., Mehta, S., and Semerad, T. (1994). Corrosion in the oil industry. *Oilfield review*, 6(2), 4-18.
- Clark, D. S., and Varney, W. R. (1962). *Physical metallurgy for engineers*: Van Nostrand Princeton, New Jersey.
- Collins, W., Weyers, R., and Al-Qadi, I. (1993). Chemical treatment of corroding steel reinforcement after removal of chloride-contaminated concrete. *Corrosion*, 49(1), 74-88.
- Dafali, A., Hammouti, B., Mokhlisse, R., and Kertit, S. (2003). Substituted uracils as corrosion inhibitors for copper in 3% NaCl solution. *Corrosion Science*, 45(8), 1619-1630.
- de Queiroz Baddini, A. L., Cardoso, S. P., Hollauer, E., and Gomes, J. A. d. C. P. (2007). Statistical analysis of a corrosion inhibitor family on three steel surfaces (duplex, super-13 and carbon) in hydrochloric acid solutions. *Electrochimica Acta*, 53(2), 434-446.
- Deng, Q., Shi, H.-W., Ding, N.-N., Chen, B.-Q., He, X.-P., Liu, G., Tang, Y., Long, Y.-T., and Chen, G.-R. (2012). Novel triazolyl bis-amino acid derivatives readily synthesized via click chemistry as potential corrosion inhibitors for mild steel in HCl. *Corrosion Science*, 57, 220-227.
- Ebenso, E. E., Arslan, T., Kandemirli, F., Caner, N., and Love, I. (2010). Quantum chemical studies of some rhodanine azosulpha drugs as corrosion inhibitors for mild steel in acidic medium. *International Journal of Quantum Chemistry*, 110(5), 1003-1018.
- Ebenso, E. E., Khaled, K., Shukla, S. K., Singh, A. K., Eddy, N., Saracoglu, M., Murulana, L. C., Kandemirli, F., Arslan, T., and Obot, I. (2012). Quantum chemical investigations on quinoline derivatives as effective corrosion inhibitors for mild steel in acidic medium.
- Eddy, N., and Mamza, P. (2009). Inhibitive and adsorption properties of ethanol extract of seeds and leaves of *Azadirachta indica* on the corrosion of mild steel in H<sub>2</sub>SO<sub>4</sub>. *Portugaliae Electrochimica Acta*, 27(4), 443-456.
- Eddy, N. O., Awe, F. E., Gimba, C. E., Ibisi, N. O., and Ebenso, E. E. (2011). QSAR, experimental and computational chemistry simulation studies on the inhibition potentials of some amino acids for the corrosion of mild steel in 0.1 M HCl. *Int. J. Electrochem. Sci*, 6(4), 931-957.
- El-Haddad, M. N. (2013). Chitosan as a green inhibitor for copper corrosion in acidic medium. *International journal of biological macromolecules*, 55, 142-149.
- El Sayed, H., El Nemr, A., Essawy, S. A., and Ragab, S. (2008). Corrosion inhibitors part V: QSAR of benzimidazole and 2-substituted derivatives as corrosion inhibitors by using the quantum chemical parameters. *Progress in Organic Coatings*, 61(1), 11-20.

- El Sayed, H., El Nemr, A., and Ragab, S. (2012). Quantitative structure activity relationships of some pyridine derivatives as corrosion inhibitors of steel in acidic medium. *Journal of molecular modeling*, 18(3), 1173-1188.
- Es-Salah, K., Keddami, M., Rahmouni, K., Srhiri, A., and Takenouti, H. (2004). Aminotriazole as corrosion inhibitor of Cu<sub>30</sub>Ni alloy in 3% NaCl in presence of ammoniac. *Electrochimica Acta*, 49(17-18), 2771-2778.
- Ezeoke, A. U., Adeyemi, O. G., Akerele, O. A., and Obi-Egbedi, N. O. (2012). Computational and experimental studies of 4-Aminoantipyrine as corrosion inhibitor for mild steel in sulphuric acid solution. *Int. J. Electrochem. Sci*, 7, 534-553.
- Fermi, I., Pasta, P., Ulam, S., and Tsingou, M. (1955). Studies of the nonlinear problems: Los Alamos Scientific Lab., N. Mex.
- Ferreira, E., Giacomelli, C., Giacomelli, F., and Spinelli, A. (2004). Evaluation of the inhibitor effect of L-ascorbic acid on the corrosion of mild steel. *Materials Chemistry and Physics*, 83(1), 129-134.
- Finšgar, M., and Jackson, J. (2016). Electrochemical Study of AISI C1018 Steel in Methanesulfonic Acid Containing an Acetylenic Alcohol-Based Corrosion Inhibitor Formulation. *Journal of laboratory automation*, 21(5), 632-641.
- Finšgar, M., and Milošev, I. (2010). Inhibition of copper corrosion by 1, 2, 3-benzotriazole: a review. *Corrosion Science*, 52(9), 2737-2749.
- Fu, J.-j., Li, S.-n., Wang, Y., and Cao, L.-h. (2010). Computational and electrochemical studies of some amino acid compounds as corrosion inhibitors for mild steel in hydrochloric acid solution. *Journal of materials science*, 45(22), 6255-6265.
- Fuentealba, P., Pérez, P., and Contreras, R. (2000). On the condensed Fukui function. *The Journal of Chemical Physics*, 113(7), 2544-2551.
- Gao, G., and Liang, C. (2007). Electrochemical and DFT studies of  $\beta$ -amino-alcohols as corrosion inhibitors for brass. *Electrochimica Acta*, 52(13), 4554-4559.
- García-Arriaga, V., Álvarez-Ramírez, J., Amaya, M., and Sosa, E. (2010). H<sub>2</sub>S and O<sub>2</sub> influence on the corrosion of carbon steel immersed in a solution containing 3 M diethanolamine. *Corrosion Science*, 52(7), 2268-2279.
- Gece, G. (2008). The use of quantum chemical methods in corrosion inhibitor studies. *Corrosion Science*, 50(11), 2981-2992.
- Gece, G., and Bilgiç, S. (2009). Quantum chemical study of some cyclic nitrogen compounds as corrosion inhibitors of steel in NaCl media. *Corrosion Science*, 51(8), 1876-1878.
- Gece, G., and Bilgiç, S. (2010). A theoretical study on the inhibition efficiencies of some amino acids as corrosion inhibitors of nickel. *Corrosion Science*, 52(10), 3435-3443.
- Gholami, M., Danaee, I., Maddahy, M. H., and RashvandAvei, M. (2013). Correlated ab initio and electroanalytical study on inhibition behavior of 2-mercaptobenzothiazole and its thiole-thione tautomerism effect for the corrosion of steel (API 5L X52) in sulphuric acid solution. *Industrial & Engineering Chemistry Research*, 52(42), 14875-14889.
- González-Olvera, R., Espinoza-Vázquez, A., Negrón-Silva, G. E., Palomar-Pardavé, M. E., Romero-Romo, M. A., and Santillan, R. (2013). Multicomponent synthesis of new 1, 2, 3-triazole derivatives of pyrimidine nucleobases: Promising acidic corrosion inhibitors for steel. *Molecules*, 18(12), 15064-15079.
- Gurudatt, D. M., Mohana, K. N., and Tandon, H. C. (2015). Synthesis of new 1, 2, 4-triazole derivatives and their anticorrosion properties on mild steel in hydrochloric acid medium. *Journal of Molecular Liquids*, 211, 275-287.
- Hansch, C., and Fujita, T. (1964).  $\rho$ - $\sigma$ - $\pi$  Analysis. A method for the correlation of biological activity and chemical structure. *Journal of the American Chemical Society*, 86(8), 1616-1626.

- Hluchan, V., Wheeler, B., and Hackerman, N. (1988). Amino acids as corrosion inhibitors in hydrochloric acid solutions. *Materials and Corrosion*, 39(11), 512-517.
- Hu, P., and Dai, W. (2012). Computer simulation and density functional theory study on relationship between structure of amino acid and inhibition performance. *Materials Research Innovations*, 16(1), 67-72.
- Jones, D. A. (1996). *Principles and prevention of corrosion*: Prentice Hall.
- Karelson, M., Lobanov, V. S., and Katritzky, A. R. (1996). Quantum-chemical descriptors in QSAR/QSPR studies. *Chemical reviews*, 96(3), 1027-1044.
- Kennard, R. W., and Stone, L. A. (1969). Computer aided design of experiments. *Technometrics*, 11(1), 137-148.
- Khaled, K. (2003). The inhibition of benzimidazole derivatives on corrosion of iron in 1 M HCl solutions. *Electrochimica Acta*, 48(17), 2493-2503.
- Khaled, K. (2008). Molecular simulation, quantum chemical calculations and electrochemical studies for inhibition of mild steel by triazoles. *Electrochimica Acta*, 53(9), 3484-3492.
- Khaled, K. (2011). Modeling corrosion inhibition of iron in acid medium by genetic function approximation method: A QSAR model. *Corrosion Science*, 53(11), 3457-3465.
- Khaled, K., and Hackerman, N. (2003). Investigation of the inhibitive effect of ortho-substituted anilines on corrosion of iron in 1 M HCl solutions. *Electrochimica Acta*, 48(19), 2715-2723.
- Kiani, M., Mousavi, M., Ghasemi, S., Shamsipur, M., and Kazemi, S. (2008). Inhibitory effect of some amino acids on corrosion of Pb–Ca–Sn alloy in sulfuric acid solution. *Corrosion Science*, 50(4), 1035-1045.
- Kokalj, A. (2010). Is the analysis of molecular electronic structure of corrosion inhibitors sufficient to predict the trend of their inhibition performance. *Electrochimica Acta*, 56(2), 745-755.
- Kraka, E., and Cremer, D. (2000). Computer design of anticancer drugs. A new enediyne warhead. *Journal of the American Chemical Society*, 122(34), 8245-8264.
- Kuznetsov, Y. I., and Kazansky, L. (2008). Physicochemical aspects of metal protection by azoles as corrosion inhibitors. *Russian Chemical Reviews*, 77(3), 219-232.
- Larif, M., Chtita, S., Adad, A., Hmamouchi, R., Bouachrine, M., and Lakhli, T. (2013). Predicting biological activity of Anticancer Molecules 3-ary 1-4-hydroxyquinolin-2-(1H)-one by DFT-QSAR models. *International Journal*, 3(12), 32-42.
- Lebrini, M., Robert, F., and Roos, C. (2011). Alkaloids extract from *Palicourea guianensis* plant as corrosion inhibitor for C38 steel in 1 M hydrochloric acid medium. *International journal of electrochemical science*, 6(3), 847-859.
- Levine, I. N., Busch, D. H., and Shull, H. (2000). *Quantum chemistry* (Vol. 5): Prentice Hall Upper Saddle River, NJ.
- Li, W., Hu, L., Tao, Z., Tian, H., and Hou, B. (2011). Experimental and quantum chemical studies on two triazole derivatives as corrosion inhibitors for mild steel in acid media. *Materials and Corrosion*, 62(11), 1042-1050.
- Lukovits, I., Kalman, E., and Zucchi, F. (2001). Corrosion inhibitors—correlation between electronic structure and efficiency. *Corrosion*, 57(1), 3-8.
- Lyon, S. (2004). Materials science: A natural solution to corrosion? *Nature*, 427(6973), 406.
- Ma, Q., Qi, S., He, X., Tang, Y., and Lu, G. (2017). 1, 2, 3-Triazole derivatives as corrosion inhibitors for mild steel in acidic medium: Experimental and computational chemistry studies. *Corrosion Science*, 129, 91-101.
- Martinez, S., and Metikoš-Huković, M. (2003). A nonlinear kinetic model introduced for the corrosion inhibitive properties of some organic inhibitors. *Journal of Applied Electrochemistry*, 33(12), 1137-1142.

- Masoud, M., Awad, M., Shaker, M., and El-Tahawy, M. (2010). The role of structural chemistry in the inhibitive performance of some aminopyrimidines on the corrosion of steel. *Corrosion Science*, 52(7), 2387-2396.
- Matheswaran, P., and Ramasamy, A. (2010). Influence of benzotriazole on corrosion inhibition of mild steel in citric acid medium. *Journal of Chemistry*, 7(3), 1090-1094.
- Moniz, B., Pollock, W. I., Gutzeit, J., Herbert, R., Schluter, J., and Siebert, O. (1986). Process industries corrosion: The theory and practice.
- Moore, J. J. (2013). *Chemical metallurgy*: Elsevier.
- Moretti, G., Guidi, F., and Grion, G. (2004). Tryptamine as a green iron corrosion inhibitor in 0.5 M deaerated sulphuric acid. *Corrosion Science*, 46(2), 387-403.
- Muralidharan, S., Quraishi, M., and Iyer, S. (1995). The effect of molecular structure on hydrogen permeation and the corrosion inhibition of mild steel in acidic solutions. *Corrosion Science*, 37(11), 1739-1750.
- Murulana, L. C., Singh, A. K., Shukla, S. K., Kabanda, M. M., and Ebenso, E. E. (2012). Experimental and quantum chemical studies of some bis (trifluoromethyl-sulfonyl) imide imidazolium-based ionic liquids as corrosion inhibitors for mild steel in hydrochloric acid solution. *Industrial & Engineering Chemistry Research*, 51(40), 13282-13299.
- Musa, A. Y., Jalgham, R. T., and Mohamad, A. B. (2012). Molecular dynamic and quantum chemical calculations for phthalazine derivatives as corrosion inhibitors of mild steel in 1 M HCl. *Corrosion Science*, 56, 176-183.
- Nimmo, B., and Hinds, G. (2003). Beginners guide to corrosion. *National Physical Library*, 200-201.
- Nwankwo, H. U., Ateba, C. N., Olasunkanmi, L. O., Adekunle, A. S., Isabirye, D. A., Onwudiwe, D. C., and Ebenso, E. E. (2016). Synthesis, characterization, antimicrobial studies and corrosion inhibition potential of 1, 8-dimethyl-1, 3, 6, 8, 10, 13-hexaazacyclotetradecane: experimental and quantum chemical studies. *Materials*, 9(2), 107.
- Nwankwo, H. U., Olasunkanmi, L. O., and Ebenso, E. E. (2017). Experimental, quantum chemical and molecular dynamic simulations studies on the corrosion inhibition of mild steel by some carbazole derivatives. *Scientific reports*, 7(1), 2436.
- Obot, I., and Gasem, Z. (2014). Theoretical evaluation of corrosion inhibition performance of some pyrazine derivatives. *Corrosion Science*, 83, 359-366.
- Obot, I., Macdonald, D., and Gasem, Z. (2015). Density functional theory (DFT) as a powerful tool for designing new organic corrosion inhibitors. Part 1: an overview. *Corrosion Science*, 99, 1-30.
- Obot, I., and Obi-Egbedi, N. (2010). An interesting and efficient green corrosion inhibitor for aluminium from extracts of *Chlomolaena odorata* L. in acidic solution. *Journal of Applied Electrochemistry*, 40(11), 1977-1984.
- Obot, I. B. (2014). Recent advances in computational design of organic materials for corrosion protection of steel in aqueous media *Developments in corrosion protection*: InTech.
- Osman, M., and Shalaby, M. (2003). Some ethoxylated fatty acids as corrosion inhibitors for low carbon steel in formation water. *Materials Chemistry and Physics*, 77(1), 261-269.
- Ouid, H., Benali, O., and Guendouzi, A. (2015). *Corrosion inhibition of mild steel in acidic media using newly synthesized heterocyclic organic molecules: Correlation between inhibition efficiency and chemical structure*. Paper presented at the AIP Conference Proceedings.
- Palomar-Pardavé, M., Romero-Romo, M., Herrera-Hernández, H., Abreu-Quijano, M., Likhanova, N. V., Uruchurtu, J., and Juárez-García, J. (2012). Influence of the alkyl chain length of 2 amino 5 alkyl 1, 3, 4 thiadiazole compounds on the corrosion inhibition of steel immersed in sulfuric acid solutions. *Corrosion Science*, 54, 231-243.

- Popova, A., Christov, M., and Deligeorgiev, T. (2003). Influence of the molecular structure on the inhibitor properties of benzimidazole derivatives on mild steel corrosion in 1 M hydrochloric acid. *Corrosion*, 59(9), 756-764.
- Popova, A., Christov, M., Raicheva, S., and Sokolova, E. (2004). Adsorption and inhibitive properties of benzimidazole derivatives in acid mild steel corrosion. *Corrosion Science*, 46(6), 1333-1350.
- Popova, A., Christov, M., and Zwetanova, A. (2007). Effect of the molecular structure on the inhibitor properties of azoles on mild steel corrosion in 1 M hydrochloric acid. *Corrosion Science*, 49(5), 2131-2143.
- Pourbasheer, E., Aalizadeh, R., Ganjali, M. R., Norouzi, P., and Banaei, A. (2014). QSAR study of mGlu5 inhibitors by genetic algorithm-multiple linear regressions. *Medicinal Chemistry Research*, 23(6), 3082-3091.
- Quraishi, M. (2013). Electrochemical and theoretical investigation of triazole derivatives on corrosion inhibition behavior of copper in hydrochloric acid medium. *Corrosion Science*, 70, 161-169.
- Quraishi, M., and Jamal, D. (2000). Fatty acid triazoles: novel corrosion inhibitors for oil well steel (N-80) and mild steel. *Journal of the American Oil Chemists' Society*, 77(10), 1107-1111.
- Quraishi, M., and Sardar, R. (2002). Aromatic triazoles as corrosion inhibitors for mild steel in acidic environments. *Corrosion*, 58(9), 748-755.
- Quraishi, M., Sudheer, Ansari, K., and Ebenso, E. E. (2012). 3-Aryl substituted triazole derivatives as new and effective corrosion inhibitors for mild steel in hydrochloric acid solution. *International journal of electrochemical science*, 7(8), 7476-7492.
- Roberge, P. R. (1999). Corrosion inhibitors. *Handbook of Corrosion Engineering*, McGraw-Hill, New York, 833.
- Roy, K., Kar, S., and Das, R. N. (2015). *A primer on QSAR/QSPR modeling: Fundamental concepts*: Springer.
- Saha, S. K., and Banerjee, P. (2015). A theoretical approach to understand the inhibition mechanism of steel corrosion with two aminobenzonitrile inhibitors. *RSC Advances*, 5(87), 71120-71130.
- Sanyal, B. (1981). Organic compounds as corrosion inhibitors in different environments—a review. *Progress in Organic Coatings*, 9(2), 165-236.
- Sastri, V. S. (1998). *Corrosion inhibitors: principles and applications*.
- Sastri, V. S. (2012). *Green corrosion inhibitors: theory and practice* (Vol. 10): John Wiley & Sons.
- Sherif, E.-S. M. (2006). Effects of 2-amino-5-(ethylthio)-1, 3, 4-thiadiazole on copper corrosion as a corrosion inhibitor in 3% NaCl solutions. *Applied surface science*, 252(24), 8615-8623.
- Shi, W., Xia, M., Lei, W., and Wang, F. (2013). Molecular dynamics study of polyether polyamino methylene phosphonates as an inhibitor of anhydrite crystal. *Desalination*, 322, 137-143.
- Silva, A., Agostinho, S., Barcia, O., Cordeiro, G., and D'elia, E. (2006). The effect of cysteine on the corrosion of 304L stainless steel in sulphuric acid. *Corrosion Science*, 48(11), 3668-3674.
- Singh, P., Ebenso, E. E., Olasunkanmi, L. O., Obot, I., and Quraishi, M. (2016). Electrochemical, theoretical, and surface morphological studies of corrosion inhibition effect of green naphthyridine derivatives on mild steel in hydrochloric acid. *The Journal of Physical Chemistry C*, 120(6), 3408-3419.
- Sun, S., Geng, Y., Tian, L., Chen, S., Yan, Y., and Hu, S. (2012). Density functional theory study of imidazole, benzimidazole and 2-mercaptobenzimidazole adsorption onto clean Cu (1 1 1) surface. *Corrosion Science*, 63, 140-147.
- Szklarska-Smialowska, Z., and ZS-Smialowska. (2005). *Pitting and crevice corrosion*: NACE International Houston, TX.

- Tanak, H., Ađar, A., and Yavuz, M. (2010). Experimental and quantum chemical calculational studies on 2-[[4-Fluorophenylimino] methyl]-3, 5-dimethoxyphenol. *Journal of molecular modeling*, 16(3), 577-587.
- Tang, Y., Zhang, F., Hu, S., Cao, Z., Wu, Z., and Jing, W. (2013). Novel benzimidazole derivatives as corrosion inhibitors of mild steel in the acidic media. Part I: gravimetric, electrochemical, SEM and XPS studies. *Corrosion Science*, 74, 271-282.
- Taylor, C., Chandra, A., Vera, J., and Sridhar, N. (2015). Multiphysics modelling, quantum chemistry and risk analysis for corrosion inhibitor design and lifetime prediction. *Faraday discussions*, 180, 459-477.
- Tong, W., Hong, H., Xie, Q., Shi, L., Fang, H., and Perkins, R. (2005). Assessing QSAR limitations-A regulatory perspective. *Current Computer-Aided Drug Design*, 1(2), 195-205.
- Tropsha, A., Gramatica, P., and Gombar, V. K. (2003). The importance of being earnest: validation is the absolute essential for successful application and interpretation of QSPR models. *Molecular Informatics*, 22(1), 69-77.
- Veerasamy, R., Rajak, H., Jain, A., Sivadasan, S., Varghese, C. P., and Agrawal, R. K. (2011). Validation of QSAR models-strategies and importance. *International Journal of Drug Design & Discovery*, 3, 511-519.
- Vema, C., Olasunkanmi, L. O., Ebenso, E. E., Quraishi, M. A., and Obot, I. B. (2016). Adsorption behavior of glucosamine-based, pyrimidine-fused heterocycles as green corrosion inhibitors for mild steel: experimental and theoretical studies. *The Journal of Physical Chemistry C*, 120(21), 11598-11611.
- Vosta, J., and Eliasek, J. (1971). Study on corrosion inhibition from aspect of quantum chemistry. *Corrosion Science*, 11(4), 223-229.
- Wang, H.-L., Liu, R.-B., and Xin, J. (2004). Inhibiting effects of some mercapto-triazole derivatives on the corrosion of mild steel in 1.0 M HCl medium. *Corrosion Science*, 46(10), 2455-2466.
- Wazzan, N. A. (2015). DFT calculations of thiosemicarbazide, arylisothiocyanates, and 1-aryl-2, 5-dithiohydrazodicarbonamides as corrosion inhibitors of copper in an aqueous chloride solution. *Journal of Industrial and Engineering Chemistry*, 26, 291-308.
- Wazzan, N. A., Obot, I., and Kaya, S. (2016). Theoretical modeling and molecular level insights into the corrosion inhibition activity of 2-amino-1, 3, 4-thiadiazole and its 5-alkyl derivatives. *Journal of Molecular Liquids*, 221, 579-602.
- Wu, W., Zhang, C., Lin, W., Chen, Q., Guo, X., Qian, Y., and Zhang, L. (2015). Quantitative structure-property relationship (QSPR) modeling of drug-loaded polymeric micelles via genetic function approximation. *PLoS one*, 10(3), e0119575.
- Wymyslowski, A., Iwamoto, N., Yuen, M. M. F., and Fan, H. (2014). *Molecular Modeling and Multiscaling Issues for Electronic Material Applications: Volume 2*.
- Xia, S., Qiu, M., Yu, L., Liu, F., and Zhao, H. (2008). Molecular dynamics and density functional theory study on relationship between structure of imidazoline derivatives and inhibition performance. *Corrosion Science*, 50(7), 2021-2029.
- Y Wong, K., R Duchowicz, P., G Mercader, A., and A Castro, E. (2012). QSAR applications during last decade on inhibitors of acetylcholinesterase in Alzheimer's disease. *Mini reviews in medicinal chemistry*, 12(10), 936-946.
- Yaro, A. S., Khadom, A. A., and Wael, R. K. (2013). Apricot juice as green corrosion inhibitor of mild steel in phosphoric acid. *Alexandria Engineering Journal*, 52(1), 129-135.
- Zeng, J., Zhang, J., and Gong, X. (2011). Molecular dynamics simulation of interaction between benzotriazoles and cuprous oxide crystal. *Computational and Theoretical Chemistry*, 963(1), 110-114.

- Zerfaoui, M., Oudda, H., Hammouti, B., Kertit, S., and Benkaddour, M. (2004). Inhibition of corrosion of iron in citric acid media by aminoacids. *Progress in Organic Coatings*, 51(2), 134-138.
- Zhang, D.-Q., Cai, Q.-R., He, X.-M., Gao, L.-X., and Zhou, G.-D. (2008). Inhibition effect of some amino acids on copper corrosion in HCl solution. *Materials Chemistry and Physics*, 112(2), 353-358.
- Zhang, F., Tang, Y., Cao, Z., Jing, W., Wu, Z., and Chen, Y. (2012). Performance and theoretical study on corrosion inhibition of 2-(4-pyridyl)-benzimidazole for mild steel in hydrochloric acid. *Corrosion Science*, 61, 1-9.
- Zhang, S., Lei, W., Xia, M., and Wang, F. (2005). QSAR study on N-containing corrosion inhibitors: quantum chemical approach assisted by topological index. *Journal of Molecular Structure: THEOCHEM*, 732(1-3), 173-182.
- Zhao, H., Zhang, X., Ji, L., Hu, H., and Li, Q. (2014). Quantitative structure–activity relationship model for amino acids as corrosion inhibitors based on the support vector machine and molecular design. *Corrosion Science*, 83, 261-271.